

y.1

# Health Physics DIVISION



3 4456 0359430 4

## *Annual Progress Report*

Period Ending July 31, 1972

OAK RIDGE NATIONAL LABORATORY  
CENTRAL RESEARCH LIBRARY  
DOCUMENT COLLECTION

### **LIBRARY LOAN COPY**

DO NOT TRANSFER TO ANOTHER PERSON

If you wish someone else to see this  
document, send in name with document  
and the library will arrange a loan.

UEN-1104  
12 3-77



## **OAK RIDGE NATIONAL LABORATORY**

OPERATED BY UNION CARBIDE CORPORATION • FOR THE U.S. ATOMIC ENERGY COMMISSION

Printed in the United States of America. Available from  
National Technical Information Service  
U.S. Department of Commerce  
5285 Port Royal Road, Springfield, Virginia 22151  
Price: Printed Copy \$3.00; Microfiche \$0.95

This report was prepared as an account of work sponsored by the United States Government. Neither the United States nor the United States Atomic Energy Commission, nor any of their employees, nor any of their contractors, subcontractors, or their employees, makes any warranty, express or implied, or assumes any legal liability or responsibility for the accuracy, completeness or usefulness of any information, apparatus, product or process disclosed, or represents that its use would not infringe privately owned rights.

Contract No. W-7405-eng-26

**HEALTH PHYSICS DIVISION  
ANNUAL PROGRESS REPORT  
For Period Ending July 31, 1972**

August 1, 1971--June 30, 1972

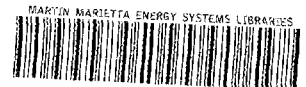
K. Z. Morgan, Director  
W. S. Snyder, Assistant Director  
E. G. Struxness, Assistant Director (August  
1, 1971--May 15, 1972; May 15, 1972 --  
Assistant Director of Environmental Sciences  
Division and liaison between Environmental  
Sciences and Health Physics Divisions)

July 1, 1972

J. A. Auxier, Director  
W. S. Snyder, Assistant Director  
D. M. Davis, Assistant Director  
K. Z. Morgan, Senior Advisor

SEPTEMBER 1972

OAK RIDGE NATIONAL LABORATORY  
Oak Ridge, Tennessee 37830  
operated by  
UNION CARBIDE CORPORATION  
for the  
U.S. ATOMIC ENERGY COMMISSION



3 4456 0359430 4

Reports previously issued in this series are as follows:

ORNL-2384	Period Ending July 31, 1957
ORNL-2590	Period Ending July 31, 1958
ORNL-2806	Period Ending July 31, 1959
ORNL-2994	Period Ending July 31, 1960
ORNL-3189	Period Ending July 31, 1961
ORNL-3347	Period Ending July 31, 1962
ORNL-3492	Period Ending July 31, 1963
ORNL-3697	Period Ending July 31, 1964
ORNL-3849	Period Ending July 31, 1965
ORNL-4007	Period Ending July 31, 1966
ORNL-4168	Period Ending July 31, 1967
ORNL-4316	Period Ending July 31, 1968
ORNL-4446	Period Ending July 31, 1969
ORNL-4584	Period Ending July 31, 1970
ORNL-4720	Period Ending July 31, 1971

# Contents

SUMMARY .....	vii
<b>PART I. RADIATION PHYSICS</b>	
1. THEORETICAL RADIATION PHYSICS .....	1
Pion Beam Dosimetry .....	1
Status of the Theory of Delta-Ray Production .....	2
Electron-Slowing-Down Spectra in Semiconductors .....	2
Inner-Shell Excitation of Atoms by Slow Heavy Charged Particles .....	3
Low-Energy Electron Scattering by Polar Molecules .....	4
Utilization of Complex Potential Operator Formalism in Electron Scattering Problems .....	8
Influence of Plasmon Damping on the Mean Free Path for Plasmon Excitation .....	9
Plasmons in Solids .....	10
The Damping of Plasma Waves in Condensed Matter .....	10
Surface Plasmons and the Image Force .....	11
2. INTERACTION OF RADIATION WITH LIQUIDS AND SOLIDS .....	13
Optical Properties of K between 4 and 10.7 eV and Comparison with Na, Rb, and Cs .....	13
Optical Properties of Glassy Carbon from 0 to 82 eV .....	15
A Slope Method for Determining Extinction Coefficients .....	16
Work Function Changes during Oxygen Chemisorption on Fresh Magnesium Surfaces .....	17
A Technique for Revitalization of Vacuum Ultraviolet Diffraction Gratings .....	18
3. PHYSICS OF TISSUE DAMAGE .....	19
Electron-Slowing-Down Studies .....	19
Optical Properties of Organic Liquids .....	21
Radiation Interactions with Nucleic Acid Bases .....	23
4. ELECTRON AND ION COLLISION PHYSICS .....	25
Metastable Anions of CO <sub>2</sub> .....	25
Electron Attachment to Organic Molecules .....	28
Chemi-Ionizing Collisions .....	29
Ion Condensation Reactions in Benzene Vapor .....	31
Collisional Ionization of Cesium by Molecules: Determination of Electron Affinities .....	32
Longitudinal Electron Diffusion Coefficient and Electron Drift Velocity Measurements in Water Vapor .....	32

Thermal and Near-Thermal Electron Transport Coefficients in O <sub>2</sub> Determined with a Time-of-Flight Swarm Experiment Using a Drift-Dwell-Drift Technique .....	33
Chlorine Gas Evolution from Irradiated Rock Salt .....	33
Florida State University–Oak Ridge National Laboratory Chemical Accelerator .....	34
<b>5. ATOMIC AND MOLECULAR RADIATION PHYSICS .....</b>	<b>35</b>
Intermediate Phase Studies for Understanding Radiation Interaction with Condensed Media: The Electron Attachment Process .....	35
Structure in the Cross Section for Capture of Slow (<0.5 eV) Electrons by O <sub>2</sub> to Form O <sub>2</sub> <sup>-</sup> .....	39
Lifetimes of Long-Lived Polyatomic Negative Ions .....	39
Unimolecular Decompositions .....	40
Mobilities of Thermal Electrons in Gases and Liquids .....	40
Scattering of Slow Electrons by $\pi$ -Electron-Containing Organic Molecules .....	43
Compound Negative-Ion Resonances and Threshold-Electron Excitation Spectra of Quinoline and Isoquinoline .....	43
Energy-Loss Spectra of <i>N</i> -Heterocyclic Benzene Derivatives .....	44
Threshold-Electron Excitation and Compound Negative-Ion Formation in Methane, Ethane, and Propane .....	44
Reactions of Molecular Rydberg States .....	45
Photophysical Studies of Organic Liquids and Solutions; Emission Spectra from Higher Excited $\pi$ -Singlet States of Aromatic Hydrocarbons in Solution .....	45
Low-Energy Electron Interactions with Liquids .....	46
<b>6. GRADUATE EDUCATION AND VOCATIONAL TRAINING .....</b>	<b>47</b>
<b>PART II. RADIATION DOSIMETRY RESEARCH</b>	
<b>7. DOSIMETRY FOR HUMAN EXPOSURES AND RADIOBIOLOGY .....</b>	<b>49</b>
Japanese Dosimetry Program .....	49
Measurements of Dose Distributions .....	50
Dose and LET Calculations .....	51
Measurements at the Biology Division <sup>252</sup> Cf Irradiation Facility .....	60
<b>8. APPLIED DOSIMETRY RESEARCH .....</b>	<b>62</b>
The Role and Nature of Activators in TSEE .....	62
TSEE Reader Development .....	64
Reproducibility and Stability of TSEE Detectors .....	66
Atmospheric, Temperature, and Other Effects on TSEE .....	67
Fading Stability of Solid-State and Film Dosimeters .....	69
Thermoluminescence Dosimetry .....	70
Track Etching .....	71
<b>9. INTERACTION OF CHARGED PARTICLES WITH MATTER .....</b>	<b>74</b>
Proton Interactions with Helium .....	74

Transport of Resonance Radiation .....	76
An Operational Rationale for Radiation Protection .....	76
10. HPRR AND ACCELERATOR OPERATIONS .....	78
Health Physics Research Reactor Operations .....	78
Calculation of the HPRR Neutron Spectrum for Simulated Nuclear Accident Conditions .....	78
11. SPECTROMETRY RESEARCH AND DEVELOPMENT .....	82
Neutron Detector .....	82
Light Pulsar .....	82
Contributions to Environmental Impact Statements .....	83
Development of a High-Sensitivity Fast-Neutron Spectrometer .....	83
A Device for Listing Punched Paper Tape Directly on a Typewriter .....	83
Distribution of Charged Particle Stopping .....	84
Zone Refining of Organic Compounds .....	84
The Natural Radiation Environment and Man's Influence on It .....	84
<b>PART III. INTERNAL DOSIMETRY</b>	
12. Estimates of Absorbed Fractions for Photon Emitters within the Body .....	86
13. Estimates of Dose to Infants and Children from a Photon Emitter in the Lungs .....	91
14. Weight of the Lungs Plus Fluids for Reference Man .....	97
15. A Metabolic Model for Magnesium in Man and an Estimate of Dose to Bone and Soft Tissue Resulting from a Single Intravenous Injection of $^{28}\text{Mg}$ .....	99
16. A Method of Interpreting Excretion Data Which Allows for Statistical Fluctuation of the Data .....	102
<b>PART IV. ENVIRONMENTAL STUDIES</b>	
17. DOSE ESTIMATION STUDIES RELATED TO PEACEFUL USES OF NUCLEAR EXPLOSIVES AND OTHER RADIONUCLIDE RELEASES .....	108
Development of Radiation Safety Guides for Environmental Releases of Radioactivity .....	108
Utilization of Natural Gas from Nuclearly Stimulated Wells .....	109
Characterization of the Radioactivity in Liquid Effluents from Light-Water Power Reactors .....	110
Environmental Impact Statements .....	111
<b>THESES, PAPERS, PUBLICATIONS, AND LECTURES</b>	
THESES .....	115
PAPERS .....	116
PUBLICATIONS .....	120
LECTURES .....	128



## Summary

### PART I. RADIATION PHYSICS

#### 1. Theoretical Radiation Physics

A theoretical study has been made of the energy deposited in water spheres and cylinders of various sizes around the site at which an oxygen or carbon nucleus captures a stopped negative pion. A review has been made of methods for calculating the spectra of delta rays produced by heavy ions and electrons, with a view toward their incorporation into microdosimetry theory. Calculations have been made of electron-slowing-down spectra in semiconductors based on the use of model cross sections for the valence band in a semiconductor and classical cross sections for excitations from inner levels. Interesting new formulas have been obtained for the inner-shell excitation of atoms by slow heavy charged particles, using the perturbed stationary state formalism of Mott. An extensive theoretical study of the effects of dipolar forces on charged-particle scattering phenomena has been made. Use has been made of Feshbach's elegant and powerful technique for determining elastic and total scattering cross sections under multichannel scattering conditions in an application to atomic scattering of electrons above the ionization potential of the target. Very satisfactory results for elastic and total scattering cross sections have been obtained for electrons on hydrogen. The mean free path of an electron in a nearly free electron gas has been investigated, yielding a result which predicts an appreciable probability for plasmon excitation by an incident electron with energy well below the threshold predicted by the usual zero-damping theory. A general review has been made of some of the interesting properties of plasmons and their manifestations in experimental physics. We have obtained analytical expressions which may be used to relate the damping of long-wavelength plasma waves to experimentally determined values of the complex dielectric permittivity of a medium. We have shown that the classical image potential outside a metal may be considered to originate in the shifted zero-point energy of the surface plasmon field and that retardation correction to this

potential gives a more rapid falloff with the distance than predicted by the classical theory at distances which are of the order of tens to hundreds of angstroms from the surface, depending upon the quantum plasma energy of the metal.

#### 2. Interaction of Radiation with Solids and Liquids

Measurements of the optical properties of a medium can yield information about the modes of energy deposition occurring when high-energy charged particles or electromagnetic radiation interact with the medium. Thus we have a continuing program to measure and interpret the optical properties of materials of basic importance. During this year the optical constants of K have been measured above the plasma energy and the results compared with those obtained previously for Na, Rb, and Cs. The most plausible explanation for the strong absorption seen above the plasma energies in all these alkali metals is that of plasmon-assisted interband transitions. The optical properties of glassy carbon have been obtained up to 82 eV and interpreted, by comparison with graphite, in terms of  $\pi$  and  $\sigma$  single-electron transitions and collective oscillations. In addition, work function changes during oxygen chemisorption on fresh Mg surfaces have been correlated with the observed exoelectron emission. A method has been developed for obtaining extinction coefficients from critical angle measurements which gives greater accuracy than the usual method of fitting Fresnel's equations for reflectance as a function of angle of incidence. A technique has also been developed for revitalizing vacuum ultraviolet diffraction gratings.

#### 3. Physics of Tissue Damage

The experimental investigation of the electron-slowing-down spectra in semiconductors was completed with a study of silicon. The shape of the spectrum was similar to that of germanium and of those conductors studied earlier, but did show some evidence of discontinuities near the silicon *L*- and *K*-shell energies.

These are attributed to electron-induced ionizations of the shells.

Electron-slowing-down studies have been extended to include insulating materials. Preliminary data have been obtained using aluminum oxide doped with a small amount of dysprosium, which served as the electron source. Electron fluxes were found to be generally higher than those for a typical conductor.

A series of studies was initiated on the influence of source thickness on the slowing-down spectra in an effort to explain the present discrepancy between theory and experiment. In the thinner sources a pronounced peak in the electron flux was observed at the *LMM* Auger range. This represents a new source which can contribute to the electron flux at lower energies and may be, in part, responsible for the poor agreement between theory and experiment at the lower energies.

Experimental studies of the optical properties of organic liquids was continued with investigations of several commonly used solvents. The measurements were made using a newly developed transmission cell which enables studies to be carried out on samples as thin as 500 Å.

An experimental investigation of the optical and dielectric properties of the nucleic acid bases has been initiated. Preliminary data have been obtained for guanine at energies up to 80 eV which, in general, show good agreement with the results of the electron-energy-loss studies obtained by scanning electron microscope techniques.

#### 4. Electron and Ion Collision Physics

The first experimental values for thermal and near-thermal electron transport coefficients have been determined for oxygen and water vapor with a time-of-flight electron swarm experiment using the drift-dwell-drift technique. Comparison with theory where available is good. Studies of the interaction of low-energy electrons with a series of organic and organometallic compounds in the gas phase have elucidated a number of new electron-molecule reaction mechanisms. Electron collisions with a series of anhydride molecules produced metastable  $\text{CO}_2^{-*}$  ions, and the lifetime of this ion was measured for the first time. Also, metastable ions of the form  $\text{C}_x\text{H}_y\text{CO}_2^{-*}$  were found to dissociate after electron detachment into energetic  $\text{C}_x\text{H}_y$  and  $\text{CO}_2$  molecules. The formation of positive and negative ions in the organometallic "sandwich" compounds ferrocene, cobaltocene, nickelocene, and magnesocene have been studied by high-resolution electron impact mass

spectrometry techniques. The electron affinities of a number of organic and inorganic molecules have been determined by the cesium collisional ionization technique. A number of positive-ion condensation reactions in the benzene system have been examined in a time-of-flight mass spectrometer. Ion-pair production by chemi-ionizing collisions of excited rare-gas atoms with molecules have been studied and show extremely large cross sections. In short, a number of gas collision problems of direct interest to radiation chemistry have been studied.

#### 5. Atomic and Molecular Radiation Physics

Intermediate phase studies for understanding radiation interaction with condensed media and for developing a coherent picture of radiation interaction with matter are discussed with emphasis on electron attachment and drift through low- and high-pressure gases and liquids. Highlights of our studies on long-lived polyatomic negative ions, moderately short-lived negative ions, compound negative-ion resonance states, threshold-electron excitation of polyatomic molecules, and thermal electron scattering by molecules are outlined. The emphasis in these studies is on key groups of organic molecules including O- and  $\text{NO}_2$ -containing organic molecules, *N*-heterocyclic benzene and naphthalene derivatives, and saturated and aromatic hydrocarbons. Reactions of molecular Rydberg states and emission spectra from higher excited  $\pi$ -singlet states of aromatic hydrocarbons in solution are also discussed.

#### 6. Graduate Education and Vocational Training

The health physics training program included fellowship students from the University of Kentucky, the University of Michigan, Georgia Institute of Technology, and Purdue University. These reported to ORNL for summer on-the-job instruction in applied and research health physics.

Division personnel visited eight colleges and universities to give seminars on various research problems of current interest and also to help recruit qualified students in the fellowship program.

The Health Physics Division provided research facilities and advisors for 13 Oak Ridge Graduate Fellows, AEC Fellows, and USPHS Fellows who were conducting thesis research.

Teaching assistance was given to The University of Tennessee for its program in radiation physics. Lectures

and tours were given for several university groups visiting ORNL.

Assistance and consultation were given to six schools that were interested in establishing health physics courses or programs in their science departments.

The Division cooperated with ORAU in the presentation of a ten-week course in applied health physics and in the screening of applicants for AEC Fellowships.

## PART II. RADIATION DOSIMETRY RESEARCH

### 7. Dosimetry for Human Exposures and Radiobiology

Calculations of dose distributions in human-size tissue-equivalent phantoms for a wide variety of radiation sources continues to be a major objective in this research. During this report period, emphasis was again placed on distributions from  $^{252}\text{Cf}$ , monoenergetic neutrons incident at  $45^\circ$  with the axis of the phantom, and monoenergetic photons incident unilaterally on a heterogeneous phantom. Local dose distributions for implanted  $^{252}\text{Cf}$  sources were determined, and tables of exposure values were prepared for regions close to the source. Neutron isodose curves in tissue were also prepared. An absolute comparison of measured dose distributions (reported in ORNL-4720) was made with calculations. The agreement was found to be within the probable errors of measurement and calculation. Values of neutron and gamma-ray dose were measured in the vicinity of a  $^{252}\text{Cf}$  source facility within the Biology Division. This was done to determine the exposure conditions for specimens irradiated at that facility. Liaison with the Atomic Bomb Casualty Commission has continued. Studies of particular importance include dosimetry for "heavy shielding" cases, determinations of organ doses, and a pilot study of the histories of survivors who were exposed to the radioactive "black rain."

### 8. Applied Dosimetry Research

Major emphasis in the solid-state dosimetry program continues to be in the area of detector research. Exoelectron emission studies were centered around the role and nature of activators in the ceramic BeO detectors, reproducibility of TSEE readout, stability of stored signals, effects on TSEE response such as atmospheric, temperature, light, etc., and the development of TSEE readers. TSEE activators such as sodium, lithium, magnesium, and aluminum were added to ceramic BeO before firing to  $1600^\circ\text{C}$ . None of these

samples exhibited a glow curve different from that of BeO 995, which has a natural content of silicon of 2000 ppm. These activators seem to promote exoelectron emission which is already intrinsic to the ceramic BeO by increasing the efficiency of exoelectron release. A significant fading study was made of a variety of new solid-state detectors as well as several film dosimeters. It was found that latent unetched fission fragment tracks in  $10\text{-}\mu\text{m}$  polycarbonate foil are stable for at least three months at  $30^\circ\text{C}$  and 95% relative humidity. Radiophotoluminescent (RPL) and thermoluminescent (TLD) detectors as well as common dosimeter films were included in this study. Three different RPL dosimeters showed less than 15% deviation in readings between one day and three months after exposure if stored at  $30^\circ\text{C}$  and 95% relative humidity. Of various TL detectors, fading in  $\text{CaSO}_4:\text{Dy}$  was barely detectable, while  $\text{CaF}_2:\text{Dy}$  showed pronounced fading under the same conditions. Studies associated with developing an alternative detector (to photographic film) for personnel neutron monitoring have continued and were centered on the registration of charged particles in plastic.

### 9. Interaction of Charged Particles with Matter

The specific objective of this research program continues to be directed at determining energy pathways after swift charged particles interact with gases. During this report period studies have centered on the interaction of 2-MeV protons with helium at pressures between  $10^{-3}$  and  $10^3$  torr. The dominating ( $2^1P$ ) state was studied by observing the time behavior of a resonance line resulting from  $2^1P\text{-}1^1S$  transitions at 584 Å. Comparing these data with the intensity and time behavior of the continuous emission, it was concluded that the atomic state  $2^1P$  is converted to two different excited molecular states in helium by three-body collisions. The energy pathways model developed in these studies suggests that the Jesse effect originates from a metastable molecule rather than from an atomic state, as previously believed. An operational rationale for radiation protection is being developed which is not encumbered by such concepts as "permissible levels" measured in terms of absorbed dose or its myriad of factors. The radiation field is defined by specifying every variable which could considerably affect the biological probabilities. Two approaches to the problem are being pursued. In the first approach an operational relationship between radiation and effect is expressed by assuming that an operator exists which transforms the radiation field directly into probabilities of ob-

serving effects. The second approach embodies an operational relationship implied in the first approach and prompted by the observation that there are no "radiation diseases." The objective here is to discover the operator  $O(N)$  which changes the natural rate of incidence to that which occurs as a result of radiation ( $N$ ). A joint program with the Biology Division is under way in which an attempt is being made to find the operator  $O(N)$  for the case of mouse cataract incidence.

### 10. HPRR Accelerator Operations

The HPRR continues to provide a reliable and versatile irradiation facility. During this report period it was operated without fault in support of a dozen different types of experiments for representatives of foreign countries, many colleges and universities, Federal contractors and licensees, and other agencies. In July 1972, the ninth in a series of intercomparisons of nuclear accident dosimeters was conducted. Participants included AEC contractors and companies holding licenses for handling large quantities of fissile material.

In support of the program in nuclear safety, an extensive calculation of the HPRR's neutron energy spectra under three different conditions was made. A comparison of these calculations with previous measurements has been completed. The close agreement promotes a feeling of confidence in the calculations. The 3-MV Van de Graaff was operated throughout this report period in support of the energy pathways studies. Dosimetry studies and the determination of detector responses were performed using the DOSAR Low-Energy Accelerator.

### 11. Spectrometry Research and Development

New applications of previously developed techniques highlighted the work in spectrometry research. For example, the capabilities developed for the zone refining of organic scintillators were applied to other organic compounds being studied by mass spectroscopy in the Radiation Physics Section. Instrument development produced a stable source of light pulses for use as a standard in the organic scintillator studies and a paper-tape-to-typewriter translator that rejects non-significant zeros to aid in the clarity of a digital readout. Two different fast-neutron detectors with high sensitivity were developed. The first was for use with the Aerial Radiological Measuring Surveys system operated for the Atomic Energy Commission by the Las Vegas Division of EG&G, Inc. The second was a fast-neutron spectrometer for measuring neutrons with

energies above 200 keV as a function of incident angle on the roof of the DOSAR Control Building during HPRR operations. These data are part of a program to evaluate the doses received by survivors in heavy-shielding buildings at Hiroshima and Nagasaki. An increasing commitment to studying radiation in the environment was expressed by the development of a computer program to calculate possible isotope concentrations produced in the environment by the operation of a power reactor. High-resolution gamma-ray and alpha-particle spectrometers were obtained and put into use for measuring natural radioactivity, particularly in situations where it is higher than average. A new program was begun to measure the distribution of stopping of low-energy protons in tissue-constituent elements, data that are of general value for dosimetry calculations.

## PART III. INTERNAL DOSIMETRY

### (Chapters 12--16)

Estimation of absorbed fractions of photon energy per gram of target organ is of great importance, since dose is proportional to this quantity and for many organs of the body, particularly the gonads, the direct Monte Carlo calculation is inaccurate. The accuracy of the estimates obtained in the report "Estimates of Absorbed Fractions for Photon Emitters within the Body" are generally well within the range expected of most dose estimates, particularly when the organ involved receives only a small fraction of the dose to the critical organ or tissue. It is hoped that this method of using the buildup factor in obtaining estimates of dose will come into general use.

The second report on "Estimates of Dose to Infants and Children from a Photon Emitted in the Lungs" is likewise an extension of previous work. It appears that the dose to the child per photon is frequently higher than for an adult, the difference being one to two orders of magnitude. The extension of these results to other source organs poses problems of great interest for clinical use of nuclear energy as well as for estimates of dose due to exposure of the population.

The study of the metabolism of magnesium and its dosimetry is one example among many of the models constructed for estimation of dose needed for the revision of ICRP Publication 2. It will be circulated for review by the ICRP.

The remaining reports on blood volume in lungs and on excretion of plutonium are examples of the continuing need for metabolic data on the behavior of radionuclides in the body and of their importance for estimation of dose.

## PART IV. ENVIRONMENTAL STUDIES

### 17. Dose Estimation Studies Related to Peaceful Uses of Nuclear Explosives and Other Radionuclide Releases

Research continued on development of the CUEx methodology for assessing radiation exposures of human populations via all important exposure pathways for environmental releases of radioactivity. Methods developed under this activity were used to complete radiological sections of environmental impact statements (utility-owned nuclear power stations) prepared at ORNL for the AEC to meet the requirements of the National Environmental Policy Act of 1969. Dose estimates were made for all significant exposure pathways following a careful study of the nuclear power station and its environment. Radiation doses, both to individuals and to total population within 50 miles of the station, were estimated. Comparisons were made of the estimated doses with the appropriate radiation safety guides and the doses due to natural background radiation.

The radioactivity release experience of light-water power reactors was analyzed in a number of ways to identify critical aquatic exposure pathways and critical radionuclides. This work was a supporting effort to the above-mentioned application of CUEx methodology. The radionuclides given consideration in the analysis were those which satisfied several criteria thought to be indicative of possible environmental impact. The work provided a standard list of radionuclides which should be considered in estimating the environmental impact of radioactivity released in the liquid effluent of current light-water power reactors.

Work on dose estimations related to the Gasbuggy project, the first experiment performed to demonstrate the feasibility of using nuclear explosives to increase production of natural gas, was completed with the preparation of three topical reports. Tritium behavior in a natural gas processing plant was studied as a part of the evaluation of consumer products from Project Gasbuggy. Data obtained during the study experiment indicate that the projected whole-body doses to plant workers, attributable to tritium releases during processing of nuclearly stimulated gas, would be less than 1% of the dose from natural background radiation. The observed distribution of tritium among plant products confirmed theoretical calculations, lending confidence in our ability to predict the quantities of radioactivity in gas and liquid products leaving a plant that processes gas from nuclearly stimulated wells.

The first phase of Rulison (the second experiment performed to demonstrate the feasibility of using nuclear explosives to increase production of natural gas) dose estimations considered the radiological impact of hypothetical introduction of gas from the Rulison well into the distribution systems of two small gas transmission systems located near the well site. Inhalation and skin absorption of tritium dispersed in the atmosphere gave doses less than 1 millirem per year, but home exposure to unvented combustion products from kitchen ranges, the critical exposure pathway, could have given a dose of 3.0 millirems per year in one system and up to 20 millirems per year in the system that provided very little dilution of the Rulison gas. Computer programs were developed to aid estimation and control of doses from natural gas produced in a nuclearly stimulated well field.



# Part I. Radiation Physics

R. D. Birkhoff      R. H. Ritchie

## 1. Theoretical Radiation Physics

R. H. Ritchie

G. D. Alton <sup>1</sup>	W. R. Garrett
V. E. Anderson <sup>2</sup>	R. N. Hamm
J. C. Ashley	J. Neufeld <sup>4</sup>
W. Brandt <sup>3</sup>	H. C. Schweinler
J. Crowell <sup>4</sup>	S. Y. Shieh <sup>4</sup>
J. Dutrannois <sup>5</sup>	J. E. Turner
J. M. Elson <sup>1</sup>	R. B. Vora <sup>1</sup>

H. A. Wright

### PION BEAM DOSIMETRY

Some modifications were made in the program for computing pion-beam depth-dose curves in water. The changes allow for charge exchange and for possible future extension of the code above its present energy limit of 125 MeV. A description of the code and experimental physical data programmed into it is in press.<sup>6</sup> Good agreement is obtained between pion-beam depth-dose curves calculated with the program and curves measured at the European Organization for Nuclear Research (CERN). Our collaboration with the CERN Health Physics Group is continuing. During this year an exchange of one staff member from each group took place.

A theoretical study has been made of the energy deposited in water spheres and cylinders of various sizes

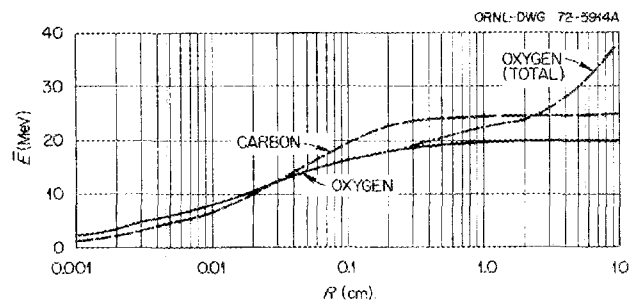


Fig. 1.1. Energy deposition in water spheres by high-LET ( $>170$  MeV/cm in  $H_2O$ ) particles produced from  $\pi^-$  capture by oxygen (solid curve) and carbon (dashed curve). Additional contribution of high-LET recoils from neutrons produced from capture by oxygen is also shown (total).

around the site at which an oxygen or carbon nucleus captures a stopped negative pion.<sup>7</sup> Figure 1.1 shows the mean energy  $\bar{E}$  deposited by high-LET ( $>170$  MeV/cm in water) particles produced directly as a result of capture as a function of the distance  $R$  from the capture site. In the case of pion capture by oxygen the added dose due to neutrons resulting from the capture is also shown. Practically all of this high-LET dose is deposited within a sphere of radius 2 mm.

1. Graduate student.

2. On loan from Mathematics Division, ORNL.

3. New York University.

4. Consultant.

5. CERN, Geneva, Switzerland.

6. J. E. Turner, J. Dutrannois, H. A. Wright, R. N. Hamm, J. Baarli, A. H. Sullivan, M. J. Berger, and S. M. Seltzer, "The Computation of Pion Depth-Dose Curves in Water and Comparison with Experiment," submitted to *Radiation Research*. Calculations of the dose resulting from electrons, which contaminate pion beams, and from subsequent electron-photon cascades were done at the National Bureau of Standards.

7. J. R. Dutrannois, R. N. Hamm, J. E. Turner, and H. A. Wright, "Analysis of Energy Deposition in Water around the Site of Capture of a Negative Pion by an Oxygen or Carbon Nucleus," submitted to *Physics in Medicine and Biology*.

## STATUS OF THE THEORY OF DELTA-RAY PRODUCTION

The characterization of secondary electrons underlies a basic physical understanding of the action of radiation on matter. A review has been made of methods for calculating the spectra of delta rays produced by heavy ions and electrons, with a view toward their incorporation into microdosimetry theory. The broad shapes of secondary electron spectra in materials of low atomic number can be predicted by using a simple binary-encounter theory, suitably scaled. The energy spectra of ejected electrons, integrated over all angles, are reproduced rather well both by the binary encounters and by use of the Born approximation. Figure 1.2 shows calculated and measured (circles) spectra from the impact of 100-keV protons on helium. A report of this review was presented at the Third Symposium on Microdosimetry.<sup>8</sup>

8. James E. Turner and Cornelius E. Klots, "Status of the Theory of Delta-Ray Production," pp. 31-65 in *Proceedings of the Third Symposium on Microdosimetry*, Stresa, Italy, October 18-22, 1971 (Euratom).

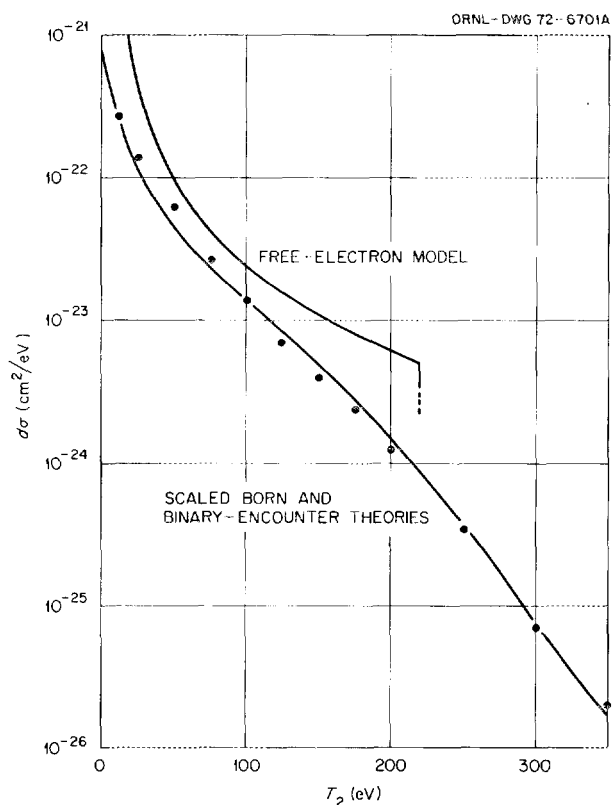


Fig. 1.2. Secondary-electron energy ( $T_2$ ) spectrum from impact of 100-keV protons on helium. Circles show experimental data of Crooks and Rudd, *Phys. Rev. A3*, 1628 (1971).

## ELECTRON-SLOWING-DOWN SPECTRA IN SEMICONDUCTORS

A theoretical program paralleling that in the Physics of Tissue Damage Group has been established to study the spectrum of slowing-down electrons in semiconductors containing beta-emitting nuclides. Progress in this effort requires detailed estimates of differential inelastic cross sections for excitation of valence-to-higher-band transitions and for transitions from inner levels by incident electrons having energies ranging from a few eV to  $\sim 10^6$  eV.

Spencer and Fano and Spencer and Attix have given theoretical treatments of electron-slowing-down spectra at energies high enough that detailed electronic structure of the material is not important. Calculations at energies comparable with transition energies from inner levels require not only detailed cross sections which account for binding effects but also require a different approach to the solution of the Boltzmann equation. The Spencer-Fano method is predicated upon the approximate validity of the continuous-slowing-down approximation; this approximation is suspect in this range of energies where the probability of large fractional energy losses in a single interaction becomes appreciable.

The work reported here has involved the use of (1) the Callaway-Tosatti model of a semiconductor to generate cross sections for excitation from the valence band, (2) classical cross sections for excitations from inner levels, and (3) the Kane cross sections for electron interaction with the phonon field. We thereby include the effects of plasmon creation and electron-hole production in the valence band and the excitation of electrons from inner levels. We have decided to use classical binary collision cross sections to represent excitations from all inner levels in the case of metals and semiconductors. Our reasons for using the classical model are (1) the quite reliable results which one obtains for the few cases in which experimental or Born approximation cross sections are available, (2) the convenient scaling properties possessed by cross sections which emerge from the model, (3) the relatively simple analytical forms possessed by such cross sections, and (4) the ease with which one may constrain these cross sections so that sum rules and high-energy stopping-power requirements are satisfied.

These cross sections have been prepared in a form suitable for use in a Monte Carlo code which was designed and written by us for another application. This code has been used to compute slowing-down spectra in neutron-activated silicon. Figure 1.3 shows the resulting fluxes presented in histogram form in the energy range

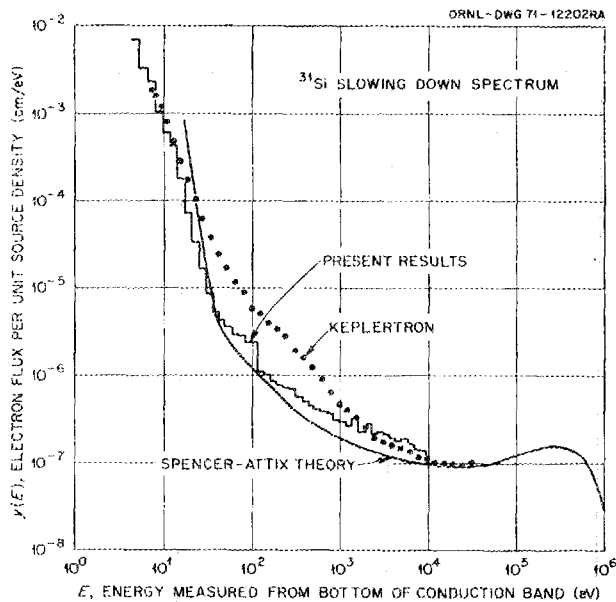


Fig. 1.3. Electron-slowing-down spectrum in silicon. The points represent experimental data corrected to the interior of the sample. The smooth curve shows the results of calculations using the Spencer-Attix theory. The histogram gives results using a Monte Carlo approach.

from 10 to  $10^6$  eV. The flux spectrum obtained experimentally is shown as the solid points, while results of a calculation using the Spencer-Attix method are shown as a solid line. Reasons for the discrepancy between theory and experiment are being sought.

#### INNER-SHELL EXCITATION OF ATOMS BY SLOW HEAVY CHARGED PARTICLES

Much effort has gone into the study of x-ray generation due to the filling of inner-shell vacancies in atomic systems. Theoretical cross sections for production of such vacancies by heavy charged particles have been much studied in the Born approximation, usually employing Coulombic wave functions to describe initial and final states. It is of interest to investigate theoretically cross sections for production of inner-shell vacancies by particles having velocities low compared with those of electrons in the shell considered. Considerable data have been accumulated in this regime.

We have obtained interesting new formulas for  $K$ -shell excitation using the perturbed stationary state formalism of Mott.<sup>9</sup> His approach yields an exact expression for the probability amplitude that the  $n$ th ionized or excited state in an atomic system is reached in an  $s$ -

to  $s$ -wave transition when a slowly moving charged particle is incident on the system with impact parameter  $b$  relative to the nucleus. This expression is exact for limiting small velocity. For a charged particle with velocity  $v$  and charge  $Z_1 e$ , incident with straight-line trajectory along the  $Z$  axis, the probability amplitude for excitation of the  $n$ th excited state is

$$a_n = (fv_1)^{-1} \int_{-\infty}^{\infty} dZ \frac{e^{ik_{0n}Z}}{k_{0n}} \times \int d^3r \psi^*(\mathbf{r}, \mathbf{R}) \frac{\partial}{\partial Z} \left( \frac{Z_1 e^2}{|\mathbf{r} - \mathbf{R}|} \right) \psi_0(\mathbf{r}, \mathbf{R}) \quad (1)$$

if the atomic system is initially in the state 0. This expression is appropriate to a one-electron atom but may be generalized immediately to apply to a many-electron atom. The basis set  $\psi_n(\mathbf{r}, \mathbf{R})$  consists of the exact, orthonormal solutions of Schroedinger's equation for the electron in the Coulomb field of the two nuclei when held stationary at a distance  $|\mathbf{R}|$  apart.  $Z$  is the  $z$  coordinate of the incident charge if the atom is situated at the origin and if  $\mathbf{v}_1$  is parallel with the  $z$  axis. The wave number  $k_{0n} = (W_0 - W_n)/fv_1$  and  $W_m(\mathbf{R})$  is the energy of the electron in the  $m$ th excited state at separation  $|\mathbf{R}|$ . This rather complicated expression may be simplified greatly using the following trick.

If the term  $|\mathbf{r} - \mathbf{R}|$  is expressed as a Fourier integral, Eq. (1) may be written

$$a_n = C \int d^3q \frac{e^{i\mathbf{q} \cdot \mathbf{R}}}{q^2} \int_{-\infty}^{\infty} dZ \left( \frac{q_z}{k_{0n}} \right) \times e^{ik_{0n}Z} G_n(\mathbf{q}, \mathbf{R}), \quad (2)$$

where

$$C = \frac{Z_1 e^2}{2i\pi^2 fv}$$

and

$$G_n(\mathbf{q}, \mathbf{R}) = (e^{i\mathbf{q} \cdot \mathbf{r}})_{n0}$$

Making the change of variable

$$q_z - k_{0n}(\mathbf{R}) = Q,$$

this expression becomes

$$a_n = C \int d^2q_1 e^{i\mathbf{q}_1 \cdot \mathbf{R}_1} \times \int_{-\infty}^{\infty} dQ \int_{-\infty}^{\infty} dZ e^{iZQ} F_{q_1, \mathbf{R}_1},$$

9. N. F. Mott, *Proc. Cambridge Phil. Soc.* 27, 553 (1931).

where

$$F_{\mathbf{q}_\perp, \mathbf{R}_\perp}(Q, Z) = \frac{(Q + k_{0n})}{k_{0n} [p_\perp^2 + (Q + k_{0n})^2]} \times \left[ e^{i\mathbf{q}_\perp \cdot \mathbf{r}_\perp} e^{i(Q + k_{0n})z} \right]_{n0} \quad (4)$$

and the vectors  $\mathbf{q}$ ,  $\mathbf{R}$ , and  $\mathbf{r}$  have been resolved into components perpendicular ( $\perp$ ) and parallel with the  $z$  axis.

If  $F$  is expanded in a Taylor series in the variable  $Q$  and if the resulting terms are integrated by parts in the variable  $Z$ , it is found that

$$a_n = 2\pi C \int d\mathbf{q}_\perp e^{-i\mathbf{q}_\perp \cdot \mathbf{R}_\perp} \left\{ F(0, 0) + \frac{1}{2!} \frac{\partial^4}{2Q^2 \partial Z^2} F + \dots \right\}.$$

Designating the  $j$ th term in this series by  $a_n^{(j)}$ , it may be shown that

$$a_n^{(1)} = 2\pi^2 C \int d^3r \psi_n^*(\mathbf{r}, \mathbf{R}_\perp, 0) K_0 \times [k_{0n}(R)|\mathbf{r}_\perp - \mathbf{R}_\perp|] e^{ik_{0n}z} \psi_0(\mathbf{r}, \mathbf{R}_\perp, 0), \quad (5)$$

where  $k_0(x)$  is the zero-order modified Bessel function of the second kind and  $\psi_m^*(\mathbf{r}, \mathbf{R}_\perp, 0)$  designates the electron eigenfunction evaluated at the position of closest approach of the incident charge. The remaining terms in this series may be shown to be negligible by comparison with  $a_n^{(1)}$  in the case of small  $v_1$ . The expression for  $a_n^{(1)}$  above is comparable in form to the Born approximation-theoretic result of Bang and Hansteen.<sup>10</sup> However, the interpretation of the various quantities in Eq. (5) is quite different. Bang and Hansteen work in the large  $v_1$  regime; the eigenfunctions which they employ correspond to those of the unperturbed atom, while the eigenfunctions appearing in Eq. (5) are perturbed strongly by the incident particle. The wave number  $k_{0n}$  is different from the corresponding wave number of Bang and Hansteen and is evaluated at the distance of closest approach.

Equation (5) yields a cross section for ionization which is quite similar to one which has been obtained by a plausible but empirical procedure applied to the Bang-Hansteen high-velocity formulas. This procedure consists of shifting the binding energy of the ground state by a stationary state perturbation energy corresponding to the distance of closest approach of the perturbing particle.

10. J. Bang and J. M. Hansteen, *Kgl. Dan. Vidensk. Selsk., Mat.-Fys. Medd.* **31**(13), 1 (1959).

This recipe has yielded theoretical cross sections in good agreement with experiment in the small  $v_1$  regime. Equation (5) puts this procedure on a sound theoretical basis and may lead to improvements, for example, through the use of variationally determined  $W_m(\mathbf{R})$  and  $\psi_m(\mathbf{r}, \mathbf{R})$  in establishing cross sections.

This work was done in collaboration with Prof. Werner Brandt of New York University.

## LOW-ENERGY ELECTRON SCATTERING BY POLAR MOLECULES

An extensive theoretical study of low-energy electron scattering by dipolar target systems has been concluded. This was the culmination of a long-range program to obtain detailed theoretical knowledge of the effects of dipolar forces on charged-particle scattering phenomena. The present study is complementary to earlier theoretical investigations<sup>1-13</sup> of the critical binding properties of dipolar fields and to experimental investigations<sup>14-17</sup> of momentum transfer cross sections for thermal electrons in polar gases.

We limit our considerations to the energy range in which the relevant experimental data are available, and in this region ( $\sim 0.03$  eV) rotational excitations are the only open inelastic channels. If we designate the projectile coordinate by  $\mathbf{r}$  measured from the center of mass, then the Schroedinger equation can be written as

$$[H_{\text{rot}} - \nabla_{\mathbf{r}}^2 + V(\mathbf{r}, \hat{\mathbf{s}})] \psi(\mathbf{r}, \hat{\mathbf{s}}) = E\psi(\mathbf{r}, \hat{\mathbf{s}}), \quad (6)$$

where  $H_{\text{rot}}$  is the rotational Hamiltonian of the target system and  $V(\mathbf{r}, \mathbf{s})$  is the total electron-molecule interaction potential. The orientation of the molecule is designated by  $\hat{\mathbf{s}}$ , and the target rotational eigenfunctions are the spherical harmonics  $Y_j^m(\hat{\mathbf{s}})$ . We have chosen Rydberg atomic units, where  $\hbar = 1$ ,  $m_e = 1/2$ ,  $e^2 = 2$ . The units of energy and distance are 13.6 eV and the Bohr radius  $a_0$ , respectively.

If the orbital angular momentum of the incident electron is designated by the quantum number  $l$  with projection  $m_l$  and the total angular momentum  $J$  is

11. J. E. Turner and K. Fox, *Phys. Lett.* **23**, 547 (1966).
12. W. R. Garrett, *Chem. Phys. Lett.* **5**, 393 (1970).
13. W. R. Garrett, *Phys. Rev. A* **3**, 961 (1971).
14. L. G. Christophorou, G. S. Hurst, and W. G. Hendrick, *J. Chem. Phys.* **45**, 1081 (1966).
15. J. A. D. Stockdale, L. G. Christophorou, J. E. Turner, and V. E. Anderson, *Phys. Lett.* **25A**, 510 (1967).
16. L. G. Christophorou and A. A. Christodoulides, *J. Phys. B (At. Mol. Phys.)* **2**, 71 (1969).
17. L. G. Christophorou and D. Pittman, *J. Phys. B (At. Mol. Phys.)* **3**, 1252 (1970).

formed from  $\mathbf{J} = \mathbf{j} + \mathbf{l}$ , then the usual coupled spherical harmonics  $\psi_{j'l}^{JM}(\hat{\mathbf{r}}, \hat{\mathbf{s}})$  are eigenfunctions of  $J^2$  and  $J_z$ . The total wave function  $\Psi_{j'l}^{JM}$  for the system having total angular momentum  $J$  can be written in terms of these functions through an expansion of the form

$$\Psi_{j'l}^{JM}(\mathbf{r}, \hat{\mathbf{s}}) = \sum_{j'} \sum_{l'} \psi_{j'l}^{JM}(\hat{\mathbf{r}}, \hat{\mathbf{s}}) U_{j'l}^{Jl}(r)/r. \quad (7)$$

Through use of expression (7), Eq. 6) is converted into a set of coupled radial equations for the functions  $U_{j'l}^{Jl}(r)$ :

$$\left[ -\frac{d^2}{dr^2} + \frac{l'(l'+1)}{r^2} - k_{j'l}^2 \right] U_{j'l}^{Jl}(r) + \sum_{j''} \sum_{l''} \langle j'' l''; J | V | j' l'; J \rangle U_{j'' l''}^{Jl}(r) = 0, \quad (8)$$

where  $k_{j'l}$  is the wave vector for the scattered electrons.

Solutions of Eq. (8) yield the scattering matrix  $\mathbf{S}$  through the asymptotic relation

$$U_{j'l}^{Jl}(r) \sim \delta_{j'l} \delta_{l'l} \exp[-i(k_{j'l}r - l\pi/2)] - \left( \frac{k_{j'l}}{k_{j'l'}} \right)^{1/2} S^J(j'l; j'l') \exp[i(k_{j'l}r - l'\pi/2)]. \quad (9)$$

Numerical solutions to Eq. (8) have been determined for a large number of dipolar systems, some of which we describe below. The  $\mathbf{S}$  matrix was obtained from these solutions, and both momentum transfer and total scattering cross sections were obtained by carrying out the proper sums over elements of the scattering matrix.

One of the primary objectives of this investigation was to determine whether the critical binding properties of the pure dipole field are reflected in the theoretical behavior of momentum transfer cross sections for polar molecules. For this purpose a model electron-molecule interaction potential was adopted which would allow an investigation of the individual and collective effects of separate terms in this interaction potential on the resultant cross sections. For this purpose we have adopted a model electron-molecule interaction potential of the form

$$V(\mathbf{r}, \hat{\mathbf{s}}) = -\frac{Ze^{-\beta r}}{r} - \frac{2De}{r^2} C(r) P_1(\hat{\mathbf{s}} \cdot \hat{\mathbf{r}}) - C(r) \times \left[ \frac{1}{3} \frac{(\alpha_{\parallel} + 2\alpha_{\perp})}{r^4} - \frac{2}{3} \frac{(\alpha_{\parallel} - \alpha_{\perp})}{r^4} P_2(\hat{\mathbf{s}} \cdot \hat{\mathbf{r}}) \right], \quad (10)$$

where  $C(r) = 1 - e^{-r^6}$  is a cutoff function which removes the strong singularity at  $r = 0$ . In this molecular

model,  $Z$  is an effective nuclear charge for the monopole term, and  $\beta$  is an effective screening parameter for the Coulomb field. The terms in brackets represent an induced dipole interaction where  $\alpha_{\parallel}$  and  $\alpha_{\perp}$  are the parallel and perpendicular polarizabilities of a linear target system. The term containing  $D$  is the dipole potential due to the permanent dipole moment  $D$  of the target molecule. With this function one can very conveniently study the effects of individual components of the interaction potential on the resulting scattering cross sections.

Some of the results of this systematic study are shown in the five curves of Fig. 1.4. The figure shows a bewildering amount of data and is somewhat hard to read, but an important conclusion can best be reached from this composite display of the results.

First, note that in Fig. 1.4 the pure dipolar case is labeled  $\alpha_{\parallel} = 0, Z = 0.0$ . ( $\alpha_{\perp}$  is always chosen to be  $\alpha_{\parallel}/2$ , thus it is not necessary to list both.) When a small polarizability term,  $\alpha_{\parallel} = 2.0\alpha_0^3$ , is added, the result labeled  $\alpha_{\parallel} = 2.0, Z = 0.0$  is obtained. Here the maxima and minima in the elastic cross section  $\sigma(0, 0)$  occur at lower values of  $D$ . This is to be expected, since the strength of the interaction is increased by the presence of an induced dipole term. However, not so readily anticipated is the magnitude of the shift. This result indicates that even a small induced dipole term has a significant effect on the elastic cross section.

The effect of a monopole term is shown in the curve labeled  $Z = 6.0, \alpha_{\parallel} = 0$ . The first maximum in  $\sigma(0, 0)$  is

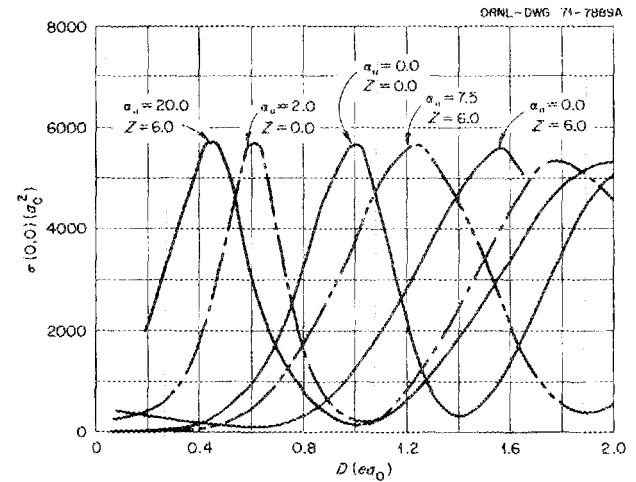


Fig. 1.4.  $J = 0$  component of the elastic cross sections as a function of dipole moment for 0.03-eV electrons on a linear polar molecule. Data are for five different choices of effective charge  $Z$  and polarizabilities  $\alpha_{\parallel}$  and  $\alpha_{\perp}$ .  $\alpha_{\perp} = \alpha_{\parallel}/2$  in every case; thus only  $\alpha_{\parallel}$  is listed.

shifted all the way down to  $D = 0$ , and the second maximum now appears at  $D \approx 1.5ea_0$ . If, in addition, an induced dipole term of magnitude  $\alpha_{\parallel} = 7.5a_0^3$  is added in with the monopole term, the curve labeled  $\alpha_{\parallel} = 7.5$ ,  $Z = 6.0$  is obtained. Here the first maximum has shifted below  $D = 0.0$ , and the second maximum now occurs at  $D \approx 1.2ea_0$ . Finally, if the strength of the polarizability term is increased to  $20a_0^3$ , the result is that shown by the fifth curve, labeled  $\alpha_{\parallel} = 20.0$ ,  $Z = 6.0$ . Here the second maximum has shifted down to  $D = 0.4ea_0$ , and a third maximum has appeared at  $D \approx 1.8ea_0$ .

From these and other results<sup>18</sup> we can make at least three general comments concerning momentum transfer cross sections for thermal energy electrons on polar molecules. (1) In the context of electron-molecule interactions there is little significance to the critical binding property of the pure dipolar field.<sup>19</sup> (2) The Born approximation forms a very inadequate description of the total momentum transfer cross section for polar molecules over the entire range of dipole magnitude, and it adequately describes the  $0 \rightarrow 1$  rotational excitation channel only in the case of very small  $D$ .<sup>18</sup> (3) If the Born result for a pure dipole rotator is used as a basis for comparing thermal energy values of  $\sigma_m$  for real molecules,<sup>14-17</sup> the present results would indicate that observed values should be greater than  $\sigma_m^B$  for molecules whose dipole moments range from 0 to  $\sim 0.6ea_0$  and tend toward values smaller than the Born result for molecules of large  $D$  ( $D \geq 1.2ea_0$ ), with a possible fluctuation as large as  $\pi/k^2$  in the observed values for different molecules possessing any particular value of  $D$ . These points are well illustrated by the results shown in Fig. 1.5. Here the total momentum transfer cross sections for 0.03-eV electrons on a model system having a screened Coulomb field represented by  $Z = 6.0$ ,  $\beta = 1.7a_0^{-1}$  and with three different values for the polarizabilities  $\alpha_{\parallel} = 0.0$ ,  $10.0a_0^3$ , and  $20.0a_0^3$  are shown. The cross section for a pure dipole target ( $Z = 0$ ,  $\alpha_{\parallel} = 0$ ) and the Born cross section for a pure dipole are also shown for reference.

Finally, we consider the question of whether the conclusions reached in the present study are consistent with experimental data or, to the contrary, whether the data support earlier claims<sup>15-17,20,21</sup> as to a demon-

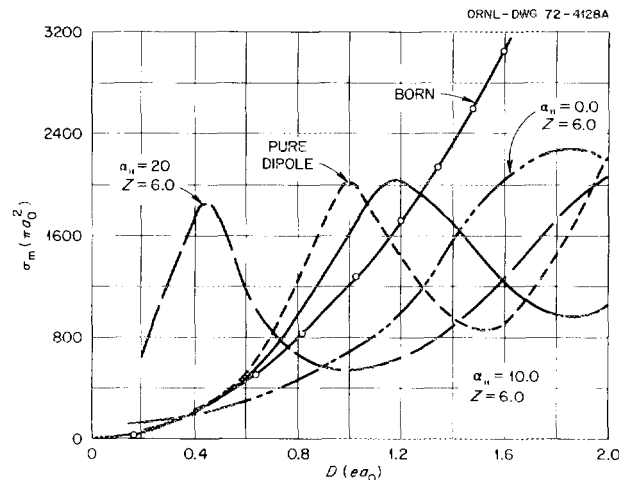


Fig. 1.5. Total momentum transfer cross sections as a function of dipole moment  $D$  for 0.03-eV electrons on a model polar molecular system. Values obtained for a pure dipole rotator in the present calculation and in the Born approximation are also shown. Moment of inertia  $I = 5.8 \times 10^4 ma_0^2$ .

strable effect of the critical binding property of dipolar fields on electron scattering by polar molecules. When all the recent data are accumulated and displayed in toto, the result is as shown in Fig. 1.6. There is a greater density of data for molecules whose dipole moments lie between 1.5 and 2.1 esu-cm and a peculiar scarcity of data for those whose dipole moments lie between  $\sim 2.1$  and 2.7 esu-cm. This nonuniformity in the distribution in  $D$  of molecules studied experimentally was probably brought about by great interest in molecules with  $D \sim 1.625$  esu-cm, which is the critical moment for electron binding to a stationary dipole. However, there appears to be no particular region in the range of  $D$  covered by these experiments where the cross section displays anomalous behavior which could be associated with binding properties of the dipolar field.

The thermally averaged momentum transfer cross section obtained from the Born approximation for a point dipole is plotted as the solid line in Fig. 1.6. We note that the general trend in the data is similar to that obtained in the present analysis; that is, the values of  $\langle \sigma_m \rangle$  tend to be significantly greater than  $\langle \sigma_m^B \rangle$  for low  $D$  and to fall below the Born result for very high  $D$ . This behavior is very clearly indicated in the most recent data for strongly polar molecules.<sup>16</sup>

18. W. R. Garrett, accepted for publication in *Molecular Physics*.

19. The importance of critical binding is reduced to the very weak assertion that the possibility of a stable negative ion is assured if  $D > D_{\text{critical}}$  for a particular molecular system. See W. R. Garrett, *Phys. Rev.* **A3**, 961 (1961).

20. K. Takayangi and Y. Itikawa, *J. Phys. Soc. Jap.* **24**, 160 (1968).

21. J. M. Levy-Leblond and J. M. Provost, *Phys. Lett.* **26B**, 104 (1967).

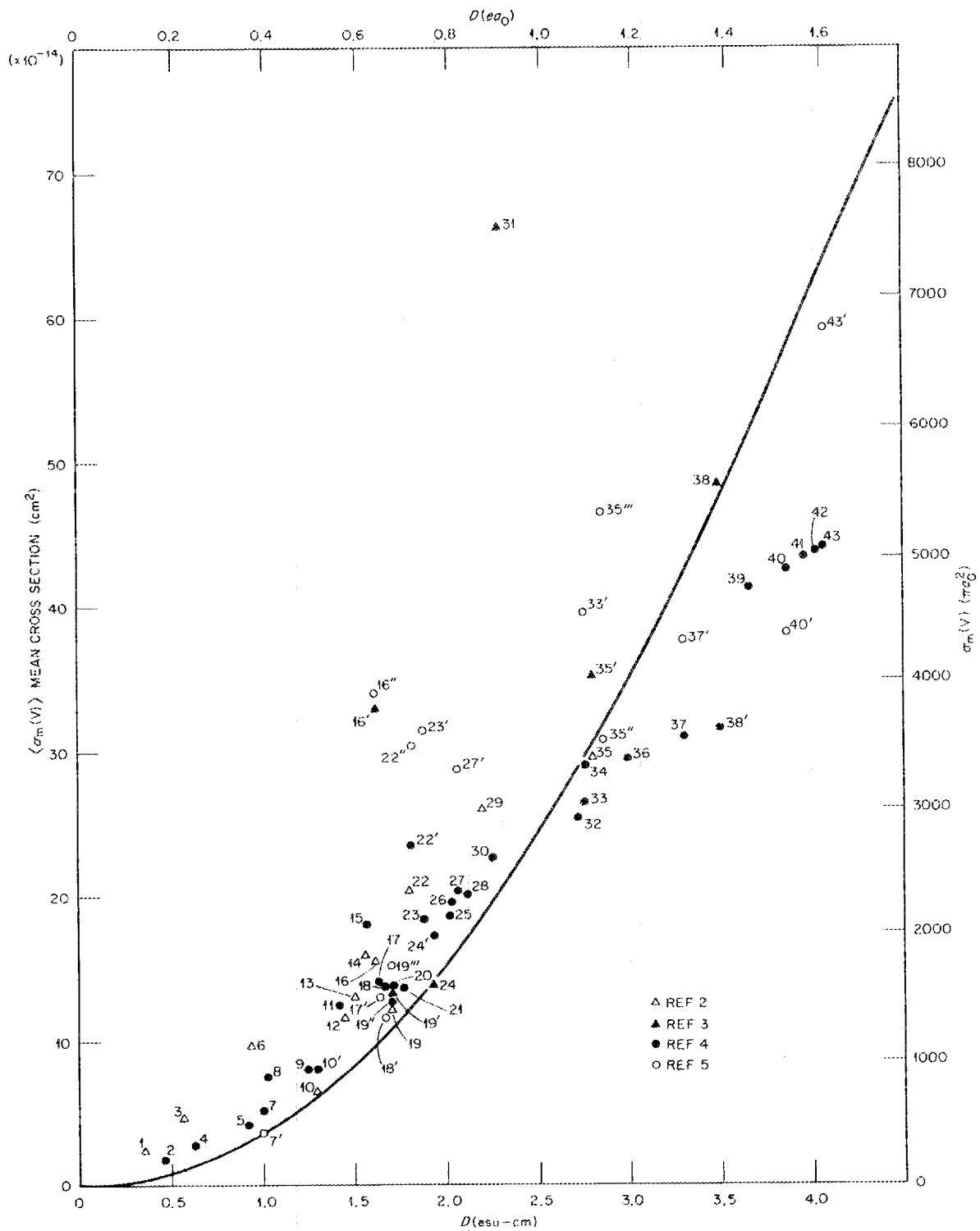


Fig. 1.6. Compilation of thermal energy ( $300^\circ\text{K}$ ) momentum transfer cross sections as derived from electron swarm experiments. The data listed consist of that published since the compilation of ref. 11 and are labeled according to the numbers given in ref. 18. The solid line represents the Born results for a pure dipole rotator.

### UTILIZATION OF COMPLEX POTENTIAL OPERATOR FORMALISM IN ELECTRON SCATTERING PROBLEMS

The theoretical determination of scattering cross sections for all atomic and molecular species is extremely complicated in the energy region above the ionization potential due to the presence of a large (usually infinite) number of open scattering channels. Thus, in order to obtain an accurate description of scattering phenomena for charged particles of modest energy (below the region where the simple Born approximation may be utilized), one must include effects due to various inelastic processes which may occur. In the usual practice of expanding the total wave functions in terms of a set of target eigenfunctions, one is led to an infinite set of coupled differential equations which describe the scattering probabilities for elastic and inelastic processes. The difficulties associated with such large coupled sets of equations preclude accurate solutions for all but a very limited range of projectile energies.

Feshbach<sup>22</sup> has developed a very elegant and very powerful technique for determining elastic and total scattering cross sections under multichannel scattering conditions. In his projection operator approach the elastic channel is projected out of the total Schrodinger equation, and all other channels are included in a complex nonlocal "optical potential" operator. The difficulties associated with a large set of coupled equations are transformed into a new set of complexities associated with the optical potential. However, the formalism is amenable to a number of different approximations which offer some distinct advantages over other methods of calculating cross sections in a difficult energy region.

We have utilized Feshbach's technique in an application to atomic scattering of electrons above the ionization potential of the target. In our analysis we define a projection operator  $P$  which selects the elastic channel from the total wave function. The remaining part of the wave function, which contains the description of all inelastic processes, is given by operation with a projection operator  $Q$  which is the complement of  $P$ . That is,  $Q = 1 - P$ .

The Schrodinger equation for the interacting system is expressed as

$$(E - H)\psi = 0, \quad (11)$$

where  $H$  and  $E$  are the total Hamiltonian and energy, respectively, for the system. By using the idempotent properties of the  $P$  and  $Q$  projection operators we can transform Eq. (11) into the following two coupled equations:

$$(E - PHP)P\psi = (PHQ)Q\psi \quad (12)$$

and

$$(E - QHQ)Q\psi = (QHP)P\psi. \quad (13)$$

Formally, we may solve for  $Q\psi$  in Eq. (13)

$$Q\psi = (E^+ - QHQ)^{-1} QHP\psi \quad (14)$$

and substitute this expression for  $Q\psi$  in Eq. (12). This gives the Feshbach equation

$$[PHP + PHQ(E^+ - QHQ)^{-1} QHP - E]P\psi = 0. \quad (15)$$

This is an integro-differential equation for the elastic scattering component  $P\psi$  of the total wave function  $\psi$  for the systems. The term  $PHQ(E^+ - QHQ)^{-1} QHP$  is referred to as the "optical potential" though it is in general a nonlocal operator with both real and complex parts. In the Green's function  $(E^+ - QHQ)^{-1}$  the term  $E^+ = E + i\eta$ , where  $\eta$  is a positive infinitesimal to ensure outgoing wave boundary conditions in the continuum.

Partial wave decomposition of Eq. (15) leads to a set of phase shifts which contain real and imaginary components, from which the elastic and total reaction cross sections may be obtained. However, before this can be accomplished one must be able to evaluate the Green's function.

The Green's function  $G(\mathbf{R}, \mathbf{R}')$  is defined through the inverse operator in Eq. (16)

$$(QHQ - E)G(\mathbf{R}, \mathbf{R}') = \delta(\mathbf{R} - \mathbf{R}'). \quad (16)$$

We have investigated an approximation in which the interaction terms between target and projectile are neglected in evaluating  $G(\mathbf{R}, \mathbf{R}')$  but are included elsewhere in Eq. (15). In order to gain some insight into the practicality of the optical potential for atomic scattering problems, we have applied the formalism to electron scattering by atomic hydrogen. In this case the Green's function may be evaluated analytically, in the approximation just mentioned, and numerical solutions for both the discrete and continuum state contributions to the optical potential may be included in the calculation.

22. H. Feshbach, *Ann. Phys.* 5, 357 (1958).

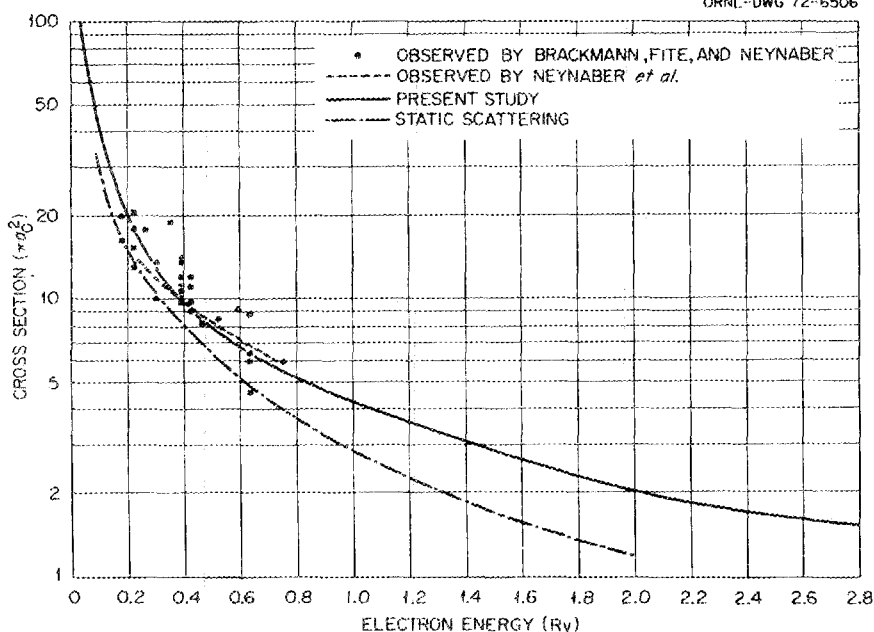


Fig. 1.7. Elastic scattering cross section for electrons on hydrogen. Experimental results are those of Neynaber et al. (ref. 23) and Brackmann et al. (ref. 24).

Very satisfactory results for elastic and total scattering cross sections have been obtained for electrons on hydrogen. These results are shown in Figs. 1.7, 1.8, and 1.9. The experimental data are from Neynaber et al.,<sup>2,3</sup> Brackmann, Fite, and Neynaber,<sup>2,4</sup> and Gilbody et al.<sup>2,5</sup> In the region where experimental data are available, the agreement with experiment is very good.

Investigations are continuing in the use of this very powerful technique for obtaining electron scattering cross sections. Other approximations in the form of the optical potential and application to other atomic and molecular systems are under investigation.

#### INFLUENCE OF PLASMON DAMPING ON THE MEAN FREE PATH FOR PLASMON EXCITATION

The mean free path of an electron in a nearly free electron gas, including the effect of damping of the plasmon states of the system, has been investigated. The results of this calculation indicate an appreciable probability for plasmon excitation by an incident

electron with energy below the threshold predicted by the zero-damping theory.

Many-body theory shows that the plasmon contribution to the self-energy of an electron in an electron gas is given by

$$\Sigma_p^{PL} = \frac{i}{\hbar} \int \frac{d^4 q}{(2\pi)^4} G_{p-q} g_q^2 D_q,$$

where  $q$  is the four vector  $(\mathbf{q}, \omega)$  and  $G_{p-q}$  is the electron Green function.  $D_q$  is the plasmon propagator given by

$$D_q \equiv D_{\mathbf{q}, \omega} = \frac{2\omega_q}{\omega^2 - \omega_q^2 + i\gamma_q},$$

where  $\gamma_q$  is the plasmon damping rate. The quantity  $g_q^2$  is given by

$$g_q^2 \equiv \frac{4\pi e^2}{q^2 (\partial \epsilon_{\mathbf{q}, \omega} / \partial \omega)_{\omega = \omega_q}},$$

where  $\epsilon_{\mathbf{q}, \omega}$  is the dielectric function for the electron gas. The  $\omega_q$ 's are the values of  $\omega$  for which  $\epsilon_{\mathbf{q}, \omega} = 0$ . The inverse mean free path of an electron for plasmon excitation is given by

$$\lambda_p^{-1} = \frac{-2 \text{Im} \Sigma_p^{PL}}{v_0},$$

23. R. Neynaber, L. Marino, E. Rothe, and S. Trujillo, *Phys. Rev.* 124, 135 (1961).

24. R. Brackmann, W. Fite, and R. Neynaber, *Phys. Rev.* 112, 1457 (1958).

25. H. Gilbody, R. Stebbings, and W. Fite, *Phys. Rev.* 121, 794 (1961).

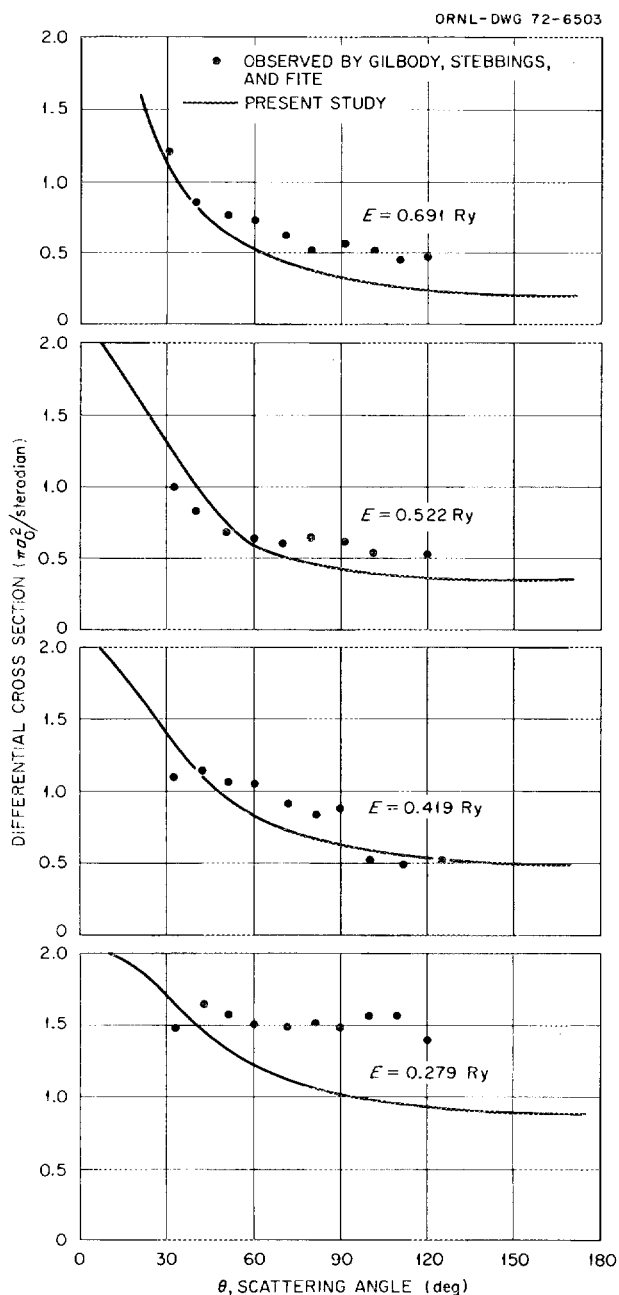


Fig. 1.8. Differential cross section for electrons on hydrogen. Experimental results are from Gilbody and Stebbings (ref. 25).

where  $v_0$  is the speed of the incident electron. For a noninteracting electron gas we find

$$\lambda_p^{-1}(E) = \frac{1}{2\pi^2 \hbar v_0^2} \int_0^{2p} q dq g_q^2 N_q \int_0^{(\hbar/m)(2pq - q^2)} \times d\omega \frac{2\omega_q \lambda_q}{(\omega^2 - \omega_q^2)^2 + \gamma_q^2} \theta(E - E_F - \hbar\omega),$$

where  $p = mv_0$ ,  $E = \frac{1}{2} mv_0^2$ ,  $E_F$  is the Fermi energy of the electron gas, and  $\theta(x) = (0, x < 0; 1, x > 0)$ .  $N_q$  is a "normalization factor" included to ensure that sum-rule requirements are not violated.

This inverse mean free path has been evaluated for an electron gas density corresponding to the conduction band in aluminum. The values for the damping  $\gamma_q$  were taken from the experimental work of Festenberg.<sup>26</sup> These new results are shown in Fig. 1.10. For comparison we show the results calculated using Quinn's formula,<sup>27</sup> in which damping of the plasmon states is not included. The effect of damping is to make plasmon excitation possible for incident particle energies lower than the threshold value predicted by Quinn. This calculation may be important in assessing the energy-loss mechanisms for low-energy charged particles in matter.

### PLASMONS IN SOLIDS

Collective electron effects in solids are increasingly important in the characterization of matter in its condensed state. A review has been made of some of the salient properties of plasmons and their manifestations, for example, in measurements of electron energy loss, optical reflectance, photoemission, low-energy electron diffraction, electron tunneling, etc. Significant progress has been made in the systematic use of the plasmon as a diagnostic tool to study matter in the bulk and at surfaces. This review has been published in the *Proceedings of the NATO Advanced Study Institute, Istanbul, Turkey, August 16--27, 1971*.

### THE DAMPING OF PLASMA WAVES IN CONDENSED MATTER

We have obtained analytical expressions which may be used to relate the damping of long-wavelength plasma waves to experimentally determined values of the complex dielectric permittivity  $\epsilon(\omega) = \epsilon_1(\omega) + i\epsilon_2(\omega)$  of the medium which supports the waves. This permittivity is obtainable from measurements of, for example, the reflectance or absorptance of the medium. Our results are obtained by two methods: (1) from energetic considerations involving the use of an expression first derived by von Laue for the energy stored in a dispersive medium which is weakly absorbing and (2) from manipulation of the basic dispersion relations.

26. C. von Festenberg, *Phys. Lett.* 23, 293 (1966).

27. J. J. Quinn, *Phys. Rev.* 126, 1453 (1962).

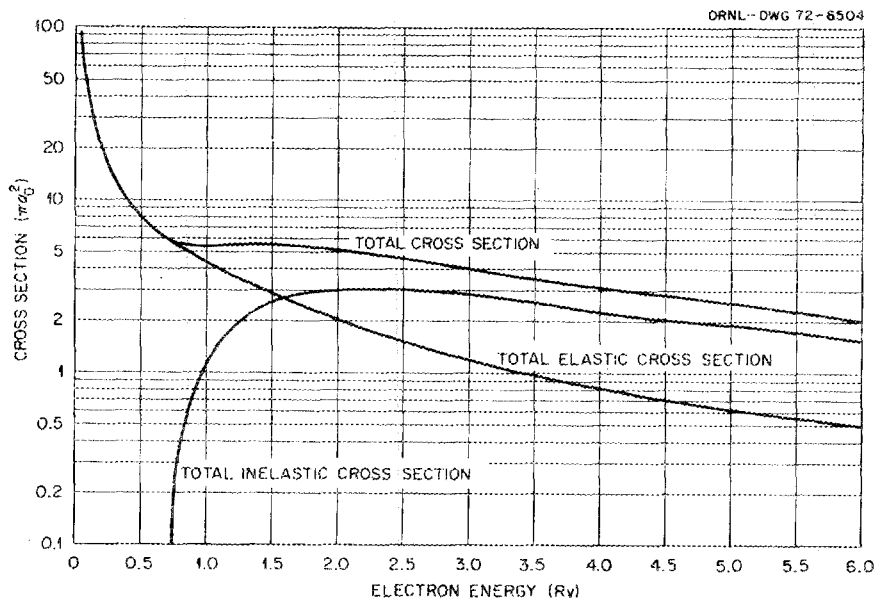


Fig. 1.9. Elastic, inelastic, and total scattering cross sections for electron-hydrogen scattering.

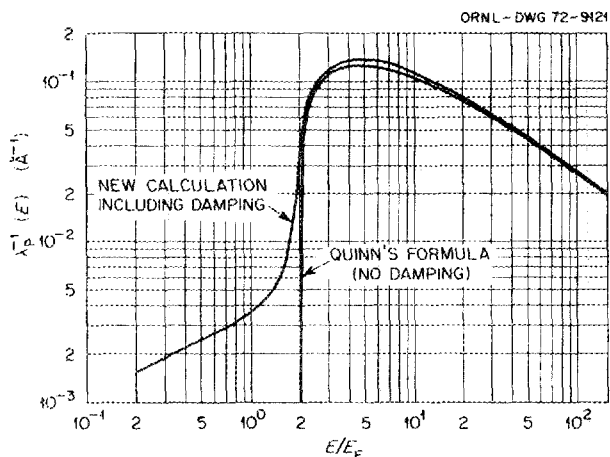


Fig. 1.10. The inverse mean free path measured in  $\text{\AA}^{-1}$  as a function of incident electron energy (in multiples of the Fermi energy) for an electron gas density equal to the conduction band electron density in aluminum.

We find that the damping rate of a volume plasma wave is given by

$$\gamma_{vp}(\omega) = \frac{\omega \epsilon_2(\omega)}{\epsilon_1(\omega) + (\omega/2)(d\epsilon_1/d\omega)},$$

and for a surface plasma wave

$$\gamma_{sp}(\omega) = \frac{\omega \epsilon_2(\omega)}{\epsilon_1(\epsilon_1 + 1) + (\omega/2)(d\epsilon_1/d\omega)}.$$

These expressions are valid when the damping rates given are small compared with the eigenfrequencies of the respective waves. This work has been published in *Surface Science* 30, 178 (1972).

### SURFACE PLASMONS AND THE IMAGE FORCE

It has been shown recently by Van Kampen and co-workers that van der Waals forces between two semi-infinite solids separated by a planar gap may be regarded as arising from interactions between polarization waves on the two surfaces. They applied this idea in a specific calculation of the force in such a system, neglecting retardation effects.

It is an interesting logical extension of this concept to regard the well-known image potential, which exists when a point classical charge is placed at a fixed distance from a solid surface, as having its origin in the interaction between this charge and the surface plasmon field existing in the neighborhood of the interface. Since the image potential is important in a number of physical processes such as the Schottky effect, electron tunneling in metal-insulator-metal (M-I-M) junctions,

and other phenomena in metals, it is important to investigate the consequences of this extension.

We have shown that the classical image potential may be considered to originate in the shifted zero-point energy of the surface plasmon field. The retardation correction to the image potential may be studied conveniently using the electron gas model. We find that the potential becomes appreciably smaller than that

predicted by classical theory at distances from the interface of the order of  $c/\omega_p$ , where  $\omega_p$  is the plasma frequency of the electron gas and  $c$  is the speed of light.

An account of this work has been published in *Physics Letters*.<sup>28</sup>

---

28. R. H. Ritchie, *Phys. Lett.* **28A**, 189 (1972).

## 2. Interaction of Radiation with Liquids and Solids

E. T. Arakawa

R. D. Birkhoff	J. A. Harter
T. A. Callcott <sup>1</sup>	B. L. Sowers <sup>2</sup>
Ada E. Carter	U. S. Whang <sup>2</sup>
J. T. Cox	C. E. Wheeler, Jr. <sup>2</sup>
L. C. Emerson	Mary W. Williams

### OPTICAL PROPERTIES OF K BETWEEN 4 AND 10.7 eV AND COMPARISON WITH Na, Rb, AND Cs

As a continuation of our studies on the alkali metals,<sup>3</sup> the optical and dielectric constants of K have been determined from reflectance and transmission measurements for photons of energy between 4.0 and 10.7 eV. Reflectance measurements were made as a function of incident angle at a K-MgF<sub>2</sub> interface in an ultrahigh vacuum system. The refractive index ( $n$ ) was determined from the critical angle for total internal reflection, and the absorption coefficient ( $k$ ) was determined from the slope of the reflectance curve at the critical angle<sup>4</sup> and from transmission measurements. The values of  $n$  and  $k$  obtained are shown in Fig. 2.1. Figure 2.2 shows a plot of  $\epsilon_1$ , the real part of the dielectric constant, vs the wavelength squared. The solid triangles are points calculated from the smooth curves for  $n$  and  $k$  of Fig. 2.1, using the relation  $\epsilon_1 = n^2 - k^2$ . Except for the open circles the other points plotted are taken from the data of other workers<sup>5-8</sup> as indicated in the

figure caption. Figure 2.3 shows the optical conductivity  $\sigma = \omega\epsilon_2/4\pi$ , where  $\epsilon_2 = 2nk$  is the imaginary part of the dielectric constant. Also shown are optical conductivities obtained previously for other alkali metals. For all four metals the solid lines at high energies have been obtained at ORNL.<sup>3</sup> The dashed curves at low energies are from the work of Smith.<sup>8</sup> The dash-dot curve for Na is a smooth extrapolation between the high- and low-energy data.

The analysis of the data in Figs. 2.2 and 2.3 follows that presented previously for the other alkali metals.<sup>3</sup> The open circles in Fig. 2.2 show the values of  $\epsilon_1$  obtained when  $\delta\epsilon_1$ , the contribution to  $\epsilon_1$  due to processes not included in the nearly free-electron

1. Consultant.
2. Graduate student.
3. E. T. Arakawa et al., *Health Phys. Div. Annu. Progr. Rep. July 31, 1971*, ORNL-4720, pp. 42-43.
4. See article entitled "A Slope Method for Determining Extinction Coefficients," this section.
5. J. C. Sutherland and E. T. Arakawa, *J. Opt. Soc. Amer.* **57**, 645 (1967); **58**, 1080 (1968); J. C. Sutherland, R. N. Hamn, and E. T. Arakawa, *J. Opt. Soc. Amer.* **59**, 1581 (1969).
6. S. Yamaguchi and T. Hanyu, *J. Phys. Soc. Jap.* **31**, 1431 (1971).
7. R. E. Palmer and S. E. Schnatterly, *Phys. Rev.* **4**, 2329 (1971).
8. N. V. Smith, *Phys. Rev.* **183**, 634 (1969); **B2**, 2840 (1970).

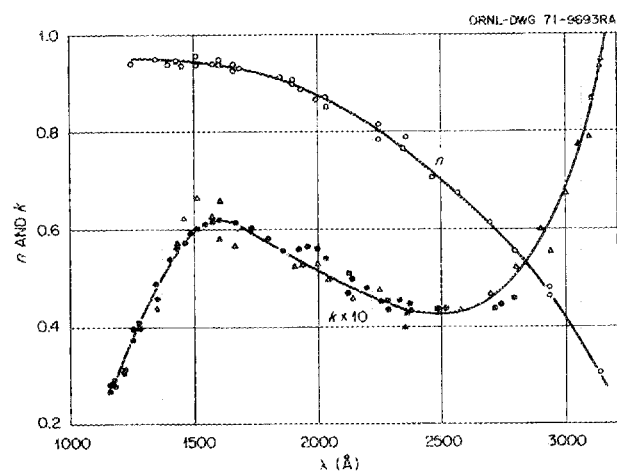


Fig. 2.1. Experimental values of  $n$  and  $k$  for K vs wavelength. Open circles are  $n$  values obtained from the critical angle method, triangles are  $k$  values obtained from the slope of  $R(\theta)$  near critical angle, and solid circles are  $k$  values obtained from transmission measurements. Solid lines give the smoothed average values of the data.

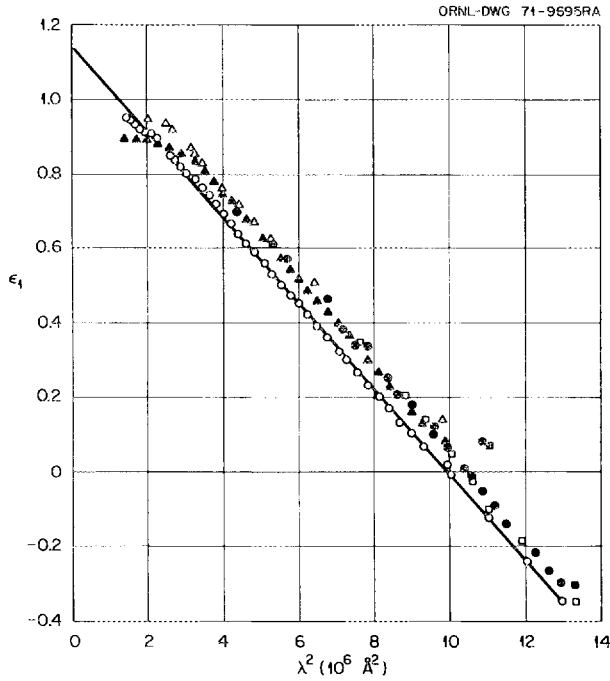


Fig. 2.2. Real part of the complex dielectric constant of K vs the square of photon wavelength. Solid triangles are the points obtained from the smooth curves of  $n$  and  $k$  values. Data points are taken from Sutherland et al. ( $\Delta$ ), Yamaguchi and Hanyu ( $\circ$ ), Palmer and Schnatterly ( $\square$ ), and Smith ( $\bullet$ ). Open circles are a plot of  $\epsilon_1 - \delta\epsilon_1$ , the free carrier contribution to  $\epsilon_1$ .

model, is subtracted from the experimental value of  $\epsilon_1$ . The value of  $\delta\epsilon_1(\lambda)$  was calculated by a Kramers-Kronig analysis of the experimentally observed deviation of  $\sigma$  from the free carrier part characterized by a damping constant  $2\pi\gamma\hbar = 0.018$  eV and a plasma energy of 3.9 eV. The straight line in Fig. 2.2 gives the best fit of  $(\epsilon_1 - \delta\epsilon_1)$  vs  $\lambda^2$  to the nearly free-electron theory. This yields an optical effective mass of  $1.01 \pm 0.01$  and an ion core polarization of  $0.15 \pm 0.01$ . The plasma energy obtained by setting  $\epsilon_1 = 0$  is found to be 3.85 eV. In Fig. 2.3, Smith's  $\sigma$  data for K, obtained from ellipsometry measurements, most clearly show the absorption peak centered at 2 eV that may be attributed to direct interband transitions and the rise in  $\sigma$  below 1 eV due to free carrier absorption. The dominant feature of the  $\sigma$  curve in the region of our measurements is a broad strong peak centered at 8 eV and extending from about 5 to 11 eV. Its interpretation will now be discussed along with similar structure observed for the other alkali metals above their plasma energies.

Our measurements clearly show the existence of an absorption process in all of the alkali metals at energies

above the plasma frequency. In each case the absorption is strong, being comparable in magnitude to the interband transition absorption at lower energies. The broad absorption peaks are found to become stronger and more to lower energies for alkali metals of larger atomic number. Finally, in each material the high-energy peak is found about  $1.5\hbar\omega_p$  above the interband peak, where  $\hbar\omega_p$  is the plasma energy. In Fig. 2.3, the separations are approximately 8, 6, 5, and 4 eV for Na through Cs. Values of  $1.5\hbar\omega_p$  for these materials are 8.4, 6.0, 5.1, and 4.3 eV, respectively. The question of interest is whether this absorption can be understood in terms of one-electron theory or whether it must be explained in terms of the excitation of collective modes of the solid.

Except for Cs, present calculations indicate that, insofar as energy separation is concerned, transitions to  $d$ - or  $f$ -like states could account for the observed high-energy peaks. We do not believe, however, that such transitions can be responsible for the observed absorption. In Cs, where the absorption is strongest, the observed peak falls at the wrong energy. In all of the materials, if this absorption is due to an interband

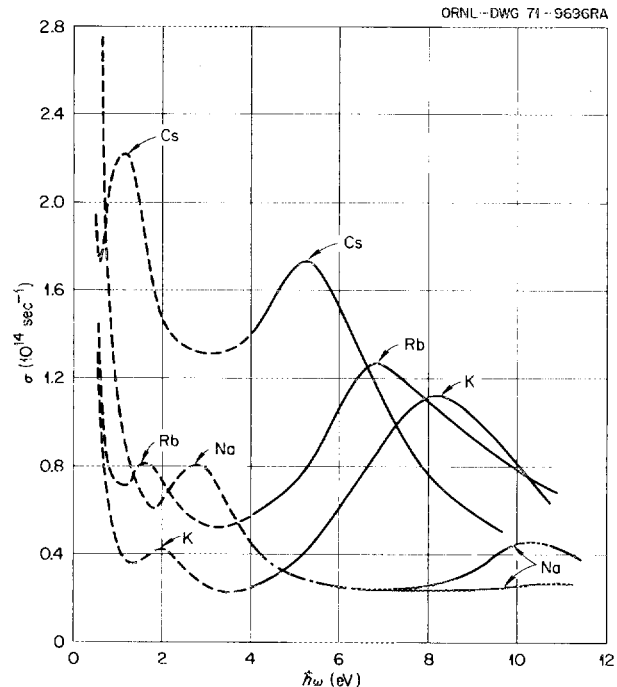


Fig. 2.3. Optical conductivity vs photon energy of Na, K, Rb, and Cs. The solid lines have been obtained at ORNL, the two solid lines for Na being from Sutherland's data with different films. The dash-dotted line is calculated from  $n$  and  $k$  values obtained by a smooth interpolation between Smith's (---) and Sutherland's data.

transition, it is very difficult to understand the large relative magnitude of the high-energy peak as compared with the interband peak for the same material. An interpretation in terms of plasmon-assisted interband transitions<sup>9</sup> seems the most plausible, but this has not been conclusively proved. The experimental observation that the peaks in question are about  $1.5\hbar\omega_p$  above an interband transition in the same metal is in agreement with this theory of plasmon-assisted transitions. However, the magnitude of the observed absorption is not in such good agreement with this theory.

#### OPTICAL PROPERTIES OF GLASSY CARBON FROM 0 TO 82 eV

Glassy carbon<sup>10</sup> is a relatively new form of hard, nongraphitizing carbon, which resembles a black glass with an extremely nonporous, smooth surface. X-ray-diffraction studies<sup>10</sup> suggest that the structure is essentially that of a turbostratic carbon<sup>11</sup> of very small crystallite size. The optical properties of a sample of glassy carbon, the surface of which had been mechanically polished, have been obtained from reflectance measurements up to 82 eV. The values of  $\epsilon_1$  and  $\epsilon_2$ , the real and imaginary parts of the complex dielectric constant, are shown in Fig. 2.4.

If glassy carbon has a turbostratic structure its properties should show some similarities with those of

9. B. I. Lundqvist and C. Lydén, in *Proceedings of the Electronic Density of States Symposium*, National Bureau of Standards, U.S. Govt. Printing Office, Washington, D.C., 1969, p. 50; B. I. Lundqvist, Ph.D. thesis, Chalmers Tekniska Högskola, Göteborg, Sweden (1969).

10. J. C. Lewis, B. Redfern, and F. C. Coward, *Solid-State Electron.* 6, 251 (1963).

11. D. B. Fischbach, p. 1 in *Chemistry and Physics of Carbon*, vol. 7, ed. by P. L. Walker, Marcel Dekker, New York, 1971.

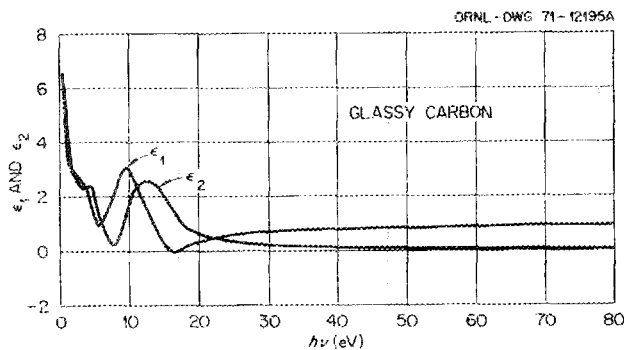


Fig. 2.4. Dielectric constants of glassy carbon vs incident photon energy.

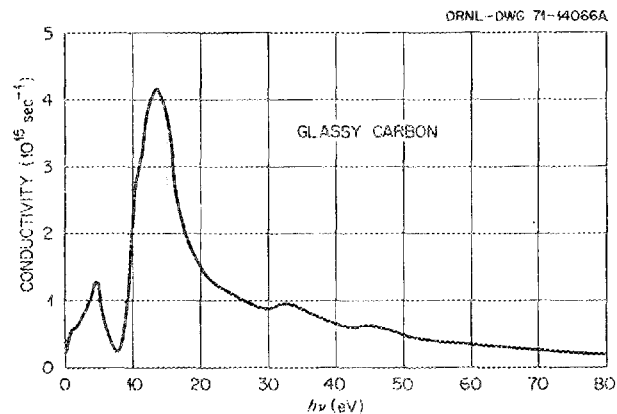


Fig. 2.5. Optical conductivity of glassy carbon vs incident photon energy.

graphite. Optical absorptions caused by single-electron transitions are identified by relative peaks in the optical conductivity. Thus, the conductivity  $E\epsilon_2/2h$ , plotted in Fig. 2.5 as a function of incident photon energy  $E$ , indicates strong interband (or single-electron) transitions at 4.7 and 13.6 eV and weaker transitions between 0 and 4 eV. The structure in  $\epsilon_2$ , and hence in the conductivity, is in fact similar to that for graphite, suggesting an interpretation in terms of  $\pi$  and  $\sigma$  electron excitations. From sum-rule calculations it was found that in glassy carbon, if there are both  $\pi$  and  $\sigma$  electrons associated with bonding, their relative participation is more complicated than in graphite. In the energy region up to 9 eV, normally associated with  $\pi$  electron excitation, considerably less than the one  $\pi$  electron per carbon atom is involved in optical transitions. This may be because of the turbostratic structure. The  $\pi$  electrons occur on either side of the planes of carbon atoms in graphite, and, since the graphitic orientation between the planes does not occur in the turbostratic structure, the  $\pi$  electron participation may be modified. However, by 80 eV nearly all of the four electrons ( $\pi + \sigma$ ) per carbon atom are involved in optical transitions. Thus, it seems reasonable to interpret the data for glassy carbon by analogy with that for graphite.

Thus the weak structure in the conductivity at about 0.9 eV (Fig. 2.5) can be identified with the onset of transitions between  $K_1^-$  and  $K_2^-$  in the band structure of three-dimensional graphite, corresponding to the point  $K_3^-$  of the two-dimensional graphite band structure. The sharp structure at 4.7 eV can be identified with an allowed transition of the  $\pi$  electrons and that at 13.6 eV with an allowed transition of the  $\sigma$  electrons, both for the electric vector perpendicular to the  $C$  axis. The energy-loss function  $-\text{Im } 1/\epsilon$  calculated from the dielectric constants of Fig. 2.4 is plotted in Fig. 2.6.

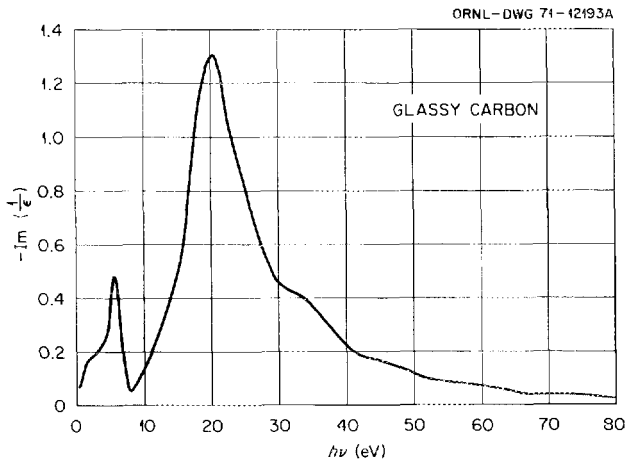


Fig. 2.6. Energy-loss function of glassy carbon vs incident photon energy.

Strong structure is seen at 5.6 and at 20.4 eV. The structure at 5.6 eV corresponds to a minimum in  $\epsilon_1$  and is associated with a collective oscillation, in this case a hybrid resonance involving both collective and single-electron effects. The structure at 20.4 eV is associated with a pure collective oscillation presumably involving both  $\pi$  and  $\sigma$  electrons.

#### A SLOPE METHOD FOR DETERMINING EXTINCTION COEFFICIENTS

Many factors, such as imperfections in the optical system or on the surface of the sample, result in inaccuracies in the measured reflectance  $R$  at a surface as a function of the angle of incidence  $\theta$  so that the optical constants  $n$  and  $k$ , obtained from the best fit of the data to Fresnel's equations, may not be the true constants for the bulk material under investigation. It is well known that for nonabsorbing media with  $n < 1$ , the critical angle for total internal reflection,  $\theta_c$ , gives a precise value of  $n$  through the relation  $n = \sin \theta_c$ . Hunter<sup>12</sup> has extended the critical angle method to yield accurate  $n$  values for slightly absorbing media ( $k < 0.2$ ). An approximate value of  $n$  is obtained from the angle  $\theta_m$  at which the slope of  $R$  vs  $\theta$  is a maximum, and then a correction is applied depending on the values of  $k$  and  $P$ , the polarization of the incident light. We have found that  $k$  may be obtained from the magnitude of the slope of  $R$  vs  $\theta$  at  $\theta_m$ . This quantity is sensitive to the value of  $k$  but relatively insensitive to surface imperfections and to the values of  $n$  and  $P$ .

12. W. R. Hunter, *J. Opt. Soc. Amer.* 54, 15 (1964); *J. Phys.* 25, 154 (1964).

In general we may write  $R_{\text{meas}}(\theta) = c(\theta) R(\theta)$ . Here  $R(\theta)$  is the reflectance for an ideal interface,  $R_{\text{meas}}(\theta)$  is the experimentally measured reflectance, and  $c(\theta)$  is a factor which may involve both instrumental uncertainties and those due to surface imperfections. For the slope we have

$$\frac{dR(\theta)_{\text{meas}}}{d\theta} = c(\theta) \frac{dR(\theta)}{d\theta} + R(\theta) \frac{dc(\theta)}{d\theta}.$$

In this method we are concerned with the case where the slope  $dR(\theta)/d\theta$  is very large. Then, to a good approximation, it is possible to neglect the second term on the right side of the equation in comparison with the first. Thus, where the critical angle method can be used and  $c(\theta_m)$  can be evaluated, values of  $n$  and  $k$  determined from  $\theta_m$  and the slope at  $\theta_m$  are more reliable than those obtained by fitting the entire  $R$  vs  $\theta$  curve. The slope  $dR(\theta_m)/d\theta$  has been calculated by differentiating Fresnel's equations for the reflectance. Figure 2.7 shows calculated values of  $dR(\theta_m)/d\theta$

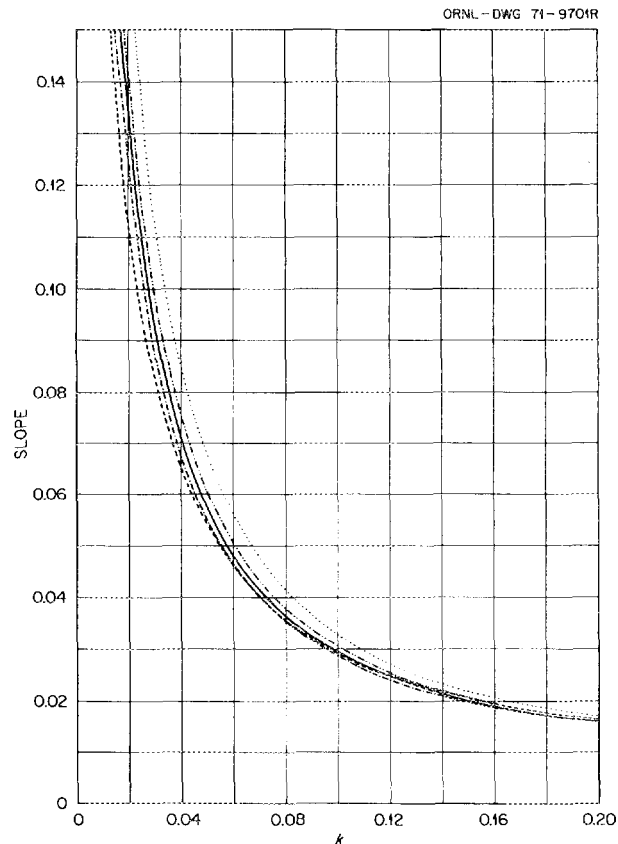


Fig. 2.7. Calculated value of  $dR/d\theta$  at  $\theta_m$  vs  $k$  for  $n = 0.5$  and  $P = 0$  (---), 0.5 (-.-.), 1 (—), 2 (.....), and  $\infty$  (.....).

plotted as a function of  $k$  for a given value of  $n$  and several values of  $P$ . It is seen that the measured slope at  $\theta_m$  is more sensitive to the value of  $k$  for the smaller values of  $k$ . A whole family of such curves can be plotted and used in conjunction with Hunter's method for getting  $n$  from  $\theta_m$ , in order to obtain values of  $k$  limited in accuracy only by the uncertainty in  $c(\theta_m)$ . In actual practice, we have found the optical constants from the theoretical expression for  $dR(\theta_m)/d\theta$  by an iterative process carried out by means of a computer program written to fit  $n$  to the observed  $\theta_m$  and  $k$  to the observed slope at  $\theta_m$  for a known value of  $P$ .

We have found this method to be very useful in measuring the optical properties of the alkali metals at photon energies above their plasma energies, where they become relatively transparent.<sup>13</sup>

#### WORK FUNCTION CHANGES DURING OXYGEN CHEMISORPTION ON FRESH MAGNESIUM SURFACES

Measurements have been made previously<sup>14</sup> of exoelectron emission during oxygen and water vapor chemisorption on fresh magnesium surfaces. At that time, preliminary measurements of the photoelectric work function indicated that some connection exists between the work function and exoelectron emission for a given surface. For a given partial pressure of oxygen, the work function changes with time after abrasion of the surface, exhibiting minima in association with maxima in the exoelectron emission. We have now obtained photoelectric data showing this phenomenon, and also show that the exoelectron emission is a maximum for an approximately monolayer coverage of oxygen on magnesium.

Figure 2.8 shows data for an oxygen pressure of approximately  $7 \times 10^{-9}$  torr. The top curve shows the work function, as determined by the onset of photoemission, as a function of time, while the lower curves show the photoemission for a photon energy of  $(1.93 \pm 0.05)$  eV and the exoelectron emission, both as functions of time. The work function goes through two minima corresponding directly to the two maxima in the photoemission and closely connected with the two

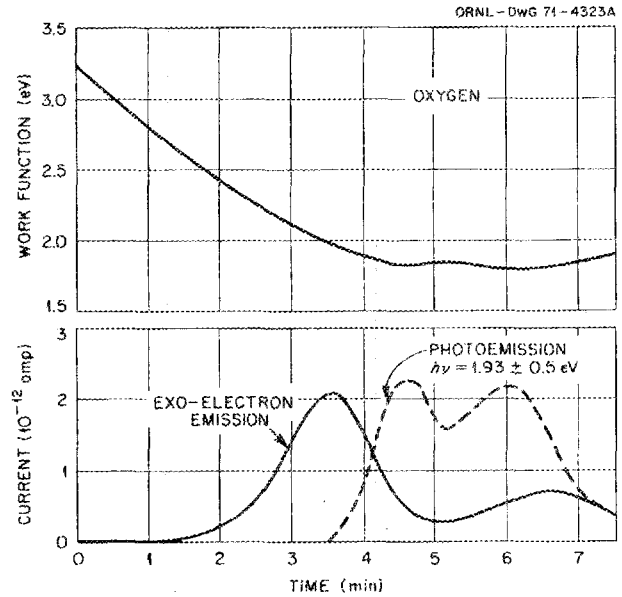


Fig. 2.8. Time development of the work function, the exoelectron emission, and the photoemission ( $h\nu = 1.93 \pm 0.05$  eV) from a fresh magnesium surface.

maxima in the exoelectron emission. The work function is seen to vary between 3.3 and 1.8 eV, as compared with previously published<sup>15</sup> values for evaporated magnesium films, which range from 3.6 to 2.2 eV.

The first maximum which occurs in the exoelectron emission with time after abrasion is very close to the monolayer formation time calculated assuming a unit sticking coefficient. This is shown in Fig. 2.9, which is a plot of the calculated monolayer formation time for oxygen as a function of pressure together with data which show the position in time of the first peak in the oxygen exoelectron emission curve as a function of pressure. The solid points are the actual data, and the open points were obtained by assuming a background partial pressure of oxygen amounting to  $2 \times 10^{-9}$  torr. For the actual data points the oxygen pressure was recorded as the increase in total pressure on admitting the oxygen into the system. For the open points the estimated background oxygen pressure was added to the measured partial pressure of oxygen. In either case the higher-pressure points follow the shape of the monolayer line very well.

13. See article entitled "Optical Properties of K between 4 and 10.7 eV and Comparison with Na, Rb, and Cs," this section.

14. T. F. Gesell, E. T. Arakawa, and T. A. Callcott, *Surface Sci.* 20, 174 (1970).

15. R. J. Cashman and W. S. Huxford, *Phys. Rev.* 48, 734 (1935).

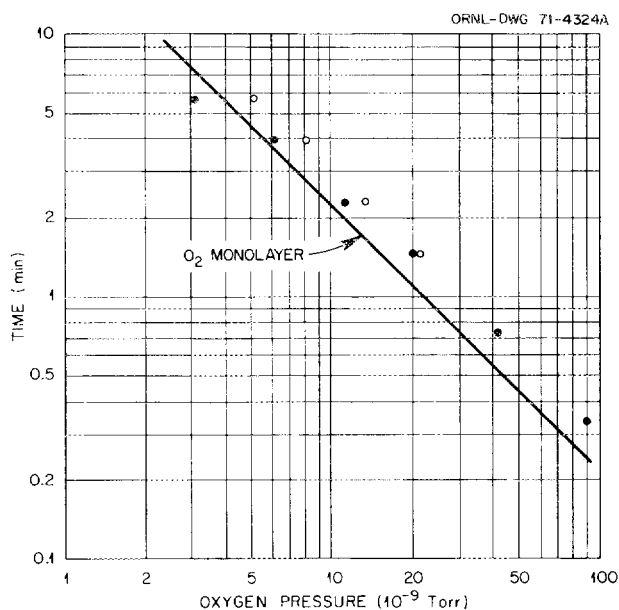


Fig. 2.9. Time to achieve a monolayer of oxygen on a surface as a function of oxygen pressure assuming unit sticking coefficient together with data which show the position in time of the first peak in the oxygen emission curves as a function of pressure.

#### A TECHNIQUE FOR REVITALIZATION OF VACUUM ULTRAVIOLET DIFFRACTION GRATINGS

A technique has been developed for revitalizing replica gratings used in the vacuum ultraviolet region. Epoxy replica gratings overcoated with a suitable metal are usually more efficient than the originals when they are new. However, after exposure to the atmosphere and to radiation and contaminants in the vacuum system, all gratings become less efficient and tend to have more scattered light.

Revitalization has been achieved by replacing the metal overcoating on the grating. So far two gratings have been treated, both of which were originally overcoated with Al. First the Al was dissolved using a dilute solution of NaOH, and then the grating was cleaned in a Freon bath. They were then recoated by vacuum evaporation, one with Au and the other with Al. In this whole procedure care had to be taken not to

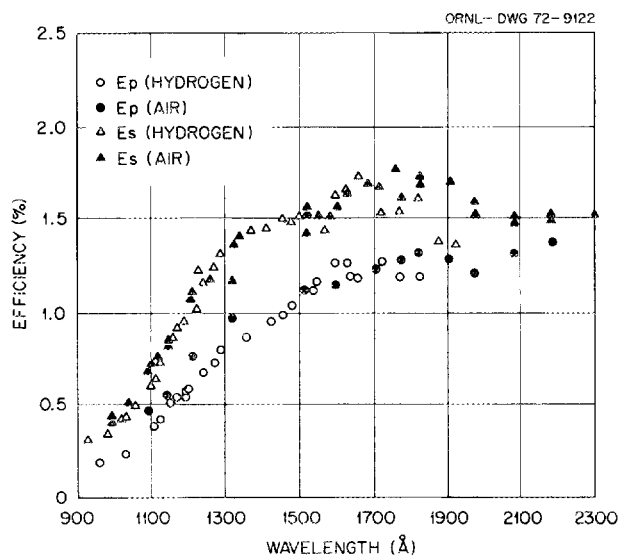


Fig. 2.10. Efficiency curves for a revitalized aluminum-coated diffraction grating.

damage the rulings in the epoxy layer of the grating. The efficiencies of the freshly overcoated gratings were then found as a function of wavelength using the grating calibrator described by Hammer<sup>16</sup> for both *s*- and *p*-polarized radiation.

Figure 2.10 shows the measured efficiencies for both *s*- and *p*-polarized radiation for the epoxy replica grating overcoated with approximately 760 Å of Al. Measurements were obtained for both air and hydrogen discharge light sources. The results shown are representative for this grating. Earlier measurements showed slightly higher efficiencies, but some decrease in efficiency was observed due to repeated exposure to the atmosphere.

In general it was found that the gratings were around 10 to 20% as efficient as a new grating but with much decreased scattered light intensity. Improvements in technique should produce revitalized gratings more nearly approaching the efficiency of a new grating.

16. D. C. Hammer, E. T. Arakawa, and R. D. Birkhoff, *Appl. Opt.* 3, 79 (1964).

### 3. Physics of Tissue Damage

E. T. Arakawa  
R. D. Birkhoff

W. T. Cochran<sup>1</sup>    W. G. McGlothlin<sup>1</sup>  
L. C. Emerson    L. R. Painter<sup>2</sup>  
R. N. Hamm    R. H. Ritchie  
R. A. MacRae<sup>2</sup>    B. L. Sowers<sup>1</sup>  
Mary W. Williams

#### ELECTRON-SLOWING-DOWN STUDIES<sup>3</sup>

The extensive series of studies previously carried out here on electron-slowing-down spectra<sup>4</sup> in a wide variety of metals was recently extended to include the semiconducting materials germanium and silicon.<sup>5</sup> The preliminary data for silicon had indicated some evidence of structure in the experimentally measured flux at 90 eV and at 2 keV. This structure took the form of discontinuities in the data very near the *L*- and *K*-shell energies in silicon and was thought to arise from electron-induced ionizations of these shells. Since this process, if true, represents a possible breakdown in the continuous slowing-down model, we made a more careful exploration of the slowing-down spectrum in silicon using a finer energy mesh and a stronger electron source.

Two single crystals of extremely high-purity (impurities <1 ppb) silicon were irradiated in the High-Flux Isotope Reactor to near saturation in a thermal flux of  $3 \times 10^{15}$  neutrons  $\text{cm}^{-2} \text{sec}^{-1}$ . The resulting activity was sufficiently high to enable us to obtain several very reproducible measurements of the electron spectrum up to 32 keV. Particular attention was paid to the region in the vicinity of the *K*- and *L*- shell binding energies. The

results of one measured spectrum are shown in Fig. 3.1 along with the spectrum calculated from the Spencer-Fano theory. Agreement between theory and experiment at the higher energies is excellent, but, as in previous comparisons, the magnitude of the measured flux exceeds that predicted by theory at lower energies. Not shown on the graph are the high densities of data points taken near the shell binding energies. The discontinuity in the data at these energies is not as pronounced as that seen earlier, but there is a distinct

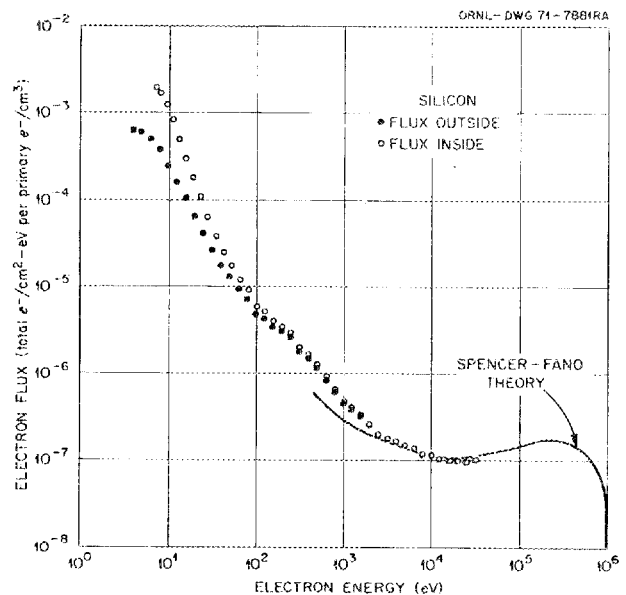


Fig. 3.1. Slowing-down spectrum of electrons in single-crystal silicon.

1. Graduate student.

2. Consultant.

3. The research reported in this section was sponsored in part by the Air Force Cambridge Research Laboratories, Office of Aerospace Research, under Contract No. Y72-923, but the report does not necessarily reflect endorsement by the sponsor.

4. W. J. McConnell, H. H. Hubbell, R. N. Hamm, R. H. Ritchie, and R. D. Birkhoff, *Phys. Rev.* **138A**, 1377 (1965).

5. E. T. Arakawa et al., *Health Phys. Div. Annu. Progr. Rep.* July 31, 1970, ORNL-4584, pp. 87-88; July 31, 1971, ORNL-4720, pp. 51-52.

change in slope just under 100 eV and near 2 keV. On the basis of the reproducibility of these features and, in particular, because of the excellent statistics afforded by the high source strength, we believe that some inner-shell ionizing events occur. These processes, while not affecting the gross features of the slowing-down spectrum, do represent a perturbation to the continuous slowing-down model.

In addition to the work on metals and semiconductors we have extended our studies to insulators to provide a comparison of existing data with that from wide-band-gap materials. Preliminary data have been obtained for a polycrystalline sample of aluminum oxide. Because of the impossibility of producing a measurable activity in pure  $\text{Al}_2\text{O}_3$ , it was necessary to introduce an impurity which could be activated by neutron irradiation. Normal isotopic dysprosium was chosen because of its convenient half-life, its clean decay spectrum, and its high activation cross section. Because of this latter feature we were able to secure sufficient electron currents with a doping level of only 0.5 wt % dysprosium. The measured slowing-down spectrum shown in Fig. 3.2 is characteristic of that of both metals and semiconductors in that the flux exhibits a minimum at the high-energy end, where the primary flux is falling faster than the secondary flux is building up, and a rise at lower energies, reaching the familiar  $1/E$  region in the vicinity of 400 eV. On an absolute basis the electron flux is generally higher than that seen for a typical metal. For example, when corrected for the differences in stopping power and densities in the two materials, the ratio of the flux in

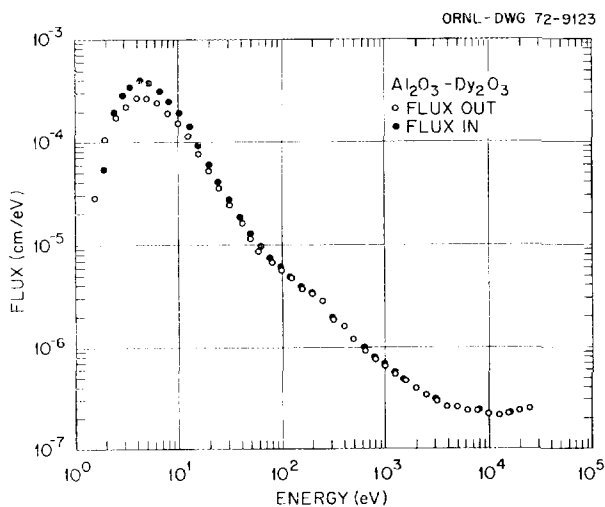


Fig. 3.2. Slowing-down spectrum of  $^{163}\text{Dy}$  beta particles in aluminum oxide.

$\text{Al}_2\text{O}_3$  to that in the metal aluminum varies between about 3 and 7, with the higher ratio occurring at the lower energies. These are preliminary data, particularly in the case of the electron flux inside the aluminum oxide, for which the details of the band gap and the work function are poorly known.

We have continued our investigations concerning the long-standing disagreement between theory and experiment at the lower energies in a material for which comparison is possible. The possibility of the existence of a low-energy photon cascade, suggested by an earlier work,<sup>6</sup> was experimentally checked last year by comparing the slowing-down spectrum from a "thin" source with that from a "thick" source. Both sources were thick compared with the beta range, but the thicker source was also thick with respect to the  $1/E$  attenuation length of the bremsstrahlung corresponding to the highest-energy beta ray. The comparison did show a higher flux at low energies, but the increase was well within the experimental error associated with the measurements, and thus the experiment was inconclusive. Additionally, the thin source was thin for only the high-energy photons, when, in actuality, there may be a much larger number of photons with energies of tens or hundreds of electron volts.

We have decided to repeat this experiment using a more extensive application of the same technique. Our plan is to measure the slowing-down spectrum from a series of sources ranging in thickness from that equal to the beta range down to the thinnest source for which we can obtain data. Gold has been chosen for the source material because of its relatively large activation cross section and because it can be obtained in the form of very thin films.

So far data have been obtained from the first four sources in this series. The sources ranged in thickness from 780 Å to 5 mils. The two thicker sources were obtained from commercial suppliers, while the two thinner sources were prepared by vacuum evaporation. The slowing-down spectra, shown in Fig. 3.3, are similar insofar as the overall shape is concerned but differ in detail. The most outstanding characteristic is the pronounced rise in the flux near 7 keV in the thinnest source. This structure can also be seen in the thicker sources, although in the thickest source it is barely discernible. This energy is almost exactly the *LMM* Auger energy, and it seems certain that the peak is due to Auger electrons augmented to some extent by photoelectrons from absorption and characteristic *L* x rays. In gold the *L*-shell fluorescent yield is only about

6. G. E. Edwards and M. L. Poole, *Phys. Rev.* **69**, 549 (1946).

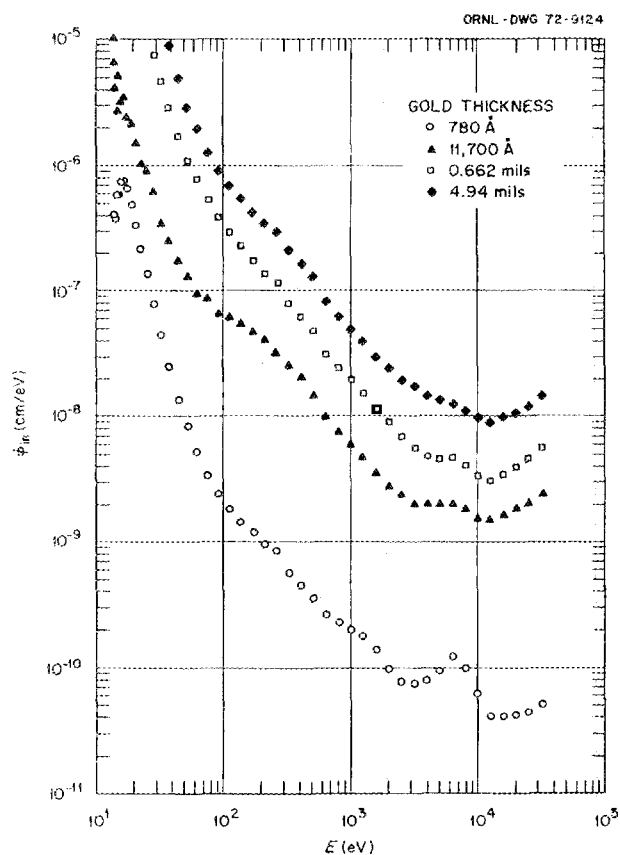


Fig. 3.3. Variation of electron flux with source thickness.

0.4, so strong Auger emission would be expected following *L*-shell ionizations. The broad rise near 1 to 5 keV in the thinnest source is probably due to *MNV* Auger electrons. The flux depression near 100 eV in the 11,700-Å source is unexplained and may be due to surface contamination. We plan to obtain more data in this region along with additional spectra from both thicker and thinner sources.

### OPTICAL PROPERTIES OF ORGANIC LIQUIDS

The study<sup>7</sup> of the optical properties of liquids in the vacuum ultraviolet has been continued. Since there is a high percentage of liquid in living matter, optical data which enable determination of the energy-loss mechanisms experienced by both electromagnetic radiation and high-energy charged particles incident on the liquid

can be of fundamental importance in the study of radiation damage in living matter.

A transmission cell<sup>7</sup> had been built which enabled samples as thin as 500 Å to be obtained, but difficulty was experienced in determining the sample thickness, so absorption spectra had to be normalized to values obtained from reflectance measurements. Techniques have now been developed for obtaining the cell thickness from interference patterns in the near-normal incidence reflectance as a function of wavelength from 1700 to 5000 Å. As the liquid fills the space between the cell walls the interference fringes in the unfilled portions are observed to remain the same, so apparently the forces associated with the surface tension and vapor pressure of the liquid do not change the cell thickness. However, thickness changes are noted if extreme care is not exercised in handling the cell. Since the transmission *T*, the sample thickness *x*, and the wavelength *λ* are known, the imaginary part of the complex index of refraction *k* is readily calculated from the Beer-Lambert law

$$I = I_0 \exp(-4\pi kx/\lambda).$$

The *k* values obtained from this method were accurate to within the experimental error of approximately 6%. To compare the absorption of the liquid and vapor phases of these molecules, the cross section for photon attenuation per molecule, *σ*, was calculated using the expression

$$I = I_0 \exp(-\sigma n_0 x),$$

where *n*<sub>0</sub> is the number of molecules per cubic centimeter and *x* is the sample thickness.

Measurements are reported here on three frequently used solvents: carbon tetrachloride (CCl<sub>4</sub>), liquid *n*-hexane (C<sub>6</sub>H<sub>14</sub>), and cyclohexane (C<sub>6</sub>H<sub>12</sub>). The molecules are simple in structure, especially carbon tetrachloride, which has tetrahedral symmetry. Thus, it is hoped that knowledge of their optical properties in the liquid state will help in the formulation of a theory for the liquid state.

The absorption cross section per molecule, *σ*, is shown for the three liquids in Figs. 3.4–3.6 together with the vapor data over the regions where such data were available.

In Fig. 3.4 for CCl<sub>4</sub> the weak structure at 6.9 eV corresponds to the vapor peak at 7.1 eV, which has been attributed to an *n* → *σ*\* transition of the nonbonding chlorine electrons.<sup>8</sup> This excitation in the

7. E. T. Arakawa et al., *Health Phys. Div. Annu. Progr. Rep.* July 31, 1971, ORNL-4720, pp. 52–55.

8. H. Tsubomura, K. Kimura, K. Kaya, J. Tanaka, and S. Nagakura, *Bull. Chem. Soc. Jap.* 37, 417 (1964).

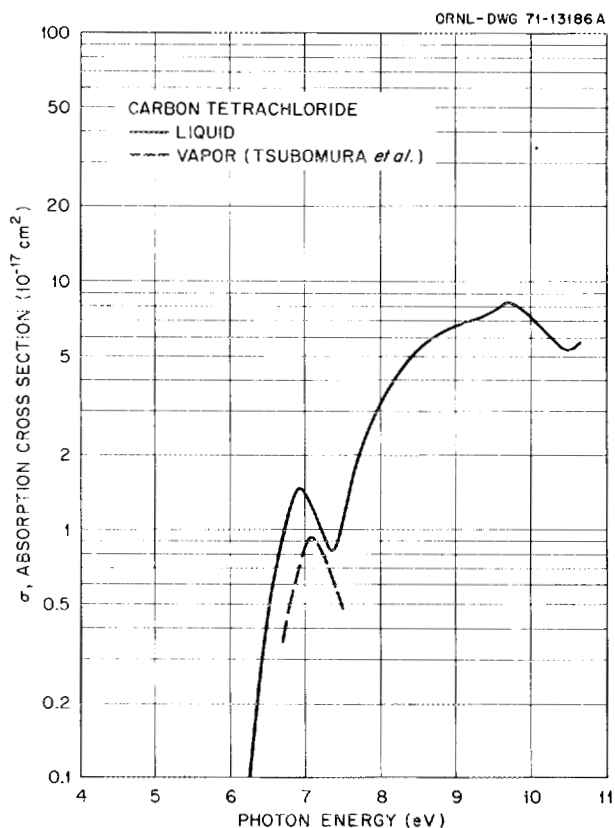


Fig. 3.4. Absorption cross section  $\sigma$  of carbon tetrachloride liquid and vapor as a function of photon energy.

liquid is shifted to lower energies and is larger in magnitude than that for the vapor. Strong absorption begins at 7.3 eV in the liquid. The two peaks centered at 9.0 and 9.7 eV are probably a result of  $\sigma \rightarrow \sigma^*$  transitions, as will be seen in the following discussion of  $C_6H_{14}$  and  $C_6H_{12}$ .

Figure 3.5 shows the cross section curves of liquid and vapor *n*-hexane from the absorption edge at 7.4 eV up to 10.65 and 11.0 eV, respectively. Since the molecule is saturated, containing only  $\sigma$  bonds, this absorption has been identified as the onset of  $\sigma \rightarrow \sigma^*$  transitions of the C-H or C-C bonding electrons.<sup>9,10</sup> For this higher-energy structure the cross section of the liquid is lower than that for the vapor, but the difference is within the experimental error of the two curves.

The cross sections of  $C_6H_{12}$  liquid and vapor are shown in Fig. 3.6 from the onset of absorption at 7.1

9. B. A. Lombos, P. Sanvageau, and C. Sandorfy, *J. Mol. Spectry.* **24**, 253 (1967).

10. J. W. Raymonda and W. T. Simpson, *J. Chem. Phys.* **47**, 430 (1967).

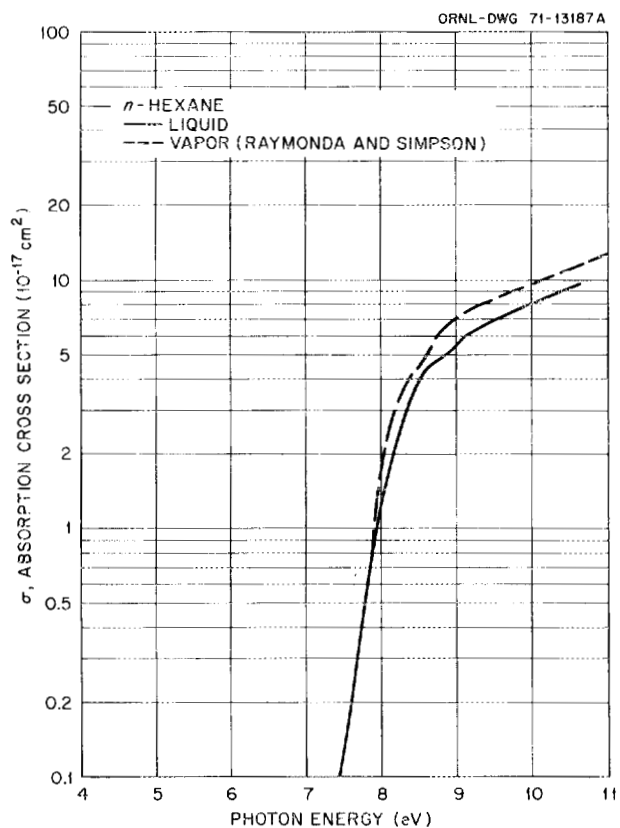


Fig. 3.5. Absorption cross section  $\sigma$  of *n*-hexane liquid and vapor as a function of photon energy.

eV up to 10.65 and 11.0 eV, respectively. The  $C_6H_{12}$  cross section is very similar to that of  $C_6H_{14}$  except for the double resonance at 8.5 and 10.4 eV in the vapor data. This structure has been attributed to a resonance effect caused by the ring structure of the  $C_6H_{12}$  molecule.<sup>10</sup> Again the molecular excitations have been identified as  $\sigma \rightarrow \sigma^*$  transitions. As for  $C_6H_{14}$ , the liquid and vapor cross sections for  $C_6H_{12}$  in this energy region are nearly equal; however, the two peaks are less pronounced in the liquid than in the vapor due to the increased damping experienced by the molecules in the liquid state.

The data presented here show that the electronic properties of these liquids are very similar to those of the vapor in the energy region from 2 to 11 eV. More data are needed for the  $CCl_4$  vapor in the higher-energy region to compare with the liquid data.

Absorption spectra measured by transmission are more reliable than those obtained from reflectance measurements when  $k$  is small. We, in fact, get differences in  $k$  by the two methods which are not within the calculated experimental errors. The reason

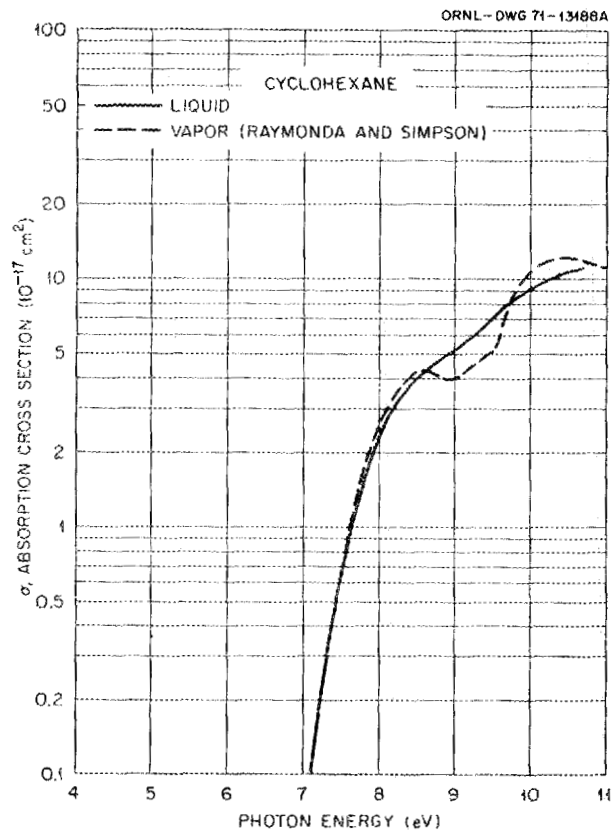


Fig. 3.6. Absorption cross section  $\sigma$  of cyclohexane liquid and vapor as a function of photon energy.

for this is not understood and indicates the need for further investigation.

#### RADIATION INTERACTIONS WITH NUCLEIC ACID BASES

An experimental investigation of the optical and dielectric properties of the nucleic acid bases has been initiated. The studies are carried out by measuring the optical reflectivity of the bases in the form of a smooth film as a function of the angle of incidence and then using an iterative procedure involving Fresnel's equations to extract the optical constants. For the reflectivity measurements it is necessary to have a specularly reflecting surface. The films are prepared by a gentle sublimation within a vacuum environment onto a suitably flat substrate of either glass or quartz.

Preliminary data have been obtained for guanine at photon energies up to 82 eV. The dielectric constants  $\epsilon_1$  and  $\epsilon_2$  are shown in Fig. 3.7 at energies above 14 eV. The broad minimum in  $\epsilon_1$  near 22 eV coupled with decreasing values for  $\epsilon_2$  gives rise to a broad maximum

in the energy-loss function shown in Fig. 3.8. These data are in general agreement with the work of Johnson,<sup>11</sup> who obtained direct measurements of the electron energy loss using a scanning electron microscope. Preliminary data which show structure in the energy-loss function have been obtained at energies below 14 eV. Modifications to the experimental apparatus are expected to result in a significant improvement in the resolution at these lower energies, allowing comparison with the electron-loss data.

11. D. E. Johnson, *Radiat. Res.* **49**, 63 (1972).

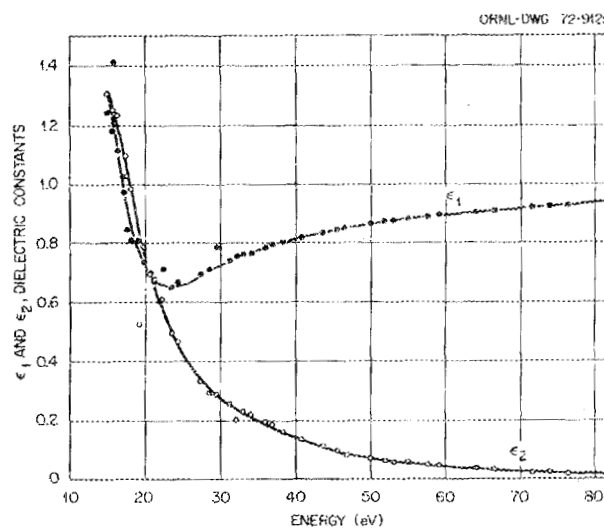


Fig. 3.7. Dielectric constants of guanine from 14 to 82 eV.

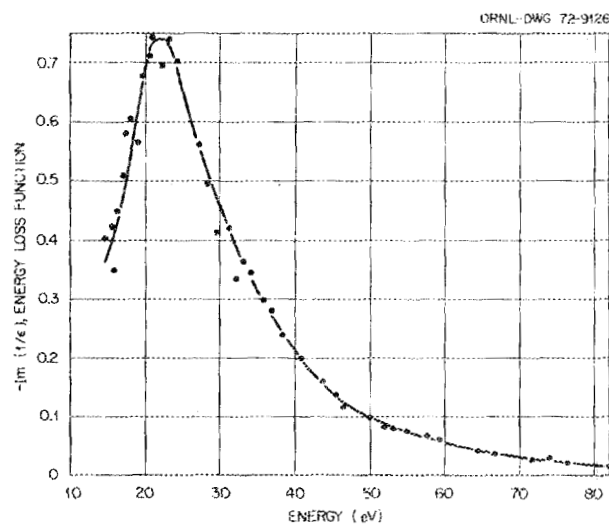


Fig. 3.8. Energy-loss function of guanine from 14 to 82 eV.

Data of these types are important in that they provide a supplement to the electron beam work and perhaps afford an independent measurement of the dielectric properties of nucleoproteins with less danger of radiation damage to the molecules. The ultimate application,

of course, is reading the nucleic acid-base sequence in DNA; that is, complete knowledge of the dielectric "fingerprint" of each base may well be the key to its identification.

## 4. Electron and Ion Collision Physics

R. N. Compton

V. E. Anderson<sup>1</sup>    W. R. Garrett  
Ada Carter        D. R. Nelson<sup>3</sup>  
C. D. Cooper<sup>2</sup>    P. W. Reinhardt  
J. T. Cox         H. C. Schweinler  
F. J. Davis        J. A. Stockdale  
J. F. Wilson<sup>4</sup>

### METASTABLE ANIONS OF CO<sub>2</sub>

According to the Walsh rules, CO<sub>2</sub><sup>-</sup> with 17 valence electrons should be bent in its ground state, whereas CO<sub>2</sub> is linear. Experimental evidence from electron-spin resonance and infrared studies of CO<sub>2</sub><sup>-</sup> in solids shows that the bond angle is 134°, and the CO bond distance of 1.25 Å is consistent with an analysis of the molecular infrared bands. Electron impact studies of gaseous CO<sub>2</sub> have failed to produce CO<sub>2</sub><sup>-</sup> ions which could be observed in a mass spectrometer. We have observed CO<sub>2</sub><sup>-</sup> ions in the gas phase as direct products of collisions of either electrons or cesium atoms with organic molecules which contain "bent" CO<sub>2</sub> as a basic unit. Figure 4.1 shows the dissociative attachment cross section for production of CO<sub>2</sub><sup>-</sup> from two such molecules, succinic anhydride (I) and maleic anhydride (II). In all cases the CO<sub>2</sub><sup>-</sup> ions were found to be metastable with respect to autodetachment, and the lifetimes were measured using a time-of-flight technique.<sup>5</sup> Lifetime measurements for CO<sub>2</sub><sup>-\*</sup> from the different dissociative reactions are listed in Table 4.1. Dissociative electron attachment to I produced CO<sub>2</sub><sup>-\*</sup> with a lifetime (26 ± 5 μsec) which differs from that observed from II (60 ± 5 μsec). However, within experimental error the lifetime of CO<sub>2</sub><sup>-\*</sup> observed from the cesium collisional ionization reaction is the same for I and II and agrees with the

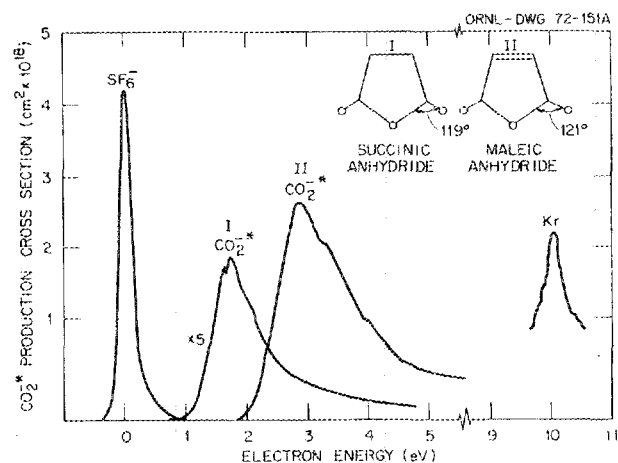


Fig. 4.1. CO<sub>2</sub><sup>-\*</sup> ion currents as a function of incident electron energy from succinic anhydride (I) and maleic anhydride (II). Automatic retarding potential difference method afforded energy resolution of 0.15 eV, and the energy scale was calibrated with the krypton energy loss peak at 10.0 eV.

values observed for II in the above experiment. In each case, the lifetime of CO<sub>2</sub><sup>-\*</sup> was not dependent on the energy of the bombarding particle. The fact that stable CO<sub>2</sub><sup>-</sup> was not observed in the Cs collision experiment supports a negative electron affinity for CO<sub>2</sub>. If the electron affinity is negative and the ground state <sup>2</sup>A<sub>1</sub> of CO<sub>2</sub><sup>-</sup> is metastable, the minimum in the <sup>2</sup>A<sub>1</sub> potential curve for CO<sub>2</sub><sup>-</sup> at 134° bond angle must lie below the ground-state potential curve for neutral CO<sub>2</sub> at 134° but above the minimum for CO<sub>2</sub> at 180°. According to the energetics of the above experiment, the minimum for the CO<sub>2</sub><sup>-</sup> curve should not be more than 0.5 eV above the ground state of CO<sub>2</sub>.

1. On loan from Mathematics Division.
2. Consultant (sabbatical leave from University of Georgia to ORNL for 1971-72).
3. On loan to Environmental Impact Studies.
4. Radiological Health Physics Fellow, University of Tennessee.
5. W. T. Naff, C. D. Cooper, and R. N. Compton, *J. Chem. Phys.* 49, 2784 (1968).

**Table 4.1. Mean lifetimes of  $\text{CO}_2^{-*}$  produced by dissociative electron attachment and collisional ionization**

The lifetimes are independent of both the incident electron energy and incident cesium atom energy.

Parent molecule	$\tau$ ( $\mu\text{sec}$ )		O-C-O angle in parent
	Electron impact	Cs collision	
Succinic anhydride (I)	$26 \pm 5$	$71 \pm 10$	$119^\circ \pm 1^\circ{}^a$
Deuterated succinic anhydride	$30 \pm 5$		
Maleic anhydride (II)	$60 \pm 5$	$62 \pm 10$	$121^\circ \pm 1^\circ{}^b$
$\beta$ -Propiolactone	$26 \pm 5$		$123^\circ \pm 6^\circ{}^c$

<sup>a</sup>M. Ehrenberg, *Acta Crystallogr.* **19**, 698 (1965).

<sup>b</sup>R. E. Marsh, E. Uhell, and H. E. Wilcox, *Acta Crystallogr.* **15**, 35 (1962).

<sup>c</sup>J. Bergman and S. H. Bauer, *J. Amer. Chem. Soc.* **77**, 1955 (1955).

Our observation of metastable  $\text{CO}_2^-$  ions prompted Krauss and Neumann<sup>6</sup> of NBS to make an ab initio calculation of the potential curve for the  ${}^2A_1$  state of  $\text{CO}_2^-$ . Using a CO bond distance of 1.16 Å [same as in  $\text{CO}_2$  ( ${}^1A_1$ )], they find that the minimum for the  ${}^2A_1$  state of  $\text{CO}_2^-$  falls below the  $\text{CO}_2$  ( ${}^1A_1$ ) curve at the  $134^\circ$  bond angle, but this minimum is still about 1.7 eV above the ground state of linear  $\text{CO}_2$ . In addition, one point on the potential curve was computed for a bond angle of  $130^\circ$  and a bond distance of 1.27 Å and found to be only 0.3 eV above the ground state of linear  $\text{CO}_2$ . A potential curve through this point, similar to the one computed for the 1.16-Å bond distance, would satisfy the experimental evidence which places the curve below 0.5 eV and permit a plausible explanation of the lifetime data. According to such a curve,  $\text{CO}_2^{-*}$  could vibrate between  $152$  and  $122^\circ$  with up to 0.45 eV of energy and still be metastable, with the lifetimes depending on the Franck-Condon overlap integrals between the ionic and neutral states. It may be fortuitous, but the  $122^\circ$  angle is approximately the same as the O-C-O bond angle in I and II (Table 4.1). If a bombarding electron or Cs atom does increase the bond-bending energy of  $\text{CO}_2^-$  and thereby decrease the bond angle below about  $119^\circ$ , the autodetachment would be much faster because of the greatly increased Franck-Condon overlap above the crossing in the potential curves, and the lifetimes would probably be too short to permit mass spectrometric observation. Thus the lifetime observed in the mass spectrometer should not be dependent upon the energy of the incident particle.

The observation of two distinct lifetimes of  $\text{CO}_2^{-*}$  can be explained if  $\text{CO}_2^{-*}$  observed from I (shorter lifetime) possesses a higher vibrational excitation than

$\text{CO}_2^{-*}$  observed from II. In this case, since the radiation lifetime between vibrational states is longer than the observed autodetachment lifetimes, autodetachment will occur primarily from the initial state, and the probability of electron ejection will depend on the different Franck-Condon-overlap integrals for the two vibrational states. The complexities of the dissociative process involved prevent a determination of the source of the higher vibrational excitation; however, it may arise from the fact that the O-C-O bond angle in I ( $119^\circ$ ) is farther from the equilibrium angle in  $\text{CO}_2^-$  ( ${}^2A_1$ ) than is the angle in II ( $121^\circ$ ).

In summary, a long-lived metastable state of  $\text{CO}_2^{-*}$  exists which lies about 0.5 eV above the ground state of  $\text{CO}_2$ . These experimental results support the ab initio calculations by Krauss and Neumann,<sup>2</sup> which show that the minimum in the  ${}^2A_1$  state of  $\text{CO}_2^-$  lies below the ground state of  $\text{CO}_2$  for a bond angle of  $134^\circ$ . It is proposed that the two observed lifetimes of  $\text{CO}_2^{-*}$  are related to different Franck-Condon-overlap integrals between two vibrational states of  $\text{CO}_2^{-*}$  and the vibrational states of  $\text{CO}_2$ . Furthermore, for practical purposes, maleic anhydride is a readily available source of metastable  $\text{CO}_2^-$  or neutral beams of  $\text{CO}_2$  of known translational energy which may be used in beam-collision experiments. In addition, the fact that  $\text{CO}_2^-$  is bent and will probably be in an excited vibrational state following autodetachment may be of importance in  $\text{CO}_2$  laser technology. Stable  $\text{CO}_2^-$  ions are produced in solutions or solids by radiation interactions, and it is hoped that future studies will elucidate the stabilizing effects of the environment on the metastable  $\text{CO}_2^-$  ion.

#### IONIZATION PHENOMENA IN SEVERAL METALLOCENES

The formation of positive and negative ions in the organometallic "sandwich" compounds ferrocene, cobal-

6. M. Krauss and D. Neumann, *Chem. Phys. Lett.* **14**, 26 (1972).

tocene, nickelocene, and magnesocene has been studied by electron impact-mass spectrometer techniques. Positive-ion appearance potentials have been determined for the products  $(C_{10}H_{10}M)^+$ ,  $(C_5H_5M)^+$ , and  $M^+$ , where M refers to Fe, Ni, or Mg. Figure 4.2 shows typical ion yields for magnesocene where krypton was added to establish the electron energy scale. The ionization potentials are derived from the onsets, and the values compare favorably with recent photoelectron data. In all cases cyclopentadienyl anions ( $C_5H_5^-$ ) were produced at low electron energies; however, their cross sections of formation differ by orders of magnitude.

The  $SF_6$  scavenger technique was used to detect an intense temporary negative-ion resonance in ferrocene at about 0.6 eV. The cyclopentadienyl anion current also peaked at this energy; however, its cross section was small ( $3.5 \times 10^{-21} \text{ cm}^2$ ). The most striking feature of the negative-ion studies was the observation of a long-lived (lifetime  $>100 \mu\text{sec}$ ) parent negative ion of nickelocene at thermal electron energies and a second broader resonance centered at about 1 eV. Figure 4.3 shows these two resonances along with the  $SF_6^-$  ion current for reference and the weaker  $C_5H_5^-$  ion current peak. The lifetime of the second  $C_{10}H_{10}Ni^-$  resonance

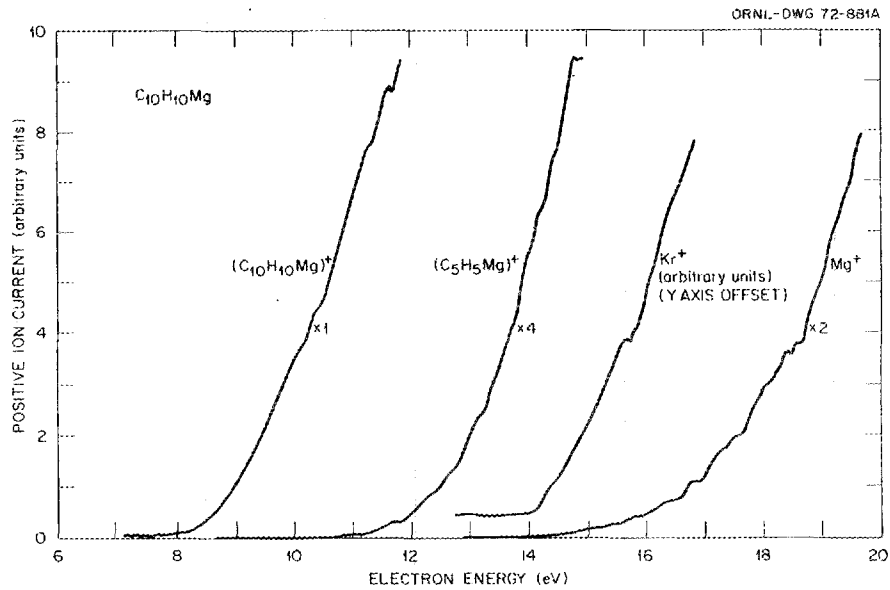


Fig. 4.2. Positive-ion yields as a function of electron energy for electron impact ionization of magnesocene. The krypton ion ( $Kr^+$ ) is recorded to calibrate the electron energy scale and to indicate electron energy resolution.

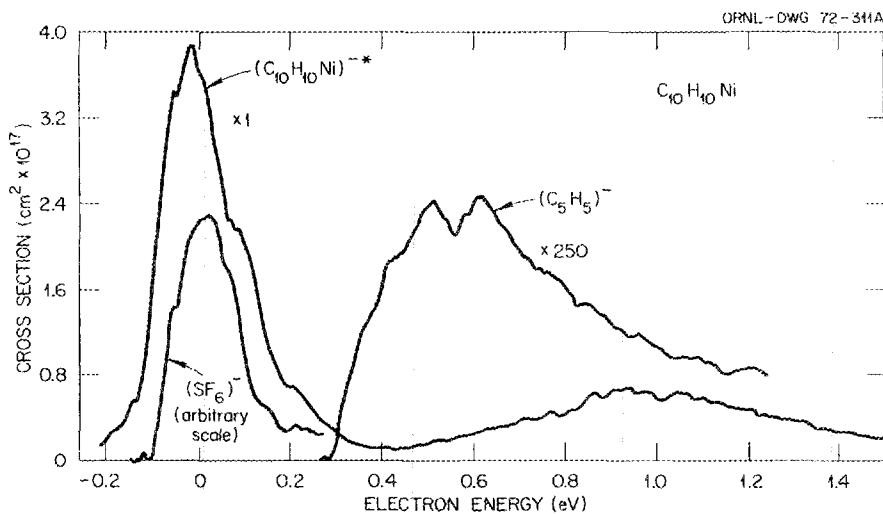


Fig. 4.3. Cross sections for production of parent negative ions ( $C_{10}H_{10}Ni^-$ ) and cyclopentadienyl negative ions ( $C_5H_5^-$ ) by electron impact upon nickelocene.

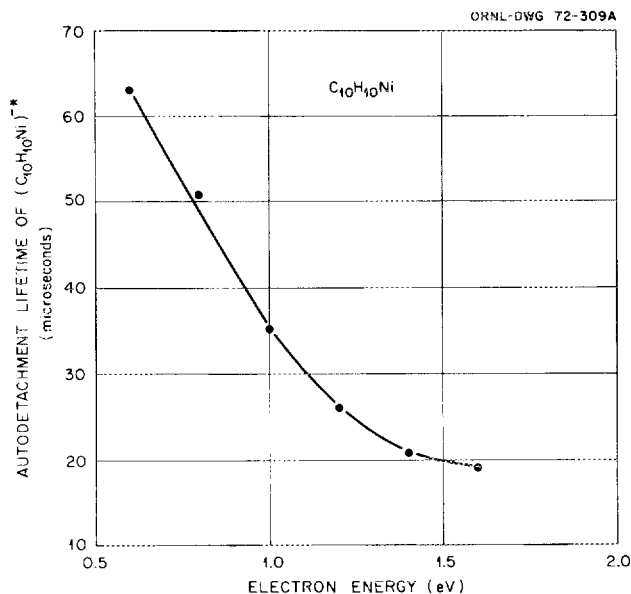


Fig. 4.4. Autodetachment lifetime of  $C_{10}H_{10}Ni^{-*}$  as a function of electron energy.  $C_{10}H_{10}Ni^{-*}$  is produced by unimolecular electron attachment to nickelocene.

decreased with increasing electron energy as shown in Fig. 4.4. Assuming that the incident electron is trapped by vibrational excitation of the ions and that unfavorable Franck-Condon factors account for the long lifetime, this marked variation in autodetachment lifetimes is being scrutinized by our previous theoretical model<sup>7</sup> of long-lived negative ions. This work was done in collaboration with H. M. Begun of the ORNL Chemistry Division.

#### ELECTRON ATTACHMENT TO ORGANIC MOLECULES

An investigation of electron attachment to several cyclic anhydrides has led to three very interesting discoveries. First, metastable negative ions have been observed which "explode" following the loss of an electron through autodetachment. Second, both parent and fragment negative ions have been observed whose lifetimes depend upon the energy of the bombarding electron. Third, cross sections for dissociative electron attachment have been observed which are as large as the attachment cross section of  $SF_6$  ( $\sim 10^{14} \text{ cm}^2$ ).

The cyclic anhydrides which have been studied are succinic, perfluorosuccinic, maleic, glutaric, perfluoroglutaric, phthalic, pyromellitic, and *cis*-1,2-cyclobutane-

dicarboxylic anhydride. All of these molecules contain the



group as part of a five- or six-member ring which may be attached to other rings. Parent negative ions were observed through the attachment of thermal electrons to maleic (284  $\mu\text{sec}$ ), phthalic (313  $\mu\text{sec}$ ), and pyromellitic anhydride ( $>8 \times 10^3 \mu\text{sec}$ ). The figure in parentheses is the lifetime of the preceding parent negative ions as measured at the peak of the cross section. The lifetimes of  $C_4H_2O_3^-$  (maleic) and  $C_8H_4O_3^-$  (phthalic) were found to decrease with an increase in the energy of the attaching electron.

The most abundant negative-ion fragments produced through dissociative electron attachment of several of the cyclic anhydrides are those in which CO is ejected from the parent molecule. Thus,  $C_2H_4CO_2^-$  (succinic),  $C_2F_4CO_2^-$  (perfluorosuccinic),  $C_2H_2CO_2^-$  (maleic),  $C_3H_6CO_2^-$  (glutaric),  $C_3F_6CO_2^-$  (perfluoroglutaric), and  $C_4H_6CO_2^-$  (cyclobutanedicarboxylic) ions were the most abundant negative ions observed from the anhydrides indicated in the parentheses. Cross sections for their production range from  $10^{-14} \text{ cm}^2$  for the perfluoro compounds to  $8 \times 10^{-19} \text{ cm}^2$  for maleic anhydride. These ions are composed of  $CO_2$  and either a hydrocarbon or a fluorocarbon. Lifetimes of the ions have been found to range from 58  $\mu\text{sec}$  for  $C_2H_2CO_2^-$  to more than 5000  $\mu\text{sec}$  for  $C_2F_4O_3^-$ . Studies of these ions are not complete, but additional data are included here on  $C_2H_4CO_2^-$ .

The lifetime of metastable  $C_2H_4CO_2^-$  varies with the energy of the bombarding electron as shown in Fig. 4.5. In making these lifetime measurements, a time-of-flight mass spectrometer was used to separate the time-of-arrival pulses for neutral and charged components. Using this technique it was noticed that the neutral peak was much broader than the ion peak (see Fig. 4.6). The relative intensities of the two peaks are not pressure-dependent, thereby indicating that collisional detachment is not involved. The only plausible explanation is that autodetachment occurs in the flight tube and that the  $C_2H_4CO_2$  fragment dissociates into two neutral molecules,  $C_2H_4$  and  $CO_2$ , which have sufficient kinetic energy to broaden the time-of-arrival pulse. Theoretical analyses of the shapes of the neutral peaks are used to determine the kinetic energies of the dissociation fragments. These dissociation energies are around 0.3 eV. Thus, the above electron attachment-detachment process is one in which a slow electron can

7. R. N. Compton et al., *J. Chem. Phys.* **45**, 4634 (1966).

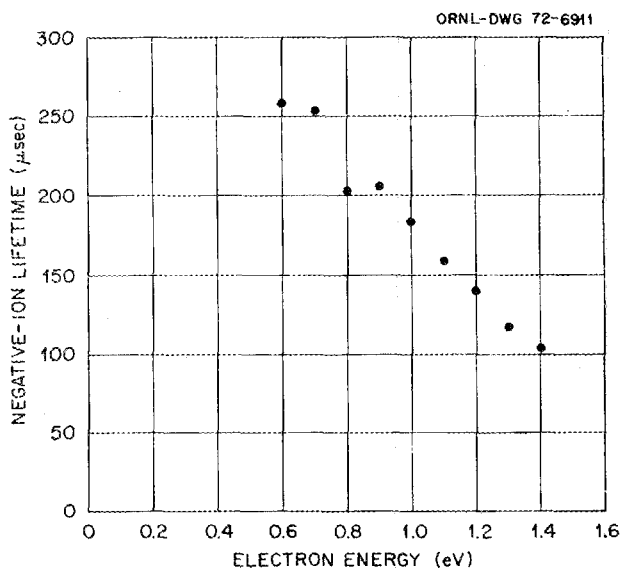


Fig. 4.5. Autodetachment lifetime for  $C_2H_4CO_2^-$  from succinic anhydride ( $C_4H_4O_3$ ).

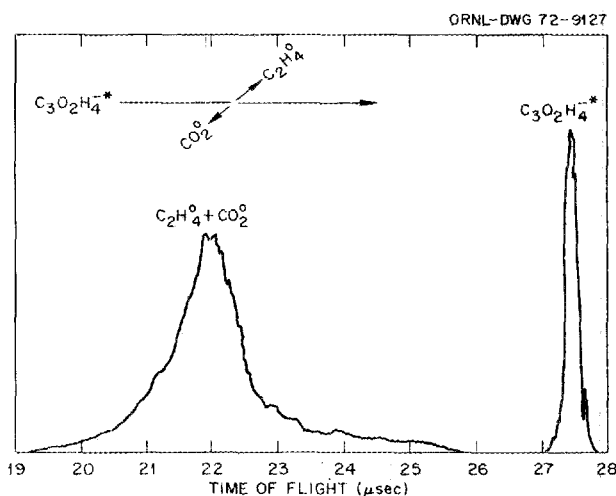


Fig. 4.6. Time-of-flight distributions of metastable negative ions ( $C_3O_2H_4^*$ ) and neutral ( $C_2H_4^0 + CO_2^0$ ) beams produced by dissociative electron attachment to succinic anhydride.

cause a molecule to explode into the fragments CO,  $CO_2$ , and a hydrocarbon. Table 4.2 summarizes some of the results of electron attachment to this series of anhydrides.

### CHEMI-IONIZING COLLISIONS

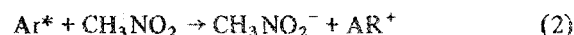
Long-lived highly excited states (Rydberg states) of the rare-gas atoms have been shown to react with molecules with extremely high cross sections of the

order of  $10^{-12} \text{ cm}^2$ .<sup>8</sup> The general form of the reaction is



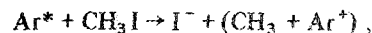
with possible variants involving products such as  $XA^+$  and/or free electrons. In both radiation chemistry and plasma physics, electron-ion recombination into high Rydberg states is probable, and the collisions of these ionizing species may be of great importance.

Figure 4.7 shows the progress in time of the reaction



observed using a pulsed electron beam to form  $Ar^*$  coupled to a time-of-flight mass spectrometer.<sup>9</sup> For the  $CH_3NO_2$  pressure used, the process is saturated (i.e., addition of further  $CH_3NO_2$  does not result in a higher  $CH_3NO_2^-$  level), indicating that all, or almost all, of the excited Ar atoms are colliding and have reacted with  $CH_3NO_2$  by the time the curve reaches its plateau value. On the assumption that this plateau value represents the original  $Ar^*$  level, we obtain an extremely high rate constant for the process of the order of  $10^{-6} \text{ molecule}^{-1} \text{ cm}^3 \text{ sec}^{-1}$ . Even if the rate constant were an order of magnitude smaller the importance of this type of process can hardly be overemphasized. Figure 4.8 shows the dependence of the observed  $CH_3NO_2^-$  current on Ar pressure over a range of electron energies and indicates that for sufficiently high argon pressures the  $CH_3NO_2^-$  current again approaches a constant level. This appears to be related to loss of  $Ar^*$  through a self-quenching process, indicating that the rate constant above should be regarded as an upper limit.

Similar studies have been made of  $Ar^*$  collisions with  $CH_3I$ ,  $C_2H_2$ ,  $C_6H_5Cl$ ,  $N_2O$ , and  $CH_3Br$ . In the case of  $CH_3I$ ,  $I^-$  is produced through the reaction



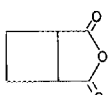
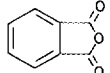
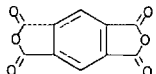
again with a rate constant in the  $10^{-6}$  to  $10^{-7} \text{ molecule}^{-1} \text{ cm}^3 \text{ sec}^{-1}$  region. A study of reaction (2) with krypton replacing argon was also made.

It would clearly be extremely important in radiation physics and chemistry if reactions of this sort occurred quite generally between molecules. Some study of this

8. H. Hottop and A. Niehaus, *J. Chem. Phys.* **47**, 2406 (1967); T. Sugiura and K. Arakawa, *Proceedings of the International Conference on Mass Spectrometry, Kyoto, 1969*, University Park, 1969, p. 848.

9. J. A. D. Stockdale, R. N. Compton, and P. W. Reinhardt, *Phys. Rev.* **184**, 81 (1969).

Table 4.2. Prominent negative ions produced by electron attachment to selected cyclic anhydrides

Compound	Structure	Negative ion	Maxima positions	Lifetime at peak cross section ( $\mu\text{sec}$ )	Approximate cross section ( $\times 10^{18}$ )
Succinic anhydride		$\text{C}_2\text{H}_4\text{CO}_2^-$	1.1 eV	150 <sup>a</sup> d	29
Also deuterated sample		$\text{C}_2\text{D}_4\text{CO}_2^-$	1.1 eV	150 <sup>a</sup> d	
Maleic anhydride		$\text{C}_4\text{O}_3\text{H}_2^-$	0 eV	248 <sup>a</sup> p	33
		$\text{C}_2\text{H}_2\text{CO}_2^-$	2.3 eV	58 d	0.8
		$\text{C}_2\text{H}_2\text{CO}^-$	2.8 eV	40 d	0.3
Glutaric anhydride		$\text{C}_3\text{H}_6\text{CO}_2^-$	0.9 eV	840 <sup>a</sup>	65
<i>cis</i> -1,2-Cyclobutanedicarboxylic anhydride		$\text{C}_4\text{H}_6\text{CO}_2^-$	1.5 eV	275 <sup>a</sup> d	11
Phthalic anhydride		$\text{C}_8\text{H}_4\text{O}_3^-$	0 eV	313 <sup>a</sup> p	
		$\text{C}_6\text{H}_4\text{CO}_2^-$	2.9 eV	Very weak	
Pyromellitic anhydride		$\text{C}_{10}\text{H}_2\text{O}_6^-$	0 eV	$8 \times 10^3$ p	
		$\text{C}_8\text{H}_2\text{O}_3\text{CO}_2^-$		Very weak	

<sup>a</sup>Lifetime depends on energy of bombarding electron; p – parent ion; d – ion dissociates following autodetachment.

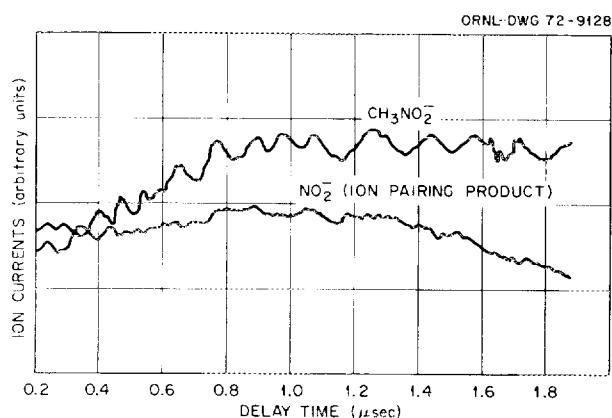
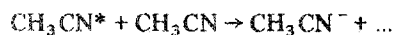


Fig. 4.7. Recorder trace showing the progress in time of the reaction  $\text{Ar}^* + \text{CH}_3\text{NO}_2 \rightarrow \text{CH}_3\text{NO}_2^- + \text{Ar}^+$ . An  $\text{NO}_2^-$  trace [from the ion-pairing process  $e + \text{CH}_3\text{NO}_2 \rightarrow (\text{CH}_3^+) + \text{NO}_2^-$ ] is included for comparison with the rising  $\text{CH}_3\text{NO}_2^-$  product. The data shown are for a  $0.4\text{-}\mu\text{sec}$  electron gate pulse width and were taken at an electron energy of 19 eV. The  $\text{CH}_3\text{NO}_2$  pressure was  $0.8 \times 10^{-4}$  torr; the Ar pressure,  $3.0 \times 10^{-4}$  torr.

possibility has been made. Collisions of  $\text{H}_2\text{O}^*$ , cyclohexane\*, and  $\text{CH}_4^*$  with both  $\text{CH}_3\text{NO}_2$  and  $\text{CH}_3\text{CN}$  have been investigated. Here complicating factors arise from the presence of negative ions (produced through ion pairing) which may charge-exchange with  $\text{CH}_3\text{NO}_2$  and  $\text{CH}_3\text{CN}$ , and from the presence of certain dissociative electron attachment resonances which may scavenge electrons which have lost some of their energy through molecular excitation. Nevertheless, evidence has been obtained which indicates that this process is probably of general occurrence. In the case of  $\text{H}_2\text{O}-\text{CH}_3\text{NO}_2$  mixtures, for instance, both  $\text{CH}_2\text{NO}_2^-$  and  $\text{CH}_3\text{NO}_2^-$  ions are observed in the vicinity of and above the ionization potential of  $\text{H}_2\text{O}$ . Water has two dissociative electron attachment resonances producing  $\text{H}^-$  (at 6.5 and 8.6 eV), and both  $\text{CH}_2\text{NO}_2^-$  and  $\text{CH}_3\text{NO}_2^-$  are observed to be produced through  $\text{H}^-$  collisions at these energies. Further, they appear to be produced in the same ratio at the two  $\text{H}^-$  resonances, but at higher energies (above the ionization potential)

$\text{CH}_3\text{NO}_2^-$  is produced at a relatively faster rate than  $\text{CH}_2\text{NO}_2^-$ , indicating that an additional production mechanism is operating here. Other evidence indicates that this is not due to a difference in  $\text{O}^-$  reaction rates. The observation of Sugiura and Arakawa<sup>b</sup> that  $\text{CH}_3\text{CN}^-$  may be produced through the reaction



has been confirmed.

### ION CONDENSATION REACTIONS IN BENZENE VAPOR

Studies of the rates of formation and decay of the condensation products  $\text{AB}^\pm$  in reactions of the type



are of considerable interest in chemical kinetics. Frequently such activated complexes have lifetimes too short for observation by present methods, but in a number of cases complexes do last long enough for information to be obtained.

The pulsed electron source time-of-flight mass spectrometer method<sup>9</sup> has been used to study thermal energy condensation reactions of  $\text{C}_6\text{H}_6^+$ ,  $\text{C}_6\text{H}_5^+$ , and  $\text{C}_6\text{H}_4^+$  with the benzene molecule. Rate constants for formation of the condensation products  $\text{C}_{12}\text{H}_{12}^+$ ,  $\text{C}_{12}\text{H}_{11}^+$ , and  $\text{C}_{12}\text{H}_{10}^+$  have been measured for several electron impact energies (see Table 4.3). An upper limit of 150  $\mu\text{sec}$  has been obtained for the lifetime against

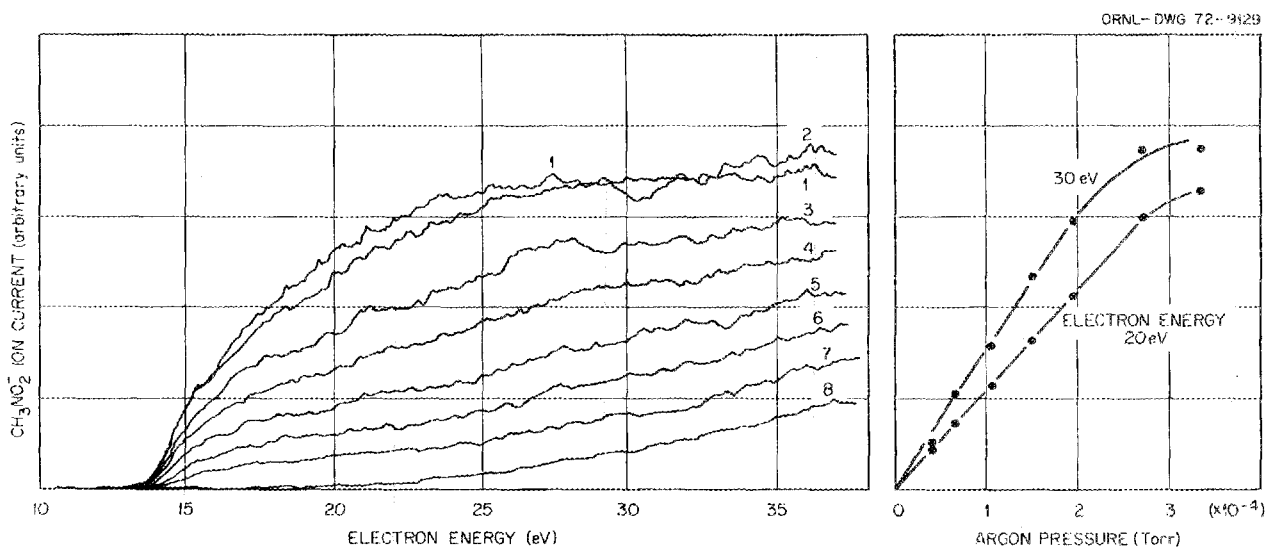


Fig. 4.8. The variation of  $\text{CH}_3\text{NO}_2^-$  ion current with electron impact energy and Ar pressure. All curves are for  $1.35 \times 10^{-4}$  torr  $\text{CH}_3\text{NO}_2$  and a 5- $\mu\text{sec}$  electron gate pulse. The circled figures refer to the following Ar pressures: (1)  $3.53 \times 10^{-4}$  torr, (2)  $2.7 \times 10^{-4}$ , (3)  $1.95 \times 10^{-4}$ , (4)  $1.5 \times 10^{-4}$ , (5)  $1.05 \times 10^{-4}$ , (6)  $0.65 \times 10^{-4}$ , (7)  $0.4 \times 10^{-4}$ , (8) zero.

Table 4.3. Thermal-energy ion condensation reactions in benzene vapor

Reaction	Rate constant $k$ (molecules <sup>-1</sup> cm <sup>3</sup> sec <sup>-1</sup> )			Lifshitz and Reuben <sup>a</sup>	Field, Hamlet, and Libby <sup>b</sup>
	$E_e = 20$ eV	$E_e = 30$ eV	$E_e = 50$ eV		
$\text{C}_6\text{H}_6^+ + \text{C}_6\text{H}_6 \rightarrow \text{C}_{12}\text{H}_{12}^+$	$7 \times 10^{-12}$	$1.2 \times 10^{-11}$	$1.3 \times 10^{-11}$	Not observed	$7 \times 10^{-12}$
$\text{C}_6\text{H}_5^+ + \text{C}_6\text{H}_6 \rightarrow \text{C}_{12}\text{H}_{11}^+$	$4.3 \times 10^{-10}$	$3.0 \times 10^{-10}$	$3.9 \times 10^{-10}$	$1.17 \times 10^{-10}$	
$\text{C}_6\text{H}_5^+ + \text{C}_6\text{H}_6 \rightarrow \text{C}_{12}\text{H}_{11}^+ \rightarrow \text{C}_{12}\text{H}_9^+ + \text{H}_2$	$7.5 \times 10^{-11}$	$4.7 \times 10^{-11}$	$7.9 \times 10^{-11}$	$4.37 \times 10^{-11}$	
$\text{C}_6\text{H}_5^+ + \text{C}_6\text{H}_6 \rightarrow \text{C}_{12}\text{H}_{11}^+ \rightarrow \text{C}_{10}\text{H}_9^+ + \text{C}_2\text{H}_2$	$9.8 \times 10^{-11}$	$1.6 \times 10^{-10}$	$2.4 \times 10^{-10}$	$3.66 \times 10^{-11}$	
$\text{C}_6\text{H}_4^+ + \text{C}_6\text{H}_6 \rightarrow \text{C}_{12}\text{H}_{10}^+$	$1.2 \times 10^{-9}$	$4.7 \times 10^{-10}$	$3.2 \times 10^{-10}$	$1.27 \times 10^{-10}$	
$\text{C}_6\text{H}_4^+ + \text{C}_6\text{H}_6 \rightarrow \text{C}_{12}\text{H}_{10}^+ \rightarrow \text{C}_{12}\text{H}_8^+ + \text{H}_2$		$8.0 \times 10^{-11}$	$1.3 \times 10^{-10}$	$1.43 \times 10^{-11}$	

<sup>a</sup>C. Lifshitz and B. G. Reuben, *J. Chem. Phys.* **50**, 951 (1969).

<sup>b</sup>F. H. Field, P. Hamlet, and W. F. Libby, *J. Amer. Chem. Soc.* **89**, 6035 (1967).

dissociation of  $C_{12}H_{11}^+$ . Rate constants for formation of  $C_{12}H_9^+$  and  $C_{10}H_9^+$  (dissociation products of  $C_{12}H_{11}^+$ ) were also obtained. The rate constants shown in Table 4.3 and the reaction sequences observed are substantially in agreement with those obtained by Lifshitz and Reuben,<sup>10</sup> who, however, did not observe the formation of  $C_{12}H_{12}^+$  from thermal energy  $C_6H_6^+$ .

#### COLLISIONAL IONIZATION OF CESIUM BY MOLECULES: DETERMINATION OF ELECTRON AFFINITIES

Studies of chemi-ionizing collisions between fast cesium beams and molecules are yielding important new information on molecular electron affinities and structures of negative ions. The experiment consists of accurately determining the threshold energy (center-of-mass system) for production of a positive- and negative-ion pair, that is,  $Cs + M \rightarrow Cs^+ + M^-$ . Electron affinities for  $O_2$ ,  $NO$ ,  $NO_2$ , and  $N_2O$  have been determined to be  $0.46 \pm 0.05$ ,  $0.1 \pm 0.1$ ,  $2.3 \pm 0.1$ , and  $\geq -0.2$  eV, respectively. Because of the activation energy required to bend  $N_2O$  to form  $N_2O^-$  the electron affinity determined for  $N_2O$  is expected to be only a lower limit. The technique has more recently been used to study a series of complex molecules: succinic anhydride, maleic anhydride, sulfur hexafluoride, and tellurium hexafluoride. Preliminary electron affinities for  $SF_6$ ,  $TeF_6$ , and maleic anhydride have been determined to be  $0.4 \pm 0.2$ ,  $3.4 \pm 0.2$ , and  $1.5 \pm 0.3$  eV, respectively.

Figure 4.9 shows the relative cross section for production of  $SF_6^-$ ,  $SF_5^-$ , and  $F^-$ . Collisions of neutral cesium with maleic anhydride produced  $C_4H_2O_3^-$ ,  $C_3H_2O_2^-$ ,  $C_3H_2O^-$ , and  $CO_2^*$ . Correspondingly,  $C_3H_4O_2^-$  and  $CO_2^*$  were observed from succinic anhydride. The cross sections at thresholds for negative-ion production appear to be a step function for some but not all ions. Figure 4.10 illustrates this for succinic anhydride. In general, the thresholds are within 0.2 eV of those observed for the same negative ions obtained by dissociative electron attachment. Parent negative ions of maleic anhydride were observed to be stable, and a preliminary measurement of the threshold gives the electron affinity of maleic anhydride to be  $\sim 1.5$  eV. The mean lifetime of  $CO_2^*$  was measured to be the same ( $60 \pm 10 \mu\text{sec}$ ) when produced by cesium collision with either maleic or succinic anhydride or by electron collision with maleic anhydride.

10. C. Lifshitz and B. G. Reuben, *J. Chem. Phys.* **50**, 951 (1969).

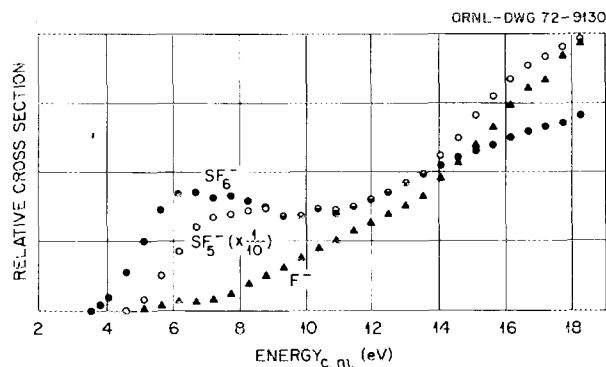


Fig. 4.9. Negative-ion production by collisional ionization of cesium by sulfur hexafluoride.

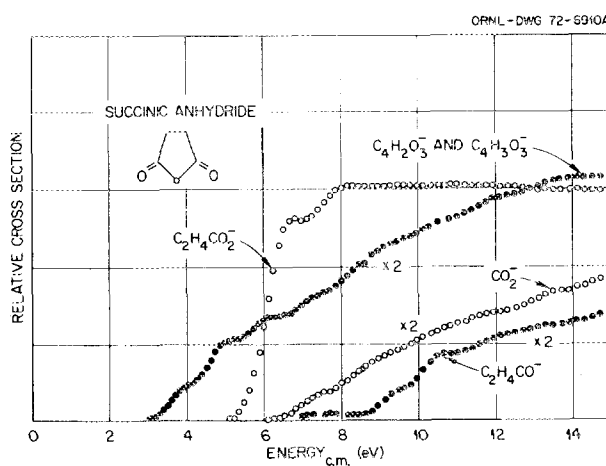


Fig. 4.10. Negative-ion production by collisional ionization of cesium by succinic anhydride.

#### LONGITUDINAL ELECTRON DIFFUSION COEFFICIENT AND ELECTRON DRIFT VELOCITY MEASUREMENTS IN WATER VAPOR

There have been no reliable measurements of electron diffusion and electron drift velocities in water vapor below an  $E/P = 20 \text{ V cm}^{-1} \text{ torr}^{-1}$ . The longitudinal diffusion coefficient  $D_L$  in most gases is usually less than the transverse diffusion coefficient  $D_T$ . For example, in  $H_2$ ,  $He$ ,  $N_2$ , and  $CO$ , the ratio of the transverse to the longitudinal diffusion coefficient is approximately a factor of 2, and in  $Ar$  the ratio is 7.<sup>11</sup> For water vapor, however, recent theoretical predic-

11. E. B. Wagner, F. J. Davis, and G. S. Hurst, *J. Chem. Phys.* **47**, 3138 (1967).

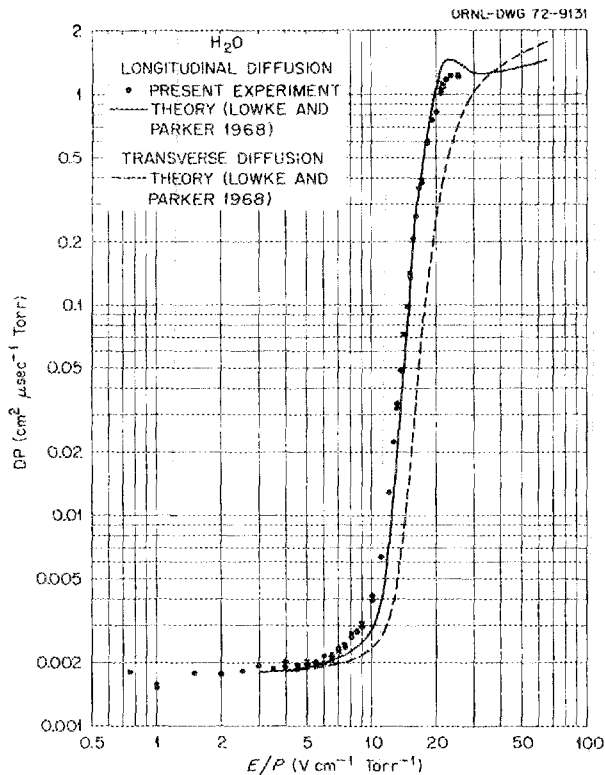


Fig. 4.11. Measurements of the longitudinal diffusion coefficients of electrons in water vapor compared with the theoretical calculations of Lowke and Parker.

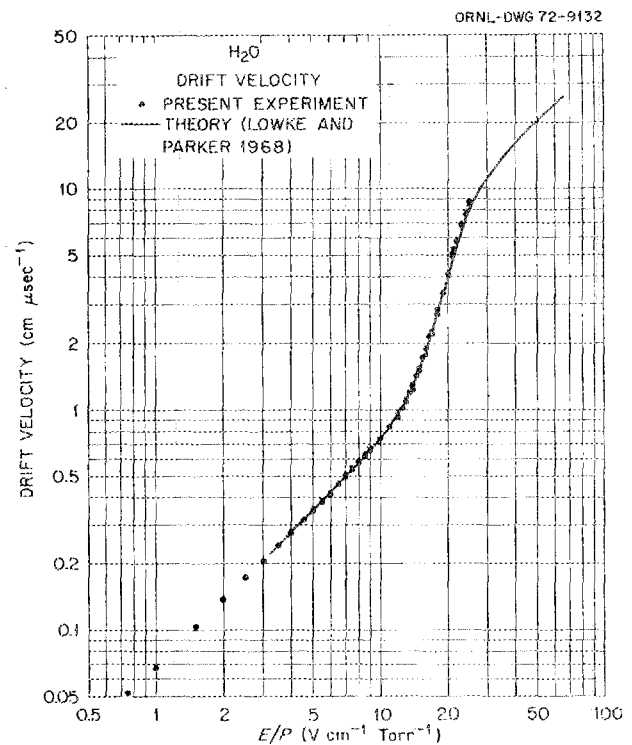


Fig. 4.12. Measurements of electron drift velocity in water vapor compared with the theoretical predictions of Lowke and Parker.

tions<sup>12</sup> indicate that the longitudinal diffusion coefficient is larger than the transverse. The measurements of  $D_L$  and drift velocity  $w$  were made using the time-of-flight method described earlier.<sup>11</sup> Our experimental values of  $D_L$  are compared with the theoretical values of Lowke and Parker<sup>12</sup> in Fig. 4.11. The experimental values of  $w$  compared with theoretical values of Lowke and Parker<sup>12</sup> are shown in Fig. 4.12 to be in very good agreement.

#### THERMAL AND NEAR-THERMAL ELECTRON TRANSPORT COEFFICIENTS IN O<sub>2</sub> DETERMINED WITH A TIME-OF-FLIGHT SWARM EXPERIMENT USING A DRIFT-DWELL-DRIFT TECHNIQUE

The drift-dwell-drift (DDD) or pulsing technique has been successfully applied to the study of low-energy electron transport coefficients in oxygen in spite of significant attachment at these energies. A thermal value of the electron diffusion coefficient times pres-

sure  $DP = 1.20 \pm 0.11 \text{ cm}^2 \mu\text{sec}^{-1} \text{ torr}$  was determined. This  $DP$  value corresponds to a momentum-transfer cross section  $Q_m = 0.82 \times 10^{-16} \text{ cm}^2$  at an energy  $\epsilon = 0.0258 \text{ eV}$  if it is assumed that  $Q_m \propto \epsilon^{1/2}$ . This thermal value of  $Q_m$  is about 40% lower than the lowest values reported from other techniques.

#### CHLORINE GAS EVOLUTION FROM IRRADIATED ROCK SALT

One question concerning the storage of radioactive wastes in salt mine repositories has to do with the generation of chlorine gas by gamma irradiation of NaCl. An experiment is in progress to search for gas evolution from irradiated rock salt. A quadrupole mass spectrometer capable of detecting  $10^{-15} \text{ mm Hg}$  residual gas pressures is pumped by a 200-liter/sec Vac-Ion pump to pressures below  $1 \times 10^{-9} \text{ torr}$ . Salt samples are sealed into Pyrex ampules at pressures of  $1 \times 10^{-9} \text{ torr}$  and irradiated by 2-MeV electrons from an electron accelerator to total doses of  $2 \times 10^{10} \text{ rads}$ . The glass ampules are smashed under high vacuum, and the mass peaks at  $^{35}\text{Cl}^+$ ,  $^{37}\text{Cl}^+$ ,  $^{35}\text{Cl}^{35}\text{Cl}^+$ ,  $^{35}\text{Cl}^{37}\text{Cl}^+$ ,

12. J. J. Lowke and J. H. Parker, *Phys. Rev.* **181**, 302 (1969).

and  $^{37}\text{Cl}^{37}\text{Cl}^+$  are monitored. No increases in these mass peaks were observed over those noted for unirradiated samples. These preliminary results are taken to indicate that no appreciable  $\text{Cl}_2$  gas is evolved from the irradiated salt. Similar experiments using salt which has been irradiated by gamma rays from spent fuel cells from the High-Flux Isotope Reactor are in progress. Experiments are also under way to determine quantitatively the amount of chlorine atom sputtering from salt samples irradiated by electron impact under high vacuum.

---

13. J. G. Skofronick, J. P. Aldridge, D. B. Greene, and R. N. Compton, *Bull. Amer. Phys. Soc.* **17**(2), 202 (1972).

**FLORIDA STATE UNIVERSITY—  
OAK RIDGE NATIONAL LABORATORY  
CHEMICAL ACCELERATOR**

An accelerator for producing fast (500 eV to 10 keV) neutral beams of a class of large molecules has been constructed at Florida State University in a cooperative effort with ORNL. The machine has successfully produced neutral beams of  $\text{SF}_6$ ,  $\text{C}_7\text{F}_{14}$ ,  $\text{CO}_2$ , and others with energy resolution ( $\Delta E/E$ ) of better than 1/100. Energy-loss processes are being studied by a time-of-flight method using a 4-m flight path, and a mass spectrometer is now being installed in the interaction region to examine reaction products. A preliminary report on the machine has been presented.<sup>13</sup>

## 5. Atomic and Molecular Radiation Physics

L. G. Christophorou

V. E. Anderson <sup>1</sup>	A. Hadjiantoniou <sup>4</sup>
J. B. Birks <sup>2</sup>	J. A. Harter
R. P. Blaunstein <sup>2</sup>	P. D. Kidd <sup>4</sup>
Ada E. Carter	C. E. Klots
J. G. Carter	D. L. McCorkle <sup>5</sup>
J. T. Cox	M. N. Pisanias <sup>4</sup>
C. E. Easterly <sup>3</sup>	D. Pittman
R. E. Goans <sup>3</sup>	

### INTERMEDIATE PHASE STUDIES FOR UNDERSTANDING RADIATION INTERACTION WITH CONDENSED MEDIA: THE ELECTRON ATTACHMENT PROCESS

Intermediate phase studies, namely, studies of radiation processes and effects as well as physicochemical reactions at densities between those corresponding to low-pressure gases and liquids, are fundamentally necessary for the development of a coherent understanding of radiation interaction with matter. There is a need for uniting our knowledge on radiation processes occurring in low-pressure gases with those in the condensed phase.

Our effort to bridge the existing gap between our knowledge on electron-molecule interaction processes in gases and liquids continued. A comprehensive study has been completed<sup>6</sup> where existing gaseous data on electron attachment have been successfully related to hydrated-electron-molecule reaction rates. On the basis of the current knowledge of electron attachment processes in gases, reaction rates for a number of molecules with the hydrated electron have been predicted.<sup>6</sup>

In an effort to further link together knowledge on electron attachment processes occurring in low-pressure gases with those in the condensed phase, a special

apparatus has been designed and built. This apparatus is presently in operation and allows electron attachment studies to be performed in the pressure range 0.5 to ~80 atm, thus bridging the density gap between low-pressure gases and liquids. The first experimental data of this nature have been obtained. Electron attachment to O<sub>2</sub> molecules in O<sub>2</sub>-N<sub>2</sub> mixtures has been studied as a function of N<sub>2</sub> pressure in the range 300 to 10,000 torrs. In Fig. 5.1 the rate of electron attachment to O<sub>2</sub> in O<sub>2</sub>-N<sub>2</sub> mixtures is plotted as a function of the mean electron energy  $\langle \epsilon \rangle$  for O<sub>2</sub> pressures  $P_{O_2} \rightarrow 0$  and for N<sub>2</sub> pressures  $P_{N_2}$  as indicated in the figure. The attachment rates are seen to increase constantly with increasing  $P_{N_2}$ . Using the actual experimental data points (solid circles in Fig. 5.1) or the smoothed-out data (broken curves in Fig. 5.1), the attachment cross sections shown in Figs. 5.2 and 5.3 as closed and open circles, respectively, were obtained<sup>7</sup> by making use of the analytical methods we have described recently.<sup>8</sup> The continuous and gradual shift of the cross section functions toward thermal energies and the pronounced increase in their sharpness at near zero energies seen in Figs. 5.2 and 5.3 suggest that as the N<sub>2</sub> density increases, electron attachment to O<sub>2</sub> cannot be described solely by a three-body process where N<sub>2</sub> acts simply as a stabilizing third body in "distant" collisions. The observed changes in  $\sigma_a(\epsilon)$  seem to suggest that N<sub>2</sub> seriously perturbs the O<sub>2</sub><sup>-</sup> potential

1. On loan from Mathematics Division, ORNL.

2. Consultant.

3. USAEC Fellow in Radiation Science.

4. Graduate Student, University of Tennessee.

5. Postdoctoral Fellow from the University of Tennessee.

6. L. G. Christophorou and R. P. Blaunstein, *Chem. Phys. Lett.* **12**(1), 173 (1971).

7. D. L. McCorkle, L. G. Christophorou, and V. E. Anderson, *J. Phys. B (At. Mol. Phys.)* (in press).

8. L. G. Christophorou, D. L. McCorkle, and V. E. Anderson, *J. Phys. B (At. Mol. Phys.)* **4**, 1163 (1971).

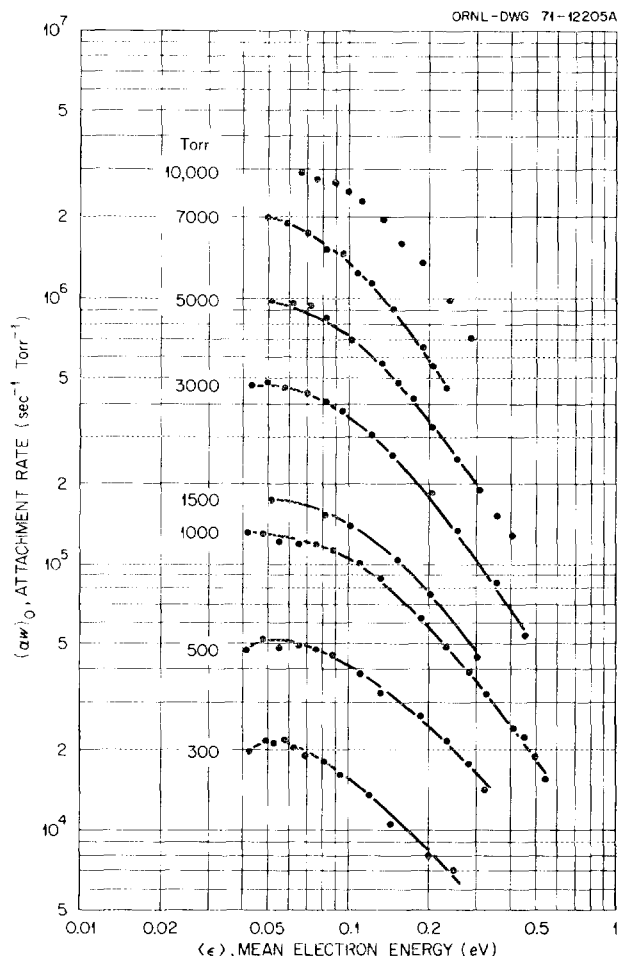
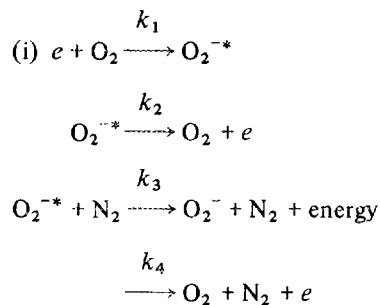


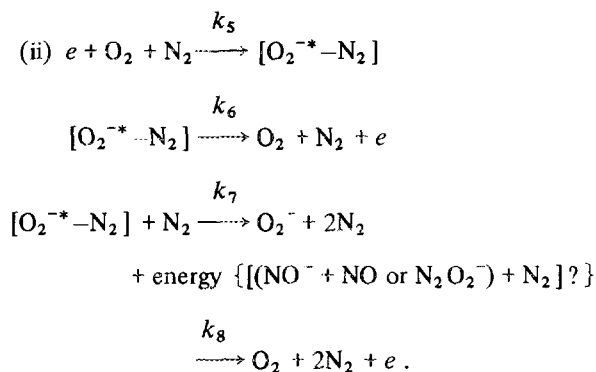
Fig. 5.1. Attachment rates  $(\alpha w)_0$ , extrapolated to zero  $O_2$  pressure, as a function of mean electron energy for various  $N_2$  pressures.

energy curves during capture with a net downward shift in what may be called "hard" or "sticky" collisions, the effect becoming more dominant the higher the  $N_2$  density. This brings to mind the familiar effect of solvation, which apparently seems to be important from these densities and above.

The data have been analyzed<sup>9</sup> on the assumption that electron attachment to  $O_2$  in  $O_2 \cdot N_2$  mixtures proceeds via the following two mechanisms:



and



The main difference between mechanisms i and ii is this: in mechanism i  $N_2$  is assumed to act simply as a stabilizing third body in "distant" collisions, not affecting the  $O_2^-$  potential energy curves, while in mechanism ii  $N_2$  is assumed to be involved in "hard," "sticky" collisions which result in a serious perturbation of the  $O_2^-$  potential energy curves during capture, with a possible formation of a transient complex  $[O_2^{-*} - N_2]$  which can be destroyed by autoionization (or collision) or lead to  $O_2^-$  upon collision with a second  $N_2$  molecule. At low pressures, mechanism i could, of course, be viewed as a one-step three-body attachment process involving "distant" collisions.

If mechanisms i and ii are taken to be plausible, the rate of change of the electron density due to electron capture by  $O_2$  can be expressed as

$$\begin{aligned}
 \frac{\partial n_e}{\partial t} = -\nu_a n_e = -k_1 n_{O_2} n_e \frac{k_3 n_{N_2}}{(k_3 + k_4) n_{N_2} + k_2} \\
 - k_5 n_{O_2} n_{N_2} n_e \frac{k_7 n_{N_2}}{(k_7 + k_8) n_{N_2} + k_6}. \quad (1)
 \end{aligned}$$

In Eq. (1)  $\nu_a$  is the overall attachment frequency,  $n_e$ ,  $n_{O_2}$ , and  $n_{N_2}$  are the number densities for electrons, oxygen, and nitrogen molecules, respectively, and  $k_1 \dots k_8$  are the rate constants for the processes considered in mechanisms i and ii. From Eq. (1) we have

$$\frac{(\alpha w)_0}{n_{N_2}} = \frac{k_1 k_3}{(k_3 + k_4) n_{N_2} + k_2} + \frac{k_5 k_7 n_{N_2}}{(k_7 + k_8) n_{N_2} + k_6}. \quad (2)$$

9. L. G. Christophorou, *J. Phys. Chem.* (in press).

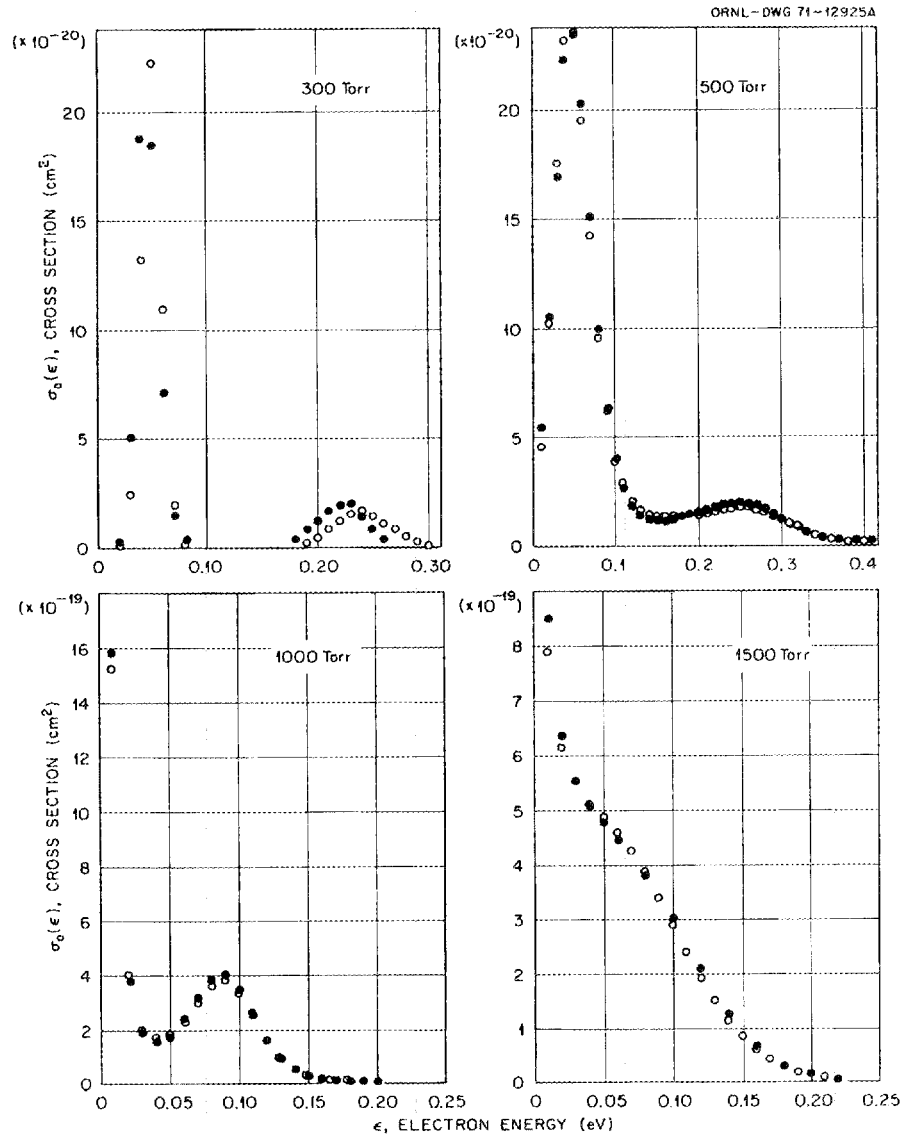


Fig. 5.2. Attachment cross sections for  $O_2$  in  $O_2-N_2$  mixtures, as a function of electron energy for  $N_2$  pressures of 300, 500, 1000, and 1500 torrs. The solid circles were obtained using the data points in Fig. 5.1 and the open circles using the smoothed-out data shown as broken curves in Fig. 5.1.

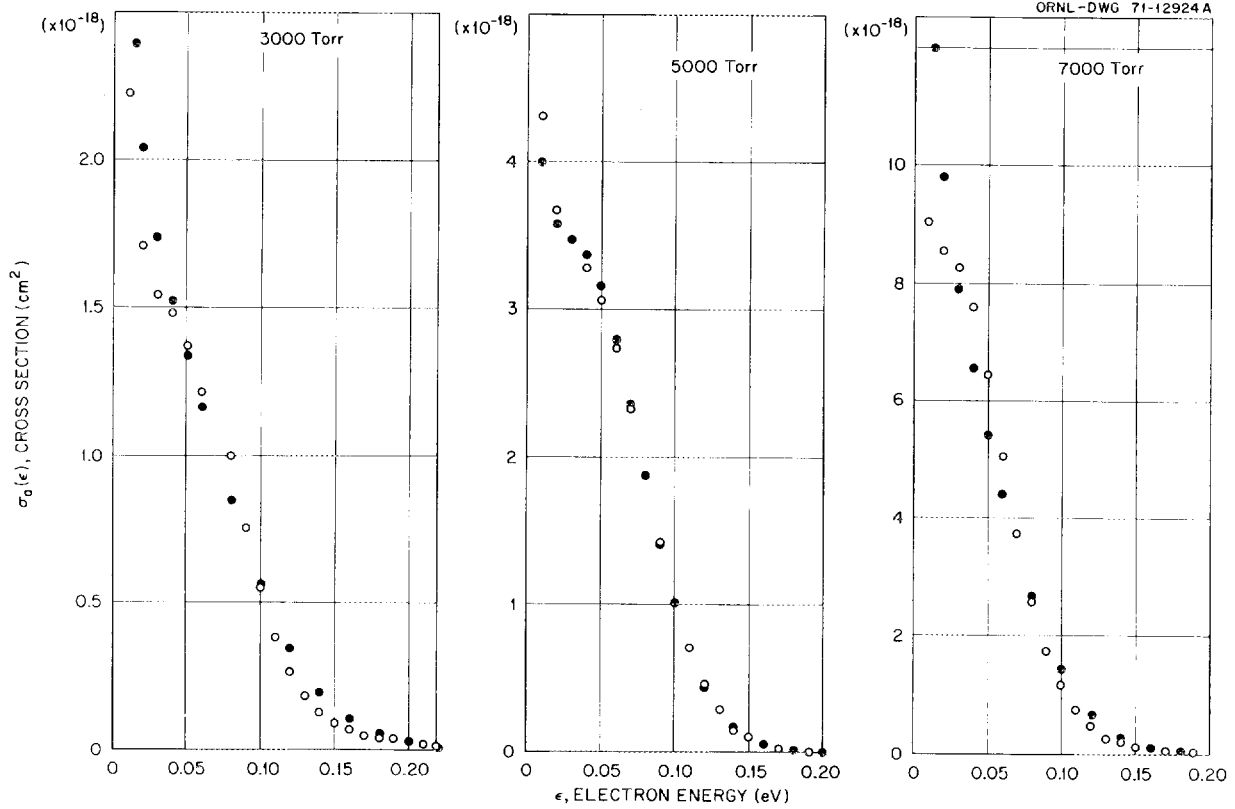


Fig. 5.3. Attachment cross sections for  $O_2$  in  $O_2-N_2$  mixtures as a function of electron energy for  $N_2$  pressures of 3000, 5000, and 7000 torrs. The solid circles were obtained using the data points in Fig. 5.1 and the open circles using the smoothed-out data shown as broken curves in Fig. 5.1.

If we now turn our attention to Fig. 5.4, where  $(\alpha w)_0/P_{N_2}$  is plotted as a function of  $P_{N_2}$ , we see that the experimental data can be represented by

$$\frac{(\alpha w)_0}{P_{N_2}} = A + BP_{N_2}, \quad (3)$$

where  $A$  and  $B$  are constants. Considering that  $n_{N_2} \propto P_{N_2}$ , Eq. (3) is consistent with Eq. (2) when

$$(k_3 + k_4)n_{N_2} \ll k_2$$

and

$$(k_7 + k_8)n_{N_2} \ll k_6. \quad (4)$$

If we now assume that the cross section for  $O_2^{-*}-N_2$  collisions is given by the Langevin expression for spiraling collisions, we obtain for the average time between  $O_2^{-*}-N_2$  collisions at 7000 torrs ( $T = 298^\circ K$ ) the value of  $\sim 4 \times 10^{-12}$  sec. Hence, we have for the

autoionization lifetime  $\tau_a(O_2^{-*})$  of  $O_2^{-*}$

$$\tau_a(O_2^{-*}) = k_2^{-1} < [(k_3 + k_4)n_{N_2}]^{-1} \approx 4 \times 10^{-12} \text{ sec}. \quad (5)$$

This value lies within the limits established by McCorkle, Christophorou, and Anderson.<sup>7</sup>

Similarly, from the second inequality (4) an upper limit to the autoionization lifetime of  $[O_2^{-*}-N_2]$  can be estimated which is of the same order of magnitude as that for  $\tau_a(O_2^{-*})$ .

From a least-squares fitting to the data in Fig. 5.4 we have

$$\frac{(\alpha w)_0}{P_{N_2}} = 88.3 + 0.025P_{N_2}. \quad (6)$$

Hence,

$$\frac{k_1 k_3}{k_2} \approx 88.3 \text{ sec}^{-1} \text{ torr}^{-2}$$

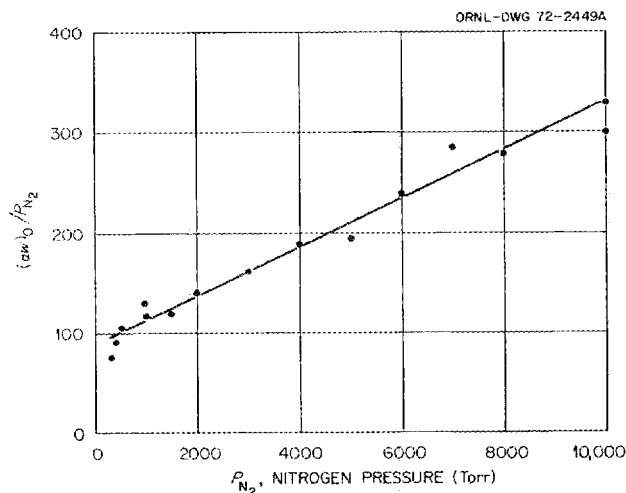


Fig. 5.4.  $(\alpha w)_0/P_{N_2}$  vs  $P_{N_2}$ . The values of  $(\alpha w)_0$  plotted are those for  $\langle \epsilon \rangle \approx 0.05$  eV, which basically correspond to the maximum value of  $(\alpha w)_0$  at each  $P_{N_2}$ .

and

$$\frac{k_5 k_7}{k_6} \approx 0.025 \text{ sec}^{-1} \text{ torr}^{-3}.$$

If it is assumed that Eqs. (2) and (3) hold over all  $N_2$  densities up to that ( $0.81 \text{ g/cm}^3$ ) of liquid  $N_2$ , from Eq. (6) we find that

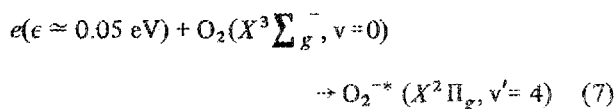
$$(\alpha w)_0(\epsilon \approx 0.04 \text{ eV}) \approx 0.74 \times 10 \text{ sec}^{-1} \text{ torr}^{-1}$$

for  $O_2$  in liquid  $N_2$ . This value compares well with the value ( $1.11 \times 10^{10} \text{ sec}^{-1} \text{ torr}^{-1}$ ) one obtains from  $\pi\lambda^2$ , where  $\lambda = \hbar/2\pi$  is the de Broglie wavelength for a 0.04-eV electron. This is an interesting observation and may indicate that mechanisms i and ii describe reasonably well the process of electron capture by  $O_2$  in the presence of  $N_2$  throughout the whole range of  $N_2$  densities up to that of the liquid. Efforts are in progress to investigate this by finding out the range of  $P_{N_2}$  over which a plot such as in Fig. 5.4 holds.

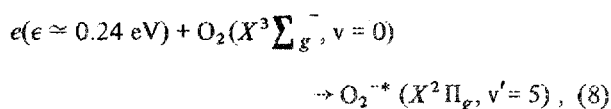
Studies of high-pressure electron attachment (electron-molecule interaction processes in general) are experimentally very difficult, the detailed analyses are obscured by the complexities of high densities and the lack of direct information as to the products formed, and any generalizations have to take careful account of the effects of many specific environments on a given process; still, such studies are important in efforts to relate and unite our knowledge on radiation interactions with low-pressure gases and with condensed media.

### STRUCTURE IN THE CROSS SECTION FOR CAPTURE OF SLOW ( $<0.5$ eV) ELECTRONS BY $O_2$ TO FORM $O_2^-$

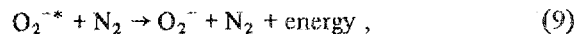
As can be seen from Fig. 5.2 the absolute cross section for the formation of  $O_2^-$  from  $O_2$  as a function of electron energy from  $\frac{3}{2} kT$  to about 0.5 eV exhibits distinct structure. The two distinct peaks in the cross section function observed for the two lowest values of  $P_{N_2}$  (300 and 500 torr) at 0.05 and 0.24 eV are interpreted,<sup>7,9</sup> respectively, as being due to the processes



and



that is, capture of the electron into the fourth and fifth vibrational levels of  $O_2^-$  from the  $v=0$  vibrational level of  $O_2$ , with a subsequent stabilization of  $O_2^{*-}$  by an  $N_2$  molecule, namely,



where the  $N_2$  molecule acts simply as an agent for removing excess energy.

### LIFETIMES OF LONG-LIVED POLYATOMIC NEGATIVE IONS

Systematic time-of-flight mass spectrometric studies have been made of key groups of organic molecules directly involved in biological reactions (e.g.,  $NO_2^-$  and O-containing aromatic molecules, amino acids, aldehydes, and quinones). For all molecules investigated the cross section for parent negative-ion formation peaked at about 0.0 eV. For quite a number of them, such as *o*-nitrophenol (see Fig. 5.5) and *o*-nitroaniline, the parent negative-ion lifetime has been found to decrease drastically with increasing electron energy above  $\frac{3}{2} kT$ . The measured lifetimes are being related to the molecular structures involved, and the techniques are being used to locate the site ("electrophore") of electron capture in a polyatomic molecule.

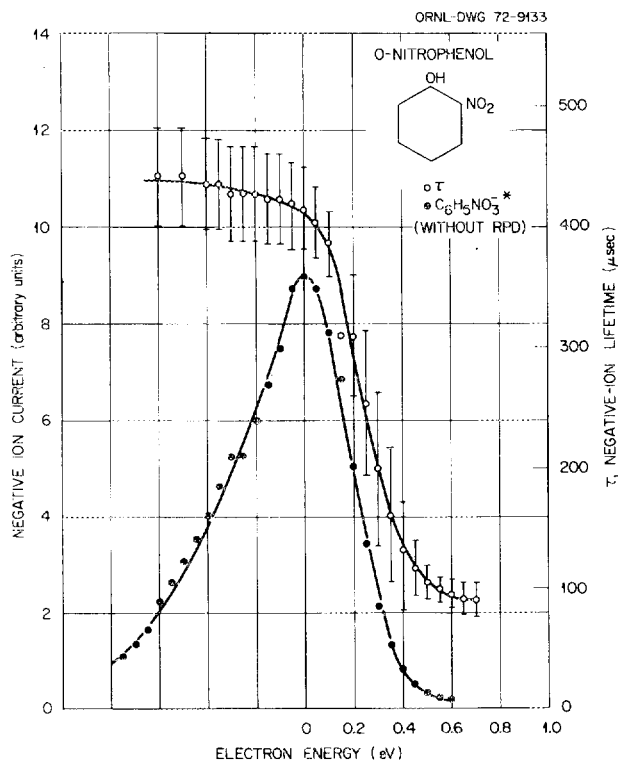


Fig. 5.5. Lifetimes of long-lived polyatomic negative ions. (○): Variation of the *o*-nitrophenol parent negative-ion lifetime with incident electron energy  $\epsilon$ . The data plotted are the average of seven runs; (●): variation of the *o*-nitrophenol parent negative-ion current (without the retarding potential difference) with incident electron energy; the data plotted are the average of six runs.

### UNIMOLECULAR DECOMPOSITIONS

The consequences of a recent reformulation of unimolecular decomposition theory have been pursued further. Especially simple formulas for calculating the rates of decomposition reactions and excess-energy disposal in the products have been obtained.<sup>10</sup> One of the most remarkable features to emerge is the effect of long-range forces on the number of bound states available to a molecular ion. The number of these states increases enormously near a dissociation threshold, as illustrated in Fig. 5.6, and serves to retard greatly the rate of an incipient reaction. Mass spectrometric data in the literature corroborate this effect.

### MOBILITIES OF THERMAL ELECTRONS IN GASES AND LIQUIDS

As part of our effort to relate studies on slow-electron-molecule interaction processes in low-pressure

10. C. E. Klots, *Z. Naturforsch.* (in press).

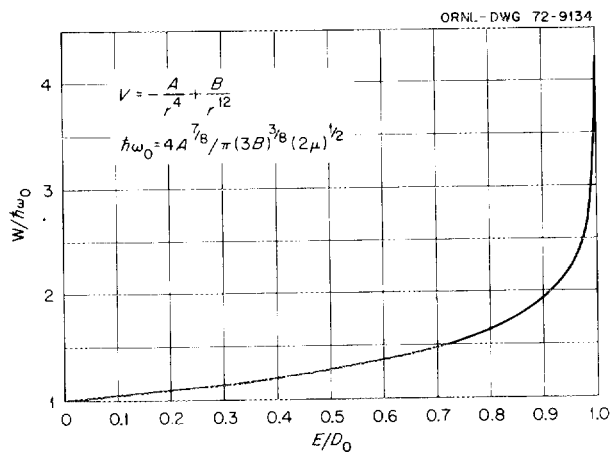


Fig. 5.6. Number of bound states of an anharmonic oscillator, normalized to that of a harmonic oscillator, as a function of energy measured from the potential minimum.

gases with studies on the same processes in condensed media, we have measured thermal ( $\sim 298^\circ\text{K}$ ) electron mobilities in a number of organic vapors for which similar measurements have been made by others in the liquid phase.

The variation of the electron drift velocity  $w$  with the pressure-reduced electric field  $E/P_{298}$  is presented in Fig. 5.7 for three groups of organic molecules: linear, cyclic, and branched hydrocarbons. These measurements were confined to the indicated low  $E/P$  regions for which  $w$  varies linearly with  $E/P_{298}$ , and thus the electron energy distribution function is Maxwellian. From a least-squares fit to the data in Fig. 5.7, the slopes

$$S \equiv \frac{w}{E/P}$$

were determined and are given in Table 5.1. In Table 5.1 similar data are presented for the rare gases. Also, in Table 5.1 besides the dipole moment  $D$  and the static polarizability  $\alpha$  the following quantities are listed:

- (i) The electron mobility  $\mu_L$  in the corresponding liquid, measured at the indicated temperature  $T$ .
- (ii) The quantity

$$\mu_G \equiv S \frac{N_{\text{torr}}}{N_L}, \quad (10)$$

where  $S = \mu P$ ,  $\mu = w/E$ ,  $P$  is the gas pressure in torrs at  $T$ ,  $N_{\text{torr}}$  is the number of molecules per cubic centimeter per torr at the specified gas temperature, and  $N_L$  is the number density of the corresponding liquid at the

Table 5.1. Data on electron mobilities in gases and liquids

Molecule	Formula	$D$ (debyes) <sup>a</sup>	$\alpha \times 10^{24}$ (cm <sup>3</sup> ) <sup>b</sup>	$\mu_L$ (cm <sup>2</sup> V <sup>-1</sup> sec <sup>-1</sup> ) <sup>c</sup>	$S = \frac{w}{E/P}$ (cm <sup>2</sup> torr V <sup>-1</sup> sec <sup>-1</sup> ) <sup>c</sup>	$\mu_G = SN_{\text{torr}}/N_L$ (cm <sup>2</sup> V <sup>-1</sup> sec <sup>-1</sup> ) <sup>d</sup>	$\mu_L/\mu_G$
<b>Linear hydrocarbons</b>							
Methane	CH <sub>4</sub>	0	2.60	300(120°K) <sup>e</sup>	$93 \times 10^5$ <sup>f</sup>	~19.3	15.5
n-Butane	CH <sub>3</sub> (CH <sub>2</sub> ) <sub>2</sub> CH <sub>3</sub>	<0.05	8.12	0.4 <sup>g</sup>	$33.1 \times 10^5$	17.9	0.022
n-Pentane	CH <sub>3</sub> (CH <sub>2</sub> ) <sub>3</sub> CH <sub>3</sub>	<0.05	9.95	0.16 <sup>g</sup> ; 0.07 <sup>h</sup>	$25.3 \times 10^5$	15.7	0.010 <sup>i</sup>
n-Hexane	CH <sub>3</sub> (CH <sub>2</sub> ) <sub>4</sub> CH <sub>3</sub>	0	11.8	0.09 <sup>g</sup> ; 0.07 <sup>h</sup>	$20.6 \times 10^5$	14.5	0.006 <sup>j</sup>
<b>Cyclic hydrocarbons</b>							
Cyclopentane	C <sub>5</sub> H <sub>10</sub>	0(?)		1.1 <sup>g</sup>	$14.9 \times 10^5$	7.5	0.146
Cyclohexane	C <sub>6</sub> H <sub>12</sub>	0; 0.61	10.9	0.35 <sup>g</sup>	$14.7 \times 10^5$	8.5	0.041
Benzene	C <sub>6</sub> H <sub>6</sub>	0	10.3	0.6 <sup>h</sup>	$5.2 \times 10^5$	2.5	0.24
Toluene	C <sub>6</sub> H <sub>5</sub> CH <sub>3</sub>	0.37	12.3	0.54 <sup>k</sup>	$3.6 \times 10^5$	2.1	0.26
<b>Branched hydrocarbons</b>							
2-Methylpropane (isobutane)	(CH <sub>3</sub> ) <sub>3</sub> CH	0; 0.13		5 <sup>e</sup>	$18.8 \times 10^5$	9.8	0.513
2-Methylbutene-2	(CH <sub>3</sub> ) <sub>2</sub> C=CHCH <sub>3</sub>			3.6 <sup>h</sup>	$1.1 \times 10^5$	0.6	6.1
2,2-Dimethylpropane (neopentane)	C(CH <sub>3</sub> ) <sub>4</sub>	<0.05		70 <sup>k</sup> ; 55 <sup>g</sup> ; 40 <sup>e</sup>	$8.3 \times 10^5$	5.3	10.4 <sup>l</sup>
2,2-Dimethylbutane (neohexane)	CH <sub>3</sub> CH <sub>2</sub> C(CH <sub>3</sub> ) <sub>2</sub>			10 <sup>g</sup>	$11.6 \times 10^5$	8.3	1.2
2,2,4-Trimethylpentane (isooctane)	(CH <sub>3</sub> ) <sub>2</sub> CHCH <sub>2</sub> C(CH <sub>3</sub> ) <sub>3</sub>	0(?)		7 <sup>g</sup>	$5.6 \times 10^5$	4.9	1.42
Helium	He		0.21	$\sim 3 \times 10^{-2}$ (3°K) <sup>m</sup>	$161 \times 10^5$ (77°K) <sup>n,o</sup>	90.3	$3.3 \times 10^{-4}$
Argon	Ar		1.63	450(80°K) <sup>p</sup>	$177 \times 10^5$ (77°K) <sup>n,o</sup>	~104	~4.3
Krypton	Kr		2.48	1310(200°K) <sup>p</sup>	$36 \times 10^5$ (195°K) <sup>n,o</sup>	~11	~119
Xenon	Xe		4.01	2200(163°K) <sup>q</sup>	$9.7 \times 10^5$ (195°K) <sup>n,o</sup>	~3	~733

<sup>a</sup>A. L. McClellan, *Tables of Experimental Dipole Moments*, W. H. Freeman and Company, San Francisco, 1963.

<sup>b</sup>H. H. Landolt and R. Bornstein, *Tables of Chemical Data, Zahlenwerte und Funktionen* (Springer-Verlag, Berlin), vol. 1, part 3, 1951, pp. 511-12 (for molecules); vol. 1, part 1, 1950, p. 401 (for atoms).

<sup>c</sup>All measurements were taken at ~298°K unless otherwise indicated.

<sup>d</sup>See text.

<sup>e</sup>P. G. Fuocho and G. R. Freeman, *J. Chem. Phys.* **56**, 2333 (1972).

<sup>f</sup>F. J. Davis and D. R. Nelson (private communication).

<sup>g</sup>W. F. Schmidt and A. O. Allen, *J. Chem. Phys.* **52**, 4788 (1970).

<sup>h</sup>R. M. Minday, L. D. Schmidt, and H. T. Davis, *J. Chem. Phys.* **54**, 3112 (1971).

<sup>i</sup>Taking  $\mu_L = 0.16$  cm<sup>2</sup> V<sup>-1</sup> sec<sup>-1</sup>.

<sup>j</sup>Taking  $\mu_L = 0.09$  cm<sup>2</sup> V<sup>-1</sup> sec<sup>-1</sup>.

<sup>k</sup>R. M. Minday, L. D. Schmidt, and H. T. Davis, *J. Phys. Chem.* **76**, 442 (1972).

<sup>l</sup>Taking  $\mu_L = 55$  cm<sup>2</sup> V<sup>-1</sup> sec<sup>-1</sup>.

<sup>m</sup>L. Meyer, H. T. Davis, S. A. Rice, and R. J. Donnelly, *Phys. Rev.* **126**, 1927 (1962).

<sup>n</sup>J. L. Pack, R. E. Voshall, and A. V. Phelps, *Phys. Rev.* **127**, 2084 (1962); Westinghouse Research Labs, Scientific Paper: 62, 928-113-P1.

<sup>o</sup>Obtained using the measured values of  $w$  for the lowest three values of  $E/P$  reported in ref. *n*.

<sup>p</sup>H. Schnyders, S. A. Rice, and L. Meyer, *Phys. Rev.* **150**, 127 (1966).

<sup>q</sup>L. S. Miller, S. Howe, and W. E. Spear, *Phys. Rev.* **166**, 871 (1968).

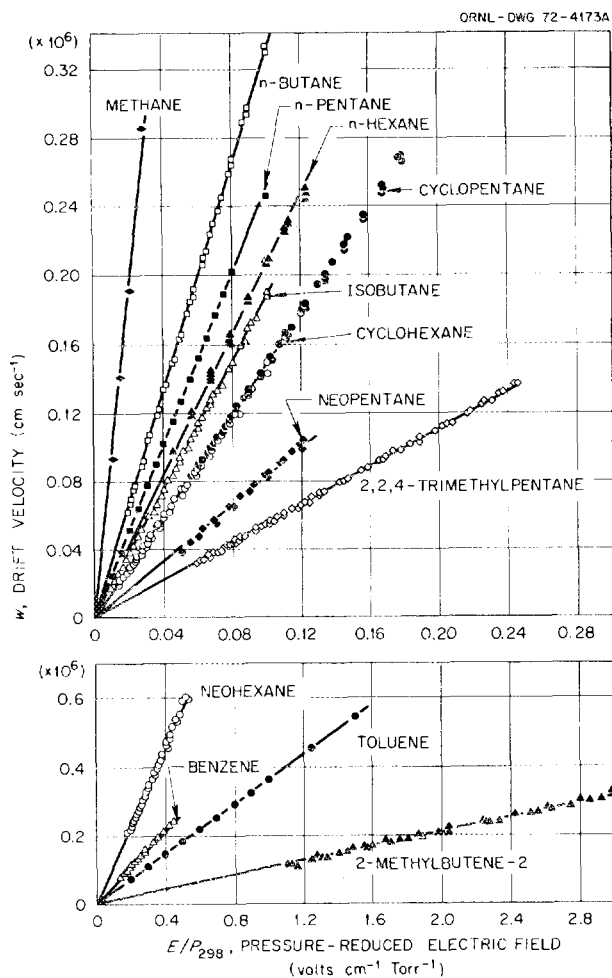


Fig. 5.7. Electron drift velocity  $w$  as a function of the pressure-reduced electric field  $E/P_{298}$  for a number of linear, cyclic, and aromatic hydrocarbons.

temperature of the liquid.  $\mu_G$  may be regarded as the gaseous electron mobility adjusted for the change in density between the gas and the liquid.

(iii) The ratio  $\mu_L/\mu_G$ .

The data in Table 5.1 offer a direct comparison between the measured values of  $\mu_G$  and  $\mu_L$  for thermal electrons which allows deduction of the following conclusions:

(1) Contrary to previous reports in the literature that the mobilities of thermal electrons in hydrocarbon vapors of the kind listed in Table 5.1 are of similar magnitude, the data in Table 5.1 show that  $\mu_G$  varies considerably ( $0.6 \lesssim \mu_G \lesssim 19 \text{ cm}^2 \text{ V sec}^{-1}$ ) from one hydrocarbon molecule (linear, cyclic, or branched) to another.

(2) For the linear hydrocarbon molecules listed in Table 5.1 except methane,  $\mu_L \ll \mu_G$  and  $\mu_L/\mu_G$  is small (0.006 to 0.022).

(3) For the cyclic aromatic and nonaromatic hydrocarbons listed in Table 5.1,  $\mu_L < \mu_G$ , but  $\mu_L/\mu_G$  is now much larger (0.041 to 0.26) than for the linear hydrocarbons in Table 5.1.

(4) In sharp contradistinction to conclusions (2) and (3) above, the branched hydrocarbons listed in Table 5.1, with the exception of isobutane, have  $\mu_L > \mu_G$ , the ratio  $\mu_L/\mu_G$  attaining as high a value as 10.4 for neopentane. For these molecules, then, on the basis of the ratio  $\mu_L/\mu_G$  thermal electrons are more mobile in the liquid than in the corresponding gas.

(5) In spite of the limitations which arise from the fact that  $\mu_L$  and  $\mu_G$  for the rare gases listed in Table 5.1 have not been measured at the same temperature, it is seen that for all rare-gas atoms but He (and Ne?)  $\mu_L > \mu_G$ , the ratio  $\mu_L/\mu_G$  increasing greatly with increasing atomic number  $Z$ . On the basis of the ratio  $\mu_L/\mu_G$ , thermal electrons are seen to be  $\sim 4.3$ ,  $\sim 119$ , and  $\sim 733$  times more mobile in liquid Ar, Kr, and Xe, respectively, than in the respective gases. It is observed that while  $\mu_G$  for Ar, Kr, and Xe decreases,  $\mu_L$  increases with increasing  $Z$ . The decrease in  $\mu_G$  with  $Z$  for Ar, Kr, and Xe is due to the increase in  $\sigma_m(v)$ <sup>11</sup> below the Ramsauer-Townsend minimum with increasing  $Z$ , while the increase in  $\mu_L$  with  $Z$  may be associated with a decrease in  $\sigma_m(v)$  with increasing  $Z$  due to a shifting of the Ramsauer-Townsend minimum to lower energies in the liquid phase.

(6) Concomitant with observation (2) above is the finding that  $\text{CH}_4$  is the only molecule known to show the Ramsauer-Townsend effect in the gas phase due to its high symmetry and, hence, compact structure.<sup>11</sup> Methane is also the only molecule for which  $\mu$  has been found to increase with gas density.<sup>12</sup> For all other molecules (or atoms) for which  $\mu$  has been measured as a function of gas pressure,  $\mu$  has been found to decrease with increasing gas density ( $\text{He}$ ;<sup>13</sup>  $\text{H}_2$ ;<sup>14,15</sup>  $\text{N}_2$ ;<sup>14</sup>  $\text{CO}_2$ ;<sup>16</sup>  $\text{C}_2\text{H}_6$ ;<sup>17,18</sup>  $\text{C}_3\text{H}_8$ <sup>18</sup>).

Similarly, concomitant with observation (5) above is the finding that He (and Ne) is the only rare-gas atom for which the Ramsauer-Townsend effect is not observed. For He,  $\mu$  decreases<sup>13</sup> with increasing gas

11. L. G. Christophorou, *Atomic and Molecular Radiation Physics*, Chap. 4, Wiley-Interscience, London, 1971.

12. H. Lehning, *Phys. Lett.* **29A**, 719 (1969).

13. R. Grünberg, *Z. Naturforsch.* **24a**, 1838 (1969).

14. R. Grünberg, *Z. Naturforsch.* **23a**, 1994 (1968); *Z. Phys.* **204**, 12 (1967).

15. A. Bartels, *Phys. Rev. Lett.* **28**, 213 (1972).

16. H. Lehning, *Phys. Lett.* **28A**, 103 (1968).

17. B. Huber, *Z. Naturforsch.* **23a**, 1228 (1968).

18. B. Huber, *Z. Naturforsch.* **24a**, 578 (1969).

pressure (>8000 torrs). The above findings were discussed<sup>19</sup> in relation to theories on electron transport through low- and high-pressure gases and liquids. It was concluded<sup>19</sup> that no direct relation between  $\mu_L$  and  $\mu_G$  is suggested by the data. Two sets of mechanisms with opposite effects seem to affect  $\mu_L$ : (1) those which decrease  $\mu_L$ , such as electron capture, electron trapping, and additional inelastic scattering processes characteristic of the liquid phase, and (2) those which increase  $\mu_L$ , such as the reduction in the effective electron mass in the liquid, coherent and forward scattering, and possibly, for spherically symmetric molecules, scattering by potentials characteristic of Ramsauer-Townsend effect conditions. For any given liquid most probably more than one of the above mechanisms is involved in determining  $\mu_L/\mu_G$ . Which mechanism is most influential in determining the magnitude of  $\mu_L/\mu_G$  appears to be intimately connected to both the molecular and the liquid structure.

#### SCATTERING OF SLOW ELECTRONS BY $\pi$ -ELECTRON-CONTAINING ORGANIC MOLECULES

A quantitative investigation of the role of  $\pi$  electrons in slow-electron scattering has been made for three classes of  $\pi$ -electron-containing organic molecules: aromatic, linear nonaromatic, and cyclic nonaromatic. The results indicated that at thermal energies the scattering cross section increases greatly (a sixfold increase was observed when the number of  $\pi$  electrons was increased from 0 to 10) with increasing number of  $\pi$  orbitals. These studies indicated also that molecular scattering of slow electrons is not only affected strongly by a large macroscopic permanent electric dipole moment,<sup>20</sup> but also by certain microscopic molecular characteristic features such as the highly polarizable  $\pi$  orbitals which give rise to large induced moments. They also indicate that double-bonded systems may efficiently thermalize slow electrons.

#### COMPOUND NEGATIVE-ION RESONANCES AND THRESHOLD-ELECTRON EXCITATION SPECTRA OF QUINOLINE AND ISOQUINOLINE<sup>21</sup>

Compound negative-ion resonances (CNIR) are of unique physical and chemical interest. Such resonances also constitute very efficient ways for thermalizing subexcitation electrons via the processes of indirect vibrational and rotational excitation of molecules. They are of general occurrence in molecules, both small and large and organic and inorganic.<sup>11</sup>

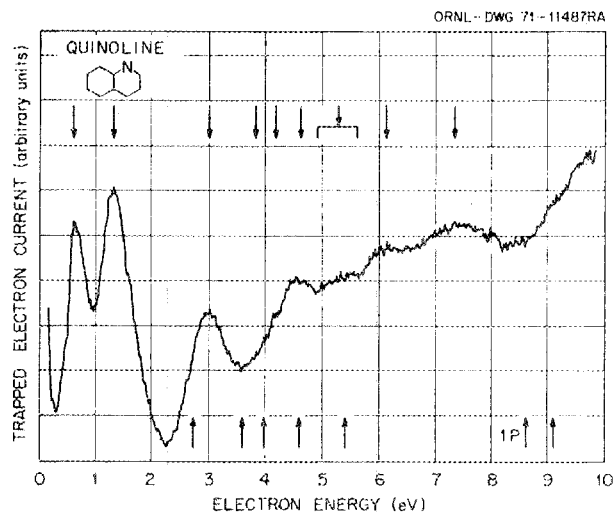


Fig. 5.8. Threshold-electron excitation spectrum of quinoline. The electron trap is 0.05 V. IP denotes the photoionization value of the ionization potential.

Two such CNI resonances have been found in the *N*-heterocyclic molecules of quinoline (Q) and isoquinoline (IQ) and the  $\pi$ -isoelectronic molecule of naphthalene (N). The two resonances showed maxima at 0.6 and 1.30 eV for Q and at 0.75 and 1.3 eV for N. For IQ, maxima were observed at 0.42, 0.55, 0.76 eV and 1.25, 1.67 eV, indicating the presence of vibrational structure in the two CNI resonances for this molecule.

Figure 5.8 shows a representative threshold-electron excitation (TEE) spectrum for quinoline. The arrows above the spectrum indicate the positions of the maxima in the TEE spectrum. The arrows shown below the spectrum in Fig. 5.8 indicate the 0-0 transitions in the optical spectra, which, both for transitions below and above the ionization potential, agree well with the onsets in the present TEE spectra.

A summary of the electronic transitions in Q and IQ, the possible types of transition, the assignment, and the multiplicity of the states involved has been given in ref. 21.

The TEE spectra of Q and IQ indicated the presence of an energy-loss process below the position of the first

19. L. G. Christophorou, R. P. Blaunstein, and D. Pittman, *Chem. Phys. Lett.* (in press).

20. L. G. Christophorou, A. A. Christodoulides, and D. Pittman, *J. Phys. B (At. Mol. Phys.)* 2, 71 (1969); 3, 1252 (1970).

21. M. N. Pisanias, L. G. Christophorou, and J. G. Carter, *Chem. Phys. Lett.* 13, 433 (1972).

$\pi$ -triplet state  $T_1(\pi \rightarrow \pi^*)$ , which was identified as the lowest excited electronic state of Q and IQ, namely, the first triplet  $n \rightarrow \pi^*$  transition at  $\sim 2.45$  eV.

The most striking feature in the TEE spectrum of Q, IQ, and N is the presence of the two strong resonances below  $\approx 2$  eV which were attributed to the formation of two compound negative-ion states in each of these molecules.

### ENERGY-LOSS SPECTRA OF *N*-HETEROCYCLIC BENZENE DERIVATIVES

The energy-loss spectra of pyridazine, pyrimidine, and pyrazine have been investigated using the trapped electron method and have been compared with photoabsorption data. Figure 5.9 shows the TEE spectrum of pyrimidine. Besides the location of low-lying  $\pi \rightarrow \pi^*$  and  $n \rightarrow \pi^*$  triplet states, the most striking feature of the threshold-electron-excitation spectra for all these molecules was the presence of two intense energy-loss processes below 2 eV attributed to two compound negative-ion resonance states. The positions of these resonances (0.70 and 1.44; 0.80 and 1.90; 1.10 and

1.53 eV for pyridazine, pyrimidine, and pyrazine, respectively) have been related to a simpler molecular orbital theory and to the electronic structure of the parent benzene molecule, for which only one compound negative-ion resonance is observed at  $\sim 1.6$  eV.

### THRESHOLD-ELECTRON EXCITATION AND COMPOUND NEGATIVE-ION FORMATION IN METHANE, ETHANE, AND PROPANE

The threshold-electron excitation spectra (TEES) of methane, ethane, and propane have been studied and compared with photoabsorption (PA) and energy-loss spectra (ELS). Distinct differences between TEES and PA or ELS exist, and these are attributed to optically forbidden transitions and/or to compound negative-ion states which are distinctly favored in TEES but are absent in PA or ELS. A compound negative-ion resonance has been clearly observed in methane (in the range 1.8 to 3.15 eV with a maximum at 2.5 eV) and in ethane (in the range 1.5 to 3.0 eV with a maximum at 2.25 eV). At higher energies the TEES of methane begins at 7.45 and shows a shoulder at 8.8 eV, a broad

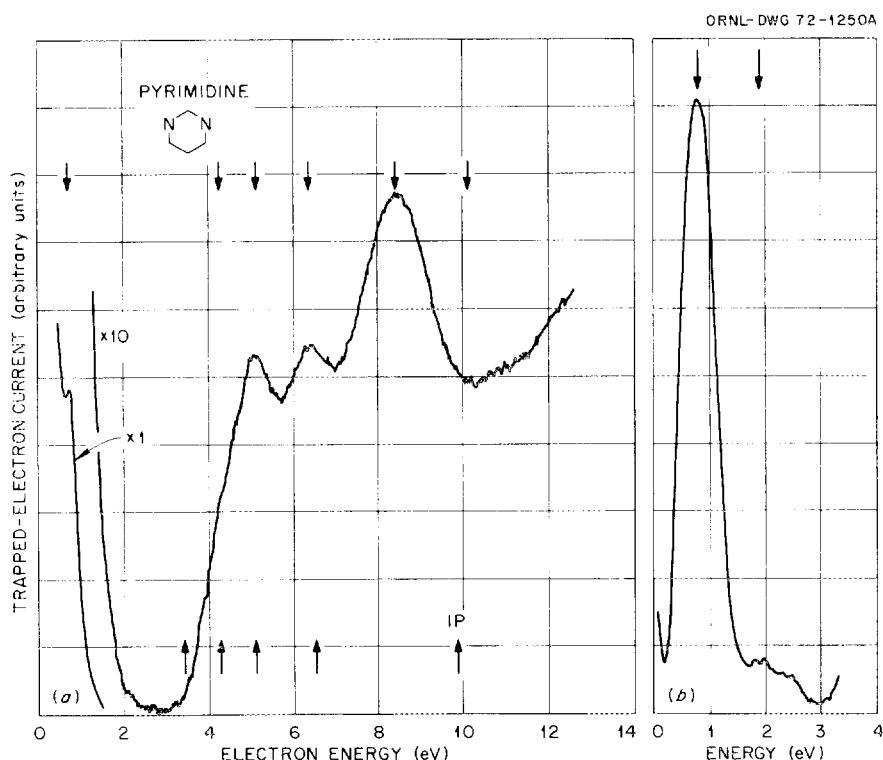


Fig. 5.9. Energy-loss spectra of *N*-heterocyclic benzene derivatives. (a) Threshold-electron excitation spectrum of pyrimidine. The electron trap is 0.14 V. IP denotes the ionization potential as obtained by electron impact. (b) The 0- to 3-eV energy region recorded with improved energy resolution showing the two compound negative-ion resonances in pyrimidine. The electron trap is 0.034 V.

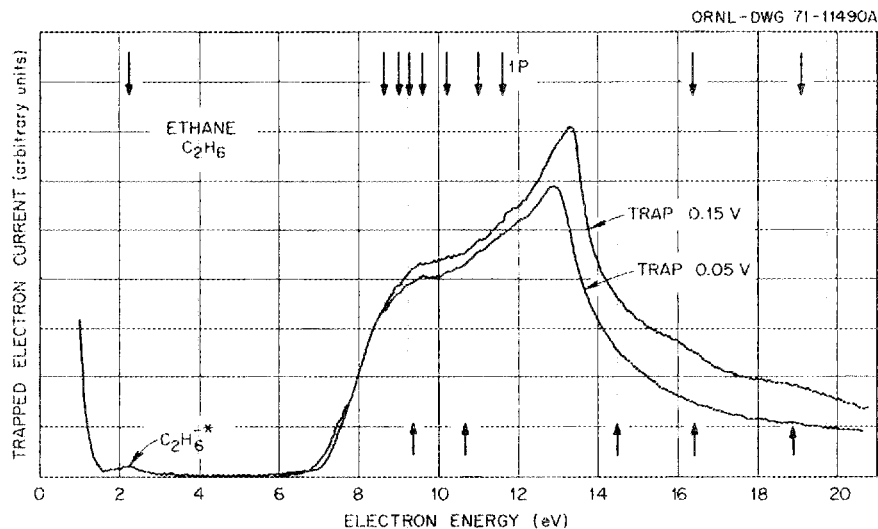
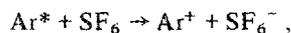


Fig. 5.10. Threshold-electron excitation spectrum of ethane. The upper arrows indicate the positions of the peaks in the TEE spectrum. The lower arrows indicate the position of the maxima in the photoabsorption spectrum of ethane. Note the compound negative-ion resonance at 2.3 eV.

peak in the range 9.9 to 10.2 eV, a shoulder at 11.05 eV and peaks at 11.72, 12.00, 12.28, 12.52, 13.8, and 14.3 eV. The TEES of ethane begins at 7.15 eV and shows peaks at 8.65, 9.0, 9.25, 9.65, 10.28, 10.98, 16.4, and 19.1 eV. The TEES of propane resembles that of ethane. Figure 5.10 gives the TEES of ethane.

#### REACTIONS OF MOLECULAR RYDBERG STATES

The charge-transfer reactions of rare-gas atoms in Rydberg states with acceptor molecules, for example,



have been known for some time. We have found that molecules such as  $\text{H}_2\text{O}$  and cyclohexane, excited to their Rydberg states by electrons or photons, can react similarly. This shows that these states are rather long-lived and upsets considerably conventional models of radiation-induced ionization in liquids and gases.

#### PHOTOPHYSICAL STUDIES OF ORGANIC LIQUIDS AND SOLUTIONS; EMISSION SPECTRA FROM HIGHER EXCITED $\pi$ -SINGLET STATES OF AROMATIC HYDROCARBONS IN SOLUTION

Our studies in this area have continued and showed that fluorescence emission from the second excited  $\pi$ -singlet states of aromatic molecules in solution is not uncommon. Detailed studies have been made of the emission spectra from the first,  $S_1$ , and second,  $S_2$ ,

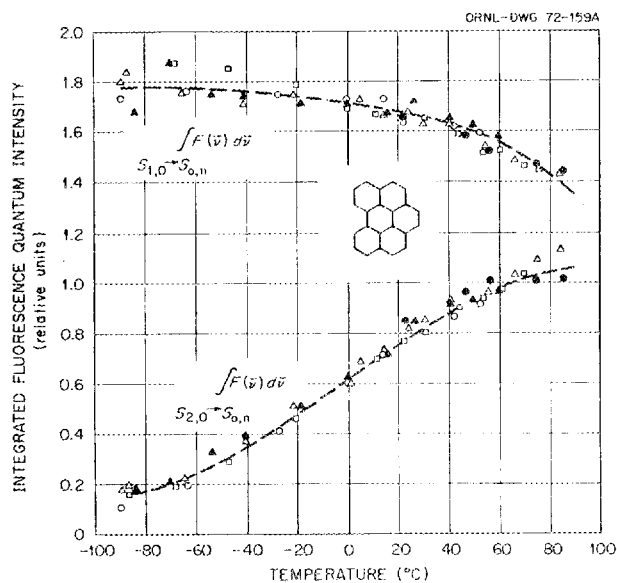


Fig. 5.11. Integrated fluorescence quantum intensities of  $S_1$  and  $S_2$  in relative units for  $5 \times 10^{-6} M$  solutions of 1,12-benzperylene in *n*-heptane. The differences seen are due to temperature differences only.

excited  $\pi$ -singlet states and also of the dependence of these light emissions on temperature  $T$ . Figure 5.11 shows the integrated fluorescence quantum intensity as a function of  $T$  for the  $S_{1,0} \rightarrow S_{0,n}$  and  $S_{2,0} \rightarrow S_{0,n}$  radiative transitions. Similar data were obtained for 3,4-benzpyrene and 1,2-benzathracene. A reasonable theoretical understanding of the radiative and nonradia-

tive processes involved has been achieved.<sup>22</sup> For 1,12-benzperylene it was concluded:

(1) The fluorescence quantum yield from  $S_2$  is primarily due to an indirect fluorescence originating from thermal repopulation of  $S_2$  from  $S_1$ .

(2) The activation energy determined for the thermal repopulation of  $S_2$  from  $S_1$  is  $690 \text{ cm}^{-1}$ . This value is significantly less than the actual energy separation of  $1400 \text{ cm}^{-1}$  between  $S_{2,0}$  and  $S_{1,0}$ , that is, between the 0-0 absorption bands for  $S_2$  and  $S_1$ . This may indicate that  $S_{2,0}$  in addition to being repopulated from  $S_{1,0}$  is also repopulated from vibrationally excited  $S_1$  (i.e.,  $S_{2,0} \rightarrow S_{1,n} \rightarrow S_{2,0}$ ,  $n > 0$ ), or possibly from an optically forbidden state located between  $S_{1,0}$  and  $S_{2,0}$ .

---

22. C. E. Easterly, L. G. Christophorou, and J. G. Carter, *J. Phys. Chem.* (submitted).

(3) The internal conversion process cannot be considered as being completely irreversible.

It has been generally concluded from these studies that fluorescence from the second excited  $\pi$ -singlet state of aromatic molecules in solution does not appear to be as uncommon as has been thought in the past. Such emissions, depending on the temperature, affect strongly the overall spectral characteristics of organic molecules. Additionally, the persistence of the excitation energy between  $S_{1,0}$  and  $S_{2,0}$  should be of importance in energy transfer from such excited molecules and warrants investigation.

#### LOW-ENERGY ELECTRON INTERACTIONS WITH LIQUIDS

Recognizing the need for physical studies on low-energy electron interactions with liquids we have developed a method for direct physical studies of low-energy electron interactions with liquids. The necessary equipment is in the final stages of construction.

## 6. Graduate Education and Vocational Training

K. Z. Morgan

M. F. Fair

R. D. Birkhoff

L. G. Christophorou

R. N. Compton

L. C. Emerson

W. R. Garrett

R. H. Ritchie

H. C. Schweinler

J. E. Turner

The demands for education in health physics have continued to rise on all levels. Education to the Ph.D. level is required to provide personnel for positions of leadership in industrial, academic, and medical institutions. Training at the master's level is needed to provide the leaders in the applied health physics field emphasizing instrumentation and procedures. The needs of the reactor and other nuclear-related professions must be met by large numbers of technicians at the B.S. level.

The field training program at ORNL during the summer months is open to all AEC Fellowship students who have completed their first academic school year under the fellowship program. The field training consists of two major phases, applied health physics and research health physics. The university program cannot, in itself, produce the desired product. The summer training program is absolutely essential in the education of a health physicist.

Six Fellows participated in the summer training program at ORNL during July and August 1971 – two from the University of Kentucky, one from the University of Michigan, one from the University of Kansas, one from Georgia Institute of Technology, and one from Purdue University. Seven Fellows were in training during May and June 1972.

The summer training began with a three-day orientation program, which was followed by five weeks with the applied health physics group and five weeks with the research health physics groups. One week was spent at the Special Training Division (ORAU) doing health physics experiments. Numerous seminars were held throughout the summer, highlighting recent advances in health physics and closely allied fields. Many of the seminar speakers were from laboratories and universities from around the world.

In the applied health physics training, the student gains practical experience in many phases of radiation protection under the supervision of a senior health physicist.

In health physics research the students are first given a brief summary of all the research projects in progress in the Division. They then choose the group in which they remain for a five-week period. They become part of the team and are truly engaged in doing health physics research under senior scientist supervision.

The summer program gives the student sufficient experience in applied health physics to enable him to take a position in this field, where with only a little additional experience he will soon qualify for a position of responsibility in radiation protection. Also, he learns of the tremendous breadth in research health physics and is made aware of the diverse problems available for thesis work should he decide to continue his education for the M.S. or the Ph.D. degree.

Twelve students were enrolled in the General Health Physics undergraduate course (Physics 4710-20-30) taught by a member of the Division at the University of Tennessee. This was a three-quarter course which met 3 hr/week.

The Division provided assistance to the staff of the University of Tennessee in updating and teaching its graduate curriculum in health physics. This included courses in General Health Physics, Radiation Chemical Physics, Physics of Polyatomic Molecules, Interaction of Electrons with Gases, Interaction of Electrons with Solids, and Interaction of Radiation with Matter. This curriculum has attracted Fellows who desire education to the master's level and also those who wish to pursue the Ph.D. degree. Help was provided to the University of Tennessee in conducting the co-op program with ORNL leading to the B.S. degree in health physics. This

type of assistance and consultation is available to any school desiring to set up a health physics program or institute courses in this field. For example, queries have been received from Georgia Institute of Technology, Southern Technical Institute, Auburn University, Oklahoma State University, Duquesne University, and Wake Forest University with regard to setting up courses in health physics. Assistance was given the University of Tennessee in the preparation of qualifying examinations in health physics. A visit to ORNL with lectures and tours was provided for students in health physics from the University of Arkansas. A series of lectures were given at the University of North Carolina. Eight universities were visited at which ORNL health physics research and educational activities were discussed.

There were a number of Oak Ridge Graduate Fellows, AEC Fellows, USPHS students, and others working on theses for advanced degrees under the supervision of Radiation Physics staff. Their thesis titles and universities are listed below:

1. G. D. Alton, "Optical Model Studies of Low-Energy Electron Interactions with Simple Atoms and Molecules"(UT)
2. J. L. Blankenship, "Gamma-Ray Damage and Annealing in Ultra-High Purity Germanium"(UT)
3. M. D. Brown, "Interaction of Uranium in Solids"(UT)
4. C. E. Easterly, "Study of Aromatic Hydrocarbons in Relation to Carcinogenesis"(UT)
5. J. M. Elson, "The Interaction of Photons at Rough Dielectric Surfaces" (Univ. Ky.)
6. R. E. Goans, "Dissociative Electron Attachment to Polyatomic Molecules"(UT)
7. A. Hadjiantoniou, "Electron Attachment to and Autoionization of Long-Lived Negative Ions of Polyatomic Molecules"(UT)
8. W. F. Hanson, "Soft X-Ray Studies of the Satellites of Na, Mg, Al, and Si and the Optical Properties of MgO and MgF<sub>2</sub>"(UT)
9. P. D. Kidd, "Electron Capture and Drift in Organic Liquids"(UT)
10. D. L. McCorkle, "Low-Energy Electron Attachment to Molecules at High Densities"(UT)
11. M. N. Pisanias, "Threshold-Electron Excitation and Compound Negative Ion Formation in Polyatomic Molecules"(UT)
12. B. L. Sowers, "Optical Properties of Liquid CCl<sub>4</sub>, C<sub>6</sub>H<sub>14</sub>, C<sub>6</sub>H<sub>12</sub>, C<sub>6</sub>H<sub>10</sub>, C<sub>6</sub>H<sub>8</sub>, and C<sub>6</sub>H<sub>6</sub> in the Vacuum Ultraviolet"(UT)
13. I-Lan Tang, "Optical Properties of Nucleic Acid Bases"(UT)
14. R. B. Vora, "Studies of Electron Transfer in Atomic Collisions with Molecules"(UT)
15. J. F. Wilson, "Mass Analysis of Ions Formed in Electron Swarm Experiments"(UT)
16. U. S. Whang, "Optical Properties of Potassium, Rubidium, and Cesium in the Vacuum Ultraviolet"(UT)
17. C. E. Wheeler, Jr., "Experimental and Theoretical Investigations of the Smith-Purcell Effect"(UT)

Assistance was given to ORAU in the presentation of a ten-week course in health physics.

Three student trainees and two faculty members spent the summer (1971) in the Division as research participants sponsored by ORAU. Two student trainees spent the summer of 1972 in the Division.

Several staff members of the Radiation Physics Section of the Health Physics Division worked with the University of Tennessee faculty in preparing preliminary examinations for the Ph.D. degree and in grading the examinations. Four of our staff hold Ford Foundation appointments at the University and in this capacity participated in student advising on matters of curricula and research. They were also active on the University Committee on Graduate Education. Our staff took part in the faculty meetings of the UT Physics Staff.

A proposal for a cooperative training program for health physics technologists was accepted by the USAEC. This program will be open to students who have completed the sophomore year at one of a number of participating colleges and who are majoring in one of the sciences, mathematics, or engineering. They will receive 20 weeks of on-the-job training at ORNL in coordination with their on-campus academic program. Ten weeks of specialized training will be given at a reactor site or hospital depending upon the student's main field of interest.

The Division is currently investigating the possibility of setting up a postdoctoral program in health physics. This would infuse new ideas into the research programs and hopefully serve as a source of new senior health physicists.

## Part II. Radiation Dosimetry Research

J. A. Auxier

---

### 7. Dosimetry for Human Exposures and Radiobiology

J. W. Poston

J. A. Auxier	Y. Okamoto <sup>1</sup>
J. S. Cheka	E. M. Robinson
W. F. Fox	W. H. Shinpaugh
H. H. Hubbell, Jr.	W. S. Snyder
J. E. Jackson	M. Sohrabi <sup>2</sup>
T. D. Jones	G. G. Warner <sup>3</sup>
H. Yamada <sup>1</sup>	

#### JAPANESE DOSIMETRY PROGRAM

##### Liaison with the Atomic Bomb Casualty Commission

One ORNL representative visited the Atomic Bomb Casualty Commission (ABCC) in Hiroshima, Japan, for six weeks during August and September 1971. At this time, two ABCC shielding technicians were assigned to ORNL to help develop and verify a dose estimation technique to be used to predict accurately radiation doses to those survivors who were inside "heavy-shielding" structures, such as reinforced concrete buildings. These classes of survivors are of special interest because they were subjected to a minimum amount of blast, shock, and thermal trauma; thus, for these survivors it is more nearly possible to isolate effects whose increases above normal incidence were induced entirely by radiation. There were 1030 survivors (379 in Hiroshima, 651 in Nagasaki) in structures which provided heavy shielding. Of these, 340 were in concrete or reinforced concrete buildings, and no estimates of dose have been made, but as pointed out earlier, these represent a very important sample of the survivors.

Except for 6 additional cases, the 340 survivors in concrete buildings represent the total number of survivors at distances less than 1400 m for which ABCC has not already calculated or assigned radiation doses.

Extensive information stored on magnetic tape was sent to ORNL and will be extremely valuable when the ABCC commences a study of the effects of radiation quality.

Calculations which permit the assignment of radiation depth doses to many organs, such as the thyroid of a survivor or to children who were in utero at the time of exposure, have been completed. These calculations should be extremely useful in studies of various radiation-inducible effects such as thyroid carcinoma, cancer of the cervix, or any of the various biological defects of children who were in utero at the time of exposure. A complete description of these calculations, the intended uses, and method of application is being written and will soon be transmitted to ABCC.

A pilot study of the histories of the survivors who were exposed to the radioactive "black rain," which fell soon after the bombings, is presently under way. The studies are still incomplete, but as expected appear to indicate that very few persons who were in the black rain and were exposed to extremely low levels of "prompt radiation" from the bombs showed significant radiation-induced symptoms.

---

1. Consultant, Atomic Bomb Casualty Commission.  
2. Alien guest.  
3. On loan from Mathematics Division.

### Heavy Shielding Research

The large collimator (15° opening and rotatable around two axes) was mounted on top of the Health Physics Research Reactor (HPRR) Control Building and used to measure the angular distribution of scattered neutron and gamma doses received at that point from the HPRR on the other side of a hill. The results are shown in Figs. 7.1 and 7.2. A Hurst recoil proton proportional counter measured the doses due to neutrons, and a "Phil" G-M counter (insensitive to neutrons) measured gamma-ray doses received in the collimators. Comparison counters of the same types measured the free air doses simultaneously for normalization.

Also plotted in the figures are the angular distributions previously derived from weapons tests and from Operation BREN using the HPRR. The neutron dose distribution is similar to the earlier result, except that the peak around 30° seems high, probably because the curves are normalized to unit area and the forward directions are blocked by a hill. The gamma-ray distribution is quite different, indicating that most of the dose arises from neutron interactions and gamma scattering in the sky overhead, probably fairly close to the detector (~1 relaxation length). For these plots the measured curves of dose per steradian have been

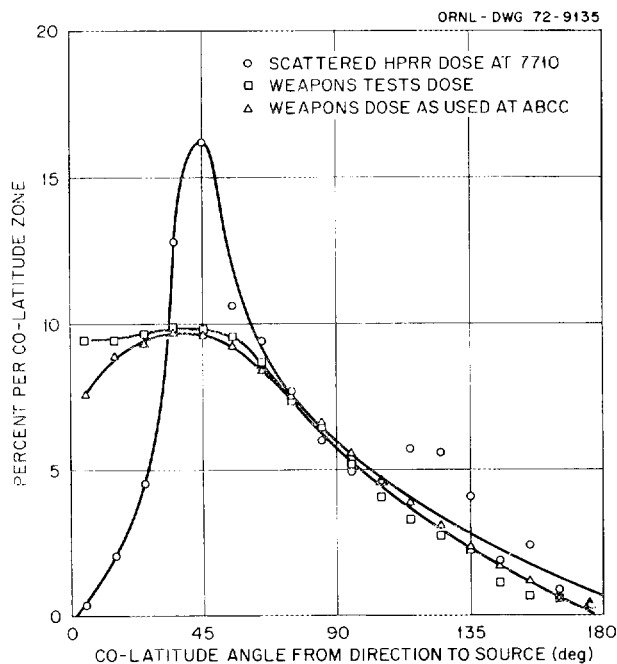


Fig. 7.1. Angular distribution of neutron dose received. Dose from hour angles (longitude) below 85° (i.e., reflection) not included.

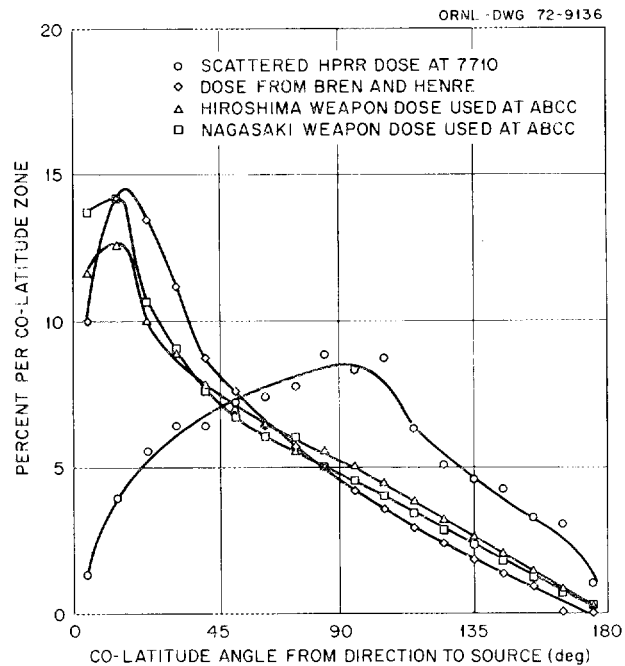


Fig. 7.2. Angular distribution of gamma dose received. Dose from hour angles (longitude) below 85° (i.e., reflection) not included.

multiplied by the solid angle per colatitude zone, assuming that the pole of coordinates was pointing at the reactor. As in weapons tests, the doses received are nearly independent of longitude angle above the horizon.

### MEASUREMENTS OF DOSE DISTRIBUTIONS

#### Dose as a Function of Depth in a Tissue-Equivalent Phantom

The study reported last year<sup>4</sup> was completed by calculating the absolute doses per neutron per square centimeter incident on a 30-cm-diam by 60-cm cylindrical tissue-equivalent phantom for neutrons from the HPRR and from 14-MeV (*d,T*) neutrons. The results are shown in Figs. 7.3, 7.4, and 7.5 and compared with T. D. Jones' Monte Carlo calculations<sup>5</sup> for the same incident neutron spectra and with a 160-keV low-energy cutoff of recoil proton dose, corresponding to the cutoff of the proportional counter used. The agreement is within the probable errors of measurement and calculation.

4. *Health Phys. Div. Annu. Progr. Rep. July 31, 1971*, ORNL-4720, p. 90.

5. *Health Phys. Div. Annu. Progr. Rep. July 31, 1971*, ORNL-4720, p. 84.

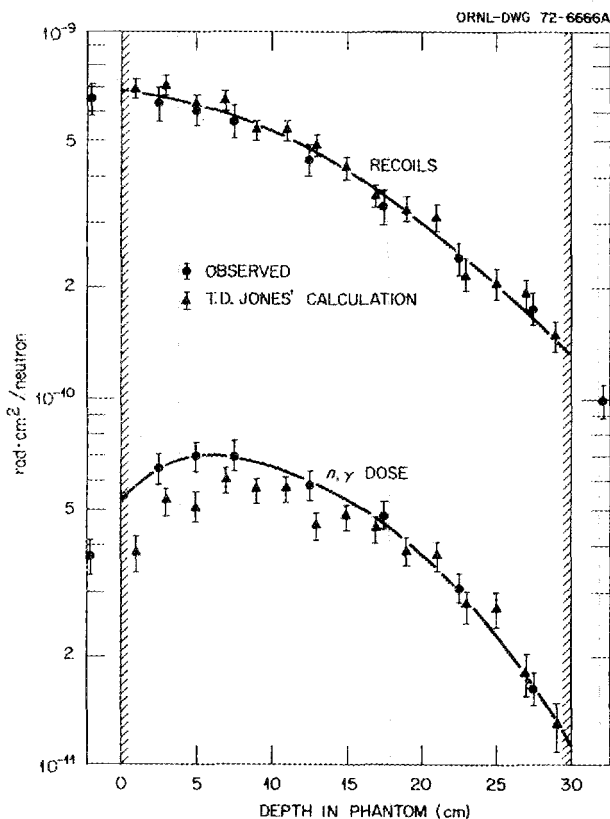


Fig. 7.3. 14-MeV neutron depth dose.

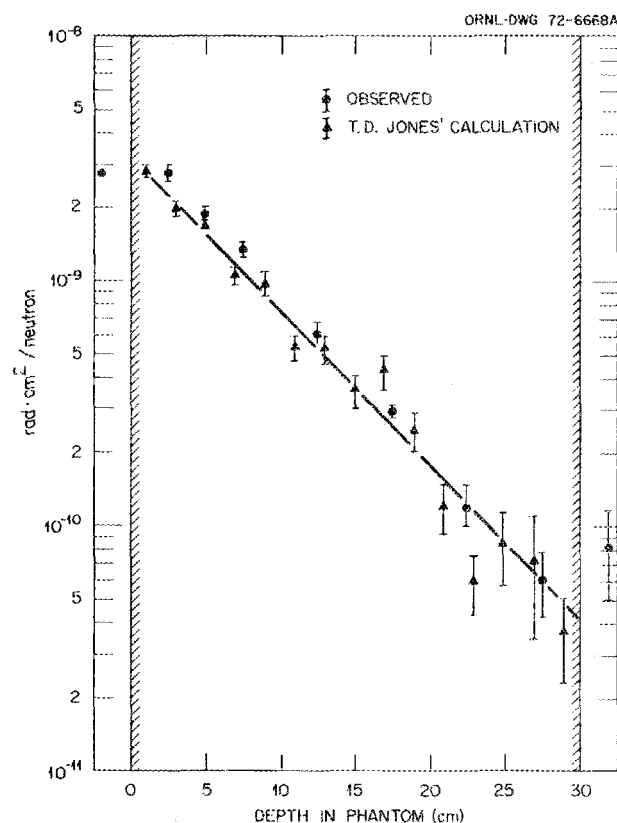


Fig. 7.4. HPRR neutron depth dose, recoils.

## DOSE AND LET CALCULATIONS

### Local Dose from Neutron-Produced Recoil Ions in the Region of a Therapeutic $^{252}\text{Cf}$ Needle

Many radiotherapists now claim<sup>6</sup> that it is possible to detect a local biological change due to a 10% variation of therapeutic radiation dose. The response of a malignant neoplasm to such slight variations in the local dose is extremely critical in therapeutic uses of implanted sources of  $^{252}\text{Cf}$  because dose decreases rapidly as distance from the source is increased. For example, the dose from  $^{252}\text{Cf}$  neutron-produced recoil ions is less by about two orders of magnitude at a distance of 4 cm from the source as compared with dose near the source. Californium-252 appears to have great potential therapeutic value, yet the spread of estimates of local dose to a small tumorous region is about 25%; therefore, techniques from previous calculations<sup>7</sup> were

6. Personal communication, meeting at New York University Medical Center, July 16, 1971.

7. T. D. Jones and J. A. Auxier, *Phys. Med. Biol.* 17(2), 206-17 (1972).

applied to determine dose distributions sufficiently accurate to satisfy the needs of most radiotherapists.

Dose distributions for  $^{252}\text{Cf}$  implants determined experimentally or calculationaly by most investigators are probably sufficiently accurate for distances greater than 4 cm; however, precision and accuracy of the local dose are extremely difficult to obtain within  $\pm 5\%$ . Experimentalists are confronted with a variety of errors which influence the estimation of dose. These errors include positioning errors of both the source and detector, variations in background radiation, and sensitivity of instruments. (In fact, a dosimeter has not yet been developed that can accurately measure local dose in a small volume without significantly perturbing the radiation field.) The basic calculational models are based on discrete ordinate and Monte Carlo transport techniques. Some limitations of using a discrete ordinate method to solve numerically the Boltzmann transport equation are: (1) the substitution of group theory for a continuous energy spectrum by groups of particles having discrete monoenergies, (2) inexactness due to oscillations in Legendre polynomials used to describe particle scattering (often observed as negative

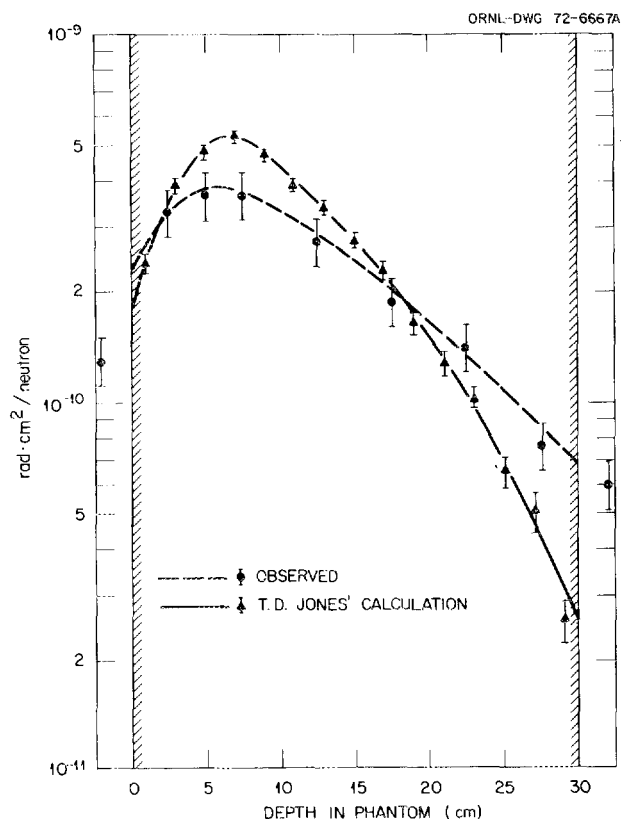


Fig. 7.5. HPRR neutron depth dose ( $n, \gamma$ ).

values of fluence or dose at a well-shielded position), (3) lack of an estimate of the statistical variance (usually replaced by apparent convergence or significant previous experience with discrete ordinate calculations), and (4) inaccurate approximations of angular quadrature (usually most notable at larger distances and for rays emanating from a point source).

Monte Carlo methods have the distinct advantages of permitting duplication of exact histories of particles and providing an estimate of the variance by standard statistical procedures. The statistical variation in a specific volume element can be decreased by the incorporation of variance-reduction techniques such as particle splitting, Russian roulette, and importance sampling; however, Monte Carlo calculations still require an extremely large number of particle histories and resulting interactions to accurately describe the effect of the particles on a small volume.

In these calculations, the areas shown in Table 7.1, which are drawn to scale, were revolved about the horizontal center line to create volumes of revolution about the needle source. Horizontal grid divisions and radial increments of the cylindrical shells were both taken as 0.5 cm.

Slight variations in atomic composition may account for significant deviations when the objective is an estimate accurate to within 10% ( $\pm 5\%$ ), so the three compositions of tissue media shown in Table 7.2 were used to investigate this effect. Composition 1 corresponds to standard soft tissue, composition 2 corresponds to whole-body average, and composition 3 corresponds to skeletal muscle tissue. Dose from neutron-produced recoil ions for each of these compositions is shown in Table 7.1. Ratios of dose from neutron-produced recoil ions to kerma from a small volume of tissue in free space were averaged to obtain an estimate for an average tissue composition, and this value was assumed to represent the value at the centroid of revolution. Exponential interpolations were done in two dimensions to produce the isodose curves shown in Fig. 7.6. The objective of combining kerma curves for the production of isodose curves is to reduce the coefficients of variation due to statistical fluctuations by  $\sqrt{3}$ . Because the distribution of dose about the source is changing so rapidly, and on the basis of experience in analyzing these and previous data, it is felt that isodose curves are of little significance if values of local dose are known with less than  $\pm 5\%$  precision.

Coefficients of variation ranged from 1 to 3.5% for this mean tissue, so the isodose curves were extremely well determined. This family of curves has a shape which differs slightly from those in previous publications,<sup>8-10</sup> but the difference is thought to be due to the

8. R. G. Fairchild, *Sources of Fission Neutrons and Their Dosimetry*, BNL-12452 and CONF-680420-2 (1968).

9. F. T. Cross, personal communication with Lowell Anderson.

10. G. D. Oliver, Jr., and C. N. Wright, *Radiology* 92, 143-47 (1969).

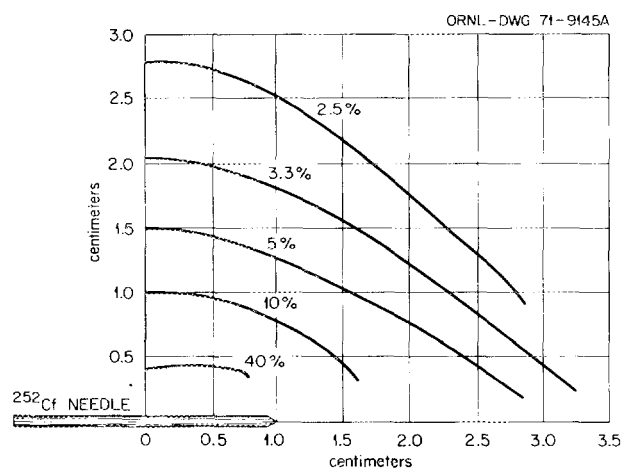


Fig. 7.6. Neutron isodose curves in tissue normalized to free space kerma.

Table 7.1. Dose from recoil ions produced by neutrons from a 20-mm <sup>252</sup>Cf needle source

A = Composition #1

B = Composition #2

C = Composition #3

D = Coefficient of Variation  
in %

A, B, & C - Dose (Rads/μg-sec)

A	D
B	D
C	D

<p style="writing-mode: vertical-rl; transform: rotate(180deg);">CM</p>	2.5	.212-3 3.1	.200-3 3.1	.174-3 3.3	.159-3 3.3	.144-3 3.5	.125-3 3.9	
		.209-3 3.0	.197-3 3.1	.183-3 3.3	.158-3 3.4	.143-3 3.5	.124-3 3.8	
		.192-3 3.1	.191-3 3.2	.178-3 3.3	.163-3 3.5	.149-3 3.7	.116-3 3.8	
	2	.243-3 3.1	.226-3 3.3	.207-3 3.8	.177-3 3.8	.156-3 4.9	.114-3 4.2	
		.262-3 3.1	.232-3 3.3	.200-3 3.4	.174-3 3.7	.149-3 3.9	.119-3 4.5	
		.243-3 3.1	.230-3 3.3	.206-3 3.4	.171-3 3.8	.146-3 3.8	.127-3 4.5	
	1.5	.398-3 3.0	.363-3 3.2	.304-3 3.4	.227-3 3.9	.181-3 4.2	.145-3 5.0	
		.435-3 2.8	.370-3 3.0	.285-3 3.5	.226-3 3.8	.196-3 4.5	.145-3 4.7	
		.372-3 3.0	.342-3 3.2	.285-3 3.6	.218-3 3.8	.169-3 4.5	.148-3 4.7	
	1	.878-3 2.7	.723-3 2.8	.454-3 3.4	.318-3 4.6	.250-3 4.9	.177-3 5.3	
		.866-3 2.7	.709-3 2.8	.482-3 3.5	.318-3 4.3	.227-3 4.8	.193-3 5.4	
		.814-3 2.7	.690-3 2.8	.477-3 3.5	.323-3 4.3	.221-3 5.0	.195-3 5.4	
	.5	.351-2 2.3	.295-2 2.5	.123-2 3.7	.618-3 5.0	.529-3 6.0	.395-3 6.4	
		.332-2 2.3	.295-2 2.4	.119-2 3.9	.578-3 5.2	.510-3 5.7	.393-3 6.0	
		.323-2 2.3	.271-2 2.5	.121-2 3.9	.641-3 5.0	.487-3 5.7	.374-3 6.5	
			.5	1	1.5	2	2.5	3
			CM					



unusual degree of accuracy believed to be associated with the calculations reported here.

**Slant Beam**

A broad beam of neutrons was programmed to impinge at an angle to the axis of a cylindrical phantom. Previous results<sup>11</sup> included broad beams of neutrons at energies of 10 keV, 1 MeV, and 7 MeV which were incident at angles of 30° with the axis of the cylinder. The results were normalized to a beam intensity of 1 neutron/cm<sup>2</sup>. Of course, this would not

be equivalent to neutrons crossing this lateral surface at a rate of 1 neutron/cm<sup>2</sup>. In fact, the “surface fluence” is not constant because of the different angles of entry at different points of the curved surface. If the monodirectional beam of neutrons, with paths parallel to the base of the cylinder, has a fluence of 1 neutron/cm<sup>2</sup>, there will be a total of 30 × 60 = 1800 neutrons impinging on the surface of the cylinder. Now the beam remains unchanged, but the cylinder is tilted so the paths of the neutrons make an angle  $\theta$  with the axis of the cylinder. The neutrons crossing the lateral surface are now decreased to (1800) (sin  $\theta$ ) neutrons, but we also have ( $\pi$ ) (15<sup>2</sup>) (cos  $\theta$ ) neutrons crossing one base of the cylinder. In Figs. 7.7–7.10 the dose and

11. Health Phys. Div. Annu. Progr. Rep. July 31, 1967, ORNL-4168, p. 220.

Table 7.2. Compositions of tissue media used in these calculations

	Composition 1		Composition 2		Composition 3	
	× 10 <sup>22</sup> atoms/g	Percent <sup>a</sup>	× 10 <sup>22</sup> atoms/g	Percent <sup>a</sup>	× 10 <sup>22</sup> atoms/g	Percent <sup>a</sup>
Hydrogen	6.266	10.5	6.169	10.3	5.975	10.0
Carbon	0.944	18.8	1.258	25.1	0.602	12.1
Nitrogen	0.133	3.1	0.107	2.5	0.172	4.0
Oxygen	2.549	67.6	2.333	62.1	2.748	73.8

<sup>a</sup>Percent of weight.

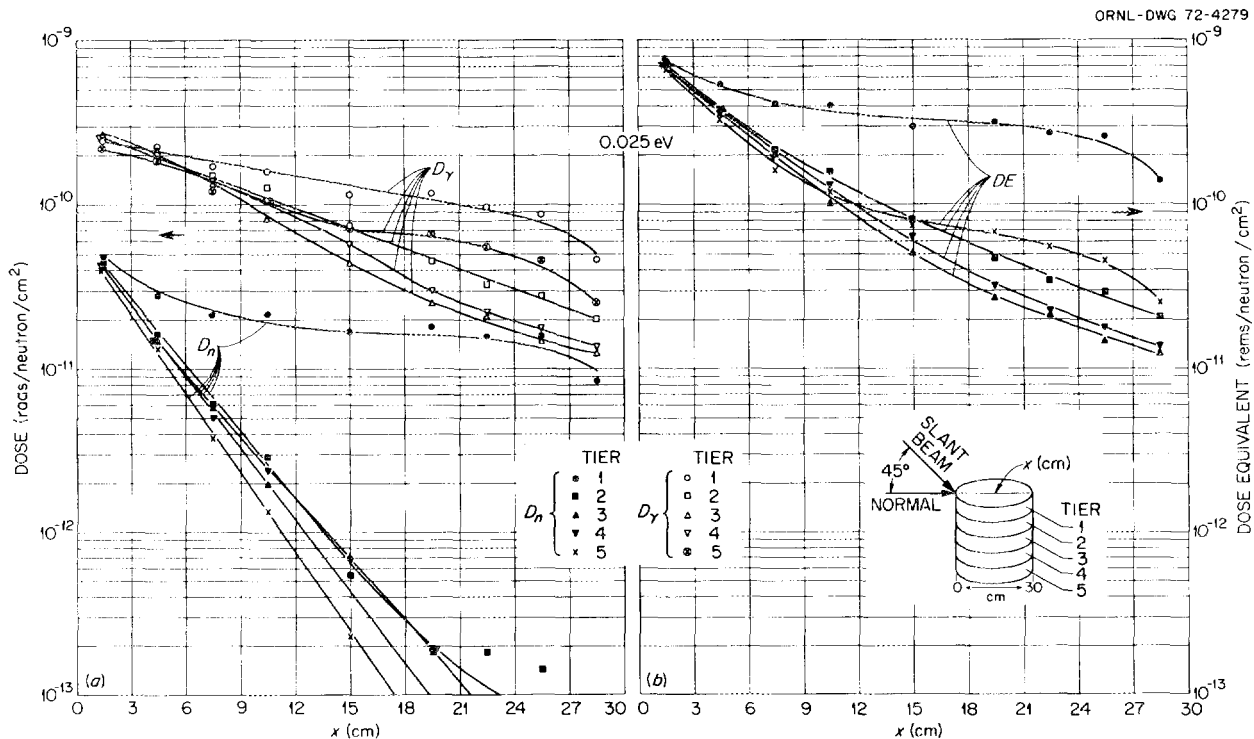


Fig. 7.7. Dose and dose equivalent in a tissue cylinder irradiated by slant beams of neutrons of energy 0.025 eV.

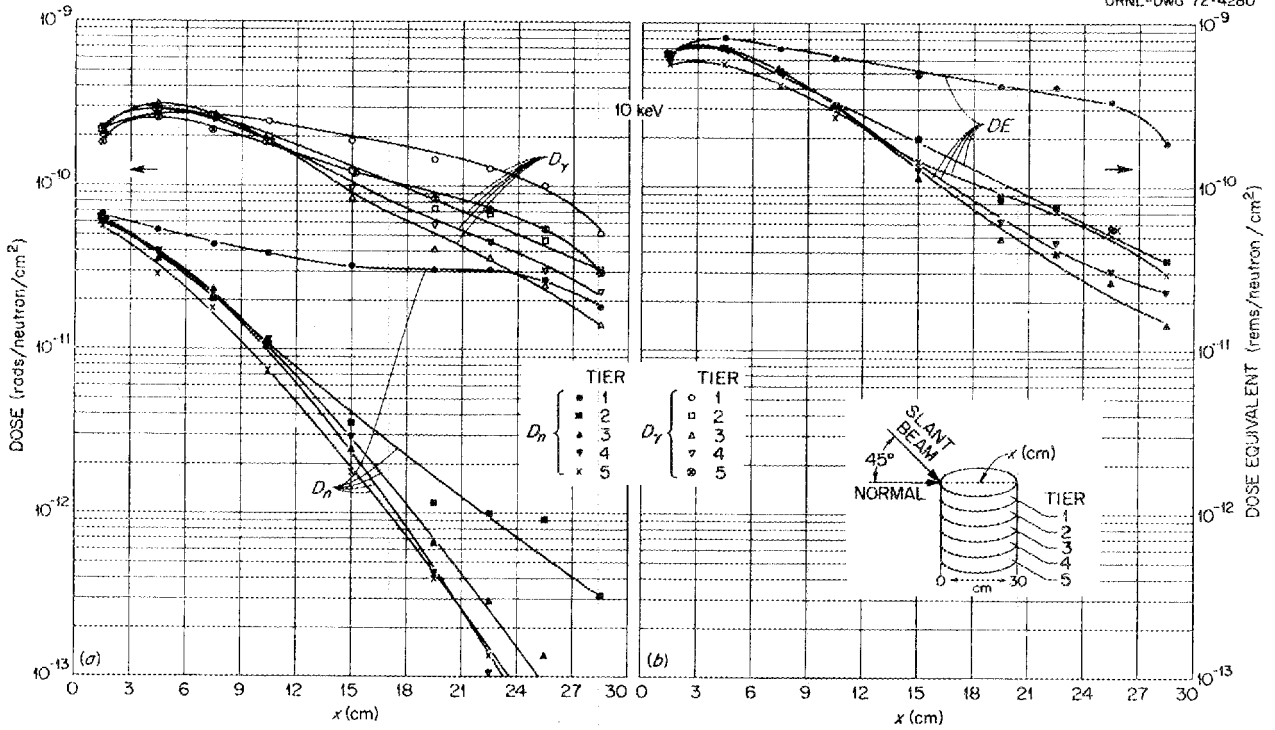


Fig. 7.8. Dose and dose equivalent in a tissue cylinder irradiated by slant beams of neutrons of energy 10 keV.

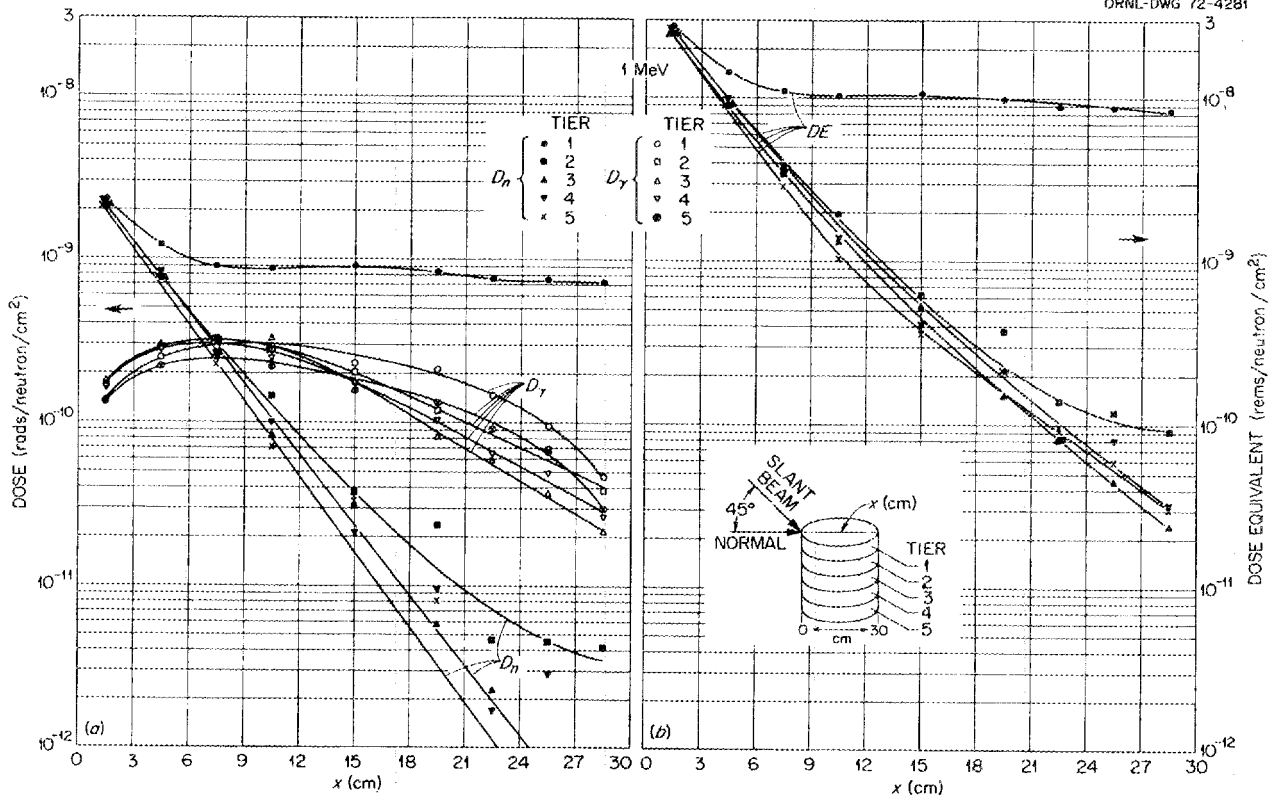


Fig. 7.9. Dose and dose equivalent in a tissue cylinder irradiated by slant beams of neutrons of energy 1 MeV.

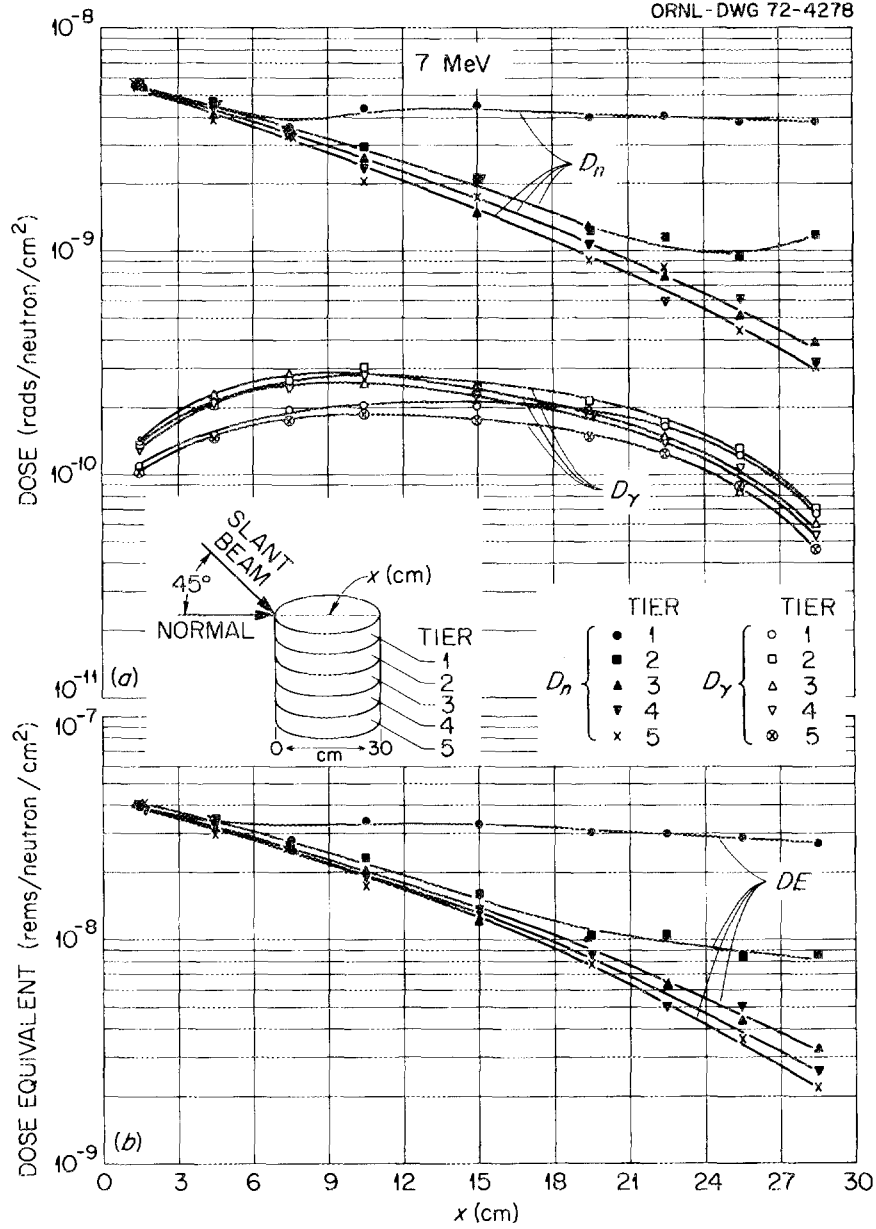


Fig. 7.10. Dose and dose equivalent in a tissue cylinder irradiated by slant beams of neutrons of energy 7 MeV.

dose equivalent are shown for neutron energies of 0.025 eV (thermal), 10 keV, 1 MeV, and 7 MeV, but now the beam makes an angle of 45° with the axis of the cylinder. The close study of the behavior of dose in the various tiers emphasizes the differences of dose in the several tiers due to neutrons entering the top of the cylinder.

In a recent paper, Keyrim-Markus et al.<sup>12</sup> reported some calculations of dose due to neutron beams

incident at various angles on a tissue phantom. They offer a number of rules for assessing maximum dose in the human body for slant beams or for other source types. They correctly point out that few neutrons traverse the body, and, consequently, for neutrons of the fission spectrum the contribution to maximum dose

12. I. B. Keyrim-Markus et al., *Health Phys.* 22(2), 187 (1972).

is largely due to neutrons which have entered the phantom near the site of the maximum on the dose — or dose equivalent — curve. However, their analysis does not indicate fully the complexity of the geometry of the body. Consider, for example, dose distributions as calculated for a beam of neutrons impinging on the phantom at an angle with the axis of the cylinder. The phantom geometry is indicated on the figures, and you will note that in tier 1 the dose is almost constant. This is due to neutrons which enter through the top of the phantom. The dose in the other tiers is much smaller than in tier 1. Actually this is still a simplified phantom. In actuality, the presence of the head would have an effect on dose. In fact, the peak dose in the body should be almost independent of the direction of the beam for neutron energies at which the peak dose is largely due to the neutrons undergoing their first collisions. On the human body, there will always be areas where the beam is almost perpendicular to the surface, and here the peak dose will be almost the same as that of the normal beam on the slab. Of course, this is not true for neutrons of all energies but only for those for which the “first collision” dose is a major contributor to the peak value, say, for neutrons of 0.5 to 10 MeV, which comprise much of the fission spectrum. For energies such that photons make a significant contribution to the peak dose, this will not

apply, and in any case it seems to apply only to the peak dose; that is, the dose from the slant beam, except at the peak, will generally be less at comparable positions than for the normal beam, as Keyrim-Markus points out, but “comparable” must be interpreted to apply to distance from the nearest irradiated surface.

**Photon Exposures**

The heterogeneous phantoms shown in Fig. 7.11 were assumed to be unilaterally irradiated by a parallel beam of monoenergetic photons limited to incidence on the torso for calculational efficiency. Figures and tables of dose distributions within the phantoms were presented in ORNL-4720.

The increase in dose along some depth-dose curves was the result of averaging dose to part of the spine into some of the volume elements, for anterior exposure to photons having source energies equal to or less than 250 keV. The statistical deviations of the points for photon source energies below 1.25 MeV were computed to be 2 to 5%, and the “increase” appeared to be due to absorption coefficients which were larger for bone than for soft tissue. The increase was only prominent for low energies, where the photoelectric process predominated, as shown in Fig. 7.12. Figure 7.12 also illustrates that relative changes in the absorption coefficients are nearly

ORNL—DWG. 71-6624

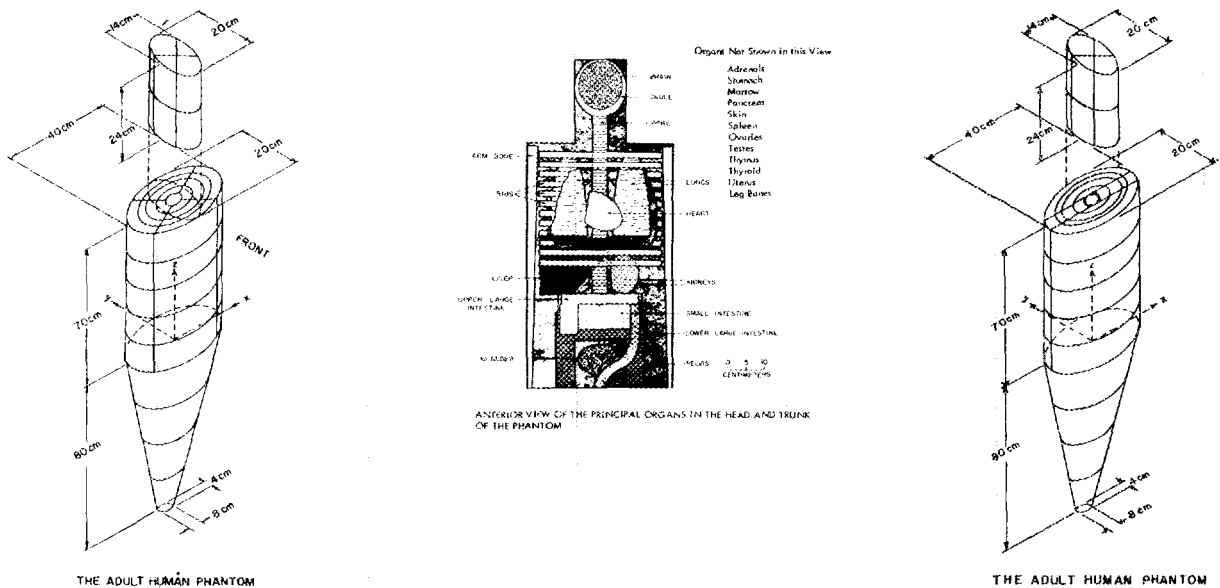


Fig. 7.11. Phantom for anterior and posterior exposures; phantom for left-side exposures.

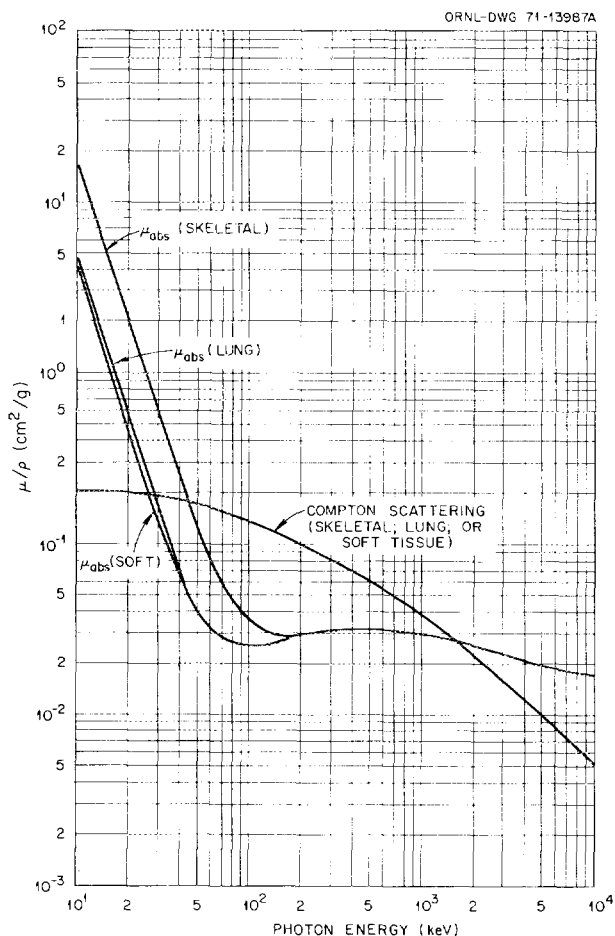


Fig. 7.12. Attenuation coefficients for skeletal, lung, and soft tissue.

independent of energy. Thus, for higher energies the effect is lost due to:

1. the convergence of the photon absorption coefficients of the three media;
2. the longer mean collision path length, which is inversely proportional to the linear absorption coefficient;
3. an increase in the variance of the dose contribution to a given volume element.

A. R. Jones<sup>13</sup> has made measurements of dose on and within a human-sized phantom from point sources of photons. Comparison of Jones' results for a heterogeneous phantom to results for homogeneous phantoms

13. A. R. Jones, *Measurement of the Dose Absorbed in Various Organs as a Function of the External Gamma Ray Exposure*, AECL-2240 (October 1964).

or to our heterogeneous results (presented in ORNL-4720) was difficult because his results were expressed as ratios of:

1. absorbed dose at a detector location normalized to the exposure in free air;
2. absorbed dose at a detector location normalized to the exposure at the site of a personnel dosimeter.

The agreement of our work with Jones' did not appear to be good; however, limits of uncertainty were large, and the exposure situations were not identical. The results of our calculations of dose to the skin for unilateral anterior exposure are shown in Table 7.3. Snyder<sup>14</sup> computed ratios of the maximum to the minimum dose to skin for a homogeneous phantom and illustrated that Jones' results tended to produce separate curves for anterior and posterior exposure. These ratios for anterior and posterior exposure were recomputed for our heterogeneous phantom, and the variances of the ratios  $Y_i/X_i$  were computed according to:

$$\text{Var}(V) \doteq \frac{y^2}{x^2} \text{Var}(x) + \frac{1}{x^2} \text{Var}(y).$$

The results shown in columns 1 and 2 of Table 7.4 appear to illustrate that there is no detectable difference in the ratios of the maximum to the minimum dose to skin for anterior and posterior irradiation except for minor statistical fluctuations. Instead, this "virtual" difference tends to illustrate the magnitude of the experimental and calculational errors and how errors of negative or opposing magnitudes can influence the results of a ratio. This point should be worth keeping in mind because experimental results are usually normalized to some other value of varying but usually known reliability.

A depth-dose value equal to that for a penetration depth of 5 cm as read from a depth-dose curve is commonly used by therapists for the dose to red marrow. Table 7.5 compares this assumption with the exposure situations from these calculations. The first column shows the source energy, and the second, third, and fourth columns give doses at penetration depths of 5 cm normalized to the average red marrow dose for anterior, posterior, and left-side irradiation. For the "rule" to be very accurate, the ratios should be near unity, and, as seen in this table, one should not expect

14. W. S. Snyder, "Variation of Dose in Man from Exposure to a Point Source of Gamma Rays," in *Congrès International sur la Radioprotection dans l'Utilisation Industrielle des Radioéléments*, Paris, December 13-15, 1965, Le Vesinet (1967).

Table 7.3. Dose to the skin from a broad parallel beam of photons, unilaterally incident on the anterior of the torso of a standard 70-kg human

Photon energy (keV)	Tier	Dose ( $10^{-9}$ rads photon $^{-1}$ cm $^2$ )			Photon energy (MeV)	Tier	Dose ( $10^{-9}$ rads photon $^{-1}$ cm $^2$ )		
		Anterior	Posterior	Side			Anterior	Posterior	Side
50	5	0.0471	0.00442	0.0182	1.25	5	0.616	0.249	0.539
	4	0.0483	0.00595	0.0304		4	0.664	0.393	0.655
	3	0.0474	0.00295	0.0293		3	0.747	0.271	0.500
	2	0.0472	0.00365	0.0315		2	0.464	0.185	0.602
	1	0.0479	0.00468	0.0314		1	0.578	0.241	0.536
		CV <sup>a</sup> =6%	CV=15-20%	CV=6%			CV=13-16%	CV=16-23%	CV=12-14%
100	5	0.0514	0.00881	0.0360	3	5	1.30	0.495	0.875
	4	0.0615	0.0143	0.0400		4	1.19	0.676	0.975
	3	0.0587	0.0105	0.0394		3	0.943	0.544	1.22
	2	0.0595	0.00796	0.0401		2	0.945	0.792	1.10
	1	0.0538	0.00678	0.0395		1	1.08	0.499	0.840
		CV=7-8%	CV=15-20%	CV=7-8%			CV=17-19%	CV=20-25%	CV=14-16%
250	5	0.146	0.0437	0.112	6	5	2.62	0.525 <sup>b</sup>	1.74
	4	0.170	0.0613	0.122		4	1.71	1.25	1.32
	3	0.135	0.0367	0.106		3	1.68	1.01	1.51
	2	0.140	0.0514	0.114		2	1.68	1.38	1.50
	1	0.146	0.0393	0.115		1	1.97	0.838	1.80
		CV=9-10%	CV=15-20%	CV=9%			CV=18-22%	CV=23-29%	CV=16-19%
660	5	0.302	0.111	0.292	10	5	2.70	2.04	2.85
	4	0.380	0.208	0.345		4	2.47	2.26	2.35
	3	0.375	0.156	0.348		3	2.86	2.30	2.49
	2	0.395	0.124	0.328		2	2.36	1.17	2.78
	1	0.355	0.158	0.333		1	2.48	1.21	2.60
		CV=12%	CV=16-20%	CV=10-11%			CV=22-24%	CV=24-31%	CV=18-20%

<sup>a</sup>Coefficient of variation in percent.

<sup>b</sup>This single number had a CV = 36%.

Table 7.4. Ratios of entrance to exit dose for monoenergetic photons

E (keV)	Ratio						Snyder, homogeneous phantom
	Beam on anterior	Beam on posterior	Normalized to free air		Normalized to film badge site		
			A. R. Jones, beam on anterior	A. R. Jones, beam on posterior	A. R. Jones, beam on anterior	A. R. Jones, beam on posterior	
38			15.6	11.7	15.8	11.1	
50	16.1 ± 3.1	17.1 ± 3.4					
60			10.6	10.6	11.0	10.5	
70							9.0
75			5.9	8.0	6.0	7.3	
100	5.6 ± 1.1	5.4 ± 0.90	3.6	6.2	3.6	6.1	
125			3.4	5.2	3.4	5.3	
165	7.5 ± 1.6	4.7 ± 0.83	2.9	5.2	3.0	5.1	4.8
240			2.9	5.9	2.9	5.9	
250	3.7 ± 0.76	3.9 ± 0.75					
400			1.9	2.8	1.8	2.8	
500							3.3
660	2.4 ± 0.52	3.7 ± 0.98	1.8	2.2	1.8	2.1	
1,000							2.4
1,250	2.8 ± 0.67	1.9 ± 0.46	1.9	2.2	1.7	2.2	
3,000	1.7 ± 0.49	1.1 ± 0.30					
6,000	1.7 ± 0.55	1.4 ± 0.43					
10,000	1.2 ± 0.39	2.5 ± 0.88					

Table 7.5. Ratio of dose at a depth of 5 cm to average red marrow dose

Energy	Ratio		
	Anterior irradiation	Posterior irradiation	Left-side irradiation
6 MeV	1.3	1	1.3
1.25 MeV	1.6	0.7	1.8
250 keV	2.0	0.5	2.0
50 keV	2.5	0.1	3.0

this rule to be more accurate than a factor of 2, and in many cases it may be even less accurate.

### MEASUREMENTS AT THE BIOLOGY DIVISION <sup>252</sup>Cf IRRADIATION FACILITY

The ORNL Biology Division operates a <sup>252</sup>Cf irradiation facility as part of a study to evaluate in mice some effects of high-dose-rate vs low-dose-rate protracted exposure to fission neutrons and gamma rays. The high-dose-rate exposures are performed at the HPRR. To allow comparison of exposures at both facilities, the Radiation Dosimetry Section was requested to perform the necessary dosimetry experiments at the <sup>252</sup>Cf facility.

The facility consists of a <sup>252</sup>Cf source (0.8 mg, nominal when installed) which when removed from the shield is positioned at the center of a 15.3-cm-diam depleted uranium sphere. The sphere is positioned directly above the <sup>252</sup>Cf storage well on a pipe stanchion. The source height during exposure is 117 cm above the concrete floor. Animals are exposed in cages placed on aluminum shelves and positioned on an arc around the source. Design of the experiment called for the animals to be exposed to 1 rad/day of fast neutrons when positioned at a distance of 2 m from the source. The study at the facility included:

1. measurement of neutron and gamma-ray dose as a function of distance from the source (see Fig. 7.13),
2. measurement of scattered to total neutron dose,
3. measurement of neutron and gamma-ray dose with and without the depleted <sup>238</sup>U sphere,
4. measurement of the effects of the shelves and animal cages on the free-field dose,
5. measurement of the symmetry of the neutron and gamma-ray dose on an arc around the source (see Fig. 7.14),
6. measurement of the neutron spectrum with and without the depleted <sup>238</sup>U sphere,

7. measurement of proton recoil spectra to allow the calculation of LET distributions for the exposure configuration.

Neutron dose was measured with the Hurst proportional counter, while gamma-ray dose was measured with the "Phil" dosimeter. All measurements were monitored with a modified long counter. Proton recoil

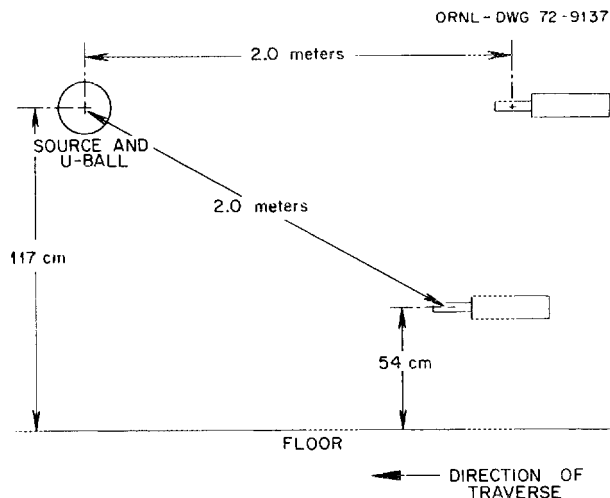


Fig. 7.13. Sketch of experiment arrangement.

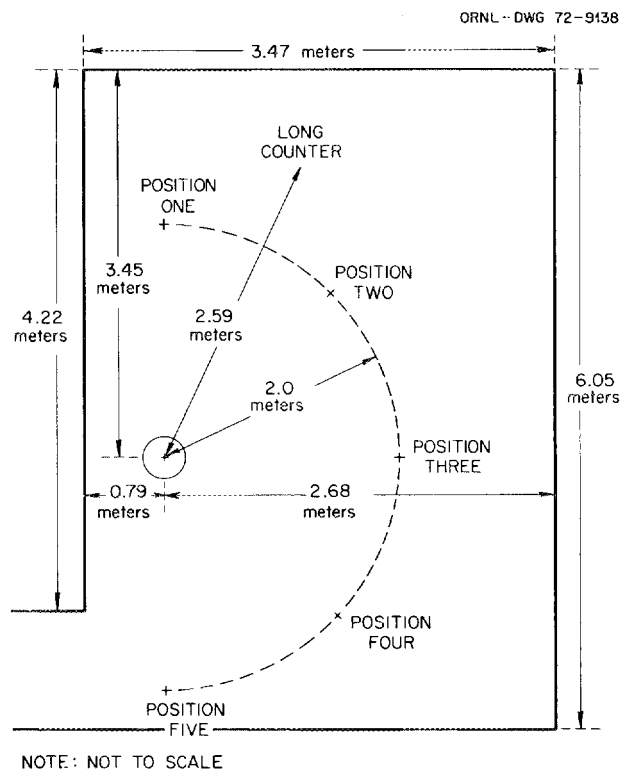


Fig. 7.14. Sketch of exposure room.

spectra were measured with the Hurst counter and a Rossi LET spherical detector. The fission-foil track etch technique was employed to measure the source spectra.

Evaluation of initial results indicated that the source strength was below optimum (consequently, the source was replaced). Figure 7.15 shows a plot of dose vs distance from the source for distances which were to be used. The detector heights correspond to the heights of two of the shelves. Table 7.6 gives the results of symmetry measurements around the source. Variations in the dose around the arc are within the errors typical of such experiments.<sup>15</sup> Table 7.7 shows the ratio of

scattered to total neutron dose measured using the shadow-cone technique. No measurements of scattered gamma dose were made.

15. D. R. Johnson and J. W. Poston, *Radiation Dosimetry Studies at the Health Physics Research Reactor*, ORNL-4113 (June 1967).

Table 7.6. Positional dependence of dose around  $^{252}\text{Cf}$  source  
2.0 m from the source

Position	Detector height (cm)	Neutron dose rate (millirads/hr)	Gamma dose rate (millirads/hr)
1	117	43.4	18.8
	54	39.2	14.7
2	117	42.5	18.5
	54	36.9	14.4
3	117	43.9	19.7
	54	38.2	15.2
4	117	42.9	19.3
	54	37.6	14.7
5	117	42.8	18.0
	54	38.1	13.8

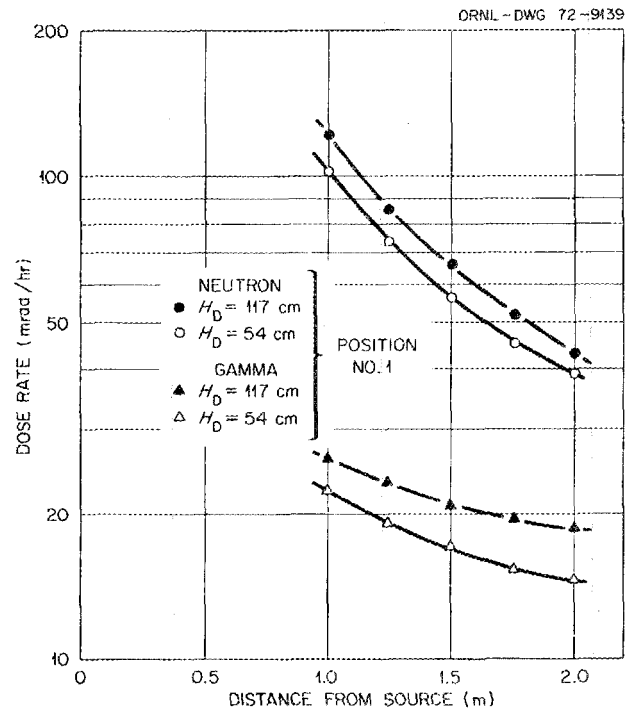


Fig. 7.15. Dose rate vs distance from source.

Table 7.7. Measurement of scattered to total dose

Position	Source condition	Neutron dose rate (millirads/hr)		Ratio of scattered to total	Gamma dose rate (millirads/hr)	
		Total	Scattered		Total	Scattered
1	U ball	43.4	18.8	0.433	18.8	
	Bare	62.9	26.1	0.415	37.4	
3	U ball	43.9	18.5	0.421	19.7	
	Bare	63.1	25.4	0.403	37.8	

## 8. Applied Dosimetry Research

Klaus Becker

J. S. Cheka            M. H. Lee<sup>2</sup>  
K. W. Crase<sup>1</sup>        J. S. Nagpal<sup>2</sup>  
R. B. Gammage       M. Sohrabi<sup>2</sup>

### THE ROLE AND NATURE OF ACTIVATORS IN TSEE

A systematic review of the existing information on thermally stimulated exoelectron emission (TSEE) from various materials,<sup>3</sup> detailed discussions with other investigators on discrepancies in the results, and extensive experimental studies led to a reshaping of ideas concerning the role of activators in exoelectron emission. It has been demonstrated that heat treatment, impregnation with silicon dioxide<sup>4</sup> or lithium,<sup>5</sup> and preirradiation with charged particles<sup>5</sup> result in pronounced qualitative and quantitative changes in the TSEE characteristics of ceramic BeO (Brush Thermalox 995). These changes were tentatively attributed to the creation or destruction of electron traps which are directly contributing to the exoelectron emission process.

It appears now that the situation is more complex. Activators seem to fall into one or both of two categories. They may perform in a traditional manner, providing the electron trap from which the exoelectron emerges. Alternately, they may act in an indirect manner, promoting the release of detrapped electrons as exoelectrons.

Exoelectron emission (EE) appears to occur only from specific surface regions and to depend strongly on a sufficient electrical surface conductivity without which local buildup of residual charge prevents further emission. Some of the "activators" which have been

studied during the last 20 years in numerous laboratories may influence TSEE indirectly by modifying such parameters as surface conductivity, work function, or irregularities of the crystal surface. Indeed, preliminary results of conductivity measurements show that the poorly emitting Thermalox 998 is less conductive by a factor of 10 than the excellent emitter Thermalox 995 ( $10^{16} \Omega$  compared with  $10^{15} \Omega$  at  $20^\circ\text{C}$ ).

Silicon and lithium activators<sup>6</sup> provide two examples of the importance of compound formation to the EE process. Substitutionally incorporated silicon in single-crystal BeO is usually less than 100 ppm,<sup>7</sup> but Thermalox 995 and 998 have silicon contents of 2000 and 81 ppm, respectively. The excess silicon, which is concentrated at grain boundaries in the form of phenacite ( $2\text{BeO}\cdot\text{SiO}_2$ ), produced in a heat treatment at  $1400^\circ\text{C}$ , helps to optimize TSEE.<sup>4</sup> The TSEE peaks, however, are intrinsic to the ceramic BeO and not to the phenacite, as shown in experiments with a natural phenacite powder (Fig. 8.1).

With lithium activation, sensitization of the EE is linked to the formation of a compound of suspected composition  $\text{Li}_2\text{BeO}_2$ .<sup>8</sup> This compound is unstable above its melting point of approximately  $950^\circ\text{C}$ , and with its decomposition the EE becomes desensitized (see also Regulla et al.<sup>9</sup>). A BeO powder activated with sodium (Matsushita, Osaka), after calcination at  $1400^\circ\text{C}$ , exhibits a TSEE curve which is similar to that

---

1. Public Health Service Radiological Health Fellow.  
2. Alien guest.  
3. K. Becker, *Crit. Rev. Solid-State Sci.* **3**, 39 (1972).  
4. R. B. Gammage, K. W. Crase, and K. Becker, *Health Phys.* **22**, 57 (1972).  
5. R. B. Gammage, K. Becker, K. W. Crase, and A. Moreno y Moreno, *Proceedings of Third International Conference on Luminescence Dosimetry, October 11 thru 14, 1971*, Risø Report No. 249, Part II, p. 573, 1972.

---

6. K. W. Crase, K. Becker, and R. B. Gammage, *Parameters Affecting the Radiation-Induced Thermally Stimulated Exoelectron Emission from Ceramic Beryllium Oxide*, ORNL-TM-3572 (November 1971).

7. D. T. Livey, "Beryllium Oxide," in *High Temperature Oxides*, Part III, Academic, 1970.

8. R. Hendricks, Jr., U.S. Patent 3,529,046 (1970).

9. D. F. Regulla, G. Drexler, and L. Boros, *Proceedings of Third International Conference on Luminescence Dosimetry, October 11 thru 14, 1971*, Risø Report No. 249, Part II, p. 601, 1972.

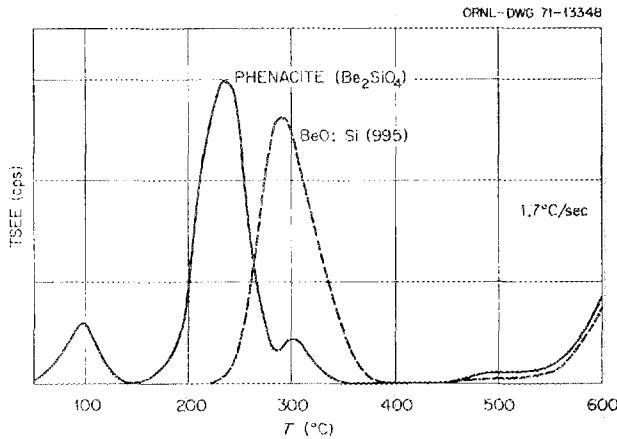


Fig. 8.1. TSEE of powdered natural Brazilian phenacite ( $\text{Be}_2\text{SiO}_4$ ) and powdered ceramic BeO (Brush Thermalox 995) mixed with graphite powder and plated on graphite carrier disk.

of BeO 995 (Fig. 8.2). Thus, lithium and sodium appear to be performing similar roles for TSEE.

The eutectic temperature for  $\text{BeO} + \text{TiO}_2$  is  $1670^\circ\text{C}$ .<sup>10</sup> After heating the titanium-impregnated surface of the poor emitter BeO 998 at  $1400^\circ\text{C}$ , no substantial changes in the TSEE characteristics occurred. At  $1600^\circ\text{C}$ , however, which is closer to the eutectic, the TSEE curve begins to look remarkably similar to that of BeO 995. The same effect was observed after diffusing silicon into silicon-depleted ceramic BeO. Apparently each of these activators is promoting EE which is already intrinsic to the ceramic BeO by increasing the efficiency of exoelectron release.

Other activators, however, resulted in the appearance of new EE peaks.<sup>11</sup> This group of activators, therefore, seems to provide new trapping sites. In Fig. 8.3 boron can be seen to have introduced some new TSEE peaks in Thermalox 998 after a diffusion treatment at  $1400^\circ\text{C}$ . Because of its small ionic radius ( $0.20 \text{ \AA}$  compared with  $0.31 \text{ \AA}$  for  $\text{Be}^{2+}$ ),  $\text{B}^{3+}$  will substitutionally displace  $\text{Be}^{2+}$  in amounts up to 0.25% with no evidence of segregation<sup>7</sup> and has the potential to act as an electron trap. For  $\text{BeO} + \text{CaO}$  the eutectic temperature is  $1384^\circ\text{C}$ .<sup>12</sup> Heating Thermalox 998 impregnated with  $\text{Ca}(\text{OH})_2$  at close to this temperature ( $1400^\circ\text{C}$ ) resulted in the TSEE spectrum of Fig. 8.4. Activation

10. S. M. Lang, C. L. Fillmore, and L. H. Maxwell, *J. Res. Nat. Bur. Stand.* 48(4), 300 (1952).

11. A. Moreno y Moreno, J. S. Cheka, J. S. Nagpal, R. B. Gammage, and K. Becker, *Further Studies on TSEE Activators in BeO*, ORNL-TM-3668 (March 1972).

12. R. A. Potter and L. A. Harris, *J. Amer. Ceram. Soc.* 45(12), 615 (1962).

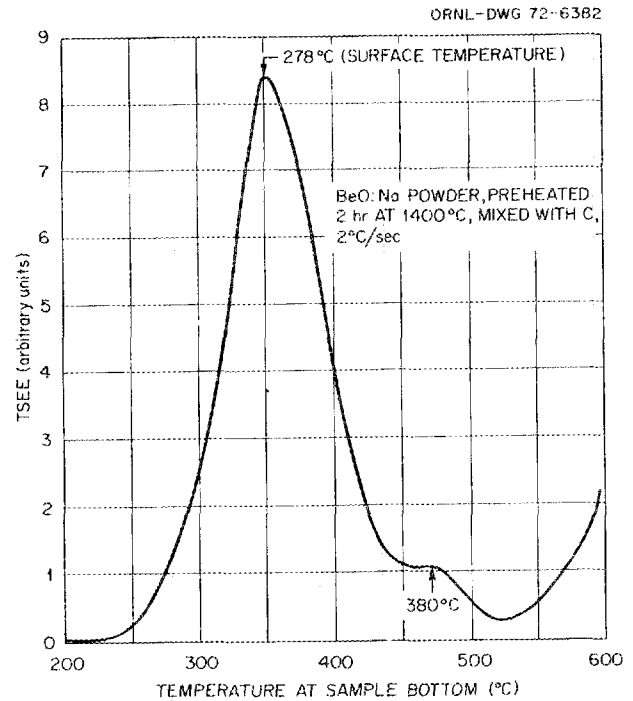


Fig. 8.2. TSEE of BeO:Na in a graphite powder matrix plated on graphite carrier disk. The actual surface temperature is below that at the carrier bottom where the thermocouple is located.

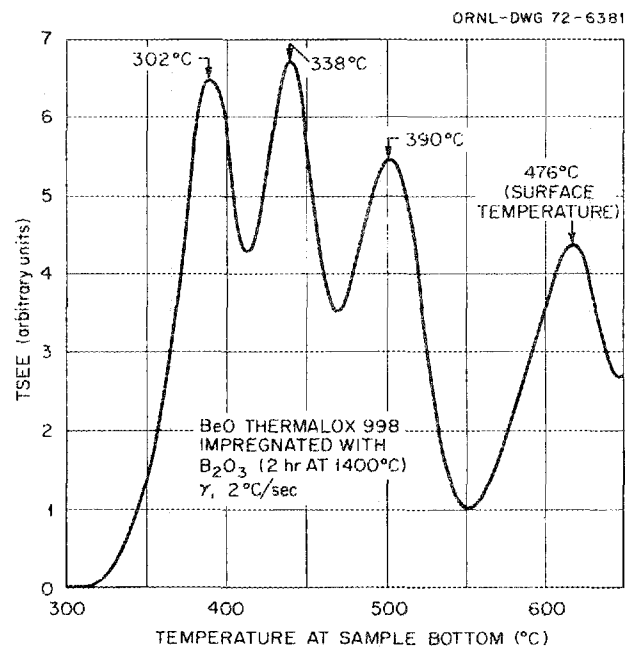


Fig. 8.3. TSEE of Thermalox 998 after impregnating the surface with a  $\text{B}_2\text{O}_3$  solution and heating for 2 hr at  $1400^\circ\text{C}$ .

with manganese at 1200°C also showed evidence for new TSEE peaks.

Cold-pressed pellets of intimately mixed high-purity beryllia powder (<20 ppm impurities) and Cabosil silica powder were prepared with silica contents up to 1% by weight (as can be seen in Fig. 8.5, an SiO<sub>2</sub> addition of about 6% would result in a minimum inherent energy dependence for photons). The pellets were fired in air at 1600°C. Preliminary results indicate that there is an increase in TSEE sensitivity with increasing SiO<sub>2</sub>

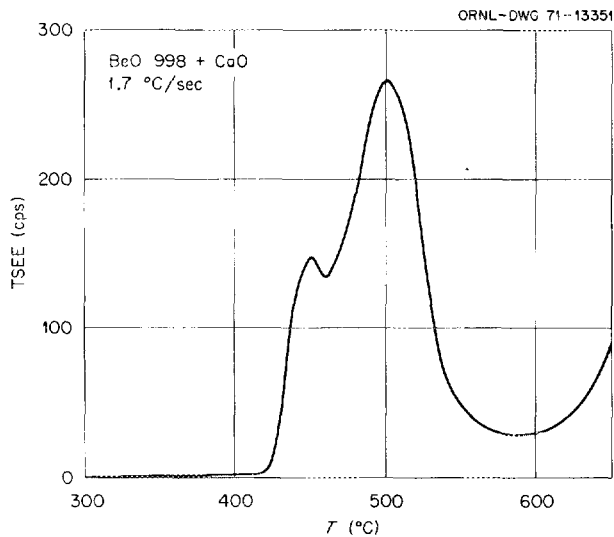


Fig. 8.4. TSEE of ceramic BeO (Thermalox 995) after impregnating the surface with a Ca(OH)<sub>2</sub> solution and heating for 2 hr at 1400°C.

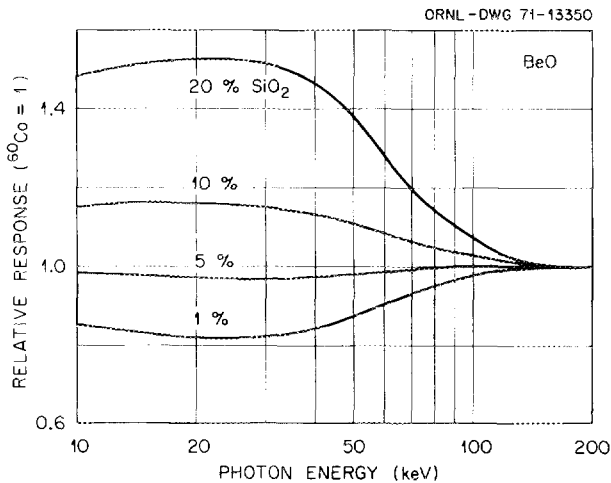


Fig. 8.5. Calculated energy dependence of the photon response of bulk BeO with varying amounts of SiO<sub>2</sub> homogeneously distributed.

content. The TSEE spectra were similar to those seen with BeO 995.

A number of ceramic BeO's containing varying amounts of MgO, SiO<sub>2</sub>, CaO, and Al<sub>2</sub>O<sub>3</sub> added before firing at 1600°C were also studied. None of these samples exhibited a glow curve (after heating at 1400°C) different from that of BeO 995. Samples with 1% by weight 5Al<sub>2</sub>O<sub>3</sub>·5SiO<sub>2</sub>·5MgO·CaO and Thermalox 995 at 1% additive level exhibit a sensitivity comparable to that of BeO 995. Heating for 4 hr at 1600°C did not change the peak locations but enhanced the sensitivity considerably. Heat-treatment experiments will be extended in the near future up to 2500°C.

### TSEE READER DEVELOPMENT

It was previously established that BeO ceramic has many desirable characteristics as a TSEE radiation detector. Before practical application of such detectors can be considered, a counting system is required wherein reproducible conditions are maintained over hundreds of readouts.

In the previously used TSEE reader, samples were not readily and rapidly interchangeable. A new routine counter, whose essential features are shown in Fig. 8.6, permits such rapid loading in a reproducible manner. A plate of Vycor glass has a central 3/8-in. hole lined with a grounded platinum strip against which the 1/2-in. BeO disk is pressed during readout. The BeO disk sits in a gold cap above the heater unit which can be raised or lowered on a weighted lever arm. Some movement in three dimensions is permitted to allow for correction of

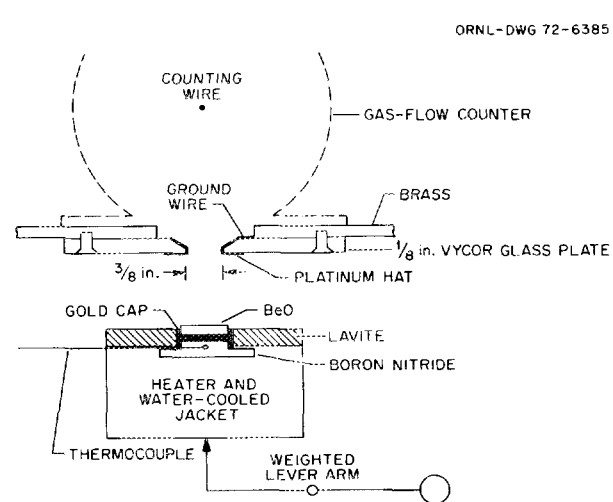


Fig. 8.6. Schematic diagram of new "routine" TSEE counter with rapidly interchangeable samples.

any geometric irregularity in a BeO disk which might otherwise prevent proper seating against the platinum strip. The  $\frac{1}{8}$ -in.-thick glass appears to be close to the optimum for mechanical strength, minimum well depth through which the exoelectrons must pass, and thermal insulation to minimize temperature gradients in the BeO and keep the counter cool.

The performance that the instrument is capable of is shown in Fig. 8.7. Over a period of two days and after exposure of the disk to a constant radiation dose, 15 consecutive readouts of the same BeO disk gave responses with a standard deviation of 2.6%. The first readout on each day, however, gave a significantly higher response than the mean, a phenomenon that is discussed later in this report.

It is important that variations in counter characteristics remain small while variations intrinsic to the BeO are being studied. Two types of counter characteristics are of particular interest: the long-term stability in the count rate obtained from a standard external source, and the daily variations that might arise from a cold or moisture-contaminated Geiger tube. Over a period of two months the response to a small  $^{60}\text{Co}$  source showed a spread of 5%. The short-term stability was

tested with a beta emitter ( $\text{UO}_2$ ) placed at the position normally reserved for the BeO and heated to  $450^\circ\text{C}$ . Readings taken with the counter, either cold or warm, were constant to approximately 1%. The stability of the counter is judged to be quite adequate, provided that the counter components and the operating conditions are held constant.

Certain limitations must be recognized, however, in the use of external or internal emitters of gamma or beta radiation for the calibration of TSEE counters because of the large energy differences compared with exoelectrons. For example, the excellent plateau which is observed with an external  $^{60}\text{Co}$  source (Fig. 8.8) is replaced by a completely different slope of 20% per 100 V when actual exoelectron emitters are used in the same G-M counter.

An "ionization chamber" type of TSEE reader for high dose measurements<sup>13</sup> has been further modified and improved to include a voltage-to-frequency converter for integral current measurements. Introduction

13. K. W. Crase, R. B. Gammage, and K. Becker, *Health Phys.* 22, 402 (1972).

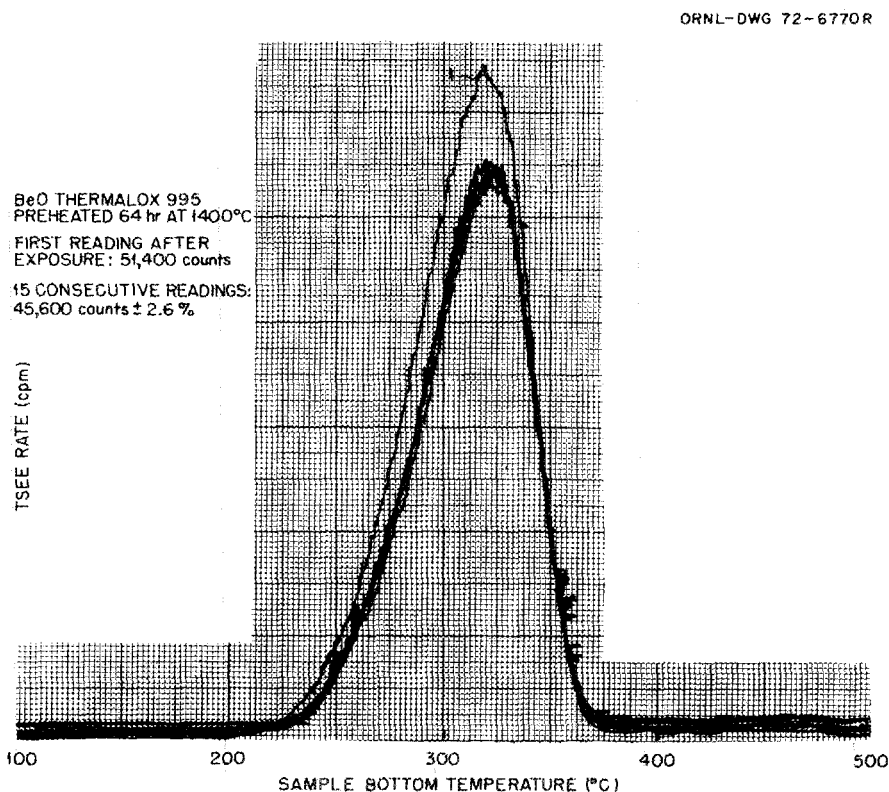


Fig. 8.7. TSEE curve of BeO 995 for the first and consecutive readouts after exposure to a constant gamma radiation dose.

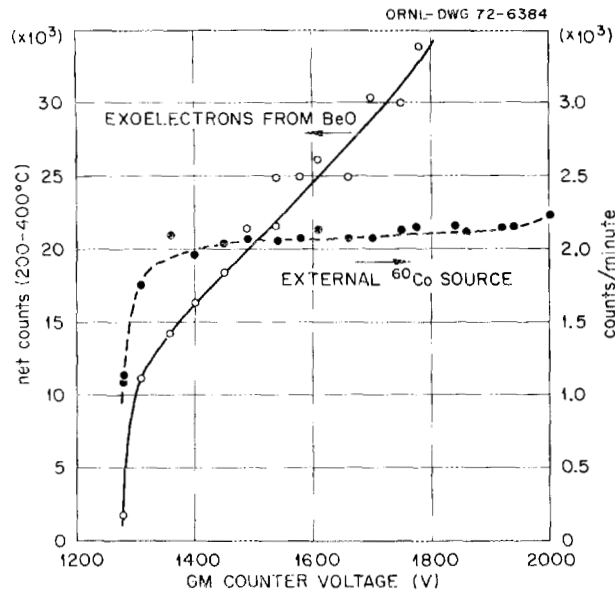


Fig. 8.8. TSEE counter plateaus for external gamma radiation and for exoelectrons from BeO.

of air into the helium-isobutane counting gas was observed to increase the sensitivity substantially, and the effect of various gases is presently being studied.

### REPRODUCIBILITY AND STABILITY OF TSEE DETECTORS

The new routine counter has been used to investigate sensitization and stabilization processes in ceramic BeO 995 disks purchased on separate dates. In a batch of 15 detectors the response was almost doubled by increasing the time of sensitization from 4 to 64 hr, and the spread in detector response (standard deviation) was reduced from 48 to 11%. The additional sensitization, however, is unstable during extended storage in an unmodified laboratory atmosphere. After about two months, the detectors had reached a stable "plateau" (Fig. 8.9). Other series of detectors were sensitized for different times and stabilized in liquid water or water vapor at 80% relative humidity. Table 8.1 shows the effects of these treatments on the mean response to 100 mR and the standard deviation. Evidently the mean response of each group settles to a level of about 20,000 counts per 100 mR for each stabilization treatment. Such results, however, have not always been confirmed by successive experiments. In one test, for example, a batch of 15 disks was heated at 1400°C for 264 hr. As Table 8.2 shows, the sensitivity of approximately 30,000 counts per 100 mR was maintained

throughout a variety of attempted "stabilization" treatments.

Another complication is an apparent "memory" effect. With increasing time after a previous readout, an increase is usually observed in the sensitivity of the dosimeter. Figure 8.7 illustrates this effect for a waiting period of one month before the first readout. Another sample (stabilized by water treatment) exhibits a nearly linear increase with time, the increase being about 25% after approximately one week (Fig. 8.10).

The effect of storage conditions (air of 0 to 100% relative humidity, temperatures of 20 and 120°C) on this memory effect has been studied. The first readouts were higher than the second and subsequent readouts under all conditions, and no clearly resolved influence

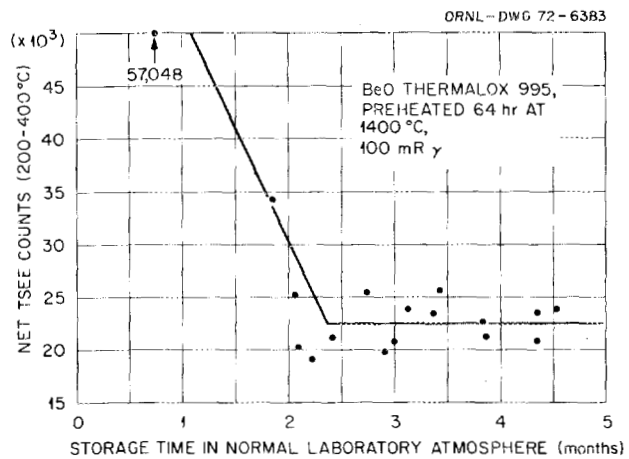


Fig. 8.9. Gamma radiation sensitivity (in net TSEE counts per 100 millirads) of a BeO 995 disk as a function of storage time in an unmodified laboratory atmosphere.

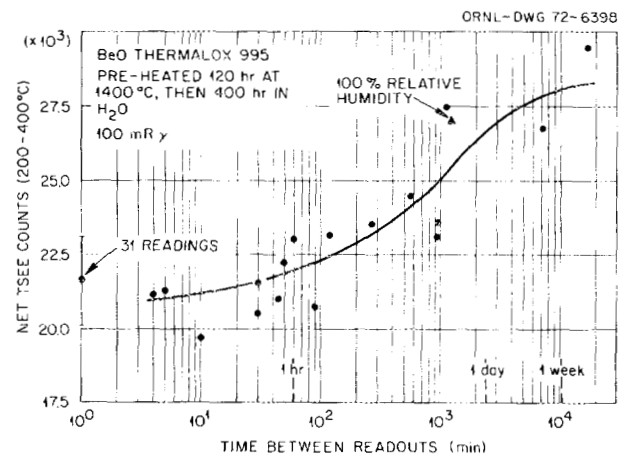


Fig. 8.10. Gamma radiation response of BeO 995 as a function of storage time between readouts.

Table 8.1. TSEE response of Thermalox BeO with varying heat sensitization and stabilization treatments

No. of disks	Heat treatment	Stabilization treatment	Mean response (net counts between 200 and 400°C)	Standard deviation (%)
15	64 hr at 1400°C	3 months in air	21,551	10.3
15	120 hr at 1400°C	400 hr in liquid H <sub>2</sub> O before drying at 600°C	20,469	8.9
6	10 hr at 1400°C	18 months in air at 80% relative humidity	18,806	4.8

Table 8.2. Invariant TSEE response of Thermalox BeO after an initial heat sensitization of 1400°C for 264 hr

Treatment	Mean response	Standard deviation (%)
Stored at 120°C and read out immediately	31,839	7.5
Storage in air at 80% relative humidity for 40 days	29,992	7.9
Heated in air at 600°C	31,818	10.4

of the storage conditions was observed. Apparently it depends principally on time. A pretreatment such as drying at 120°C just prior to readout for removal of absorbed humidity has no influence (on 12 occasions involving a whole spectrum of storage conditions, a single sample gave mean responses of 22,400 for the first readouts and 18,200 counts for immediately following second readouts, with a standard deviation of 10%).

However, there have been instances where the memory effect has worked in reverse (second readout higher). The rate of cooling of the samples from high temperatures apparently is significant for this effect. After the liquid water treatment, batches of samples were heated to 600°C and cooled either slowly or quickly. After rapid cooling the first readout proved to be high by a mean value of 20%, and after slow cooling, low by a mean value of 10%. Readout in the routine counter to 500°C includes fast cooling, which wipes out the effects of any prior slow cooling treatments.

Evidently, the dosimetric characteristics of ceramic TSEE detectors based on BeO are more complex than originally assumed, and several problems remain unresolved. By putting an accelerating potential on the gold cap in the reader, it is hoped to overcome some of the problems related to exoelectron "extraction." Also, sealed G-M tubes with bodies made of ceramic BeO, which are expected to simplify the use of TSEE dosimeters, are under development.

### ATMOSPHERIC, TEMPERATURE, AND OTHER EFFECTS ON TSEE

Having previously identified several parameters which can change the TSEE response of BeO 995, some experiments have been conducted under more closely controlled conditions. To eliminate inconsistencies related to the removal of samples from the readout instrument, they have been inserted and left undisturbed during repetitive irradiations and readouts. Particular care has been exercised to ensure constancy of counter characteristics, and attention has also been paid to gas flow effects (Fig. 8.11).

Irradiations in air at elevated temperatures, contrary to expectations, resulted in a significant reduction in the integral counts for the main peak (Fig. 8.12); a

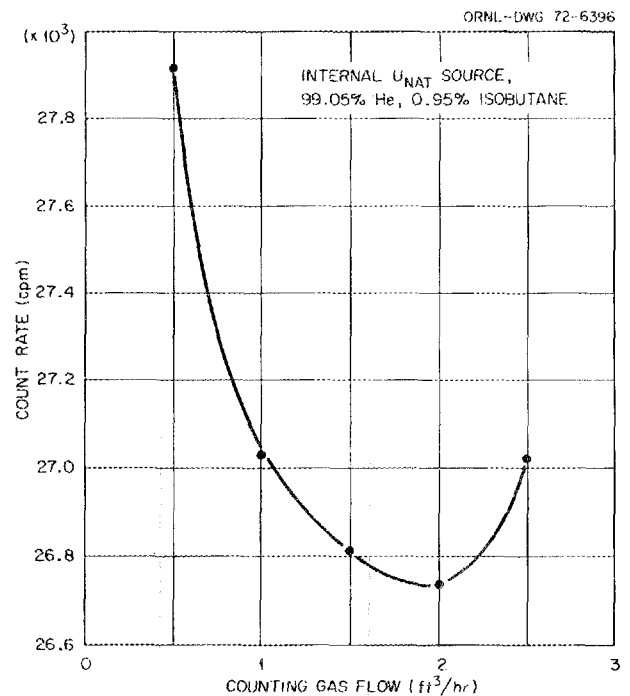


Fig. 8.11. Effect of counting gas flow on the G-M counter efficiency.

reduction of about 20% occurs between room temperature and 150°C.

To study the effect of the gaseous environment during irradiation, exposures were carried out in bottled (dry) breathing air, oxygen, nitrogen, and the helium-isobutane counting gas. Some TSEE curves for the

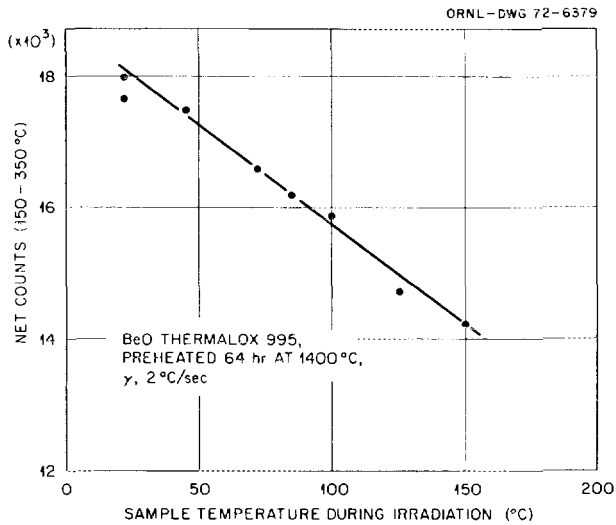


Fig. 8.12. Sensitivity of BeO 995 as a function of temperature during exposure to gamma radiation.

irradiations and readouts in helium-isobutane are shown in Fig. 8.13. A smaller but significant increase in response is seen when a nitrogen atmosphere is used, but a decrease in response occurs in an oxygen environment. In dry air the response remains constant. A possible explanation for the observed changes is that outgassing of the surface of the BeO takes place, with subsequent changes in the emission characteristics.

In the case of breathing air with added water vapor, a 30-min exposure prior to irradiation and readout produced a 6% reduction in the net counts. A similar effect was seen for moisture-containing helium-isobutane, the magnitude of the reduction being related to the amount of water present. It seems, therefore, that differences in the apparent sensitivity occur between well-outgassed surfaces and those covered with adsorbed water. The results for the oxygen atmosphere indicate that adsorbed oxygen also has a detrimental effect on the counting rate. (Under practical conditions, the oxygen effect, of course, can be ignored.)

If the detector is exposed to artificial room light prior to irradiation, there is also a reduction of the observed TSEE. The changes in the net counts are listed in Table 8.3. Obviously, the drop in response is greater for the combined exposure to light and air than for air alone. It can be concluded that several parameters may have to

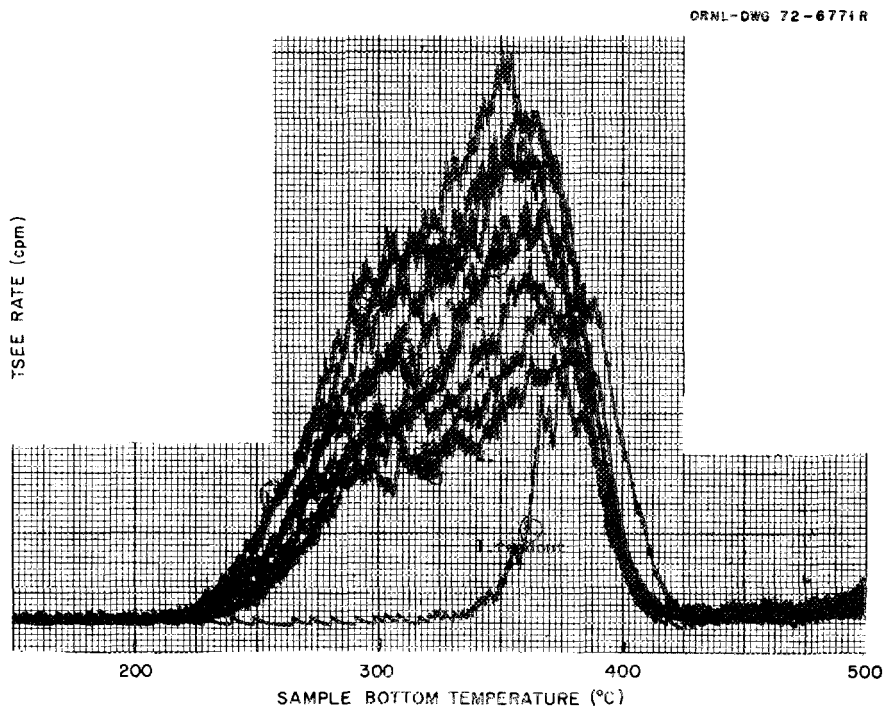


Fig. 8.13. Effect of repeated irradiation and readout in the counting gas (99.05% He, 0.95% isobutane) on the gamma radiation response of BeO 995.

Table 8.3. Effect of exposure to light and atmosphere on the TSEE response of Thermalox 995

No. of readout	Preirradiation treatment	Net counts (200–450°C)
1	Maintained in breathing air without exposure to light or atmosphere	8,817
2	Maintained in breathing air without exposure to light or atmosphere	10,057
3	Maintained in breathing air without exposure to light or atmosphere	10,675
4	Maintained in breathing air without exposure to light or atmosphere	10,793
5	Maintained in breathing air without exposure to light or atmosphere	11,163
6	Exposed in light and atmosphere	8,332
7	Exposed in light and atmosphere	8,655
8	Exposed to the atmosphere under dark conditions	9,710
9	Exposed to the atmosphere under dark conditions	9,696

be considered during irradiation, emission, and readout processes if high accuracy and/or reproducibility of the detectors is desirable.

#### FADING STABILITY OF SOLID-STATE AND FILM DOSIMETERS

Although much scattered information is available on the storage stability of radiation effects in various integrating detectors, the conditions under which their fading kinetics have been measured vary substantially, and few reliable data concerning the long-term exposure to higher temperatures and humidities are available. Therefore, fading experiments with some of the more interesting detector systems have been carried out under actual and simulated "tropical" climate conditions. Only a few of the results<sup>14</sup> can be given here.

Latent, unetched fission fragment tracks in 10- $\mu$ m polycarbonate (Kimfol) foil are stable for at least three months at 30°C and 95% relative humidity (Fig. 8.14). At 60°C and the same humidity, 25% fading was observed during three weeks after etching and spark counting. Three radiophotoluminescence (old and new Toshiba glass, C.E.C. glass) dosimeters also showed less than 15% deviation in their readings between one day and three months after exposure, if stored at 30°C and

95% relative humidity (Fig. 8.15). Of various thermoluminescent detectors,  $\text{CaSO}_4:\text{Dy}$  exhibited a barely detectable fading;  $\text{LiF}:\text{Mg,Ti}$  (TLD-100) and  $\text{CaSO}_4:\text{Tm}$  comparable fading rates (Table 8.4); and  $\text{CaF}_2:\text{Dy}$  a rather pronounced fading under the same conditions.

The results of the tests involving common Kodak dosimeter films were very discouraging, in particular when the films had been equilibrated with the ambient humidity prior to exposure (humidity requires some time to penetrate the film wrapping). The sensitive emulsion in the Kodak type 2 Personnel Monitoring films, as well as many of the NTA films, was completely destroyed after three months at 30°C and 95% relative humidity. The more resistant, insensitive emulsion of the type 2 film exhibited a large increase in fog density as well as pronounced fading (Fig. 8.16).

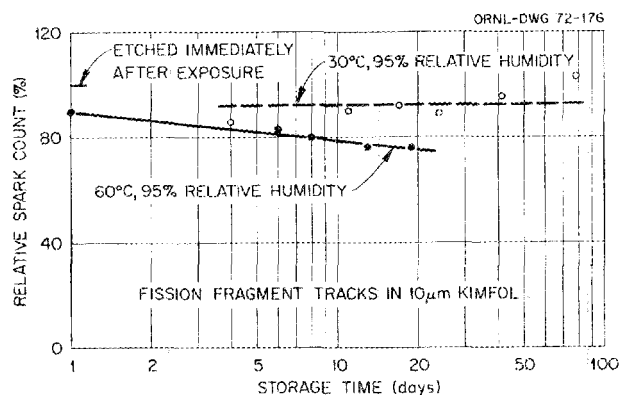


Fig. 8.14. Spark count of fission-fragment-irradiated polycarbonate foils as a function of storage time at elevated temperatures between exposure and etching.

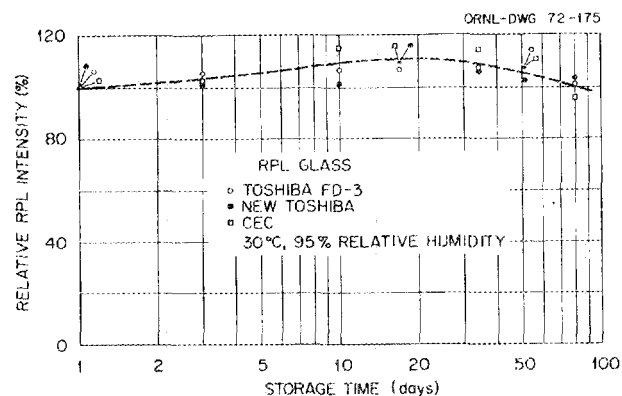


Fig. 8.15. Radiophotoluminescence in three different glass dosimeters as a function of storage time in a simulated tropical climate.

14. K. Becker, J. S. Cheka, J. S. Nagpal, and M. Sohrabi, an ORNL-TM report in preparation.

Table 8.4. Sensitivity and stability of some TLD phosphors

Material	Relative sensitivity		Fading during six weeks storage at 32°C (%)
	Harshaw 2000 reader	Teledyne 7710 reader	
LiF (TLD-100)	1	1	10
CaSO <sub>4</sub> :Dy (Harshaw)	25	30.5	1.5
CaSO <sub>4</sub> :Tm (Matsushita)	23	38	12.5

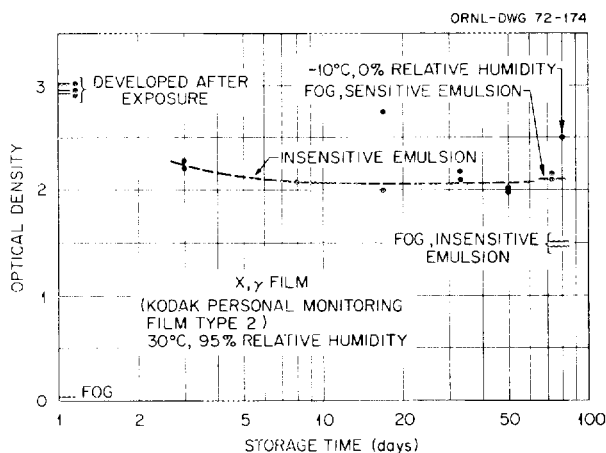


Fig. 8.16. Fading and fogging in the insensitive emulsion of a standard personnel monitoring film during three months of storage in a simulated tropical climate. The sensitive emulsion was totally destroyed.

A long-term stability study with three types of RPL glasses (Bausch and Lomb High-Z, Bausch and Lomb Low-Z, and Toshiba FD-1),<sup>15</sup> which was started in 1962, has been concluded. Considering the background buildup, the readings agreed within the accuracy limits of the reader with those taken four years ago. The Toshiba FD-1 glass read within  $\pm 6\%$  in the time interval between one day and ten years after exposure. Only in glasses which had been exposed to doses exceeding  $10^4$  R, fading of the radiation-induced absorption band simulated a further buildup of RPL.

### THERMOLUMINESCENCE DOSIMETRY

Work in this field was limited to some studies on the practical use of more recent phosphors in environmental dosimetry<sup>16</sup> and on the TL properties of some materials which had been prepared for TSEE activation studies.

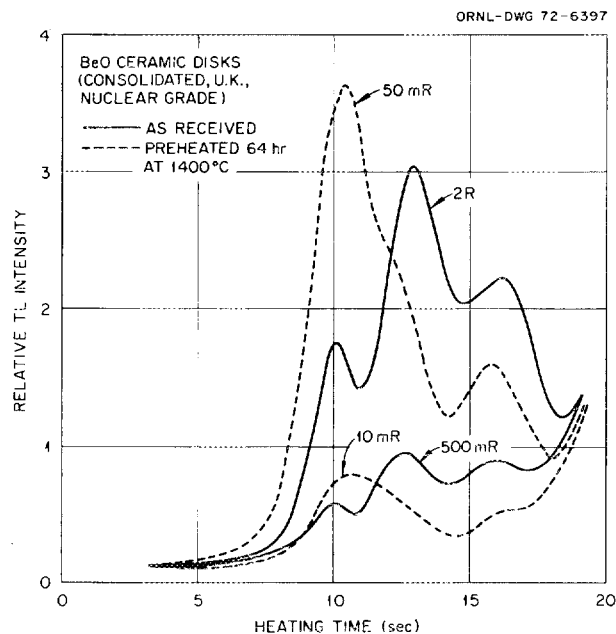


Fig. 8.17. TL curves of ceramic BeO disks prior to and after preheating for 64 hr at 1400°C.

As there is only a small contribution of low-energy photons to the total external dose, energy independence of the detectors is not important for most applications (in various background radiation measurements, no difference was observed in the reading of low-Z and unshielded high-Z detectors<sup>17</sup>). It is essential, however, to use detectors which are sufficiently sensitive, reliable, stable, and easily available. CaSO<sub>4</sub>:Dy powder, which exceeds the sensitivity of LiF:Mg,Ti (TLD-100) by a factor of about 30 (Table 8.4), is highly stable, can be easily prepared with minimal equipment and costs, and is, therefore, well suited for such measurements.

Naturally, the performance of the system will also depend on the quality of the reader and readout procedure. With one of the better commercial instruments such as the Harshaw 2000 or the Teledyne/Isotopes 7710, an optimized heating cycle, and a constant flow of clean nitrogen, gamma radiation doses as low as 0.3 millirad can be detected. Doses in the 1- to 10-millirad range are measured with a precision of 0.3

15. J. S. Cheka, *Health Phys.* 10, 303 (1964); 15, 363 (1968).

16. K. Becker, *Nucl. Instrum. Methods* (in press).

17. K. Becker, R. Lu, and P. S. Weng, *Proceedings of the Third International Conference on Luminescence Dosimetry, October 11 thru 14, 1971, Risø Report No. 249, Part III, p. 960, 1972.*

millirad for one standard deviation, which becomes about 4% at 10 millirads and 2% at doses exceeding 20 millirads.

Preliminary results indicate that a comparable sensitivity may be obtainable also with low-Z detector materials. Certain ceramic BeO samples are very sensitive if evaluated in a uv-sensitive TL reader and sensitized by proper pretreatment. It is interesting to note that heating for extended periods to 1400°C, which increases the TSEE sensitivity, also has a marked effect on the TL response (Fig. 8.17).

### TRACK ETCHING

Research continued on the possibilities of replacing the unsatisfactory method of recoil proton registration for photographic fast-neutron personnel dosimetry by etching techniques. Two approaches have been studied in some detail.

The hazards involved in the use of a combination of thin polycarbonate foils (to be spark counted after etching) and a thin layer of  $^{237}\text{Np}$  which is plated on the surface of an inert carrier had to be reduced. The best results so far have been obtained by "burning in" several layers of evaporated organic solutions of neptunium nitrate into a metal disk at high temperatures, resulting in a well-sticking neptunium oxide layer. The  $^{237}\text{Np}$  layer is additionally protected from potential rub-off of alpha activity by sealing into a 2- $\mu\text{m}$  polycarbonate foil.<sup>18</sup> This results in a sensitivity drop of about 20%. However, the sensitivity range of a combination containing about 8 mg of  $^{237}\text{Np}$  still covers well the desirable dose range from about 1

18. M. Sohrabi and K. Becker, *Some Studies on the Application of Track Etching in Personnel Fast Neutron Dosimetry*, ORNL-TM-3605 (December 1971) and *Health Phys.* (in press).

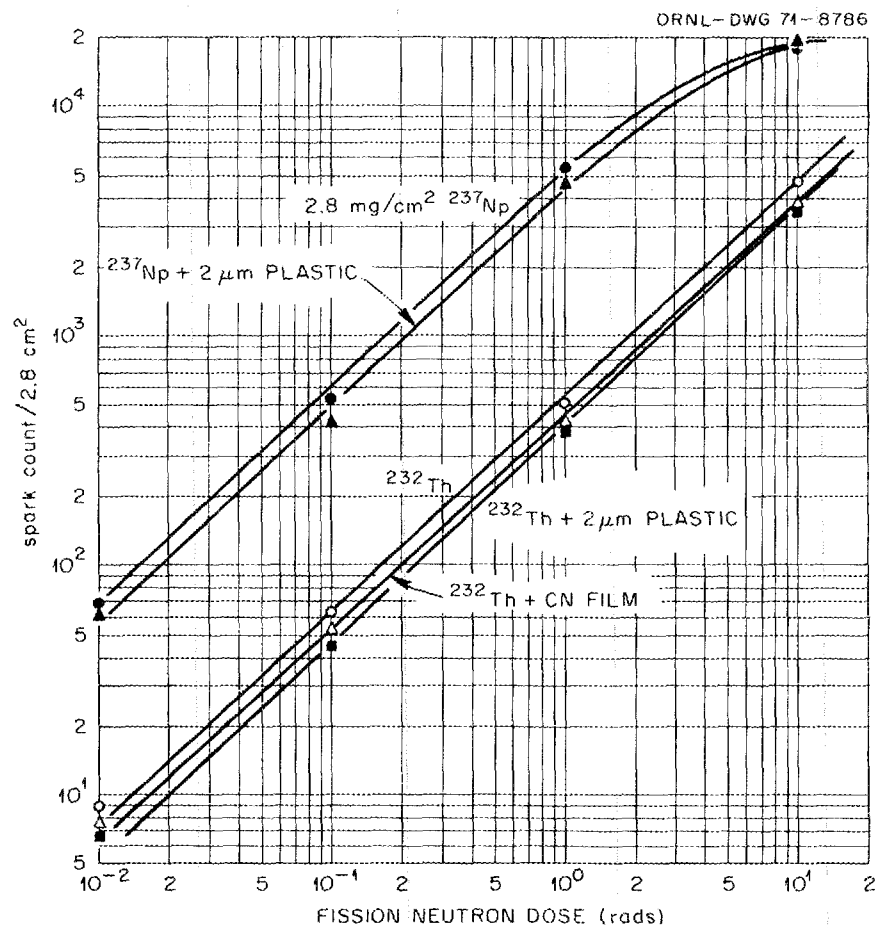


Fig. 8.18. Fission fragment spark counts of etched polycarbonate foils as a function of neutron dose from a fast reactor (HPRR) with different radiations and protective plastic covers.

PHOTO 2567-72

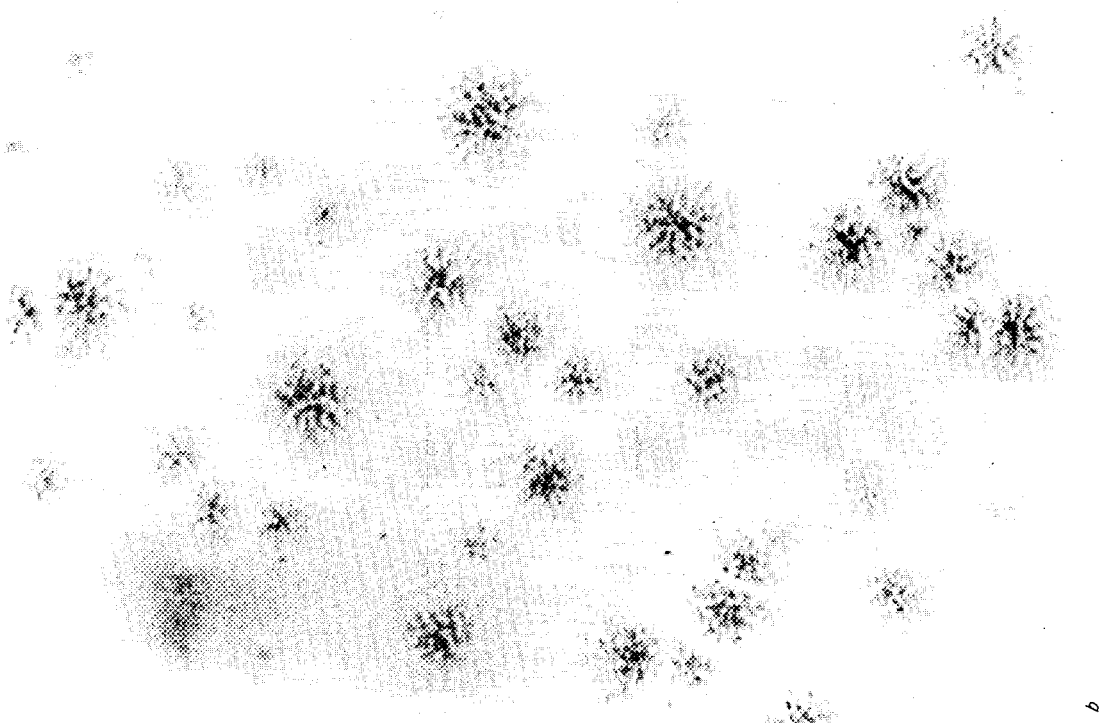
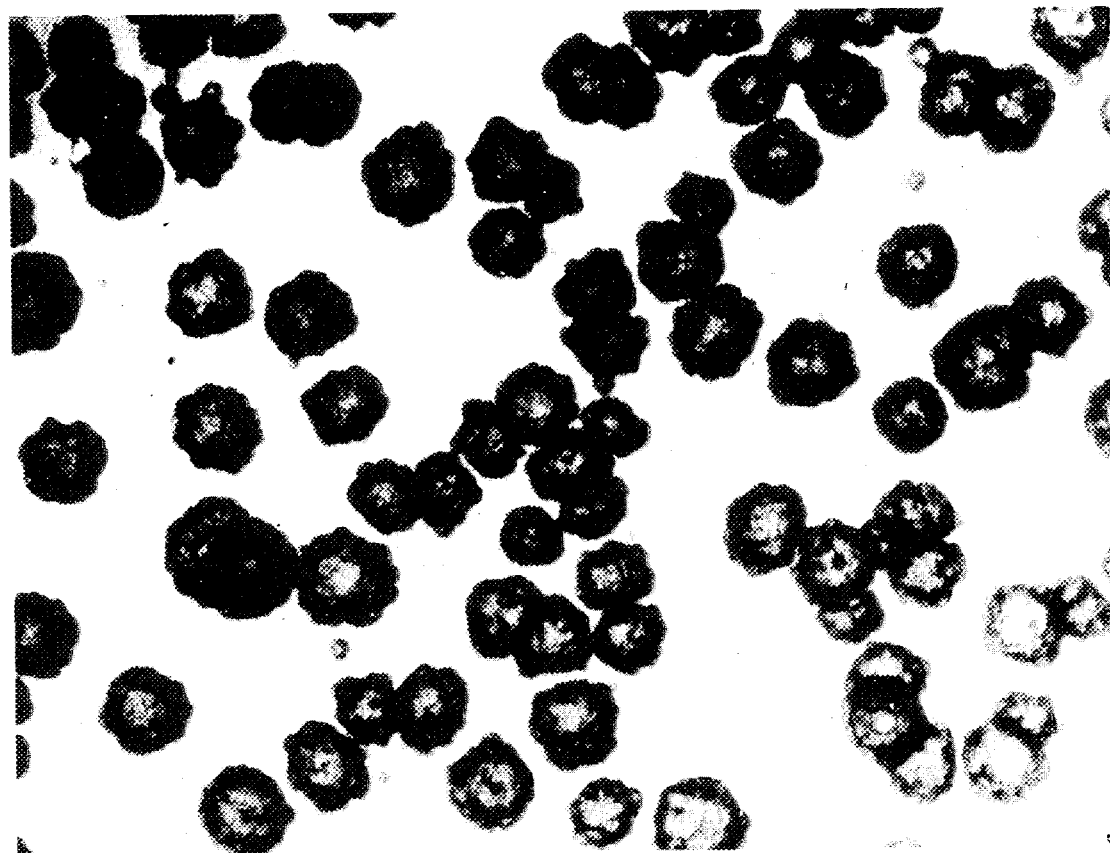


Fig. 8.19. Microphotograph of fission fragment (a) and recoil nuclei (b) etch pits in cellulose acetobutyrate (backing of Kodak NTA films) enlarged by electrochemical etching (20 hr at 1 kHz, room temperature, 28% KOH).

millirad (six sparks, no background sparks in the unexposed foil) to about 10 rads (Fig. 8.18) of HP RR fission spectrum neutrons. Higher doses can be evaluated by microscopic track counting. Reduction of the  $^{237}\text{Np}$  content or replacement of the neptunium by thorium leads to a decrease in sensitivity.

The visibility of small tracks should be improved with the purpose of simplifying the counting of fast-neutron-induced recoil particle tracks in polymers. One technique consisted in the etching of transparent holes into thin, intensely red-dyed cellulose nitrate layers which are coated on a thicker and less-sensitive polyester carrier (Kodak Pathé LR 115). The optical density reduction of such foils is a linear function of the alpha particle or fission fragment track density after optimized etching. However, this method lacks reproducibility and sensitivity. Another technique is based on locally heating the etchant by the conductive energy loss in tracks caused by application of a high-frequency electrical field during etching.<sup>19</sup> The foils were placed between two plastic containers which are filled with the etchant, and a field of 200 V and 1 kHz was applied. In thick acetobutyrate foils, such as the NTA film backing, fission fragments as well as recoil nuclei tracks could thus be amplified to visibility with the unaided eye (Fig. 8.19). Counting can be done by projecting "electroetched" foils onto the screen of a microfilm reader.

bility and sensitivity. Another technique is based on locally heating the etchant by the conductive energy loss in tracks caused by application of a high-frequency electrical field during etching.<sup>19</sup> The foils were placed between two plastic containers which are filled with the etchant, and a field of 200 V and 1 kHz was applied. In thick acetobutyrate foils, such as the NTA film backing, fission fragments as well as recoil nuclei tracks could thus be amplified to visibility with the unaided eye (Fig. 8.19). Counting can be done by projecting "electroetched" foils onto the screen of a microfilm reader.

---

19. L. Tommasino, *Proceedings Seventh International Colloquium on Track Detectors*, Barcelona, 1970.

## 9. Interaction of Charged Particles with Matter

G. S. Hurst

D. M. Bartell<sup>1</sup>    W. R. Garrett<sup>3</sup>

T. E. Bortner<sup>2</sup>    J. E. Talmage<sup>1</sup>

E. B. Wagner

### PROTON INTERACTIONS WITH HELIUM

The interaction of a swift charged particle with helium gas is perhaps the most elementary example which nature provides of the interaction of radiation with matter, a subject of intensive study since the discovery of x rays and of radioactivity. Yet the work reported here during the past year has shown many surprising energy pathways following the interaction of 2-MeV protons with helium gas at modest pressure ( $10^{-3}$  to  $10^3$  torr).

Theory can be used to determine the number of excited states and ion pairs which are "optically" excited by the primary particle, and even to follow the secondary electrons as they ionize and excite states until they fall into the subexcitation electron category. Such an energy degradation scheme for the primary particle and the secondary electrons is shown in Fig. 9.1 and Table 9.1.

The time behavior of the dominating excited state ( $2^1P$ ) was studied by doing lifetime studies at 584 Å (a

resonance line resulting from  $2^1P-1^1S$  transitions). The strong pressure dependence of the decay rate of this radiation (Fig. 9.2) shows that collisional processes convert the atomic state to some other species at a very high rate. Combining the above results with studies of the intensity and the time behavior of the continuous emission (around 675 Å and around 825 Å), we concluded that the main energy pathways are those shown in Fig. 9.3. From the diagram one sees that the atomic state  $2^1P$  is converted to two different excited molecular states in helium by three-body collisions. One of these (the *D* molecular state) radiates a fast component of the vacuum ultraviolet continuum, while the *B* state is metastable and is collisionally converted to a radiating *A* state. The latter indirect process accounts for a slow component in the vacuum ultraviolet continuum.

1. Oak Ridge Graduate Fellow, University of Kentucky.
2. Consultant.
3. Radiation Physics Section.

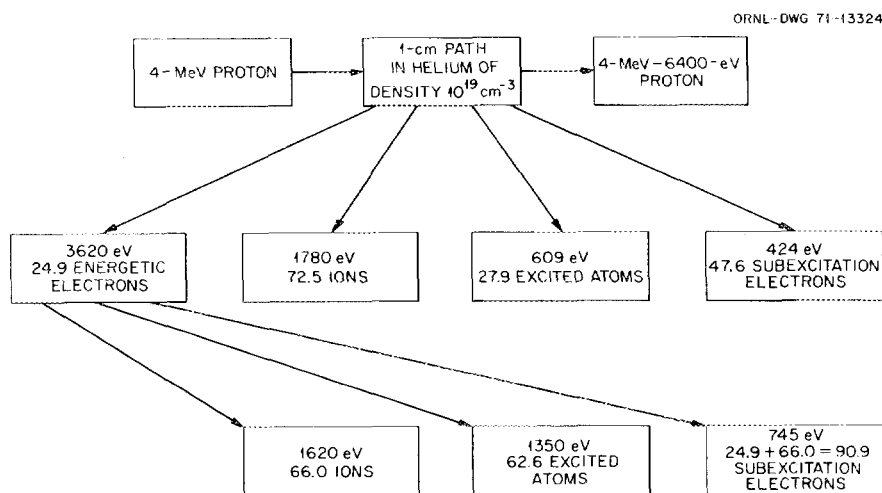


Fig. 9.1. Energy degradation in helium, based on theoretical calculation.

Table 9.1. The resulting species and relative yields of excited states and ions resulting from the action of 1- and 4-MeV protons in helium

Products	4-Mev proton		1-MeV proton (scaled)	
	Primary proton	Secondary electrons	Primary proton	Secondary electrons
$2^1S$	0.99	6.24	1.33	6.30
$3^1S$	0.22	1.21	0.30	1.22
$2^1P$	17.9	19.5	17.0	18.1
$3^1P$	4.41	4.47	4.20	4.14
$3^1D$	0.05	0.73	0.07	0.73
$2^3S$		11.3		11.5
$3^3S$		1.10		1.12
$2^3P$		6.13		6.27
$3^3P$		1.25		1.31
$3^3D$		1.31		1.18
Other atomic levels	4.30	9.30	4.25	9.05
Ions	72.5	66.0	76.1	60.2
Subexcitation electron energy	424 eV	745 eV	435 eV	710 eV

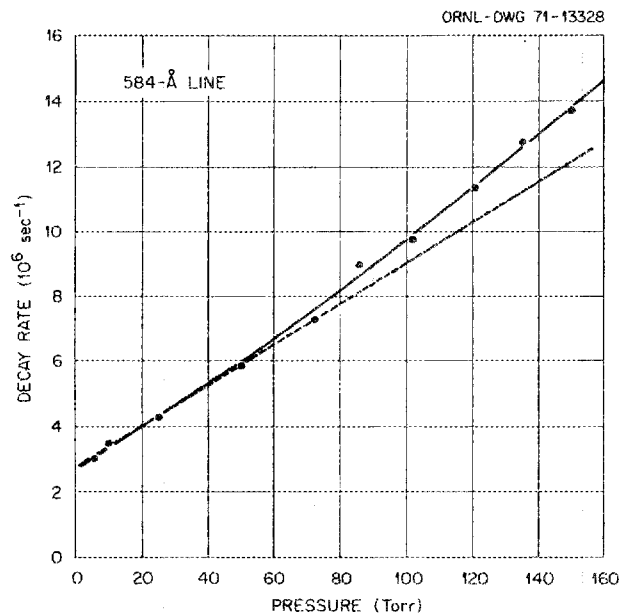


Fig. 9.2. Pressure dependence of the 584-Å decay rate for helium.

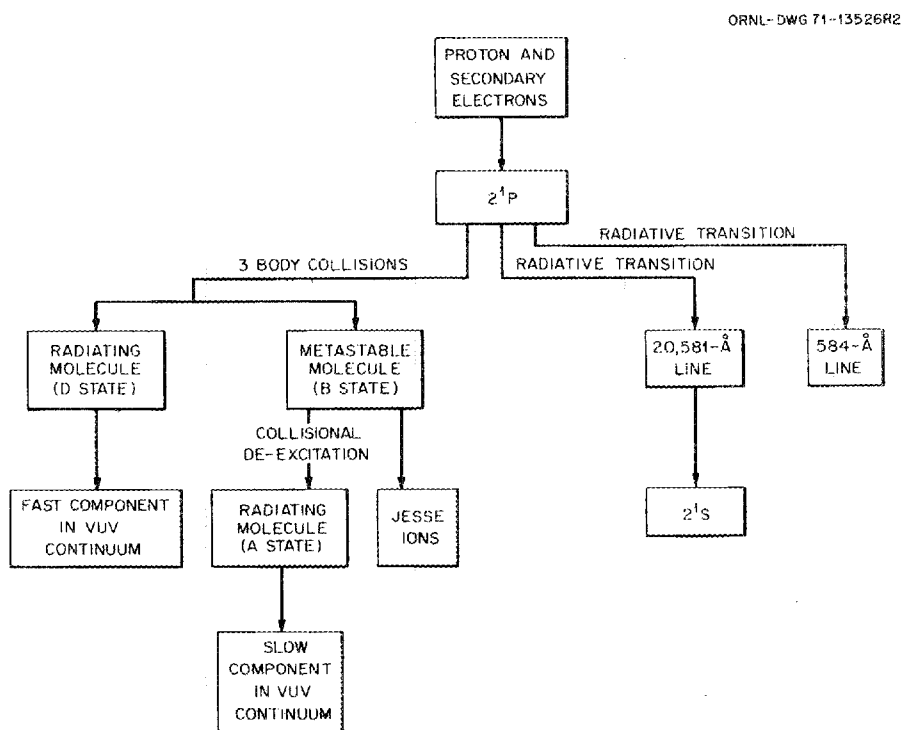
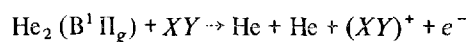


Fig. 9.3. Energy pathways model suggested to explain continuum formation and Jesse effects in helium.

Interestingly, the energy pathways model suggests that the Jesse effect originates from a metastable molecule, that is,



rather than from an atomic state, as previously believed.

A complete report on this work is available as a dissertation.<sup>4</sup>

### TRANSPORT OF RESONANCE RADIATION

In energy pathways models which attempt to interpret the interaction of fast charged particles with matter, resonance states play important roles because of their large oscillator strengths which couple them to the time-dependent electric field of the moving charged particle. Thus, in argon the resonance  $^1P_1$  (1048 Å) state is crucial because it is strongly excited, and its fate in the gaseous system determines to a large extent the ensuing energy pathways. Theoretical studies of the transport of resonance radiation involve approximations and, particularly, assumptions about the line shape in the region of pressure broadening.

We are involved in a fundamental experimental study of this problem in which use is made of a proton beam to excite resonance states initially confined to a small region around the axis of a cylindrical emission cell. These studies involve (1) measuring the escape rate of resonance radiation following excitation which lasts about 1 nsec, (2) measuring the intensity of resonance radiation as a function of pressure, and (3) measuring the intensity and time evolution of continuous emission characteristic of molecules formed when the atom is collisionally converted.

We find in argon evidence for the destruction of resonance states by three processes: (1) transport to the walls of the apparatus, (2) two-body conversion to slightly longer wavelengths (1048 Å) in a Franck-Condon process, and (3) conversion to argon molecules in three-body collisions. Our data should provide the first critical test of resonance radiation transport theory under the following necessary conditions: (1) good experimental geometry, (2) measurements of several features over wide pressure ranges, for example,  $10^{-5}$  to  $10^3$  torr, and (3) explicit corrections for the two-body and three-body sink terms.

Since we are also interested in the role which resonance states play in producing Jesse effects, we have arranged a companion ionization cell to have the

same geometry as the emission cell. Measurements of the ionization produced in the cell filled with a mixture of gases (such that Jesse effects are occurring) as a function of the total gas pressure can then be combined with measurements of the decay rate of resonance states to provide verification of the role of resonance states in producing the Jesse effect. Additionally, the rate constants for producing these effects in various impurities can be obtained.

### AN OPERATIONAL RATIONALE FOR RADIATION PROTECTION

The processes in which radiation interacts with man are so complex that one must accept an operational basis for correlating radiation fields with biological effects. We are seeking an operational rationale which is not encumbered by such concepts as "permissible levels" measured in terms of absorbed dose or its modification by a myriad of factors. The premise on which we base a formulation is the following. If the changes brought about in a biological system are governed by the ordinary laws of physics and probability, then specification of the radiation field during the life of the system determines the probability that changes have occurred or will occur in that system due to radiation.

We will define the radiation field by specifying every variable which could conceivably affect the biological probabilities. Thus, the radiation field  $N_k(E, \phi, \mathbf{r}, t)$  is defined such that

$$N_k(E, \phi, \mathbf{r}, t) dE d\phi d^3r dt$$

is the number of particles of type  $k$  lying in the energy range between  $E$  and  $E + dE$  in the solid angle  $d\phi$ , in the volume element  $d^3r$ , and in the time interval  $dt$ . The operational premise can be stated in a symbolic form if one chooses to specify the state of a biological system with respect to effect  $i$  in species  $j$  through a quantity  $S_{ij}$ . Thus, we can write an operator equation

$$G \{N(\tau), S_{ij}(t)\} = P_{ij}(t > \tau). \quad (1)$$

Here  $P_{ij}(t > \tau)$  is the probability as a function of time that effect  $i$  will be observed in species  $j$  at any future time  $t > \tau$  after the radiation  $N_k(\tau)$ , and  $G$  is an operator which yields a transformation of the system from its initial state to the  $i$ th biological end point (for convenience we have suppressed the arguments  $E, \mathbf{r}$ , etc.).

4. D. M. Bartell, Ph.D. thesis, University of Kentucky.

The idea expressed in Eq. (1) serves only as a logical framework within which a more explicit operational approach may be sought. We are pursuing two different approaches to the problem, each of which offers a degree of conceptual and mathematical beauty without total sacrifice of utilitarian purposefulness.

In the first approach, which might be described as a biological operator formulation, we express an operational relationship between radiation and effect by assuming that an operator exists which transforms the radiation field directly into probabilities of observing effects. Thus

$$O_{ij} N_k(E, \phi, \mathbf{r}, \tau) = P_{ij}(t > \tau), \quad (2)$$

where  $O_{ij}$  is an operator which leads to effect  $i$  in species  $j$  as a result of a radiation field  $N$ . The operator obviously would include integration over the multi-dimensional coordinate space of  $N$ . In actual measurements the readings obtained by a detector in a radiation field would yield a set of numbers which are indirectly related to  $N$ , say  $R_k(\epsilon, \phi, \mathbf{r}, \tau)$ . Then if the instrument is adequately designed, it is possible to learn the real nature of the field through a transformation of the readings of  $R$ . Thus

$$O_d R_k(\epsilon, \phi, \mathbf{r}, \tau) = N_k(E, \phi, \mathbf{r}, \tau), \quad (3)$$

where  $O_d$  is an operator characteristic of the "detector" which allows one to transform the readings into knowledge of the field. Thus if  $O_d$  exists, then from Eq. (2)

$$\begin{aligned} O_{ij} O_d R_k(\epsilon, \phi, \mathbf{r}, \tau) \\ = O'_{ij} R_k(\epsilon, \phi, \mathbf{r}, \tau) = P_{ij}(t > \tau), \end{aligned} \quad (4)$$

and one can transform the instrument response directly into a table of probabilities; that is, unfolding  $R$  to obtain  $N$  is unnecessary.

A second mathematical expression of the operational relationship implied by Eq. (1) has been prompted by the observation that there are no "radiation diseases."

That is, radiation only enhances the rate of incidence of certain maladies which occur naturally with probabilities  $B_{ij}(t)$  (i.e., effect  $i$  in species  $j$ ). With this in mind one is led to an operational relationship between radiation and effect which can be expressed in a form

$$O(N) B_{ij}(t) = P_{ij}(t > \tau), \quad (5)$$

where  $O(N)$  is an operator which has some as yet unspecified functional dependence on the radiation field  $N$ . ( $P_{ij}$  is now the total probability of occurrence, including the natural rate; thus if  $N = 0$ ,  $O = 1$ ). The objective here is to "discover" the operators  $O(N)$  which change the natural rate of incidence to that which occurs as a result of radiation  $N$ . Operators independent of  $i$  and  $j$  are probably outside the realm of possibility, but if it should happen that  $O = O_i$ , that is, the operator is specific to effect  $i$  but independent of species, then one could easily extend biological data to humans. This would be tantamount to the discovery of a macroscopic "law" of radiation effects. If one is unable to find operators of this degree of generality, that is, if both  $i$  and  $j$  have to be specified, the formalism, though still very useful, would require human data.

Even now it is clear that research in physical instrumentation should increasingly involve spectroscopic approaches and multiparameter computer storage technology in contrast to simpler devices which can only provide a single parameter indication.

A joint program with the Biology Division is under way in which we are attempting to find the operator  $O(N)$ , Eq. (5), for the case of mouse cataract incidence. The data  $B_{ij}(t)$  are available, and so are  $P_{ij}(t)$  for some radiation fields. Additional experiments will be performed as the effort to find operators suggests them. While the present formalism leads quite naturally to suggestions on new directions for physical instrumentation and on new experimental approaches to radiation biology, the more immediate benefits to be gained from the present investigation come in the nature of provocative and conceptual values.

## 10. HPRR and Accelerator Operations

F. F. Haywood  
D. R. Ward<sup>1</sup>

W. F. Fox            J. W. Poston  
C. P. Littleton<sup>2</sup>    E. M. Robinson  
R. L. Shoup<sup>3</sup>

### HEALTH PHYSICS RESEARCH REACTOR OPERATIONS

The HPRR has continued to be used as a source of fission neutrons for health physics and radiobiological research activities. The reactor was employed, not only by the Health Physics Division, but by other Laboratory divisions (e.g., Biology and Environmental Sciences), representatives of several foreign countries, many colleges and universities, and other Federal contractors and agencies. Typical experiments performed during this period include:

1. long-term effects of acute nonlethal doses of fission neutrons in mice;
2. study of crypt cell survival in the intestine of laboratory mice;
3. radiation-induced cancer in mammary glands of Sprague-Dawley rats;
4. radiosensitivity and mutation induction in agricultural and ornamental plants and seeds;
5. nuclear radiation pumping of a gas laser;
6. effects of fission neutrons in producing chromosome aberrations in the peripheral blood of swine;
7. the effectiveness of radioprotectants applied in vivo to laboratory mice;
8. angular distribution of neutron and gamma-ray dose incident on HPRR control building;
9. intercomparison and calibration of radiation detectors and accident dosimetry systems;
10. training for graduate nuclear engineering students.

- 
1. On loan from Neutron Physics Division.
  2. On loan from Instrumentation and Controls Division.
  3. National Science Foundation Presidential Intern.

No major modifications or changes in the reactor have been made in the past year. The annual inspection of the fuel and associated equipment showed no significant change in the condition of the reactor components.

### CALCULATION OF THE HPRR NEUTRON SPECTRUM FOR SIMULATED NUCLEAR ACCIDENT CONDITIONS

Since 1964, the Health Physics Research Reactor at the Oak Ridge National Laboratory has been used to simulate nuclear excursions to allow intercomparisons of accident dosimetry systems.<sup>4-12</sup> Generally, activation foils or threshold-activation foils are used to measure the neutron fluence. Data from these detectors are used to provide the neutron dose and some general shape to the neutron energy spectrum. However, some participants have calculated a spectral distribution to fit

---

4. J. A. Auxier, "Multi-Laboratory Intercomparisons and Standardization: Nuclear Accident Dosimetry Systems," in *Nuclear Accident Dosimetry Systems*, STI/PUB/241, IAEA, Vienna, 1970.

5. J. A. Auxier et al., *Health Phys. Div. Annu. Progr. Rep. July 31, 1965*, ORNL-3849, pp. 172-73.

6. J. A. Auxier et al., *Health Phys. Div. Annu. Progr. Rep. July 31, 1966*, ORNL-4007, pp. 192-95.

7. J. A. Auxier et al., *Health Phys. Div. Annu. Progr. Rep. July 31, 1967*, ORNL-4168, pp. 208-13.

8. J. A. Auxier et al., *Health Phys. Div. Annu. Progr. Rep. July 31, 1968*, ORNL-4316, pp. 238-44.

9. J. A. Auxier et al., *Health Phys. Div. Annu. Progr. Rep. July 31, 1969*, ORNL-4446, pp. 271-77.

10. J. A. Auxier et al., *Health Phys. Div. Annu. Progr. Rep. July 31, 1970*, ORNL-4584, pp. 191-97.

11. J. A. Auxier et al., *Health Phys. Div. Annu. Progr. Rep. July 31, 1971*, ORNL-4720, pp. 112-13.

12. F. F. Haywood, *1970 Intercomparison of Nuclear Accident Dosimetry Systems at the Oak Ridge National Laboratory*, ORNL-TM-3551 (February 1972).

the experimental results.<sup>13,14</sup> Spectrum measurements by other methods (e.g., a  $^7\text{Li}$ -sandwich detector) provide spectral information over only a portion of the neutron energy range. Since the entire neutron energy spectrum is necessary, a calculational study was begun to provide the HPRR neutron spectrum for three typical accident exposure conditions.

Calculations of the HPRR spectrum were performed using the DOT<sup>15</sup> two-dimensional transport code. The cross sections used in the calculations were obtained from several sources.<sup>16</sup> All materials except calcium and the hydrogen thermal data were obtained from the ENDF/B version II data files. The calcium data are those given in the data files for the GAM II<sup>17</sup> code, and the thermal data for hydrogen are derived from the Nelkin thermal model for bound hydrogen. The many-group (93 fast groups and 30 thermal groups) data were reduced to 33 fast groups and a single thermal group using the spectral weighting code XSDRN.<sup>18</sup> Since the calcium data consisted of 99 fast groups, these were reduced to 33 groups; the thermal group data were added using values from BNL-325.<sup>19</sup> The DOT calculations were then performed using the 34-group set in the  $P_1$  approximation.

Two calculations were made for each shielding configuration in an effort to minimize "ray effects."<sup>20</sup> The first was done in the S6 (30 discrete angles) approximation. The scalar fluxes from this run were used as a starting flux for the subsequent case, which was for a total of 328 discrete angles. The use of this number of angles reduced the ray effect to a level consistent with the accuracy limitations of the other discrete parameters.

For purposes of the calculation, the center of the reactor was placed 150 cm above a 30-cm-thick concrete slab, which extended to a radius of 3 m from the reactor center line. Shielding configurations were calculated with no shield, a Lucite shield 12 cm thick and rising to 282 cm above the concrete, and a steel shield 13 cm thick and rising to 213 cm above the concrete. These shields were at 200 cm from the reactor center. Due to limitations of the DOT code, these flat shields were represented for calculations as cylindrical annuli located as described above. Figure 10.1 shows the idealized model of the core, having cylindrical symmetry, which was used in this calculation. Rather than attempt to describe the equipment and instruments located above the reactor, only three stainless steel plates and two polyethylene slabs were included in the model. The neutron energy spectrum was divided into 34 energy groups ranging from thermal to 14 MeV.

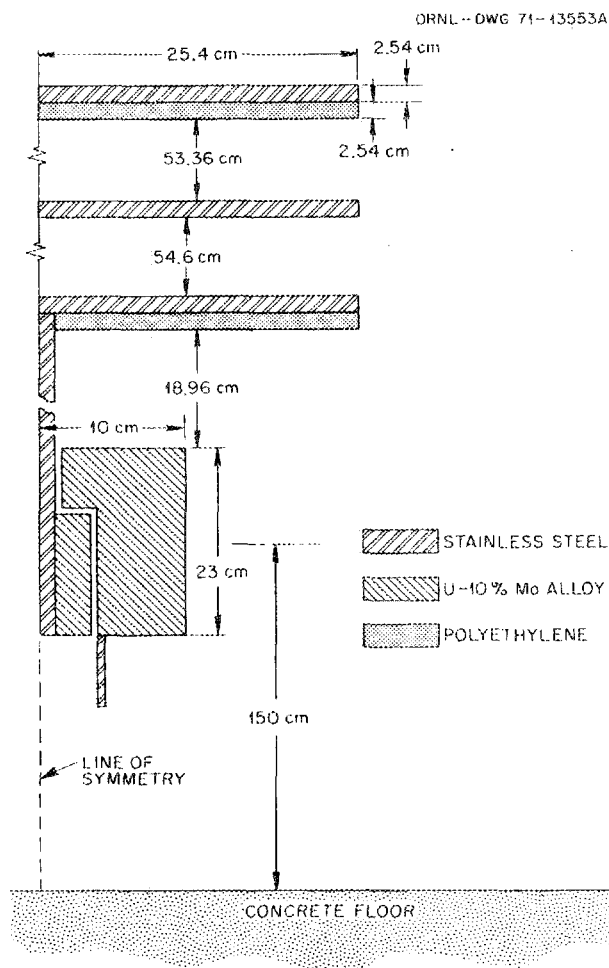


Fig. 10.1. Calculational model of the HPRR.

13. P. Candes and J. Lamberieus, "Dosimetry in Nuclear Accidents," in *Nuclear Accident Dosimetry Systems*, STI/PUB/241, IAEA, Vienna, 1970.

14. J. C. Bailey, *A New Neutron Dosimeter and Neutron Spectrum Model for Nuclear Accident Dosimetry*, K-1763 (Oct. 2, 1969).

15. F. R. Mynatt et al., *Development of Two Dimensional Discrete Ordinates Transport Theory for Radiation Shielding*, CTC-INF-952 (August 1969).

16. J. L. Lucius et al., *The INDEX Data System: An Index of Nuclear Data Libraries Available at ORNL*, ORNL-TM-3334 (March 1971).

17. G. D. Joanon and J. S. Dudek, *GAM II, A B<sub>3</sub> Code for the Calculation of Fast-Neutron Spectra and Associated Multi-group Constants*, GA-4265 (September 1963).

18. N. M. Green and C. W. Craven, *XSDRN: A Discrete Ordinates Spectral Averaging Code*, ORNL-TM-2500 (July 1969).

19. John R. Stehn et al., *Neutron Cross Sections*, BNL-325, 2d ed. (May 1964).

20. K. D. Lathrop, *Nucl. Sci. Eng.* 32, 357 (1968).

The energy grouping is given in Table 10.1. In addition to neutron spectrum, the calculation also provided neutron dose at each position in the grid. Fluence-to-dose conversion factors were those of Auxier, Snyder, and Jones.<sup>21</sup>

The calculated HPRR neutron spectra for the three conditions described above (i.e., bare, steel, and Lucite shields) are shown in Fig. 10.2. The effects of the two shields on the bare spectrum are obvious. For the Lucite shield, the spectrum appears to be about  $1/E$  up to 100 keV. Neutron dose in tissue as a function of distance is given in Fig. 10.3. For comparison, the figure also includes threshold detector results from the 1971 intercomparison study. The agreement between the calculated and measured values at a distance of 3 m adds some confidence to the calculations.

21. J. A. Auxier, W. S. Snyder, and T. D. Jones, "Neutron Interactions and Penetration in Tissue," in *Radiation Dosimetry*, vol. I, ed. by Attix and Roesch, Academic, New York, 1968.

Table 10.1. Energy groups for HPRR spectrum calculations

Group No.	Upper energy limit	Group No.	Upper energy limit
1	14.9 MeV	18	7.10 keV
2	10.0	19	3.35
3	6.7	20	1.23
4	4.97	21	583 eV
5	3.01	22	214
6	1.50	23	101
7	907 keV	24	47.9
8	408	25	29.0
9	111	26	17.6
10	86.5	27	10.7
11	67.4	28	5.04
12	52.5	29	3.06
13	40.9	30	1.56
14	31.8	31	1.00
15	24.8	32	0.65
16	19.3	33	0.45
17	15.0	34	0.10

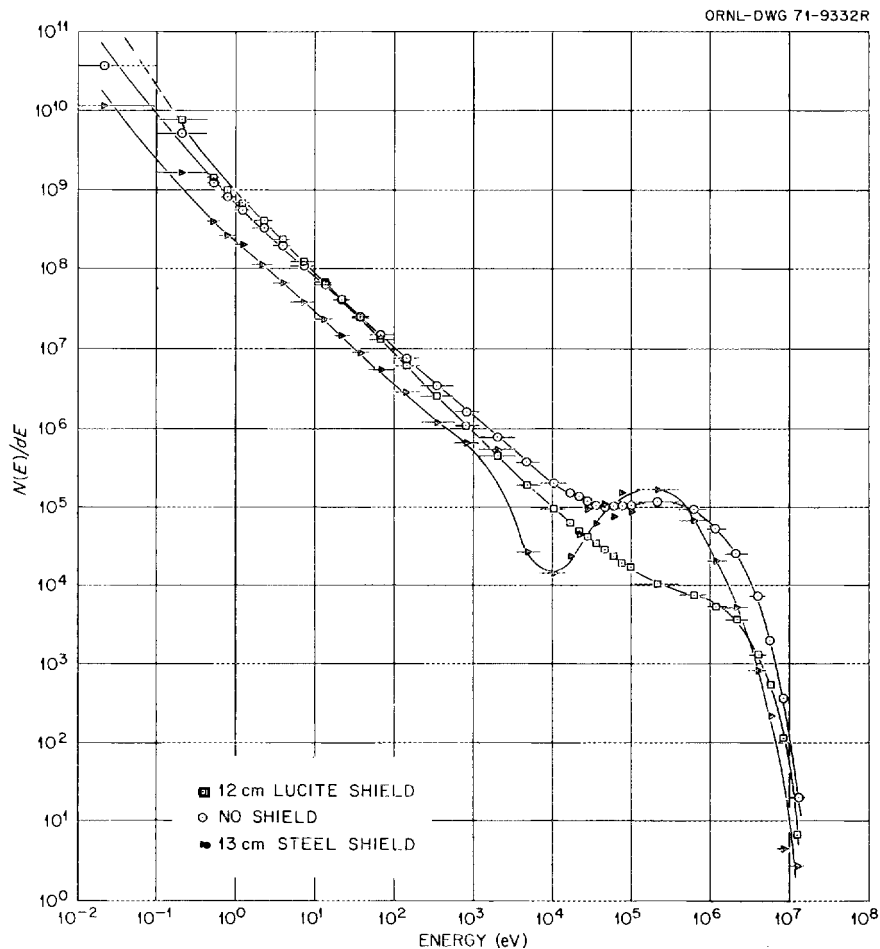


Fig. 10.2. Calculated HPRR leakage spectrum at 3.0 m from the center line of the core.

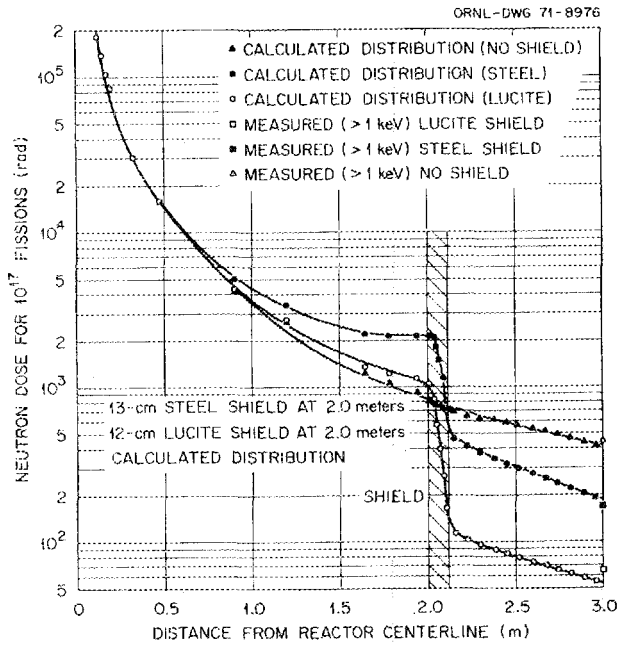


Fig. 10.3. Neutron dose vs distance from HPRR.

## 11. Spectrometry Research and Development

J. H. Thorngate

J. A. Auxier    P. T. Perdue

G. D. Kerr    M. M. Abd-El Razeq<sup>1</sup>

### NEUTRON DETECTOR

The Aerial Radiological Measuring Surveys (ARMS) system is operated for the Atomic Energy Commission by the Las Vegas Division of EG&G, Inc. A package of fourteen 4 × 4 in. NaI(Tl) crystals is used in a light two-engine aircraft to measure the terrestrial radiation signature of large areas. With the increase in the number of nuclear power stations, some ability to detect neutrons is also desirable. The first unit used was a single 12-in.-long BF<sub>3</sub> proportional counter. Next, an array of long BF<sub>3</sub> counters was tried. In support of this program the Spectrometry Group has studied the available neutron detectors. The requirements for light weight, ruggedness, and sensitivity led to the evaluation of a detector composed of a 5-in.-diam by 1/8-in.-thick glass scintillator coupled with a 5-in. photomultiplier tube. To provide neutron sensitivity the glass contains 7.5% by weight of lithium enriched in <sup>6</sup>Li to 95%, which is adequate to make it black for thermal neutrons. Actual efficiency is 0.997 at 0.025 eV, decreasing to 0.028 at 1 keV. This results in a sensitivity of 125 counts cm<sup>2</sup> neutron<sup>-1</sup> at thermal energies, which is roughly three times that obtained from the BF<sub>3</sub> counter. The particular glass chosen also has pulse-shape characteristics that allow electronic rejection of gamma-ray-produced pulses if necessary.

A series of runs were made using an AmB neutron source at a fixed distance from the glass detector and varying the thickness of a polyethylene moderator in front of the glass in 1/4-in. steps. The maximum sensitivity obtained was 6.2 counts cm<sup>2</sup> neutron<sup>-1</sup> for this neutron spectrum with 2.5 in. of polyethylene. A similar run for PuBe neutrons gave 7.7 counts cm<sup>2</sup> neutron<sup>-1</sup> for a 2.25-in. moderator thickness. These results were encouraging enough to warrant further investigation by the EG&G staff in Las Vegas.

---

1. Alien guest.

### LIGHT PULSER

Experiments using photomultipliers often require a standard source of light for calibration. An example is the pulse measurements made in conjunction with studies of the purification and development of organic scintillators.<sup>2,3</sup> A light pulser has been used that consists of a small amount of <sup>241</sup>Am in an NaI crystal of about 1-cm dimensions, but the light output of this source cannot be controlled easily, and it has limited resolution. Therefore, a light pulser was designed that uses low-cost gallium arsenide phosphide light-emitting diodes. The spectrum of light produced by these diodes makes their use more suitable with photomultiplier tubes with an S-20 response than with S-11 response tubes, although such applications are still possible. This light source is variable and can be turned on or off at will. It also yields pulse distributions with good resolution, typically less than 3%.

A major problem with light-emitting diode light sources is instability caused by temperature fluctuations. The light produced by a light-emitting diode is proportional to the forward current through the diode and is a reasonably linear function of current except at the limits of low and high current. Temperature changes affect the voltage-current characteristics of the diode, so voltage control provides inadequate stability. By using integrated circuits and regulating the diode current rather than voltage, stability of 0.5% was achieved. To achieve maximum stability the diode should be selected. Pulse height and length are variable over a wide range, and the pulses may be turned on and off reproducibly.

---

2. P. T. Perdue and M. D. Brown, *Nucl. Instrum. Methods* 71, 113-16 (1969).

3. J. H. Thorngate et al., *Health Phys. Div. Annu. Progr. Rep. July 31, 1971*, ORNL-4720, p. 110.

## CONTRIBUTIONS TO ENVIRONMENTAL IMPACT STATEMENTS

As part of a three-fourths man-year effort devoted to this project by the Spectrometry Group, a computer program was developed to convert source term data given as radionuclide concentrations in water to estimates of dose to man. It is being used in the assessment of radiological impact on man from aquatic releases of radionuclides. Estimates of the dose to man in millirems from the individual radionuclides and the total dose from all the radionuclides in water can be made for both external and internal pathways of exposure to man. The pathways included in the program are external exposure of man by submersion in contaminated water and by standing above a shore contaminated by sedimentation of radionuclides from the water, and internal exposure of man by drinking contaminated water or by eating fish or shellfish living in the water. Dose to the total body from penetrating radiation is calculated for external exposures, and the dose to the total body, bone, thyroid, kidneys, liver, and gastrointestinal tract is calculated for internal exposures.

### DEVELOPMENT OF A HIGH-SENSITIVITY FAST-NEUTRON SPECTROMETER

In the past the use of a single organic scintillator to measure fast-neutron spectra has not been adopted for measurements related to radioprotection around the HPRR due to the extreme difficulty of reducing the data. This type of detector, usually an NE-213 liquid scintillator, has received wide use for physical measurements where the delay involved in the computer reduction of data is not a problem.<sup>4,5</sup> There are also certain applications in radioprotection where the delay in data reduction does not cause a problem.<sup>6</sup> Such a problem was encountered in conjunction with the study of the effects of heavy shielding on the survivors at Hiroshima and Nagasaki. Because angular distribution of the fast-neutron spectrum incident on the roof of the DOSAR Control Building was desired, a 2 X 2 in. cylindrical NE-213 scintillator was obtained to provide adequate sensitivity.

4. V. V. Verbinski et al., *Nucl. Instrum. Methods* **65**, 8-25 (1968).

5. W. R. Burnas and V. V. Verbinski, *Nucl. Instrum. Methods* **67**, 181-96 (1969).

6. G. Burger, W. Eckl, and H. Gredel, *Advances in Physical and Biological Radiation Detectors, Proceedings of a Symposium, Vienna, November 23-27, 1970*, pp. 467-74, IAEA, Vienna, 1971.

A number of preliminary measurements were required to obtain the response function of this detector. Published values of light output vs proton energy were inadequate. In fact, there is some evidence that this varies significantly for every detector.<sup>7</sup> A method of comparing the measured response to 3- and 15-MeV neutrons to a proton energy distribution calculated with a Monte Carlo code in order to obtain the light response has been worked out but is not finished due to a delay in obtaining the calculated data. When these data become available and the light vs proton energy response is obtained, the data will be reduced by a modification of the technique developed by Turner et al. for unfolding LET spectra from pulse-height data.<sup>8</sup>

A simplified technique of pulse-shape discrimination to separate electron and proton pulses was developed for use in this experiment. It uses commercially available NIM compatible equipment throughout and requires only the anode signal from the photomultiplier. One requirement of this technique is that the photomultiplier output signal be integrated by the preamplifier. Commercially available integrating (charge-sensitive) preamplifiers were found to have an insufficient dynamic range for this application, so a simple preamplifier was designed that has performed well with good dynamic range and low noise. Its simplicity allows it to be constructed in a small size and mounted directly to the photomultiplier tube base assembly. The resulting short input leads optimize the output pulse rise time.

### A DEVICE FOR LISTING PUNCHED PAPER TAPE DIRECTLY ON A TYPEWRITER

Using punched paper tape to read out digital data from multichannel analyzers has two distinct advantages when a limited number of channels are to be read out. First, the tape punch runs faster than the mechanical printing devices commonly used for the readout of digital data; second, the data are computer compatible if the tape punches the data in the standard ASC II format. Analyzers that do not use this format can usually be adapted to do so with a translator.<sup>9</sup> Data in this form can subsequently be listed on any Teletype having a tape reader.

7. A. Bertin, A. Vitale, and A. Placii, *Nucl. Instrum. Methods* **91**, 649-52 (1971).

8. J. E. Turner et al., *Health Phys.* **18**, 15-24 (1970).

9. P. T. Perdue and J. H. Thorngate, *Conversion of the Nuclear Data 130A Pulse-Height Analyzer to ASC II Paper Tape with Manual Entry for Data Identification*, ORNL-TM-2936 (May 1970).

A circuit was designed to operate with a tape reader and an electric typewriter of the sort normally used to read out multichannel analyzers. This arrangement provides a central facility for analyzer users who need to list numerical data previously put on paper tape. A feature of this circuit is that it omits insignificant zeros, thus making the typed data much easier to read. Maxima in the data are particularly easy to identify with such a format. To perform this function the circuit is set by the space command to ignore zeros until some nonzero number has occurred. Since some channels contain nothing but zeros, the circuit also counts leading zeros and resets to type just the last zero in a channel to provide a marker. Insignificant zeros are interpreted as spaces, so that the data are kept in even columns. A detailed description of the circuit and its functioning is available.<sup>10</sup> The unit uses integrated circuits as much as possible to increase reliability.

#### DISTRIBUTION OF CHARGED PARTICLE STOPPING

A knowledge of the energy loss per unit track length by a charged particle is basic for dosimetry. While good values of the stopping power have been measured for many charged particles in tissue-constituent elements, little knowledge is available on the distribution of the energy losses. Because most of the energy lost by a charged particle is imparted to the electrons of the target nuclei in a random manner, no single value of energy loss but some distribution with energy will be obtained for a given charged particle at a specific energy incident on a particular target. For a thin target and incident protons, the energy distribution of the emerging protons will not be symmetric.

At low proton energies there is ample evidence that Bragg's additivity rule does not hold for certain types of molecules.<sup>11</sup> A program has been begun to relate the stopping distribution with this lack of additivity. To that end two electrostatic analyzers have been constructed that have energy resolutions just under 0.1%. One analyzer will be used as a proton monochromator over the energy range 50 to 200 keV so that a precisely known proton energy with a narrow energy spread can be used as the input to the stopping material. The second analyzer will be used to measure the energy

distribution of the proton beam after it emerges from the stopping media.

Because the present plans call for the measurement of the distribution of stopping for the major tissue constituents H, C, D, O, and simple two-element compounds of these materials, provisions for handling both gaseous and solid targets must be made. Therefore, a differentially pumped gas cell is under construction as well as a simple chamber to hold thin foil targets.

One additional piece of information may possibly be inferred from these data, namely, the distribution in energy of the secondary electrons produced by the interactions with the incident protons. These distributions can be measured directly for very thin gaseous targets, but no solid target can be made thin enough for an adequate measurement. Some relation between the measured distribution of secondary electrons and proton stopping in thin gaseous targets may be obtained that would allow deductions about the secondary electron distributions from solid targets to be made from the stopping distributions measured.

#### ZONE REFINING OF ORGANIC COMPOUNDS

Often the particular expertise developed to solve problems in spectrometry proves to be of value for other projects. For example, the electronics expertise that had to be developed to solve spectrometry problems has been repeatedly applied to other dosimetry problems within the section. More recently the zone refining capability established as part of the studies into organic scintillators has been applied to the purification of samples used in the negative-ion research conducted by the Radiation Physics Section. The mass-spectrometric techniques used for these studies can produce ambiguities unless the sample is extremely pure. For example, purification of maleic anhydride and phthalic anhydride by zone refining has removed questionable impurities and allowed unambiguous results to be obtained.

#### THE NATURAL RADIATION ENVIRONMENT AND MAN'S INFLUENCE ON IT

Because of proposed changes to 10 CFR 50 and the generally increased pressures to lower radiation exposures of the population, the need for a better understanding of the natural radiation environment has increased markedly. It has been assumed rather generally that there is not much that can be done to decrease the exposures to the natural environment without, for example, having people move away from

10. P. T. Perdue and J. H. Thorngate, *A Paper Tape to Typewriter Translator That Suppresses Insignificant Zeros*, ORNL-TM-3692 (March 1972).

11. J. T. Park and E. J. Zimmerman, *Phys. Rev.* **131**, 1611-18 (1963).

high altitudes or out of areas having higher than average concentrations of U, Th, or K. However, some modifying factors introduced by man, such as using uranium-bearing aggregate for roads and buildings, may be significant and may be controllable to some extent. Roadways and sidewalks in some areas of Florida have sufficient U, Th, and/or K to cause doses greater than 1000 mR/year for continuous exposure; for genetically significant dose it is assumed that it makes no difference whether one person receives a given dose or two persons each receive half of the same given dose, etc. Further, Gabrysh and Davis<sup>1,2</sup> pointed out in 1955 that uranium-bearing concrete used in some areas might result in high radon levels in buildings. To measure low levels of contaminating radionuclides in the environment, the use of high-resolution spectrometers appears necessary. To interpret measurements with such devices, notably Ge(Li), a detailed knowledge of the spectra of the natural environment as a function of several variables, including the concentrations of the

---

12. A. F. Gabrysh and F. J. Davis, *Nucleonics* 13(1), 50 (1955).

radionuclides of the U and Th series, terrain features, soil and rock types, etc., will be required in order to account for their contribution to the total response of the detector.

A mobile laboratory used for research at the DOSAR Facility was modified slightly to use for surveys of the natural environment outside ORNL. It carries the gamma-ray spectrometry system, air sampling equipment, and alpha spectrometers for the air samples (filter paper).

Preliminary measurements and calculations have shown that a 50-cm<sup>3</sup> detector of Ge(Li) is adequate for measurements of the natural gamma-radiation environment and of gamma-emitting nuclides to levels of the order of 1 to 15 mR/year, depending on the energy and half-life of the contaminant. They have shown also that the U and/or Th concentrations in the huge slag and slate dumps of the coal fields are sufficient to warrant detailed study for both the direct gamma-ray exposure and the radon progeny-produced dose to the lungs. The initial results for some roadways in Florida and Georgia are surprisingly high, that is, several times the average "natural" dose when measured inside an automobile or truck.

# Part III. Internal Dosimetry

W. S. Snyder

## 12. Estimates of Absorbed Fractions for Photon Emitters within the Body

W. S. Snyder M. R. Ford G. G. Warner<sup>1</sup>

This report extends the preliminary study reported last year for obtaining reliable estimates of specific absorbed fractions at energies where the corresponding Monte Carlo estimates have a large coefficient of variation.

### Introduction

The authors have published absorbed fractions computed by the Monte Carlo method for a variety of organs of an anthropomorphic phantom.<sup>2</sup> The photon source is assumed uniform in 16 different organs, and absorbed fractions  $\varphi$  are estimated in some 22 organs whenever the coefficient of variation for a sample of 30,000 photons is less than 50%. Unfortunately, for many organs the coefficient of variation was greater than 50%, and subsequent experience tends to confirm earlier impressions that estimates with a coefficient of variation of 50% or more may easily be inaccurate by a factor of 2 or even more. A number of attempts to produce estimates to supply these missing entries have not been entirely successful.<sup>3</sup> The present paper describes a method which is quite general, whose accuracy is not dependent on organ size, and which, for the adult body, appears to be accurate for organs of the trunk to within a factor of 2, being generally within some 20 to 30% of the values reliably estimated by the Monte Carlo calculation.

### Methods

Berger<sup>4</sup> has given estimates of the buildup factor  $B(\mu x)$  for a point source of photons in an infinite

medium of water or of tissue. The range on  $x$  is to 20 mean free paths, but he has later made available to the authors prepublication results which extend the distance to 40 mean free paths. The specific absorbed fraction  $\Phi$  (fraction of energy absorbed per gram) in the infinite medium at distance  $x$  cm from the point source of a fixed energy  $E$  is given by:

$$\Phi(\mu x) = \frac{\mu_{ab} e^{-\mu x}}{4\pi x^2} B(\mu x), \quad (1)$$

where  $\mu$  and  $\mu_{ab}$  are the mass attenuation and mass absorption coefficients for photons of energy  $E$ .

It is easy to adapt Eq. (1) to the case of a source and target organ of finite size. Let  $S$  denote a source organ of arbitrary size and shape in the medium with a source density of one photon of a fixed energy  $E$  per cubic centimeter. Consider a fixed point  $Y$  of the medium.

1. Mathematics Division.
2. W. S. Snyder et al., "Estimates of Absorbed Fractions for Monoenergetic Photon Sources Uniformly Distributed in Various Organs of a Heterogeneous Phantom," MIRD Pamphlet No. 5, Suppl. No. 3, *J. Nucl. Med.* **10**, 5 (1969).
3. W. S. Snyder, "Estimation of Absorbed Fraction of Energy from Photon Sources in Body Organs," *Medical Radionuclides: Radiation Dose and Effects*, USAEC Division of Technical Information, Oak Ridge, June 1970, p. 33.
4. M. J. Berger, "Energy Deposition in Water by Photons from Point Isotropic Sources," MIRD Pamphlet No. 2, Suppl. No. 1, *J. Nucl. Med.*, 15 (1968).

The specific absorbed fraction at  $Y$  due to the extended source in  $S$  is given by:

$$\frac{1}{\rho|S|} \int_S (dX) \frac{\rho \mu_{ab} e^{-\mu|X-Y|}}{4\pi|X-Y|^2} B(\mu|X-Y|), \quad (2)$$

where the integration is over the source organ  $S$ ,  $\rho$  is the density of the medium,  $dX$  is a volume element of  $S$ , and the expression is independent of  $\rho$ . Multiplying (2) by  $\rho dY$ , integrating over an arbitrary "organ"  $T$  of the medium, and dividing by  $\rho|T|$ , one has (by additivity of the absorbed fraction) the specific absorbed fraction from  $S$  to  $T$ , which, in the notation of MIRD Pamphlet No. 1,<sup>5</sup> is:

$$\Phi(T \leftarrow S) = \frac{1}{|S||T|} \int_T dY \frac{\mu_{ab} e^{-\mu|X-Y|}}{4\pi|X-Y|^2} B(\mu|X-Y|). \quad (3)$$

S. R. Loevinger and M. Berman, "A Schema for Absorbed-Dose Calculations for Biologically Distributed Radionuclides," MIRD Pamphlet No. 1, Suppl. No. 1, *J. Nucl. Med.*, 7 (1968).

The direct integration of formula (3) is rather forbidding, especially if the boundaries of  $S$  and  $T$  are complicated. For this reason we resort to evaluation of Eq. (3) by use of the Monte Carlo method. It is well known that if points  $(X_i, Y_i)$  are selected randomly in the six-dimensional subregion  $S \times T$ , then (3) is the expectation of the expression

$$\frac{1}{N} \sum_i \frac{\mu_{ab} e^{-\mu|X_i-Y_i|}}{4\pi|X_i-Y_i|^2} B(\mu|X_i-Y_i|). \quad (4)$$

It is clear that this method is straightforward but is subject to one difficulty — namely, if  $S$  coincides with  $T$  or shares a common boundary with  $T$ , expression (4) may be unbounded. To avoid this difficulty, we replace the term

$$\frac{\mu_{ab} e^{-\mu|X_i-Y_i|}}{4\pi|X_i-Y_i|^2} B(\mu|X_i-Y_i|)$$

by an approximation to its average value over a small sphere of radius  $r$ . In the practical use of (4),  $r$  will be

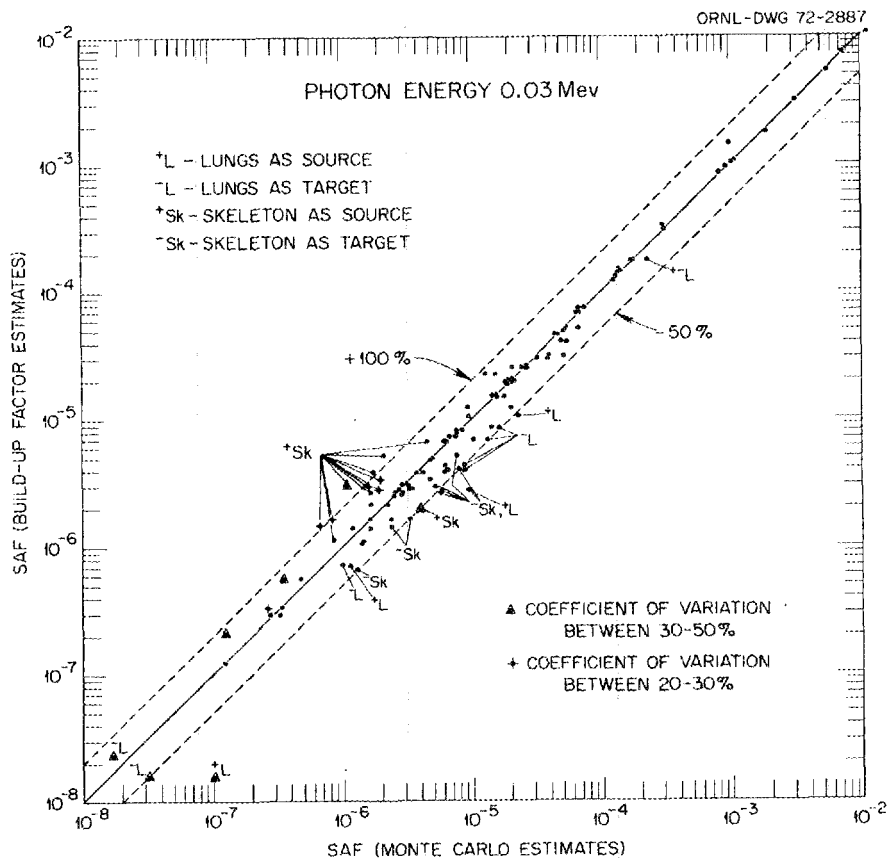


Fig. 12.1. Monte Carlo estimates of specific absorbed fractions compared with buildup factor estimates.

taken as 0.1 cm, although other values of  $r$  have been used. Thus we set

$$\bar{\Phi}(T \leftarrow S) = \frac{1}{N} \sum_i f(X_i, Y_i), \quad (5)$$

where

$$f(X_i, Y_i) = \frac{\mu_{ab} e^{-\mu|X_i - Y_i|}}{4\pi|X_i - Y_i|^2} B(\mu|X_i - Y_i|)$$

if  $|X_i - Y_i| > r$ , but

$$f(X_i, Y_i) = \frac{1}{\frac{4}{3}\pi r^3} \int_{|X_i - Y_i| \leq r} dY_i \times \frac{\mu_{ab} e^{-\mu|X_i - Y_i|}}{4\pi|X_i - Y_i|^2} B(\mu|X_i - Y_i|)$$

if  $|X_i - Y_i| \leq r$ . Changing to polar coordinates and setting  $B(\mu|X_i - Y_i|) \cong 1$ , one obtains

$$f(X_i, Y_i) \cong \int_0^r \mu_{ab} e^{-\mu\tau} d\tau \left/ \frac{4\pi r^3}{3} \right. = \frac{3\mu_{ab}(1 - e^{-\mu r})}{4\pi r^3 \mu}$$

in this latter case. This relative stability of the formula is obtained only at the expense of a certain indefiniteness in the boundary. Sometimes the entire sphere with center at  $X_i$  and of radius  $r$  is not within the region to be sampled, so we have preferred to keep  $r$  small. With  $r = 0.1$  cm, the maximum contribution of a term is about  $5000\mu_{ab}$ , and if  $N$  is taken as 30,000, this yields a contribution of  $\mu_{ab}/6$  due to this one term.

### Discussion

Data on the specific absorbed fraction are plotted in Figs. 12.1--12.7 for photons of energies 0.03, 0.05, 0.1, 0.5, 1, 1.5, and 4 MeV. The position of each point is determined by the two estimates of  $\bar{\Phi}$ ; that is, the abscissa represents the estimate of  $\bar{\Phi}$  by the Monte Carlo program used for the anthropomorphic phantom,<sup>2</sup> and the ordinate represents the estimate of  $\bar{\Phi}$  by use of the buildup factor. When the point is on the heavy line, the two estimates are equal. It will be noted that (1) generally, the points lie above the heavy line as they should (backscatter is maximal in the infinite space of tissue or water), (2) the points lie increasingly close to the line as the coefficient of variation of the Monte Carlo anthropomorphic estimates is decreased, and (3) very few points lie outside the two lines which

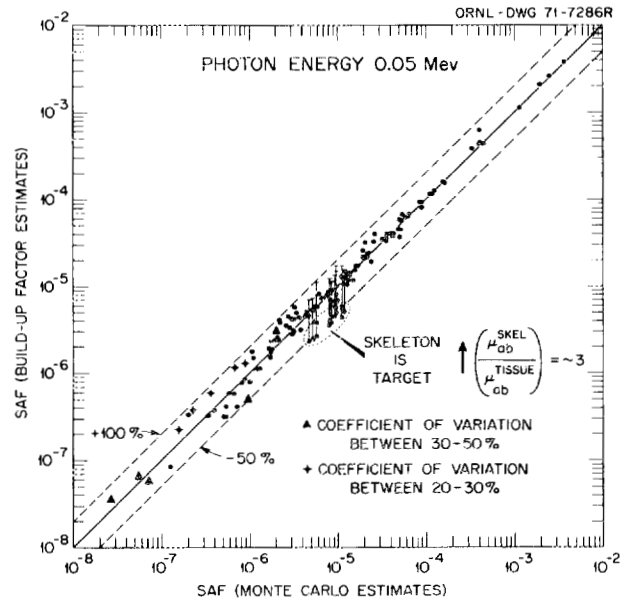


Fig. 12.2. Monte Carlo estimates of specific absorbed fractions compared with buildup factor estimates.

bound the region  $0.5 < \Phi_1/\Phi_2 < 2$ , where  $\Phi_1$  and  $\Phi_2$  are the two corresponding estimates.

There are a few exceptions to the above. When the skeleton is the target organ, the point should be raised by the factor  $\mu_{ab}^{\text{bone}}/\mu_{ab}^{\text{tissue}}$ , since the composition of bone will produce a greater abundance of secondary electrons than will water or soft tissue. This correction is important mainly for the energies below 0.1 MeV. Also, when the lung is the source organ, it appears the results might be multiplied by a factor of about 3, although the evidence is not entirely clear. In the buildup factor calculation, the lung region has a mass of about 3000 g, and this allows fewer photons to escape than if the mass were about 1000 g. Probably the factor to be used is dependent on the energy of the photon. Similarly, when bone is the source, the result obtained from the calculation using the buildup factor might be multiplied by two-thirds. However, these are "rule-of-thumb" corrections which are not rigorous, but they do generally improve the correspondence of the two estimates. We are continuing to explore this method but expect that the inclusion of an adjustment factor for bone and lungs is advisable, although its value is probably not always the reciprocal of the density.

### Acknowledgments

The authors gratefully acknowledge the assistance of James Hickey in analyzing the results and preparing the graphs.

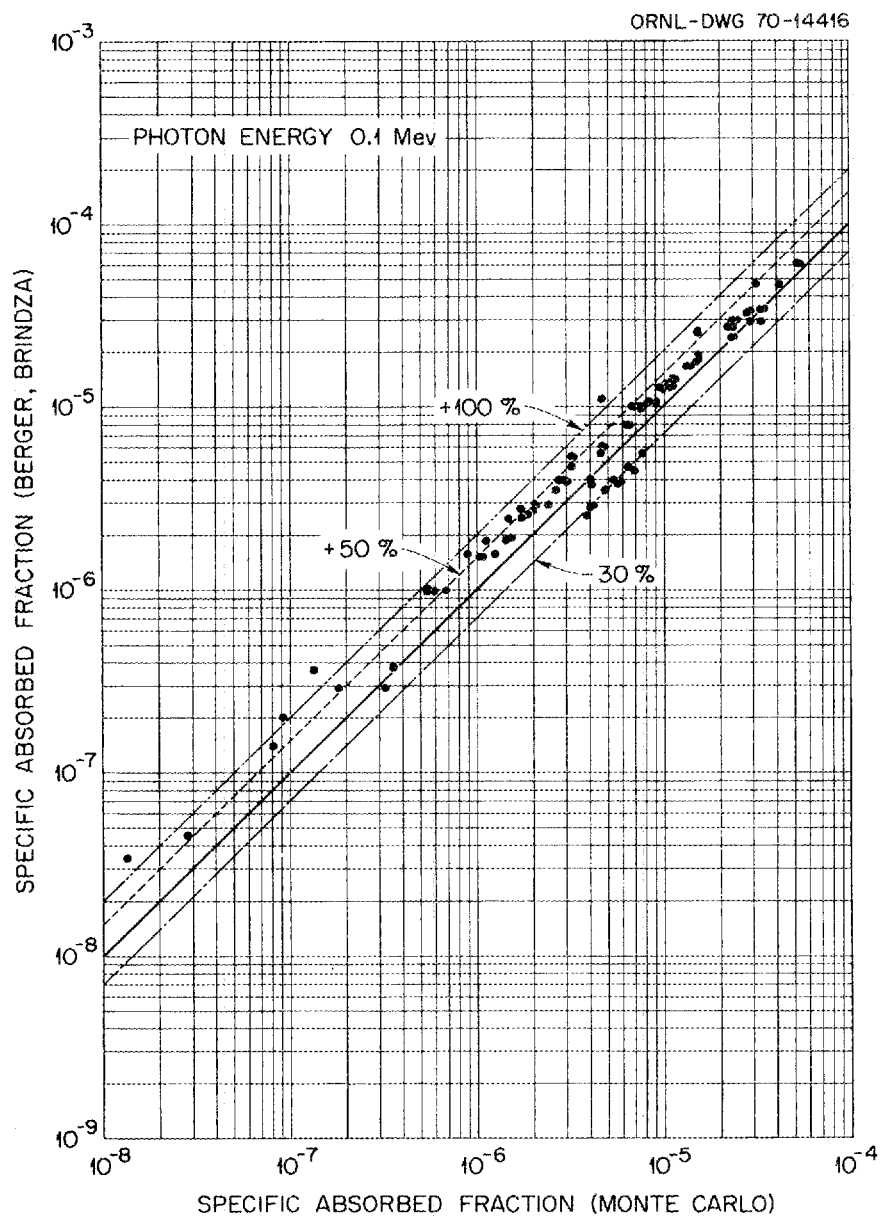


Fig. 12.3. Specific absorbed fraction in an anthropomorphic phantom and in an infinite homogeneous medium.

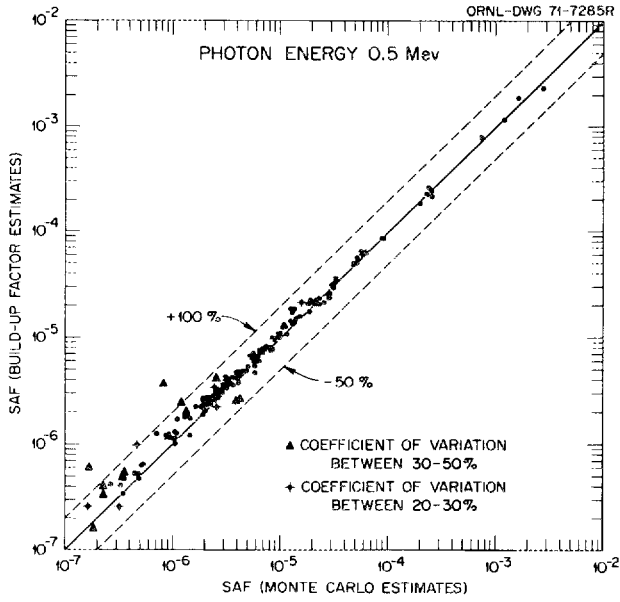


Fig. 12.4. Monte Carlo estimates of specific absorbed fractions compared with buildup factor estimates.

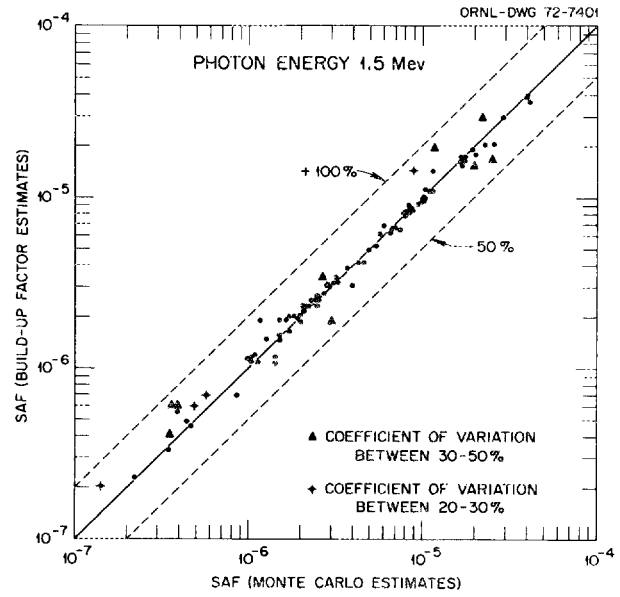


Fig. 12.6. Monte Carlo estimates of specific absorbed fractions compared with buildup factor estimates.

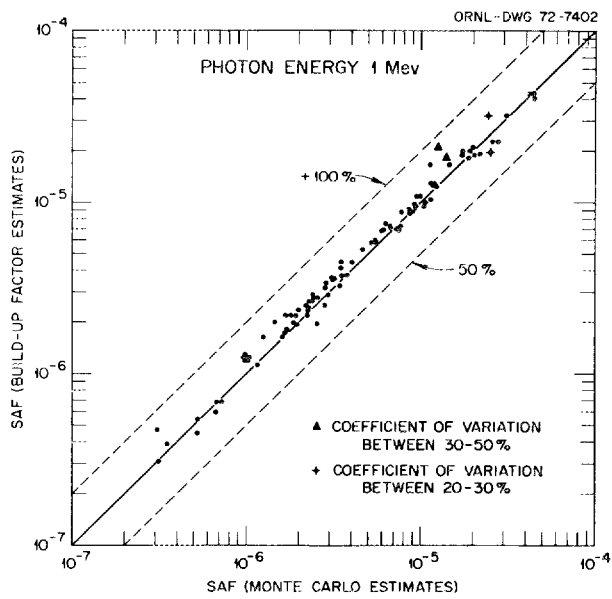


Fig. 12.5. Monte Carlo estimates of specific absorbed fractions compared with buildup factor estimates.

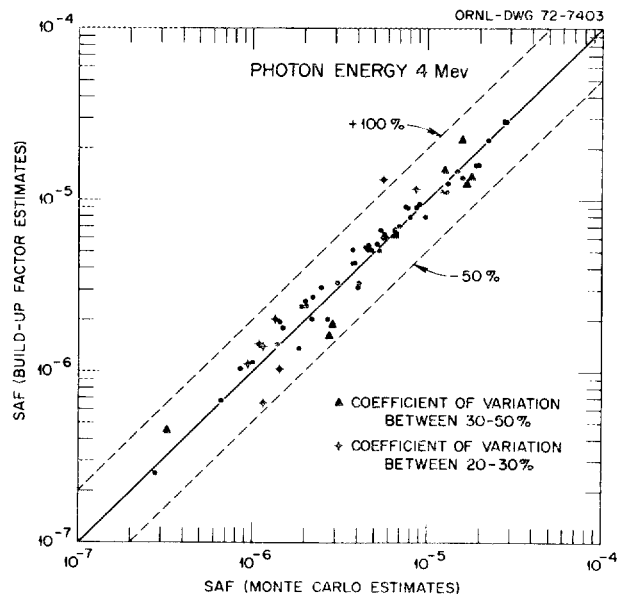


Fig. 12.7. Monte Carlo estimates of specific absorbed fractions compared with buildup factor estimates.

## 13. Estimates of Dose to Infants and Children from a Photon Emitter in the Lungs

M. J. C. Hilyer    W. S. Snyder    G. G. Warner<sup>1</sup>

When a monoenergetic photon source is distributed uniformly in any organ (called the source organ  $S$ ), the dose rate to any other organ (called the target organ  $T$ ) is proportional to the specific absorbed fraction (SAF or  $\Phi$ ). This SAF is simply the fraction of energy emitted which is absorbed per gram of the target organ, that is,

$$\Phi(T \leftarrow S) = \frac{\text{energy absorbed in } T}{(\text{energy released in } S) (\text{mass of } T \text{ in grams})}$$

In most practical situations there will be photons emitted of a variety of energies and intensities, and the concept of the SAF can be extended to include such cases,<sup>2</sup> but for simplicity only the case of a monoenergetic source is considered in this report. Values of SAF for a "reference man" may be obtained from the absorbed fraction (AF) by dividing by the mass of the target organ ( $T$ ). Some AF's for adults have been published in MIRP Pamphlet No. 5.<sup>3</sup> These estimates take account approximately of size, shape, location, composition, and density of the organ or tissue. Although similar estimates for other ages are not believed to be available, some preliminary estimates of the age variation of the SAF for photons were

published in ORNL-4720<sup>4</sup> for a photon emitter in the stomach for ages 0, 1, 5, 10, 15, and adult and for six energies: 0.2, 0.5, 1.0, 1.5, 2.0, and 4.0 MeV. This study has been continued for a photon emitter in the lungs using the same six ages but extending it to include 12 energies, namely, 0.01, 0.015, 0.02, 0.03, 0.05, 0.1, 0.2, 0.5, 1.0, 1.5, 2.0, and 4.0 MeV.

On the basis of the inverse square law, for the same source of photons in the organ of a child and of an adult, the child will receive the greater dose rate. Data on the total body, as well as on the various organs, reveal that individuals of the younger age group are not merely adults reduced proportionately by a constant factor. However, designing phantoms for a series of ages is a formidable task, particularly when data on certain ages are sparse.

For this purpose, the adult phantom was reduced by scale factors selected separately for the head section, trunk section, and leg section of the adult phantom. All of the organs and tissues within these sections were reduced by the scale factors for that section. Explicit transformation formulas were applied so that these transformations were similitudes. Therefore, loci (organs) which are nonintersecting in one phantom are nonintersecting in the other phantom. The new phantoms obtained in this way correspond to typical individuals of ages 0, 1, 5, 10, and 15 years. These phantoms are presented in outline in Fig. 13.1, and for comparison the adult phantom is shown also.

Using this transformation, it is easy to adapt the computer program for the new phantom. Whenever one needs to determine whether a point in the transformed phantom is in an organ of that phantom, one simply applies the inverse transformation and tests the corresponding point in the adult phantom. Thus, the part of the computer code concerned with recording data is not changed, and this is advantageous, since it constitutes a major complexity of that code.

1. Mathematics Division.

2. Robert Loevinger and Mones Berman, "A Schema for Absorbed-Dose Calculations for Biologically Distributed Radionuclides," MIRP Pamphlet No. 1, Suppl. No. 1, *J. Nucl. Med.* February 1968).

3. W. S. Snyder et al., "Estimates of Absorbed Fractions for Monoenergetic Photon Sources Uniformly Distributed in Various Organs of a Heterogeneous Phantom," MIRP Pamphlet No. 5, Suppl. No. 3, *J. Nucl. Med.* (August 1969).

4. W. S. Snyder, M. J. Cook, and G. G. Warner, "Preliminary Indications of the Age Variation of the Specific Absorbed Fraction for Photons," presented at Health Physics Society Meeting, New York, July 16, 1971; published in *Health Phys. Div. Annu. Progr. Rep. July 31, 1971*, ORNL-4720, pp. 116-18.

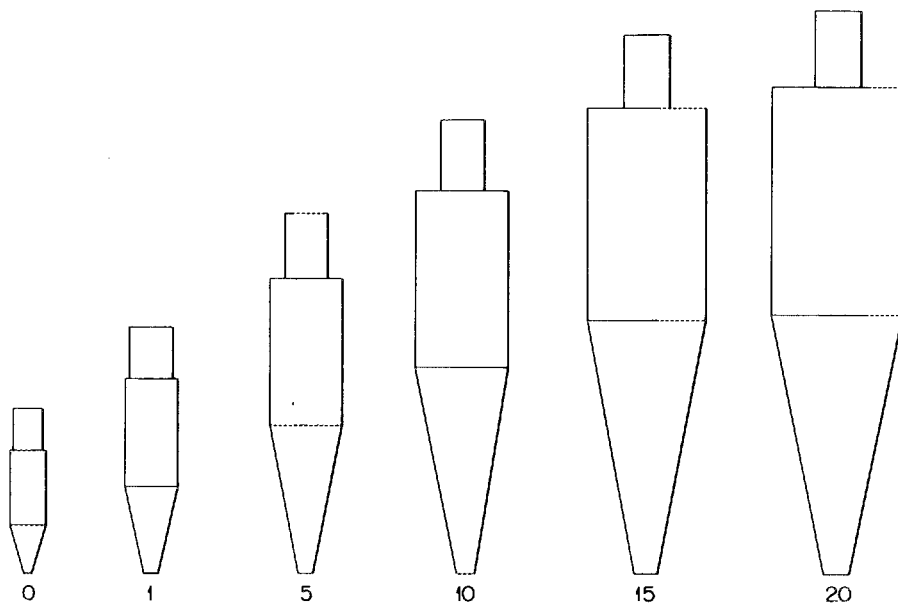


Fig. 13.1. Relative size of phantoms for 0, 1, 5, 10, 15, and 20 years.

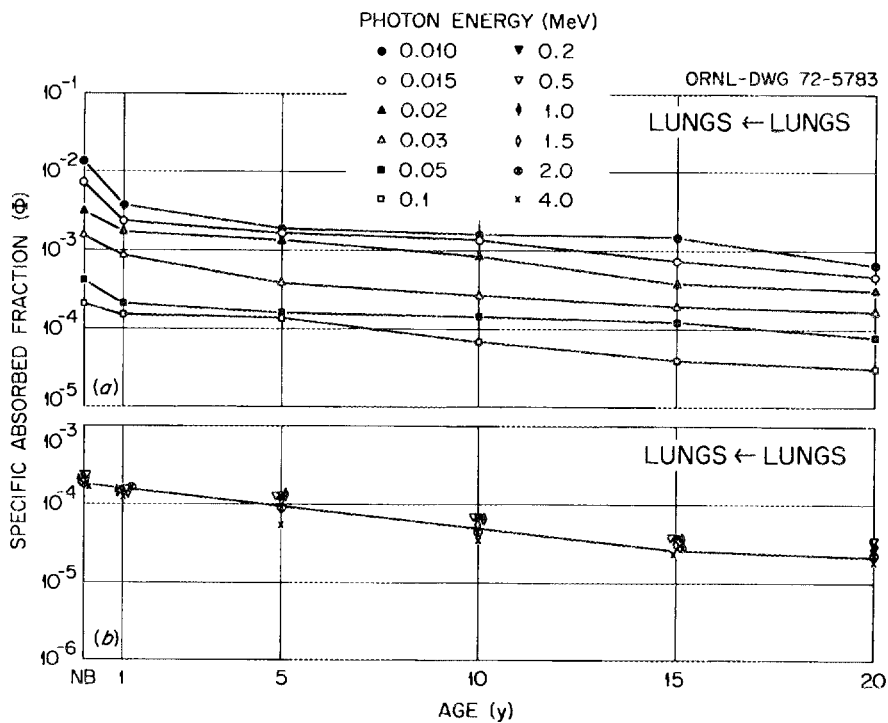


Fig. 13.2. Specific absorbed fraction as a function of age and photon energy. Lungs ← lungs.

For the six lower energies, namely, 0.01, 0.015, 0.02, 0.03, 0.05, and 0.1 MeV, 60,000 photons were programmed for each photon energy. For the six higher energies, namely, 0.2, 0.5, 1.0, 1.5, 2.0, and 4.0 MeV, 30,000 photons were programmed for each photon energy. Previous calculations had shown that the statistics were so poor for the 30,000 photons at the six lower energies that it was decided to program the lower energies using 60,000 photons. The statistics showed that these results were improved and fairly reliable.

Because inhalation could be an important route of exposure for the population, it was decided to program the source of monoenergetic photons in the lungs. For illustration, estimates of the SAF from lungs to lungs which were obtained by the Monte Carlo method are presented in Fig. 13.2. One may compare the SAF for one energy at different ages, and one may compare the SAF for one age at different energies. Using the lungs as the source organ and the lungs as the target organ, the SAF's decrease as the age increases; thus, the newborn always has the highest SAF. This behavior is undoubtedly typical and may be largely due to the inverse square law. For example, last year we showed data on the SAF using the stomach contents as the source organ and stomach as the target organ, and here also the SAF

decreases regularly as age increases. It is also instructive to compare the ratios of the SAF at a specified age with the SAF for an adult. It is found that this ratio decreases regularly as age increases,  $(SAF)_{x \text{ age}} / (SAF)_{\text{adult}}$ . At 0.01 MeV, the factor between lungs of the newborn and the lungs of the adult is about 19, but for the lungs of a five year old to the lungs of the adult, the factor is about 4. Similarly, the SAF for different energies at one age may be compared. For the newborn, there is a factor of about 64 in the SAF of lungs to lungs between 0.01- and 4-MeV values. Also, in Fig. 13.2 the SAF's for lungs as the source organ and lungs as the target organ for the six higher energies (0.2 to 4.0 MeV) have been plotted. They are all rather close for each of the chosen ages; therefore, only one curve has been used for illustration of the difference of the SAF between the newborn (and any other age) and the adult. However, the previous remarks still apply; that is, the SAF decreases as age increases, and so does the ratio of the SAF for any age to that for an adult. However, the values do not change much with energy, and so only a single curve is shown.

For a second example (Fig. 13.3) the SAF's are shown for the lungs as the source organ to liver as the target organ for the same energies and ages. At the

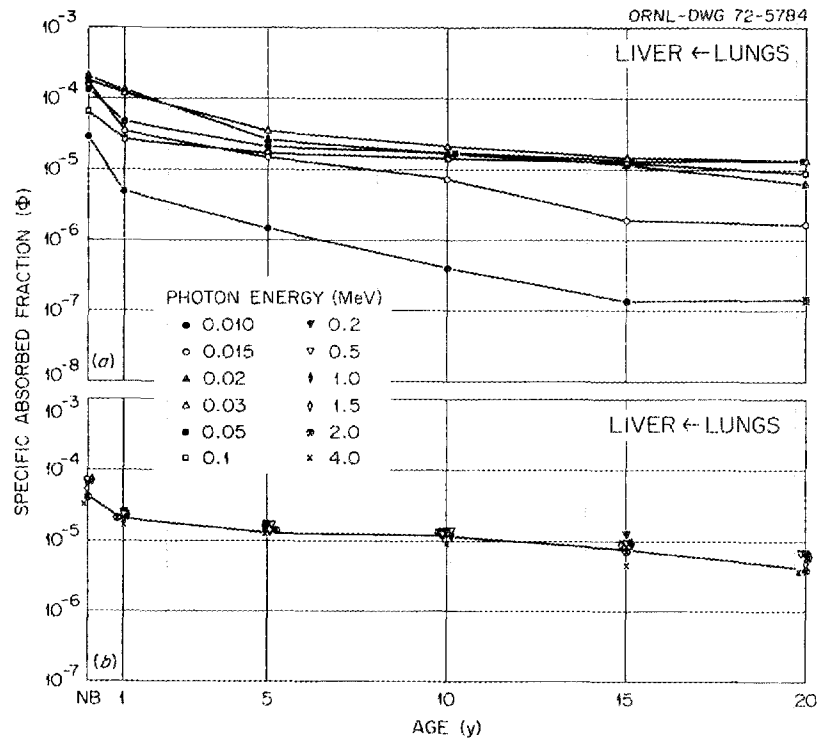


Fig. 13.3. Specific absorbed fraction as a function of age and photon energy. Liver ← lungs.

lowest energy of 0.01 MeV, the SAF for the newborn to the adult differs by a factor of about 300. From the previous illustration (Fig. 13.2) of lungs to lungs for the newborn to the adult at 0.01 MeV, this factor was about 19. This behavior seems general; that is, the ratio  $(SAF)_{x \text{ age}} / (SAF)_{\text{adult}}$  decreases as the age increases. The SAF decreases as the energy increases, which is also true at the six higher energies.

Because the ICRP has recommended lower dose limits for blood-forming organs than for the majority of other body organs, it is important to have an accurate estimate of the dose to this tissue. Estimates have been calculated for the dose to the red bone marrow for adults for these same 12 energies when the source organ was the lungs,<sup>5</sup> but comparable estimates for other ages have not been available. For example, the distribution of red bone marrow is much different for the younger ages than for the adult. For this reason the dose to total marrow has been examined as well as dose to the red bone marrow and dose to the skeleton. No systematic difference was found in these results. This does not exclude the fact that the values may differ by a factor of 2 in some cases. It appears that one may use dose to skeleton as being approximately the dose to the red bone marrow, even at younger ages. Because of the complexity of the skeletal system, red bone marrow, and total bone marrow, this rule is to be regarded as approximate only. The SAF's were calculated for these three tissues and organs and for the same six ages and 12 energies, and the data were found always to be within a factor of 2, but are usually much closer. In all cases the coefficient of variation was less than 26%. The SAF's for the skeleton as the target organ and the lungs as the source organ are presented in Fig. 13.4. Thus, these values also may be used when red bone marrow and total bone marrow are the target organs.

In a previous report<sup>4</sup> the SAF's were presented when the contents of the stomach were the source organ and the liver and lungs were the target organs for the six higher energies, namely, 0.2 to 4.0 MeV. At that time the SAF's for the six lower energies were not believed to be statistically reliable enough to present; however, more effort has been given to studying the SAF for these six lower energies when the source organ is the contents of the stomach and the target organs are the liver and lungs.

5. M. J. Cook, W. S. Snyder, and G. G. Warner, "Estimates of Dose to Red Bone Marrow from Monoenergetic Sources of Photons in Lungs and Other Organs," *Health Phys. Div. Annu. Progr. Rep. July 31, 1970*, ORNL-4584, pp. 200-203.

When the source is the contents of the stomach and the target organ is the liver, the SAF for these six lower energies is presented in Fig. 13.5. In each case the newborn receives the highest dose rate. In fact, for the 0.02-MeV energy, the newborn receives almost 300 times the dose for the adult. Also, for the newborn, the liver receives 11 times greater dose from the 0.015-MeV than from the 4-MeV photon source.

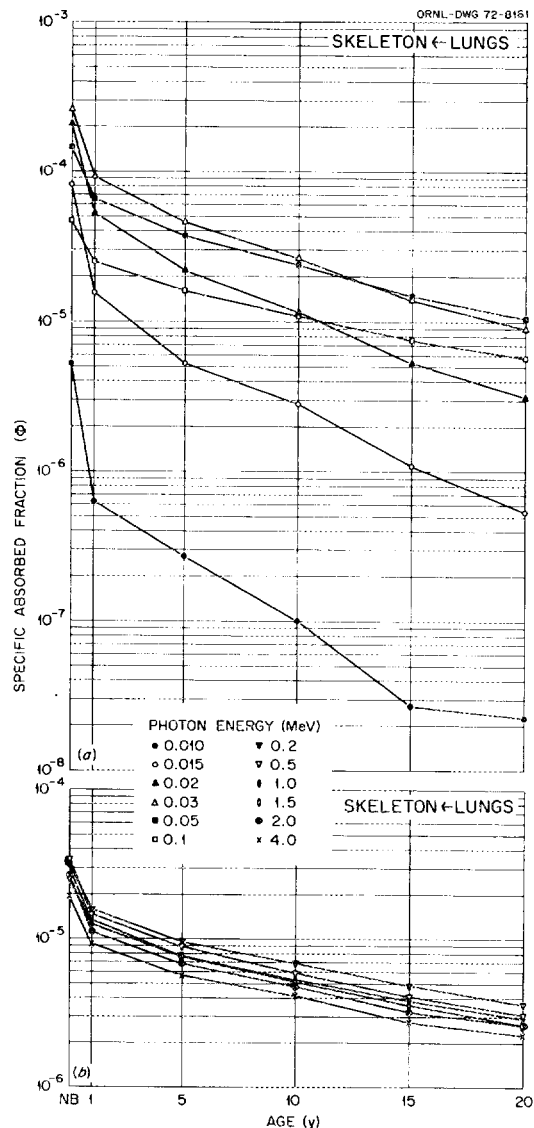


Fig. 13.4. Specific absorbed fraction as a function of age and photon energy. Skeleton ← lungs.

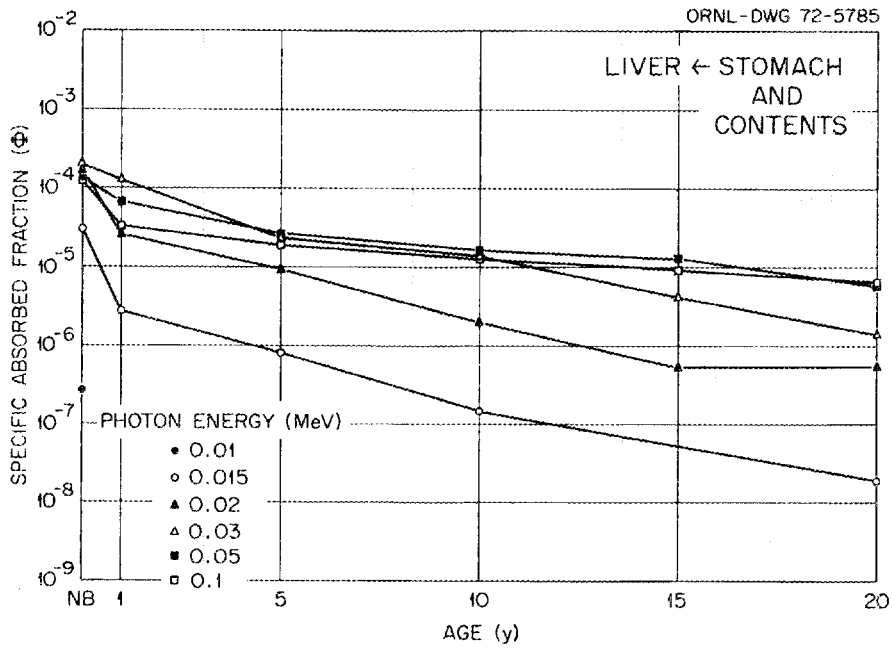


Fig. 13.5. Specific absorbed fraction as a function of age and photon energy. Liver ← stomach and contents.

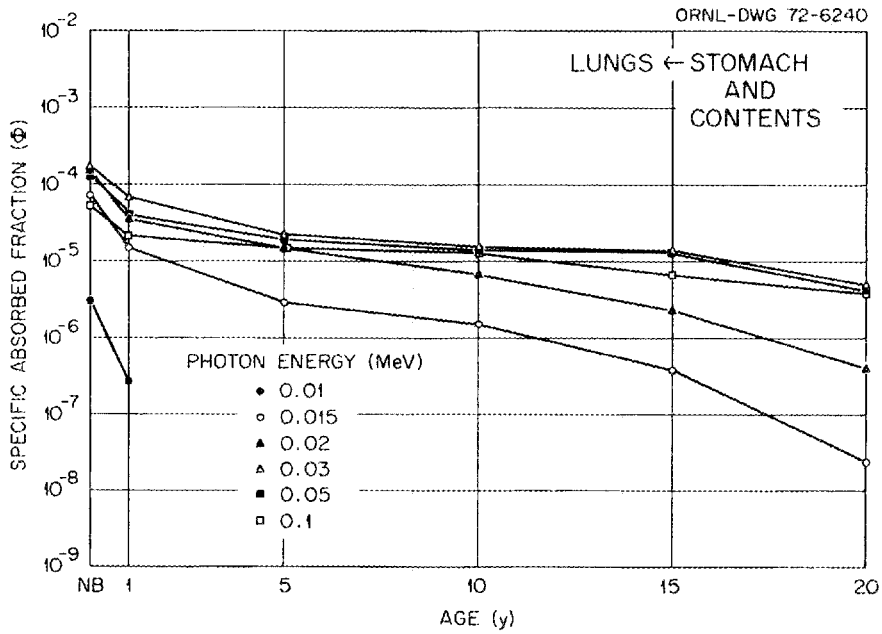


Fig. 13.6. Specific absorbed fraction as a function of age and photon energy. Lungs ← stomach and contents.

In Fig. 13.6 with the contents of the stomach as the source organ and the lungs as the target organ, the same general relationship is seen that the SAF decreases as age increases. The SAF seems to reach a maximum at about 30 keV. Also, the ratio  $(SAF)_{x \text{ age}}/(SAF)_{\text{adult}}$  generally decreases as the energy increases.

In these few examples, when the lungs or the contents of the stomach were the source organ and the target organs were the liver, skeleton, lungs, kidneys, or small intestine plus contents, the results which might be expected are (1) that generally the SAF will be greater

for the younger ages, (2) that, for a given age and for the target organ being different from the source organ, the SAF passes through a maximum which seems to occur at 30 to 50 keV, (3) that when the source and target organs are the same, the SAF generally increases as energy decreases, (4) that the ratio  $(SAF)_{x \text{ age}}/(SAF)_{\text{adult}}$  seems generally to increase as energy decreases, and (5) the published values for the absorbed fractions for the adults should not be used for calculating the dose rate for the newborn and children.

## 14. Weight of the Lungs Plus Fluids for Reference Man

W. S. Snyder    M. J. C. Hilyer    A. P. Stoholski<sup>1</sup>

For purposes of dosimetry, either external or internal to the body, an ICRP (International Commission on Radiological Protection) reference man has been established.<sup>2</sup> Reference man has a total body weight of 70 kg, and thus the weight of all his organs, tissues, and fluids must total 70 kg. One of the problems encountered in establishing reference man was determining the weight for the lungs, including a normal amount of blood. Most anatomical textbooks and anatomical studies do not state the conditions under which the lung weights they report were obtained. For example, most sources do not state whether a near-normal amount of blood is included, and seldom do they indicate the body weights or dimensions of the individual. The lungs may accumulate fluids after the death of the individual, but the references seldom, if ever, give the length of time between death and autopsy. The lungs are a very vascular tissue, so it is necessary for dosimetry to know the weight of the parenchyma and blood separately, as well as the total for parenchyma and blood. Energy from gamma rays will be absorbed in blood as well as in the lung tissue, but for radiation of less penetration — say, weak betas or alpha particles — the blood in the larger vessels might absorb little energy.

Because of these difficulties in establishing weights of total lung, parenchyma, and lung blood, a special study was set up with the cooperation of the Department of Forensic Medicine, New York University, for obtaining

these data from individuals whose age, sex, total body weight, total body height, and cause of death are known.

Because fluids accumulate in the lungs after death, these lung weights were obtained as soon as possible after death but not longer than 24 hr. Before removing the lungs from the body the largest veins and arteries were tied below the bifurcation of the trachea and severed beyond the position of the tie; so little blood was lost from the lungs. Thus, the tissue was weighed with a near-normal amount of pulmonary blood. In Table 14.1 this weight is referred to as total lung weight and represents the weight of the bronchial tree, pulmonary lymph nodes, and arterial, venous, and residual blood, as well as parenchyma. After the weight was obtained the tourniquets were cut, and the lung was drained of all blood which could be removed by gentle pressing and patting. The lung was reweighed. This weight represents the weight of the above-listed tissues except the removable blood (mostly arterial and venous) and in Table 14.1 is referred to as drained lung weight. Residual blood is defined here as that quantity of blood which remains in an organ or tissue after it has been allowed to bleed freely. This is assumed to be equivalent to capillary blood.

Twenty cases, sixteen males and four females, have been obtained, and the data are presented in Table 14.1. The data have been treated statistically as (1) a group of 20, (2) 16 males only, and (3) 4 females only. The weight of the lungs plus blood is somewhat better correlated with total body weight than with total body height or surface area. Less variation was found for the lungs plus blood as a percentage of the total body weight than for correlation with other parameters tested. The data obtained for the correlation with total body weight are presented in Table 14.1.

1. New York University.

2. Report of Committee II on Permissible Dose for Internal Radiation (1959), *Recommendations of the International Commission on Radiological Protection*, ICRP Publication 2, Pergamon, London, 1959, p. 30.

Table 14.1. Weights of lungs and of lung fluids for 20 adults

	Mean	Standard deviation	Median	Low	High	80% range	
						10th percentile	90th percentile
<b>Male (n = 16)</b>							
Age (years)	33.3	8.6	32	20	44	25	43
Total body weight (kg)	77.3	7.6	78	61	93	68	82
Total body height (cm)	171.4	6.8	170	160	185	165	178
Total lung weight (g)	946.3	115.4	960	730	1120	810	1090
Drained lung weight (g)	770.6	86.8	768	625	895	670	880
Drained blood weight (g)	169.4	47.8	173	90	240	115	225
$\frac{\text{Total lung weight (kg)}}{\text{Total body weight (kg)}} = \%$	1.23	0.134	1.25	0.95	1.46	1.07	1.33
$\frac{\text{Drained blood weight (g)}}{\text{Total lung weight (g)}} = \%$	17.60	3.37	17.93	12.33	23.83	13.69	21.43
<b>Female (n = 4)</b>							
Age (years)	29	8	29	21	37		
Total body weight (kg)	66	8.9	65.6	55.8	77.1		
Total body height (cm)	163.2	8.4	162.6	154.9	172.7		
Total lung weight (g)	879	173	845	715	1110		
Drained lung weight (g)	728	132	710	595	895		
Drained blood weight (g)	151	43	135	120	215		
$\frac{\text{Total lung weight (kg)}}{\text{Total body weight (kg)}} = \%$	1.33	0.087	1.31	1.24	1.44		
$\frac{\text{Drained blood weight (g)}}{\text{Total lung weight (g)}} = \%$	17.05	2.73	16.67	15.47	19.37		
<b>Males and females (n = 20)</b>							
Age (years)	32.5	8.5	32	20	44	21	43
Total body weight (kg)	75.1	8.9	77.1	55.8	93.4	63.5	81.7
Total body height (cm)	170.4	71.3	170.2	154.9	185.4	160	177.8
Total lung weight (g)	932.8	129.3	937.5	715	1120	765	1090
Drained lung weight (g)	759.5	94.4	760	595	895	640	880
Drained blood weight (g)	166	46	168	90	240	115	225
$\frac{\text{Total lung weight (kg)}}{\text{Total body weight (kg)}} = \%$	1.25	0.13	1.26	0.95	1.46	1.07	1.44
$\frac{\text{Drained blood weight (g)}}{\text{Total lung weight (g)}} = \%$	17.49	3.06	17.91	12.33	23.83	13.69	21.43

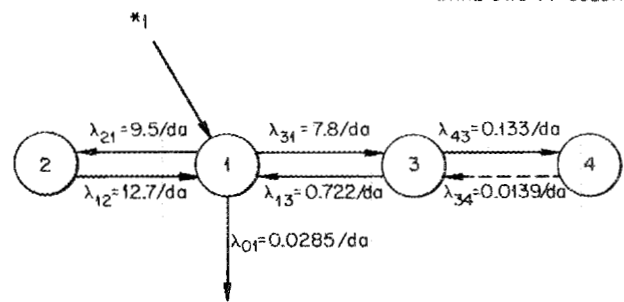
# 15. A Metabolic Model for Magnesium in Man and an Estimate of Dose to Bone and Soft Tissue Resulting from a Single Intravenous Injection of $^{28}\text{Mg}$

S. R. Bernard

The metabolic model of Avioli and Berman,<sup>1</sup> based on measurements of blood, urine, and feces of 15 human subjects who had been administered tracer doses of  $^{28}\text{MgCl}_2$  intravenously, appears in Fig. 15.1. Compartments 1, 2, 3, and 4 are "body" compartments, with 1 representing blood and 2, 3, and 4 only stated to be extravascular compartments. Avioli and Berman did not identify the other three body compartments, because they only had measurements on blood and excreta. These data only yield the four eigenvalues of the  $4 \times 4$  matrix of rate transfer constants and some information on the constraints on the  $\lambda$ 's. To estimate all  $4^2$  rate transfer constants uniquely, data are needed on all four compartments. Further details on the uniqueness of compartment models may be found in the paper by Berman and Schoenfeld.<sup>2</sup> The arrow pointing down from compartment 1 represents excretion. The starred arrow identifies the site of the initial  $^{28}\text{Mg}$  injection. The  $\lambda_{ij}$ 's are the rate transfer constants given by Avioli and Berman. These values appear in Fig. 15.1. Although Avioli and Berman give ranges of values and standard deviations, the present model uses only the means. The dashed arrow from compartment 4 to 3 indicates that this pathway connection was not observed directly but was estimated from literature data on stable Mg levels in bone and muscle and with the tracer data.

In estimating internal dose, equations for retention in organs and tissues and total body are needed. From the data in Fig. 15.1, the linear differential equations for the "body" compartments of the model of Avioli and Berman, written in matrix form, are:

$$\dot{Y}(t) = \begin{pmatrix} \dot{y}_1(t) \\ \dot{y}_2(t) \\ \dot{y}_3(t) \\ \dot{y}_4(t) \end{pmatrix} = - \begin{pmatrix} 17.8 & -12.7 & -0.722 & -0.0 \\ -9.5 & 12.7 & -0.0 & -0.0 \\ -7.8 & -0.0 & 0.855 & -0.0139 \\ -0.0 & -0.0 & -0.133 & 0.0139 \end{pmatrix} \begin{pmatrix} y_1(t) \\ y_2(t) \\ y_3(t) \\ y_4(t) \end{pmatrix} \quad (1)$$



ORNL-DWG 71-8329A

**Fig. 15.1. Berman's compartmental model assumed for  $^{28}\text{Mg}$  analysis.** Compartment 1 refers to ultrafilterable plasma Mg; compartments 2, 3, and 4 represent extravascular compartments. Compartment 4 is depicted as a slowly exchanging magnesium pool postulated to exist under steady-state conditions with slow turnover rate ( $\lambda_{34}$ ).

The time  $t$  is expressed in days. Here  $y_i(t)$  ( $i = 1, 2, 3, 4$ ) corresponds to the amount present in compartment  $i$  at time  $t$ , and  $\dot{y}_i(t)$  is the derivative  $dy_i(t)/dt$ . A computer code written by J. A. Carpenter, ORNL Mathematics Division, was used to obtain the solutions of (1). These appear in Eq. (2), which is also in matrix form, and apply to the case of unit intake into compartment 1 at zero time. Here  $Y(t)$  stands for the column vector of  $y_i(t)$ ,  $i = 1, 2, 3, 4$ . Equation (3)

1. L. V. Avioli and Mones Berman, " $^{28}\text{Mg}$  Kinetics in Man," *J. Appl. Physiol.* **21**(6), 1688-94 (1966).
2. M. Berman and R. Schoenfeld, "Invariants in Experimental Data on Linear Kinetics and the Formulation of Models," *J. Appl. Phys.* **27**, 1361 (1956).

represents retention for the total body, which was obtained from (2) by summing the rows of (2), that is, it is the sum of all the body compartments.

$$Y(t) = \begin{pmatrix} 0.00473 & 0.0709 & 0.310 & 0.614 \\ 0.00354 & 0.0538 & 0.360 & -0.418 \\ 0.0544 & 0.787 & -0.656 & -0.186 \\ 0.676 & -0.696 & 0.0193 & 0.000927 \end{pmatrix} \begin{pmatrix} e^{-0.00320t} \\ e^{-0.164t} \\ e^{-4.54t} \\ e^{-26.7t} \end{pmatrix} \quad (2)$$

$$R(t) = 0.738e^{-0.00320t} + 0.216e^{-0.164t} + 0.034e^{-4.54t} + 0.0115e^{-26.7t} \quad (3)$$

As a test of this model, we employ the daily intake of Mg in reference man's diet of 0.34 g per day<sup>3</sup> and an absorption into blood from gut of 0.45,<sup>1</sup> as given by Avioli and Berman. In studies by Yun et al.<sup>4</sup> (the compound was not stated) on two human subjects, the values found are 0.53 to 0.93, higher than Avioli and Berman's value. Integrating over time, we obtain the equilibrium body burden

$$q = \int_0^\infty 0.34 \times 0.45 \times d\tau R(t - \tau) = 36 \text{ g}, \quad (4)$$

which is in agreement with reference man's burden of 29 g of Mg. Aikawa indicates that about 60% of this is in skeleton, 20% in muscle, and the remainder in other soft tissues. This is not a close estimate of the distribution obtained from the model, that is, 92% in one compartment, which might be identified with the skeleton, 7% in a second compartment (muscle), and only 1% in the other two compartments. It might be preferable to regard the compartment containing 92% of the body content as consisting not only of skeleton but also of portions of muscle and other soft tissues, and thus more nearly approximate the distribution of the stable element.

Figure 15.2 shows a revised model in which the long-term compartment is subdivided into two separate compartments. Two of these each receive 50% of  $\lambda_{43}$  while one receives 60%, and the flow back  $\lambda_{34}$  is the same for each one. This compartment model is the same

3. J. K. Aikawa, *The Role of Magnesium in Biologic Processes*, C. C. Thomas, Springfield, Ill., 1963, pp. 65, 67.

4. T. K. Yun, R. Lazzara, W. C. Black, J. J. Walsh, and G. E. Birch, "The Turnover of Magnesium in Control Subjects and in Patients with Idiopathic Cardiomyopathy and Congestive Heart Failure Studies with Magnesium-28," *J. Nucl. Med.* 7, 177 (1966).

as Avioli and Berman's when the two compartments 4' and 4'' are combined. Then Eqs. (2) apply, and the fourth equation corresponds to the sum of compartments 4' and 4''. This can be proved easily by writing out the linear differential equations and then summing Eqs. 4' and 4''. The equations for the burden in the two additional compartments are

$$y_{4'}(t) = y_{4''}(t) = 0.50 (0.676e^{-0.00320t} - 0.696e^{-0.164t} + 0.0193e^{-4.54t} + 0.000927e^{-26.7t}) = 0.50 y_4(t).$$

The radiation dose to the total soft tissues and skeleton is estimated with this model and the decay scheme data shown in Table 15.1. From the data on absorbed fractions of photon energy, we estimate the effective energy per disintegration to be, from Table 15.2 and adding the electron plus beta energies from <sup>28</sup>Mg and <sup>28</sup>Al, for skeleton

$$\epsilon_{SK} = \begin{cases} 0.0474 \text{ MeV for source in soft tissues} \\ 1.566 \text{ MeV for source in skeleton} \end{cases}$$

while for soft tissue

$$\epsilon_{ST} = \begin{cases} 1.803 \text{ MeV for source in soft tissues} \\ 0.275 \text{ MeV for source in skeleton} \end{cases}$$

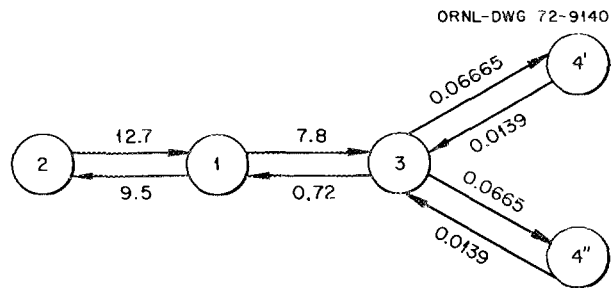


Fig. 15.2. Revised compartment model for Mg metabolism.

In the above we assume that the short-lived  $^{28}\text{Al}$  undergoes decay in situ. Later, when more data on Al metabolism are available, we may not have to make this assumption.

Table 15.1. L. T. Dillman's decay scheme data<sup>a</sup> for  $^{28}\text{Mg}$  and  $^{28}\text{Al}$

Radiation	Percent per decay	Energy (MeV)
$^{28}\text{Mg}$ : $T_{1/2} = 0.875$ day; $\beta$ , average energy = 0.1586 MeV		
$\gamma_1$	96.899	0.0310
Internal conversion electrons	3.101	0.0294
$\gamma_2$	30.00	0.4000
$\gamma_3$	30.00	0.9500
$\gamma_4$	69.999	1.3500
$KA_1$ x rays	0.171	0.0015
$KLL$ Auger electrons	2.587	0.0014
$KLX$ Auger electrons	0.344	0.0015
$LMM$ Auger electrons	5.688	0.0001
$^{28}\text{Al}$ : $T_{1/2} = 2.3$ min; $\beta$ , average energy = 1.2392 MeV		

<sup>a</sup>Decay scheme data in files of Information Center for Internal Exposure, ORNL.

From Eq. (3) we obtain the residence time of  $^{28}\text{Mg}$ ,  $Q_x$ , as 1.1  $\mu\text{Ci-days}$  for the soft tissues and 0.063  $\mu\text{Ci-day}$  for skeleton. Thus the dose commitment is

$$DE_{\text{bone}} = \frac{51}{7000} (1.6Q_{\text{bone}} + 0.047Q_{\text{soft tissues}})$$

$$\cong 0.0011 \text{ rad to bone per } \mu\text{Ci into blood}$$

and

$$DE_{\text{soft tissues}} = \frac{51}{63,000} (1.8Q_{\text{soft tissues}} + 0.3Q_{\text{bone}})$$

$$= 0.0017 \text{ rad to soft tissues per } \mu\text{Ci injection into blood.}$$

This compares favorably with the ICRP Publication 17<sup>5</sup> value for intravenous injection of 1  $\mu\text{Ci}$ . The 37-kg muscle pool receives 2.7 millirads, while it is estimated the bone hot spots receive 2.1 millirads.

5. Protection of the Patient in Radionuclide Investigations, ICRP Publication 17, Pergamon, Oxford, 1971.

Table 15.2. Absorbed fractions of photon and electron (plus beta) energies  $\phi_{T \leftarrow S}$  and specific absorbed energies for  $^{28}\text{Mg}$  and  $^{28}\text{Al}$

Radiation	Energy (MeV)	Specific absorbed fractions from target $\leftarrow$ source <sup>a</sup>				Effective energies, target $\leftarrow$ source <sup>b</sup> (MeV)			
		$\phi_{\text{SKSK}}$	$\phi_{\text{SKTB}}$	$\phi_{\text{TBTB}}$	$\phi_{\text{TB SK}}$	$\&_{\text{SKSK}}$	$\&_{\text{SKST}}$	$\&_{\text{STSK}}$	$\&_{\text{STST}}$
$\gamma_1$	0.031	0.7	0.19	0.78	0.85	0.021	0.00357	0.00014	0.0199
$\gamma_2$	0.400	0.12	0.05	0.34	0.33	0.0144	0.00456	0.0252	0.0364
$\gamma_3$	0.950	0.11	0.046	0.32	0.32	0.0314	0.00998	0.0599	0.0798
$\gamma_4$	1.350	0.105	0.042	0.31	0.30	0.0992	0.0293	0.190	0.267
$KA_1$ x ray	0.0015	1	0	1	1	0.000003	0	~0	0
Absorbed photon energy						0.166	0.0474	0.275	0.403

<sup>a</sup>These values were obtained from MIRD Suppl. No. 3, Pamphlet No. 5, 1969. The following identity is used to calculate the appropriate specific absorbed fractions  $\phi$ : TB stands for total body, SK for skeleton, and ST for soft tissues; SKTB means that the source is the total body and the target is the skeleton.

$$\phi_{\text{SKST}} = 70/60 \phi_{\text{SKTB}} - 10/60 \phi_{\text{SKSK}},$$

$$\phi_{\text{STSK}} = \phi_{\text{TB SK}} - \phi_{\text{SKSK}},$$

$$\phi_{\text{STST}} = 70/60 (\phi_{\text{TB TB}} - \phi_{\text{SKTB}}) - 10/60 (\phi_{\text{TB SK}} - \phi_{\text{SKSK}}).$$

In the above the masses of the skeleton (10 kg), the soft tissues (60 kg), and total body (70 kg) enter as weighting factors, for example, 70/60, etc.

This is obtained from the data in Table 15.1 on energy emitted times the appropriate specific absorbed fraction shown in the third column of the above table.

## 16. A Method of Interpreting Excretion Data Which Allows for Statistical Fluctuation of the Data

W. S. Snyder

Personnel monitoring for plutonium and certain other alpha emitters of similar characteristics poses one of the most difficult problems for the health physicist. While some methods have been developed for monitoring these radionuclides by in vivo counting of the chest, the activity present in the rest of the body – bone and liver, particularly – must be inferred largely on the basis of interpretation of data on excretion of the nuclide. A number of methods have been developed for interpreting excretion data to estimate what may be called the systemic body burden, that is, the activity which has entered the blood stream and thus been transferred to other organs.

There are some who have doubted whether it is important to estimate the systemic burden when the exposure is by inhalation. The animal experience has indicated that malignancies of the thoracic region far outweigh malignancies due to the systemic burden. However, there are reasons why one should not dismiss lightly the hazard of a systemic burden. From injection experiments, it is quite clear that a bone burden or a liver burden does pose a considerable hazard. Although such experiments have been designed at lower levels than those originally contemplated, no basis has yet been found for assuming a threshold. In fact, the results on rodents indicate the likelihood that quite low doses to bone may induce malignancies.

Moreover, the inhalation experiments have been at quite high levels. In Fig. 16.1 the accumulation of dose to lung and to bone following exposure of man to inhaled  $^{239}\text{PuO}_2$  is indicated. The lung model of ICRP for a Class Y aerosol (clearance half-time of 500 days) has been used to calculate dose to lung,<sup>1</sup> and dose to bone was calculated assuming equal deposition in liver and bone with only 10% elimination from bone. It is

clear that during the first five years postexposure, the lung has a far higher dose; but if the animal survives this period, the dose to bone will continue to accumulate while the lung receives little more dose, and eventually the skeleton accumulates the greater dose. It is not suggested that bone or liver replace lung as our only organ of concern but rather that we should be concerned for all three and not be swayed too much by results of animal experiments which are not representative of human exposure either in level or in the duration of the exposure. Thus it seems important to have some estimate of the systemic burden, and the principal means of estimating this is by interpreting excretion data. The dose to lung is delivered relatively soon following exposure, and thus at high levels of exposure the lung cancers tend to occur earlier and, if the incidence is severe enough, will preclude the occurrence of bone or liver cancers. At lower levels of exposure such that mortality from lung malignancies is not high,

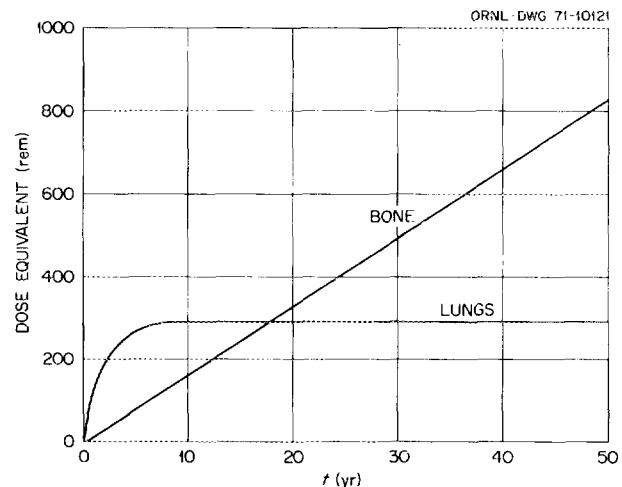


Fig. 16.1. Accumulated dose equivalent to lungs and bone following inhalation of  $1 \mu\text{Ci}$  of  $^{239}\text{Pu}$  (class Y material, AMAD =  $1 \mu\text{m}$ ).

1. ICRP Task Group on Lung Dynamics, "Deposition and Retention Models for Internal Dosimetry of the Human Respiratory Tract," *Health Phys.* 12(2), 173 (1966).

it is quite possible that bone and liver malignancies might appear. Man, with his much longer life span, has every likelihood of accumulating far more dose in bone and liver than in lungs. We should not assume lightly that extra dose will not be a hazard. Of course, there is another reason for being interested in the systemic burden, namely, a frequent route of exposure is by way of a contaminated wound, and in such a case, estimation of the systemic burden is a matter of the greatest importance.

The only plutonium excretion data we have on humans from carefully designed and controlled experiments are those obtained by Langham and Hamilton in 1945-1946. Urinary and fecal excretion data were obtained on 15 terminal patients who were given plutonium nitrate or dioxide complexed with citrate and followed until death. These data were analyzed by Langham et al.,<sup>2</sup> who expressed the general trend of the urinary and fecal excretion in terms of power functions. Later they studied the excretion of employees and found substantially the same trend in their excretion data for a period of about five years. These power functions obtained by Langham by fitting the curves to all the excretion data of the hospital patients have been the basis for most, if not all, of the methods described for interpretation of plutonium excretion data.

In most routine cases one has available only urinary excretion data for evaluating an internal exposure. Although Langham gave one power function ( $bt^{-\beta}$ ) fit to the urinary data of all the patients, there was considerable variation about this curve. In a previous study<sup>3,4</sup> the author has obtained a power function  $bt^{-\beta}$  fit to the data of each patient. This has been done by several techniques of curve fitting, and the designations "point fit," "area fit," "absolute deviations," and "percent deviations" on the figures identify the procedure used. However, these methods are not discussed here, but the interested reader may consult the references. Needless to say, there was a considerable range of

variation of the parameters  $b$  and  $\beta$  in the individual cases. The power functions so obtained are shown graphically in Fig. 16.2. When fitted to all the urinary data, a curve (called here the "typical curve") was obtained, and the parameters ranged by a factor of about 3 above and below these "typical" values. In the case of an employee, there is no way to determine a priori which of these power functions might best represent his excretion.

The existence of this variation and the occurrence of day-to-day fluctuations of the daily urinary excretion about the power function which defines the trend of the data are some of the complications which make estimation of the amount of plutonium reaching blood rather difficult. In principle, having chosen a power function as a model for excretion, one attempts to choose intakes to blood whose excretion by the model will reproduce, or essentially reproduce, the excretion data. Generally this is done sequentially. Having chosen a first intake, perhaps with reference to a known "incident," which provides for the first sample excretion, one then calculates by the model how well, or poorly, this reproduces the rest of the excretion record.

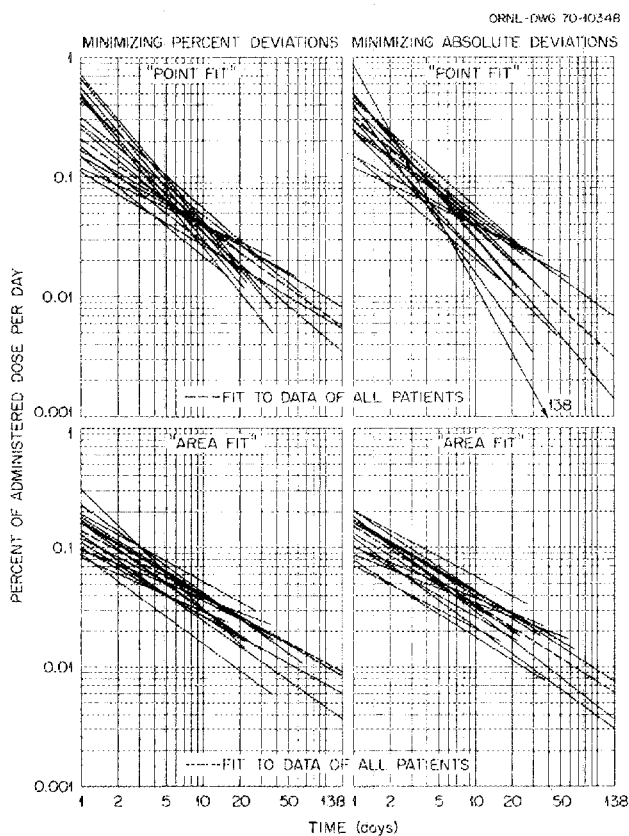


Fig. 16.2. Individual models for excretion of plutonium.

2. W. H. Langham et al., *Distribution and Excretion of Plutonium Administered Intravenously to Man*, LA-1151 (1950).

3. W. S. Snyder, M. R. Ford, and G. G. Warner, "The Use of Excretion Data to Predict the Systemic Body Burden of Plutonium," p. 279 in *Diagnosis and Treatment of Deposited Radionuclides*, ed. by H. A. Kornberg and W. D. Norwood, Reidel, Dordrecht, Holland, 1968.

4. W. S. Snyder, M. R. Ford, and G. G. Warner, "A Study of Individual Variation of Excretion of Plutonium by Man and of Its Significance in Estimating the Systemic Burden," *Proceedings 13th Annual Bioassay and Analytical Chemistry Meeting, October 12-13, 1967, Berkeley, California*, CONF-671048, p. 123 (1968).

If the excretion on certain days is significantly higher, one puts in additional intake just preceding that day to provide for the excess. If this procedure is followed, one will produce a pattern of intake which suffices to produce the excretion data, or rather to overestimate it, for clearly if one puts in intakes to reproduce all the high excretion values and ignores the lower values, one would expect to obtain an overestimate of intake. This is illustrated schematically in Fig. 16.3. The solid line suggests a power function trend of data which fluctuate about it. The dotted line represents the hypothetical excretion obtained by postulating an intake for the first daily sample, a second intake for the next daily sample which chances to lie above this line, a third intake for the next sample exceeding the new power function, and so on. Clearly, much of this intake is a result of statistical fluctuations and is not required by the data if one recognizes that the data may be expected to fluctuate about the trend curve. The effect of the above method can be demonstrated for the hospital patients whose intake to blood is known. In a previous study, the author produced estimates as described above for the hospital patients, and the results, expressed as a ratio to the activity of plutonium injected, are shown in Fig. 16.4. As will be noted, these estimates tend to be high.

The remedy is easy to find. If one examines the ratio of actual urinary excretion to that predicted by the model for the hospital patients, one has a measure of the extent to which the daily urinary excretion  $U(t)$

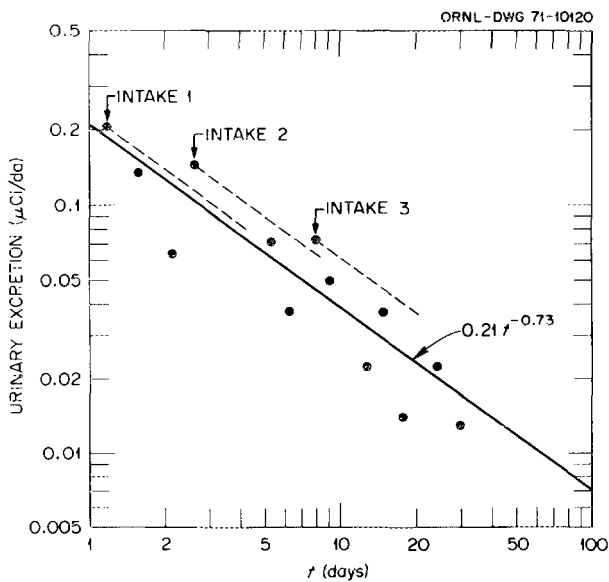


Fig. 16.3. Schematic illustration of result of introducing new intake for each high-excretion sample.

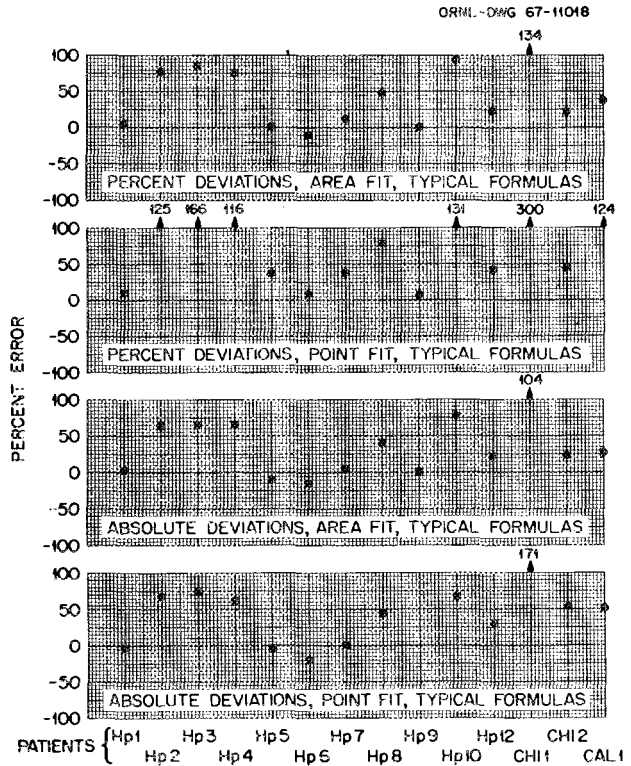


Fig. 16.4. Percent error of estimated intake.

exceeds the excretion predicted by the power function. The cumulative distribution of these ratios is shown in Fig. 16.5, where every line represents the cumulative distribution of the ratio for one of the patients. It can be noted that the ratio lies between  $1/2$  and 2 for all of the patients except for 40% of the days and between  $1/3$  and 3 except for 20% of the days. Thus, while fluctuations by a factor of 2 are not unusual, fluctuations by a factor of 3 or more are fairly rare. When one is not sure whether a high excretion level of an employee is due to a new intake or whether it represents a chance fluctuation, one may disregard any fluctuation which is by less than a factor of 3 and be rather confident that any new and significant intake to blood is not missed. Of course, there is a 10% chance that such a high value is due to a new and significant intake; if this is the case, the excretion should run high for later values as well, and thus one would expect to find the intake required for some of the later data. This game may be played at any level of significance one chooses. One can easily design a computer program which allows one to preassign a level of significance, and only when the ratio  $U(t)/bt^{-\beta}$  exceeds this level will one select an additional intake. When this program was used to estimate the intake to blood of the hospital

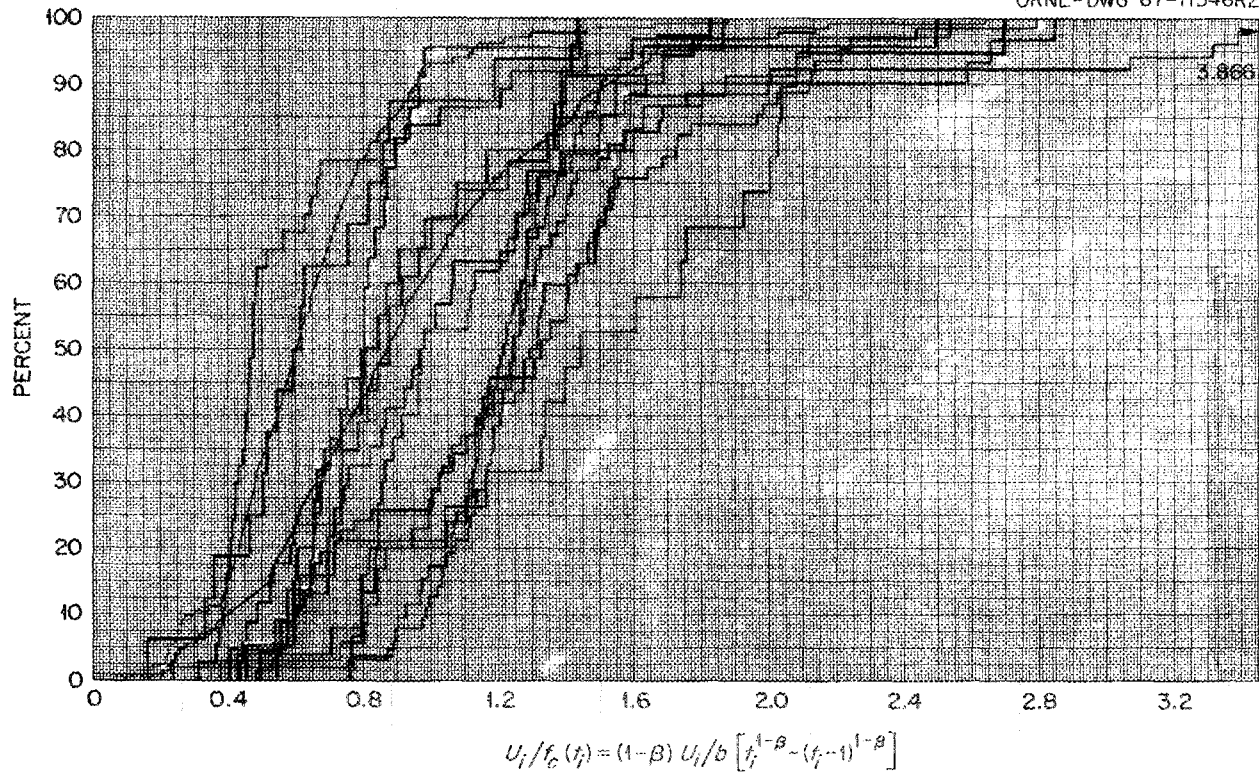


Fig. 16.5. Fluctuations of daily urinary excretion data of all patients (Langham-1950) about the typical formula of best fit—"area fit" formula obtained by minimizing the sum of absolute deviations.

patients, it produced the estimates shown in Fig. 16.6, where the ratio of the estimate to the injected amount is shown. Comparison with Fig. 16.4 reveals that the results do not run systematically high as formerly. Of course, one may make no allowance for fluctuations and obtain a conservative estimate as before. These cases were programmed for the computer using the "typical formula" fit to the data of all the patients and not using the patients' own formulas, since such information would not be available in the case of an employee.

If one has a considerable amount of excretion data, he may hope to approximate, roughly, to something like the particular excretion curve of the employee. The basis for this is the fact that if the trend of the curve is not steep enough, then there should be a preponderance of points below the curve. Now a new intake might make the excretion higher than the trend curve, but nothing can place them too low except (1) faulty collection or analysis of samples (and even a computer must have good data!) or (2) chance fluctuations. If the chance fluctuations are systematically too low, then it is likely that the curve should be steeper.

The computer program can be modified to include such a change in the slope of the excretion curve. In doing this, it seems best to start with a low value of the exponent  $\beta$  since, as mentioned above, new intakes might make excretion values be high; but it is difficult to imagine a reason, short of faulty data, which would cause them to be lower than the proper curve for an individual. This concept is illustrated in Fig. 16.7. Beginning with a power function with too low an exponent, the computer tests and finds that the data will largely fall below the line. It increases the exponent step by step until the fraction of points below does not exceed a preset level. The excretion data of the hospital patients have been analyzed from this point of view, using the starting slope of  $\alpha = 0.2$ , which is well below the exponent found for any of the patients. Whenever the proportion of excretion values below the curve exceeded the highs by more than a factor of  $1 + k$ , the exponent was increased,  $k$  being a preassigned value. The results are shown in Fig. 16.8, where the value of the exponent  $\beta$  obtained by the curve-fitting procedures mentioned earlier is shown together with the value produced by the computer in the course of its estimate

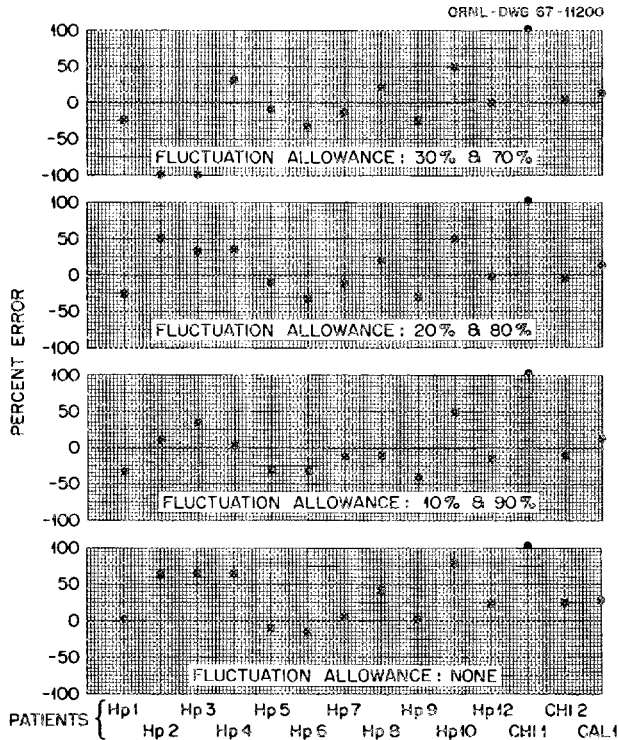


Fig. 16.6. Percent error of estimated intake.

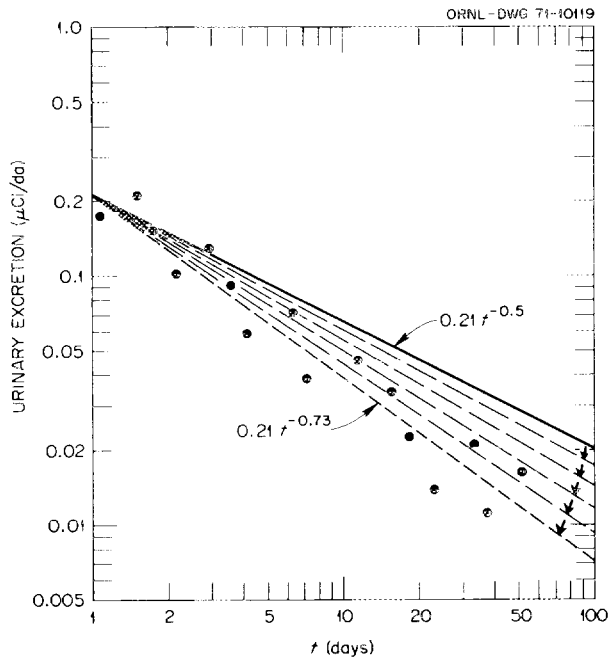


Fig. 16.7. Basis for adjustment of slope of the excretion model.

of the intake to blood. No doubt these cases, which correspond to a single intake to blood, are simpler than one will usually find in analyzing data on exposure of employees, but you will note that the computer did rather well in approximating to the correct slope for the individual. The results in Fig. 16.8 are the best of many cases tried for different choices of  $k$  and the other parameters used in the computer code. The method of adjustment seems to do best when there is little allowance for statistical fluctuations of the data and when the value of  $k$  is rather small. These results seem of interest because they demonstrate the possibility, at least in these cases of a single intake to blood, of letting the excretion data provide the information needed concerning the slope of the power function used in the model. How well the procedure will work for more complex patterns of exposure remains to be determined, and further exploration of cases is under way. Evidently, the present study is only a first attempt to develop computer techniques which take some account of individual differences, and it is realized that the present method is only a demonstration of a principle. It is clear that one must have a considerable amount of data before one can hope to apply the method and that cases of multiple exposure may pose more difficulties than are encountered here.

There seem to be only two cases of actual employee exposures where a reasonable amount of excretion data are available and where autopsy data on the systemic burden were obtained later. In neither case did the death of the subject result from his exposure to

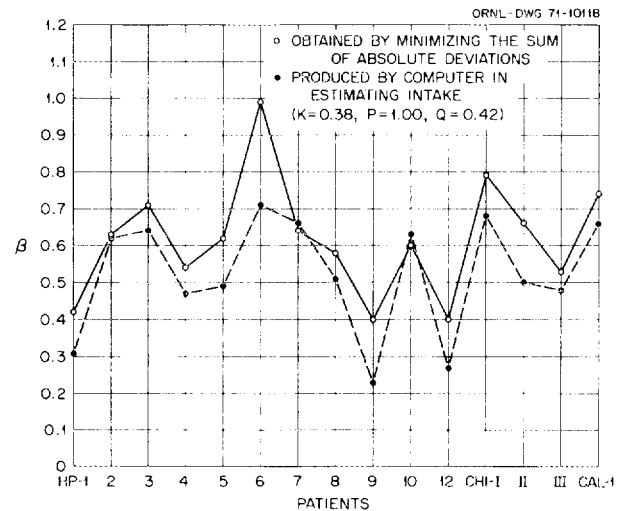


Fig. 16.8. Exponents of power function  $bt^{-B}$  for excretion of plutonium (Langham's patients).

plutonium. When the excretion data of these employees are analyzed by the methods outlined above, the predictions of the systemic body burden agree surprisingly well with the estimates based on autopsy specimens. The first case, reported by Foreman et al.,<sup>5</sup> has been analyzed by these methods and reported previously.<sup>6</sup> By all the methods tried, the estimate by the computer was higher than that based on autopsy specimens, but by a factor of less than 2. This employee's exposure to plutonium was sporadic but extended over about 11 years. The second case is reported by Lagerquist et al.,<sup>7</sup> and the urinary excretion data extend over about five years. The report indicated that the computer estimate was high by about a factor of 5. When the methods of analysis discussed

here are used, the computer estimates are well within a factor of 2, and, undoubtedly, this is largely due to the fact that allowance is made for fluctuations of the data.

---

5. H. Foreman, W. Moss, and W. H. Langham, "Plutonium Accumulation from Long-Term Occupational Exposure," *Health Phys.* 2(4), 326 (1960).

6. W. S. Snyder, "Major Sources of Error in Interpreting Urinalysis Data to Estimate the Body Burden of Pu<sup>239</sup>: A Preliminary Study," *Health Phys.* 11(11), 1177 (1965).

7. C. R. Lagerquist et al., "Plutonium Content of Several Internal Organs Following Occupational Exposure," *Proceedings 13th Annual Bioassay and Analytical Chemistry Meeting, October 12-13, 1967, Berkeley, California*, CONF-671048, p. 103 (1968).

## Part IV. Environmental Studies

E. G. Struxness<sup>1</sup>

---

### 17. Dose Estimation Studies Related to Peaceful Uses of Nuclear Explosives and Other Radionuclide Releases

C. J. Barton<sup>2</sup>    M. J. Kelly<sup>2</sup>  
R. S. Booth<sup>3</sup>    R. E. Moore<sup>2</sup>  
S. V. Kaye<sup>4</sup>    P. S. Rohwer<sup>4,5</sup>  
E. G. Struxness<sup>4,5</sup>

#### DEVELOPMENT OF RADIATION SAFETY GUIDES FOR ENVIRONMENTAL RELEASES OF RADIOACTIVITY

P. S. Rohwer    S. V. Kaye  
R. S. Booth    E. G. Struxness

The primary objective of this continuing research is to develop a methodology that is reasonable, practical, and accurate for assessing radiation exposures of human populations via all important exposure modes for environmental releases of radioactivity. The approach is to develop mathematical simulations of selected environmental systems which can be used as modules in construction of environmental models to predict the fraction of each released radionuclide exposing man as a function of time at any given location. One end point of the radiological assessment is an index identified by the acronym CUEx, which stands for CUmulative Exposure IndeX. The numerical value of CUEx for a specific radionuclide release reflects the magnitude of the estimated total dose to individuals or populations relative to a selected dose limit. In the most recent

previous annual progress report of the Health Physics Division,<sup>6</sup> the formulations for calculating CUEx values are detailed, and the generalized model used to quantitatively predict radionuclide movement through terrestrial food pathways is described. An aquatic food pathway model to complement the terrestrial model is in a preliminary stage of development.

Comprehensive demonstrations of the CUEx methodology are just as important as the modeling refinements within the methodology. A prime area for application of CUEx is the assessment of radionuclide releases from nuclear power stations. Such releases may range from the effluents of normal station operation to a massive radioactivity escape via containment breach experienced during a major reactor accident. To prepare for a demonstration of CUEx in this application, the potential source term (radioactivity to be released) must be characterized in detail. A portion of that work has been completed,<sup>7</sup> and it is summarized elsewhere in this section of this report.

Methods developed under this activity were used to complete radiological sections of all environmental

---

1. Liaison between Environmental Sciences and Health Physics Divisions.

2. Reactor Chemistry Division.

3. Instrumentation and Controls Division.

4. Environmental Sciences Division.

5. Formerly Health Physics Division.

---

6. *Health Phys. Div. Annu. Progr. Rep. July 31, 1971*, ORNL-4720, pp. 24-28.

7. R. S. Booth, S. V. Kaye, M. J. Kelly, and P. S. Rohwer, *A Compendium of Radionuclides Found in Liquid Effluents of Nuclear Power Stations*, ORNL-TM-3801 (1972).

impact statements (utility-owned nuclear power stations) prepared at ORNL, during the time period covered by this report, for the AEC to meet the requirements of the National Environmental Policy Act of 1969. The radiological assessments utilized site-specific population data, meteorological observations for each site, hydrologic dilution data, food-chain pathway models, etc., to predict doses to individuals (rems) and populations (man-rems) out to 50 miles from each power station. Participation in the in-depth technical analysis of radiological aspects of nuclear power stations and writing of environmental impact statements were valuable tests for the relevance of techniques and skills developed under this research activity.

### UTILIZATION OF NATURAL GAS FROM NUCLEARLY STIMULATED WELLS

C. J. Barton    M. J. Kelly    R. E. Moore

Work on the Gasbuggy project was confined to preparation of topical reports on Phase I<sup>8</sup> and Phase II studies<sup>9</sup> and completing the evaluation of the tritium tracer test described in the previous report.<sup>10</sup> Dose estimations related to Project Rulison are still in progress. Computer programs are being developed to aid dose calculations and plans to minimize doses due to exposure to combustion products of natural gas from a multiple-well field stimulated with nuclear explosives.

#### Rulison Dose Studies

Doses that people living in a number of small Colorado communities might receive from the hypothetical use of Rulison gas were calculated in the first phase of the Project Rulison dose estimations.<sup>11</sup> Two gas transmission systems are located close enough to the Rulison well to be potential recipients of its gas: the Rocky Mountain Natural Gas Company (RMNGC) and

the Western Slope Gas Company, Rifle Division (WSGC). We assumed that one million cubic feet per day of dry, CO<sub>2</sub>-free Rulison gas was introduced into either system operating under normal (1970 average) conditions. Rulison production testing removed all but a small fraction of the tritium originally present in the dry cavity gas, but we estimated whole-body doses that would have been received through inhalation and skin absorption if the Rulison gas had been used commercially instead of being flared (burned). Rulison gas was only about 10% of the gas used in communities served by the RMNGC system, and the maximum average dose was estimated to be 6 millirems per year from exposure to combustion products from an unvented kitchen range and refrigerator. In confirmation of results of the Gasbuggy studies, home exposure to combustion products from unvented devices was found to be the critical exposure pathway. In the two communities served by the WSGC system that could hypothetically receive Rulison gas, this source supplied either 36.8 or 68.6% of the gas used. Because of the low gas dilution factor, the maximum average dose in homes receiving the larger amount of Rulison gas and having both unvented appliances was 39 millirems per year. Inhalation and skin absorption of tritium dispersed in the atmosphere gave doses estimated to be less than 1 millirem per year.

If the gas present in the well in August 1971, following the well testing program and a period of pressure buildup in the well, had been used under the conditions described above, the tritium whole-body dose would have been 0.03 millirem per year. Whole-body doses from <sup>85</sup>Kr in Rulison gas were estimated to be about 1% of the tritium doses.

#### Computer Programs for Estimating and Controlling Doses from Nuclearly Stimulated Gas

The Rulison dose studies described above, as well as the earlier Gasbuggy studies, assumed that gas was drawn from a single nuclearly stimulated well. Larger-scale usage requires development of a number of wells, with the tritium concentration in the gas from each well declining as a function of the volume of gas removed. To deal with this situation, an equation was derived to express the tritium concentration in terms of gas produced from a single well. Computer programs based on this equation were developed to calculate the tritium concentration in the gas flowing from a multiple-well

8. D. G. Jacobs et al., *Theoretical Evaluation of Consumer Products from Project Gasbuggy - Final Report, Phase I: Impact of Hypothetical Releases of Contaminated Gas in the San Juan Basin*, ORNL-4646 (September 1971).

9. D. G. Jacobs et al., *Theoretical Evaluation of Consumer Products from Project Gasbuggy - Final Report, Phase II: Hypothetical Exposures Outside San Juan Basin*, ORNL-4748 (February 1972).

10. *Health Phys. Div. Annu. Progr. Rep. July 31, 1971*, ORNL-4720, p. 23.

11. C. J. Barton, R. E. Moore, and S. R. Hanna, *Quarterly Progress Report on Radiological Safety of Peaceful Uses of Nuclear Explosives: Hypothetical Exposures to Rulison Gas*, ORNL-TM-3601 (October 1971).

field.<sup>12</sup> These programs are designed to aid in scheduling the opening of wells so as to control the tritium concentration and the tritium doses received by persons exposed to gas combustion products.

One program permits the computation of the annual whole-body dose received through inhalation and skin absorption of combustion products of gas emitted from the stack of a gas-fired electric generating plant. A related program will compute the maximum tritium concentration in the gas, averaged over a one-year period, which could be burned in such a power plant without exceeding a predetermined annual dose that people living in the vicinity of the plant could receive. Efforts to extend the usefulness of these computer programs and to obtain better input data than are presently available are continuing.

#### Tritium Behavior in a Natural Gas Processing Plant

The sample analyses required to calculate potential doses to the operating personnel of a natural gas processing plant using nuclearly stimulated gas, as well as the distribution of tritium among the various plant products, were completed and evaluated, and a final report was issued.<sup>13</sup> The experiment that provided these samples, which involved the processing of 40,000 ft<sup>3</sup> of Gasbuggy gas mixed with 1.8 million ft<sup>3</sup> of field gas through a small plant during a 12-hr period, was described in the previous report.<sup>10</sup>

The data obtained indicate that processing of natural gas containing tritiated hydrocarbons at levels expected to prevail in large-scale exploitation of the nuclear-gas-stimulation technique will not present significant problems for plant operating personnel. No evidence of tritium exchange between tritiated hydrocarbons and the plant processing oil was found. Data on airborne tritium provided by atmospheric moisture samples taken during the experiment, extrapolated to large plant conditions with conservative assumptions, indicate that plant workers would receive tritium whole-body doses of less than 1% of natural background from breathing air containing combustion products resulting

from in-plant usage of gas as fuel for compressors, boilers, and generators.

The observed distribution of tritium among plant products (gas, butane, propane, and natural gasoline) confirmed theoretical calculations of the relative amounts of tritium in the various separated hydrocarbons, lending confidence in our ability to predict the quantities of radioactivity in gas and liquid products leaving a plant that processes gas from nuclearly stimulated wells.

#### CHARACTERIZATION OF THE RADIOACTIVITY IN LIQUID EFFLUENTS FROM LIGHT-WATER POWER REACTORS

R. S. Booth    M. J. Kelly  
S. V. Kaye    P. S. Rohwer

The radioactivity release experience of light-water power reactors has been analyzed in a number of ways to identify critical aquatic exposure pathways and critical radionuclides. The report describing this work<sup>14</sup> is, in effect, a collection in tabular form of various indexes of radiological impact which may be useful in assessing the environmental impact of radionuclides released from power reactors in their liquid effluents. Typical release rates under normal operation conditions (Ci/year) from both pressurized-water reactors and boiling-water reactors were tabulated. A concerted effort was made to derive numerical values from published measurements and experience, to ensure that these values were reasonably conservative, and to document these values with literature citations. Numerical values selected for environmental parameters are published values associated with operating power stations or power stations under construction. The radionuclides given consideration in this study are those which satisfied several criteria thought to be indicative of possible environmental impact.

The radionuclides were ranked according to their dose to man by the critical exposure pathway for several environmental half times considering typical release rates from the reactor, radioactive half-lives, concentration factors from water to aquatic biota and to sediments, typical dietary and recreational habits for man, and dose rate factors for ingestion and external exposure. Tabulations are included listing typical releases, concentration factors, dose rate factors, concen-

12. R. E. Moore and C. J. Barton, *Progress Report on Radiological Safety of Peaceful Uses of Nuclear Explosions: Preliminary Equations and Computer Techniques for Estimating and Controlling Tritium Doses from Nuclearly Stimulated Natural Gas*, ORNL-TM-3755 (June 1972).

13. M. J. Kelly, C. J. Barton, A. S. Meyer, E. W. Chew, and C. R. Bowman, *Theoretical Evaluation of Consumer Products from Project Gasbuggy - Final Report: Tritium Behavior in a Natural Gas Processing Plant*, ORNL-4775 (July 1972).

14. R. S. Booth, S. V. Kaye, M. J. Kelly, and P. S. Rohwer, *A Compendium of Radionuclides Found in Liquid Effluents of Nuclear Power Stations*, ORNL-TM-3801 (1972).

tration in water which could result in a certain dose to man through selected exposure pathways, and concentrations in water which could result in a certain dose to the aquatic biota. Another index provided in the report,<sup>14</sup> the concentration factor from water to various aquatic biota, indicates the importance of bioaccumulation for each radionuclide on the list in the assessment of its radiological impact. A tabulation of dose rate factors for man shows the dose commitment to man per microcurie ingested or per unit concentration in the environment. A listing of the concentrations in water that deliver 500 millirems per year to standard man for each radionuclide and several exposure pathways may serve as a source of radiological significance indices and dose conversion factors. Maximum permissible concentrations (MPC)<sub>w</sub> of radionuclides listed in Table 2 of 10 CFR 20 (ref. 15) are inadequate indices of radiological significance of liquid effluents, because they do not include considerations for all of the applicable exposure pathways. The final index, the ranking of the radionuclides for a typical environmental situation, is the most comprehensive, since it is a calculated dose to man from a typical release rate from the power station. The specific considerations included in this index are:

1. the pathways for ingestion (drinking water; eating fish, waterfowl, invertebrates); being exposed to contaminated sediment, or swimming in contaminated water;
2. the radioactive half-life;
3. the environmental half time (for example, some elements have different residence times in freshwater systems than in estuaries);
4. the concentration factors for the various pathways mentioned above;
5. the dose rate factor for man (millirems per microcurie ingested or millirems per unit concentration in the environment for external exposures);
6. the expected release rate of the radionuclide from the reactor;
7. the dietary and recreational habits of the population under study.

The work provides a standard list of radionuclides (see Table 17.1) which should be considered in estimating the environmental impact of radioactivity released in the liquid effluent of current light-water

Table 17.1. List of radionuclides and decay chains which should be assessed in the liquid effluent of current light-water power reactors

<sup>3</sup> H	<sup>90</sup> Y	<sup>130</sup> I
<sup>14</sup> C	<sup>91</sup> Sr- <sup>91m</sup> Y- <sup>91</sup> Y	<sup>131m</sup> Te- <sup>131</sup> Te- <sup>131</sup> I
<sup>22</sup> Na	<sup>91</sup> Y	<sup>131</sup> I
<sup>24</sup> Na	<sup>93</sup> Y	<sup>132</sup> Te- <sup>132</sup> I
<sup>32</sup> P	<sup>95</sup> Zr- <sup>95</sup> Nb	<sup>133</sup> I
<sup>35</sup> S	<sup>95</sup> Nb	<sup>134</sup> Cs
<sup>46</sup> Sc	<sup>97</sup> Zr- <sup>97m</sup> Nb- <sup>97</sup> Nb	<sup>135</sup> I
<sup>51</sup> Cr	<sup>99</sup> Mo- <sup>99m</sup> Tc	<sup>136</sup> Cs
<sup>54</sup> Mn	<sup>103</sup> Ru- <sup>103m</sup> Rh	<sup>137</sup> Cs- <sup>137m</sup> Ba
<sup>55</sup> Fe	<sup>105</sup> Rh	<sup>140</sup> Ba- <sup>140</sup> La
<sup>59</sup> Fe	<sup>106</sup> Ru- <sup>106</sup> Rh	<sup>140</sup> La
<sup>57</sup> Co	<sup>110m</sup> Ag- <sup>110</sup> Ag	<sup>141</sup> Ce
<sup>58</sup> Co	<sup>122</sup> Sb	<sup>143</sup> Ce- <sup>143</sup> Pr
<sup>60</sup> Co	<sup>124</sup> Sb	<sup>143</sup> Pr
<sup>63</sup> Ni	<sup>125</sup> Sn- <sup>125</sup> Sb- <sup>125m</sup> Te	<sup>144</sup> Ce- <sup>144</sup> Pr
<sup>64</sup> Cu	<sup>125</sup> Sb- <sup>125m</sup> Te	<sup>147</sup> Nd- <sup>147</sup> Pm
<sup>65</sup> Zn	<sup>125m</sup> Te	<sup>147</sup> Pm
<sup>69m</sup> Zn- <sup>69</sup> Zn	<sup>127</sup> Sb- <sup>127m</sup> Te- <sup>127</sup> Te	<sup>182</sup> Ta
<sup>86</sup> Rb	<sup>127m</sup> Te- <sup>127</sup> Te	<sup>185</sup> W
<sup>89</sup> Sr	<sup>127</sup> Te	<sup>187</sup> W
<sup>90</sup> Sr- <sup>90</sup> Y	<sup>129m</sup> Te- <sup>129</sup> Te	<sup>239</sup> Np

power reactors, be the assessment one for a single nuclear power station or one for all such stations contributing to the environmental radioactivity in a given region.

## ENVIRONMENTAL IMPACT STATEMENTS

D. R. Nelson

H. H. Abee      M. F. Fair  
 R. S. Booth    S. V. Kaye  
 T. J. Burnett   M. J. Kelly  
 T. G. Clark    G. D. Kerr  
 P. S. Rohwer

### Radiological Impact to Man

The rising concern and quest for quality in man's environment reached national status when the United States Congress passed the National Environmental Policy Act of 1969 (NEPA). The NEPA imposed a broad scope of environmental responsibility upon federal agencies. Although the acceptance of the concept of the NEPA was easy, few foresaw the great difficulties that lay ahead for federal agencies in implementing it. Not until the federal Appeals Court ruled on July 23, 1971, involving the Calvert Cliffs nuclear plant on the Maryland shore of Chesapeake Bay, was there any substantial beginning to understand the intent of Congress in its formulation of the NEPA or to fully appreciate the impact of judicial enforcement.

15. Title 10, "Atomic Energy," Part 20, "Standards for Protection against Radiation," *Code of Federal Regulations*.

Basically, the NEPA requires federal agencies to thoroughly review the impact of all projects, to weigh the costs and benefits of the projects, and to examine alternatives to projects. In response to the Calvert Cliffs decision, the Atomic Energy Commission revised its rules for assessing the effects of nuclear power plants on the environment with Appendix D of Title 10, Code of Federal Regulations, Part 50 (10 CFR 50) on September 9, 1971 [Appendix D -- Interim Statement of General Policy and Procedure: Implementation of the NEPA of 1969 (Public Law 91-190)].<sup>16</sup> The new rules required both the utilities and Commission staff to make a thorough assessment of all effects, not just radiological. The primary result of these rules was that the AEC would be responsible for evaluating the entire environmental impact of nuclear plants, including thermal, chemical, biological, etc.

In general, the comprehensive preparation of detailed environmental statements by ORNL was well received by the AEC. The assessment of radiological impact to man at ORNL, in particular, set the mark after which AEC's detailed environmental statements are now patterned. It was early and generally conceded that radiological effects produced by the operation of nuclear power plants would be small compared with other effects such as thermal impacts. This is especially true since both utility applicants and the Commission have sought to reduce radioactive effluent emissions to "as low as practicable." The currently used basis for what is "as low as practicable" is the proposed rule making of Appendix I, 10 CFR 50 [Appendix I -- Numerical Guides for Design Objectives and Limiting Conditions for Operation to Meet the Criterion "As Low as Practicable" for Radioactive Material in Light-Water-Cooled Nuclear Power Reactor Effluents, June 9, 1971].<sup>17</sup> Even though this proposed Appendix I is not yet law, there have not been any final environmental statements for which the assessment did not indicate that there was reasonable assurance that the proposed numerical guides would be met. Though the estimated radiological impacts have been small, the ORNL assessments have maintained a thorough, comprehensive, and credible approach which is intelligible to both the layman and expert. Each nuclear power station was

regarded as unique and different from any other station.

One excellent example of how both the layman and the expert might be expected to easily understand the radiological assessment is given in Fig. 17.1. Here the pathways for external (radiation source outside the body) and internal (radiation source inside the body) exposures are schematically illustrated. Immersion in the gaseous effluent as it is diluted and dispersed could lead to external exposure, while the deposition of radioactive particulates on the land surface could lead to direct external exposure and to internal exposure by the ingestion of food products through various food chains. Similarly, swimming in waters in which radionuclides have been discharged could lead to external exposure, while the harvest of fish from or the utilization of these waters for drinking, irrigation, or food preparation could lead to internal exposures.

The general development of the radiological impact to man assessment will be briefly given below.

After a careful study of the nuclear power station and its environment, dose estimates are made for all significant exposure pathways. Radiation doses, both to individuals (in millirems) and the population (in man-rems) within 50 miles, are estimated. The man-rem or population dose is the sum of the total body doses to all individuals in the population considered. Estimates of dose to the individual are made for total body, liver, lungs, kidneys, bone, thyroid, and gastrointestinal tract. Where significant, the estimates of dose to organs other than total body are discussed.

Factors for converting internal radiation exposures to dose were obtained with models and data published by the International Commission on Radiation Protection<sup>18</sup> and other recognized authorities.<sup>19</sup> These models and data have been incorporated in computer programs<sup>20,21</sup> to facilitate estimation of dose. Factors for converting external radiation exposures to dose

16. Title 10, "Atomic Energy," Part 50, "Licensing of Production and Utilization Facilities, *Code of Federal Regulations*.

17. Title 10, "Atomic Energy," Part 50, "Licensing of Production and Utilization Facilities," Appendix I, "Numerical Guides for Design Objectives and Limiting Conditions for Operation," *Code of Federal Regulations*.

18. International Commission on Radiological Protection, *Recommendations of the International Commission on Radiological Protection*, ICRP Publication 2, Pergamon, London, 1959.

19. G. J. Hine and G. L. Brownell, eds., *Radiation Dosimetry*, Academic, 1956.

20. W. Doyle Turner, S. V. Kaye, and P. S. Rohwer, *EXREM and INREM Computer Codes for Estimating Radiation Doses to Populations from Construction of a Sea-Level Canal with Nuclear Explosives*, K-1759 (Sept. 16, 1968).

21. W. Doyle Turner, *The EXREM II Computer Code for Estimating External Doses to Populations from Construction of a Sea-Level Canal with Nuclear Explosives*, CTC-8 (July 21, 1969).

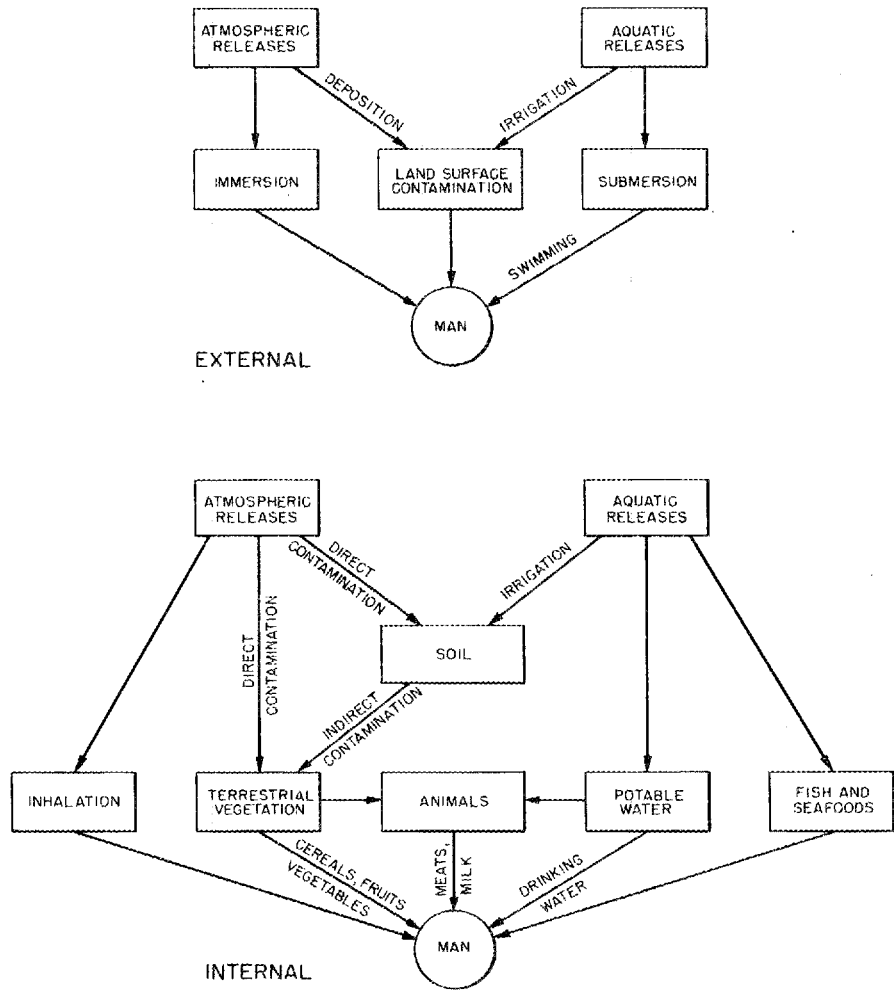


Fig. 17.1. Pathways for radiation exposure of man.

were obtained with a computer code containing models adapted from standard texts.<sup>19,22</sup>

Average annual concentrations of radionuclides contained in the air and deposited on the ground at distances up to 50 miles from the plant site were obtained from an atmospheric transport model<sup>23,24</sup> for which a computer program was developed.<sup>25</sup> The deposition velocities used in the calculations for the noble gases (krypton and xenon), methyl iodide (CH<sub>3</sub>I), elemental iodine (I<sub>2</sub>), and particulates were

10<sup>-6</sup>, 10<sup>-3</sup>, 1, and 1 cm/sec, respectively. In this model, the reduction of radionuclide concentrations in the air at ground level by radioactive decay and deposition on the ground is taken into account.

The concentration of radionuclides in a body of water receiving liquid effluents depends primarily on the half-lives of the radionuclides and the effective volume of water. The complex nature of most rivers, estuaries, and some lakes may lead to large variations in the estimates of radionuclide concentrations in the water, on the bottom sediment, and in the biota. Careful consideration was given to all the variables so that realistic instead of grossly conservative estimates of dose were obtained.

Finally, a summary of individual and population doses is given in a dose assessment section. Comparisons are made of the estimated doses with the numerical guides of proposed Appendix I (10 CFR 50) and natural background.

---

22. K. Z. Morgan and J. E. Turner, eds., *Principles of Radiation Protection*, Wiley, 1967.

23. D. H. Slade, ed., *Meteorology and Atomic Energy 1968*, TID-24190 (July 1968).

24. W. M. Culkowski, *Sixth Air Cleaning Conference, July 7-9, 1959*, TID-7593.

25. M. Reeves III, P. G. Fowler, and K. E. Cowser, *A Computer Code for Routine Atmospheric Release of Short-Lived Radioactive Nuclides*, ORNL-TM-3613 (in preparation).

# Theses, Papers, Publications, and Lectures

## Theses

Gerald Alton

*Study of Low-Energy Electron Molecule Interactions* (in preparation).

J. A. Auxier

*Contribution of Natural Terrestrial Sources to the Total Radiation Dose to Man* (in preparation).

D. M. Bartell

*Time-Dependent VUV Emission of Helium* (in preparation).

K. W. Crase

*Parameters Affecting the Radiation Induced Thermally Stimulated Exoelectron Emission from Ceramic Beryllium Oxide* (August 1971).

C. E. Easterly

*Study of Aromatic Hydrocarbons in Relation to Carcinogenesis*, ORNL-TM-2616 (in preparation).

J. M. Elson

*The Interaction of Photons at Rough Dielectric Surfaces*, ORNL-TM-3752 (May 1972).

R. E. Goans

*Dissociative Electron Attachment to Polyatomic Molecules* (in preparation).

A. Hadjiantoniou

*Electron Attachment to and Autoionization of Long-Lived Negative Ions of Polyatomic Molecules* (in preparation).

W. F. Hanson

*Soft X-Ray Studies of the Satellites of Na, Mg, Al, and Si and the Optical Properties of MgO and MgF<sub>2</sub>*, ORNL-TM-3564 (in preparation).

G. D. Kerr

*An Experimental Study of the Optical and Dielectric Properties of Liquids in the Vacuum* (August 1971).

Paul D. Kidd

*Electron Capture and Drift in Organic Liquids* (in preparation).

D. L. McCorkle

*Low-Energy Electron Attachment to Molecules at High Densities* (in preparation).

M. N. Pisanias

*Threshold-Electron Excitation and Compound Negative Ion Formation in Polyatomic Molecules* (in preparation).

M. Sohrabi

*Some Studies on the Application of Track Etching in Personnel Fast Neutron Dosimetry* (August 1971).

B. L. Sowers

*Optical Properties of Liquid CCl<sub>4</sub>, C<sub>6</sub>H<sub>14</sub>, C<sub>6</sub>H<sub>12</sub>, C<sub>6</sub>H<sub>10</sub>, C<sub>6</sub>H<sub>8</sub>, and C<sub>6</sub>H<sub>6</sub> in the Vacuum Ultraviolet*, ORNL-TM-3665 (March 1972).

- R. B. Vora  
*Optical Model Studies of Ion Molecule Interactions* (in preparation).
- J. F. Wilson  
*Mass Analysis of Ions Formed in Electron Swarm Experiments* (in preparation).
- U. S. Whang  
*Optical Properties of Potassium, Rubidium, and Cesium in the Vacuum Ultraviolet*, ORNL-TM-3649 (March 1972).

## Papers

- E. T. Arakawa  
*Experimental Studies of Surface Plasmons*, Third International Conference on Vacuum UV Radiation Physics, August 30–September 2, 1971, Tokyo, Japan.
- J. A. Auxier, T. D. Jones, W. S. Snyder, and G. G. Warner  
*Dose from Monoenergetic Photons Unilaterally Incident on the Torso of Standard Reference Man*, Health Physics Society Annual Meeting, June 12–16, 1972, Las Vegas, Nevada (presented by J. A. Auxier).
- C. J. Barton, R. E. Moore, and S. R. Hanna  
*Dose Estimates for Hypothetical Uses of Rulison Gas*, Health Physics Society Meeting, June 1972, Las Vegas, Nevada.
- K. Becker  
*New Developments in Solid-State Radiation Dosimetry*, First Latin American Conference on Physics in Medicine and Radiation Protection, February 28–March 3, 1972, Sao Paulo, Brazil.  
*Principles of Personnel Radiation Monitoring*, First Latin American Conference on Physics in Medicine and Radiation Protection, February 28–March 3, 1972, Sao Paulo, Brazil.  
*Applications of Track Etching in Neutron Dosimetry*, American Nuclear Society Annual Meeting, June 18–22, 1972, Las Vegas, Nevada.  
*Recent Developments in Solid-State Dosimetry*, Seminar, Laboratory for Environmental Studies, New York University Medical Center, July 13, 1972, New York.
- K. Becker, J. S. Nagpal, J. S. Cheka, and M. Sohrabi  
*Fading Characteristics of Various Film and Solid-State Dosimeters in a Warm and Humid Climate*, Health Physics Society Annual Meeting, June 12–16, 1972, Las Vegas, Nevada (presented by K. Becker).  
*Fading of Solid-State Dosimeters and Film at Increased Temperatures and Humidities*, Third International Conference on Medical Physics, July 30–August 4, 1972, Göteborg, Sweden.
- G. M. Begun and R. N. Compton  
*Electron Impact Ionization Studies of Several Metallocenes*, Symposium on Molecular Structure and Spectroscopy, June 12–16, 1972, Columbus, Ohio.
- S. R. Bernard  
*A Metabolic Model for Magnesium in Man and Dose Estimates for  $^{28}\text{Mg}$* , Health Physics Society, June 12–16, 1972, Las Vegas, Nevada.
- R. D. Birkoff, J. T. Cox, L. R. Painter, and G. D. Kerr  
*A Reflectometer for Studying Liquids in the Vacuum Ultraviolet*, American Physical Society, Southeastern Section, November 4–6, 1971, Columbia, South Carolina.
- A. J. Braundmeier, Jr. and E. T. Arakawa  
*Radiative Decay of Nonradiative Surface Plasmons in Aluminum*, American Physical Society, Southeastern Section, November 4–6, 1971, Columbia, South Carolina.

- L. G. Christophorou  
*Intermediate Phase Studies for Understanding Radiation Interaction with Condensed Media: The Electron Attachment Process*, Conference on Elementary Processes in Radiation Chemistry, April 4–7, 1972, Notre Dame, Indiana.
- L. G. Christophorou, R. P. Blaunstein, and D. Pittman  
*Scattering of Slow Electrons by  $\pi$ -Electron Containing Organic Molecules*, American Physical Society, March 27–30, 1972, Atlantic City, New Jersey.
- R. N. Compton  
*Negative Ion Processes*, Conference on Elementary Processes in Radiation Chemistry, April 4–7, 1972, Notre Dame, Indiana.  
*Chemi-Ionizing Collisions*, Gordon Research Conference on Dynamics of Molecular Collisions, July 24–28, 1972, Plymouth, New Hampshire.
- R. N. Compton, P. W. Reinhardt, and C. D. Cooper  
*Anions Produced by Cesium Collisions with Succinic and Maleic Anhydride*, 20th Annual Conference on Mass Spectrometry and Allied Topics, June 4–9, 1972, Dallas, Texas.
- C. D. Cooper and R. N. Compton  
*Metastable Negative Ions of  $CO_2$* , American Physical Society, January 31–February 3, 1972, San Francisco, California.
- C. D. Cooper, R. N. Compton, and H. C. Schweinler  
*Dissociative Electron Attachment to Maleic and Succinic Anhydride*, 20th Annual Conference on Mass Spectrometry and Allied Topics, June 4–9, 1972, Dallas, Texas.
- K. E. Cowser  
*Evaluation of the Potential Radiological Impact of Gaseous Effluents on Local Environments*, International Symposium on Radioecology Applied to the Protection of Man and His Environment, September 7–10, 1971, Rome, Italy.
- J. Dutrannois, H. A. Wright, J. Baarli, R. N. Hamm, A. H. Sullivan, and J. E. Turner  
*Computed RBE for Positive and Negative Pions Based on Radiobiological Data for Individual Reaction Products*, Health Physics Society, June 12–17, 1972, Las Vegas, Nevada.
- C. E. Easterly, L. G. Christophorou, and J. G. Carter  
*Fluorescence Emission from the Second Excited  $\pi$ -Singlet State of Aromatic Molecules in Solution*, Radiation Research Society, May 14–18, 1972, Portland, Oregon.
- B. R. Fish  
*Models of Soluble Gas Retention in the Nasal-Pharyngeal Airways*, Health Physics Society, June 12–16, 1972, Las Vegas, Nevada.
- B. R. Fish and J. R. Duncan  
*Measurement of Liquid Droplet Emissions from Cooling Towers and Process Stacks*, Air Pollution Control Association, June 18–22, 1972, Miami Beach, Florida.
- M. R. Ford, W. S. Snyder, and G. G. Warner  
*Dose to the GI Tract from a Gamma Emitter Present in the Contents – A Comparison of Three Models*, Health Physics Society, June 12–16, 1972, Las Vegas, Nevada.
- R. B. Gammage and J. S. Cheka  
*Recent TSEE Dosimetry with BeO Ceramic Disks*, Health Physics Society Annual Meeting, June 12–16, 1972, Las Vegas, Nevada (presented by R. B. Gammage).
- W. R. Garrett  
*Low-Energy Electron Scattering by Polar Molecules*, 24th Annual Gaseous Electronics Conference, October 5–8, 1971, Gainesville, Florida.

- F. F. Haywood  
*Intercomparison Studies in Accident Dosimetry; Recent Progress and Anticipated Progress*, Health Physics Society Annual Meeting, June 12–16, 1972, Las Vegas, Nevada.
- J. M. Heller, R. D. Birkoff, M. W. Williams, and L. R. Painter  
*The Optical and Dielectric Properties of Glycerin in the Vacuum Ultraviolet*, American Physical Society, Southeastern Section, November 4–6, 1971, Columbia, South Carolina.
- M. J. C. Hilyer, W. S. Snyder, and G. G. Warner  
*Estimates of Dose for Infants and Children for a Photon Emitter in the Lungs*, Health Physics Society, June 12–16, 1972, Las Vegas, Nevada.
- H. H. Hubbell, Jr., W. L. Chen, and W. H. Shinpaugh, Jr.  
*Dose Distributions from Neutrons Incident on a Tissue-Equivalent Phantom*, Health Physics Society Annual Meeting, June 12–16, 1972, Las Vegas, Nevada (presented by H. H. Hubbell, Jr.).
- G. S. Hurst  
*An Idealized Approach to Radiation Protection*, Health Physics Society Annual Meeting, June 12–16, 1972, Las Vegas, Nevada (presented by W. R. Garrett).
- J. E. Jobst, Z. G. Burson, and F. F. Haywood  
*A Self-Replenishing Tritium Target*, American Nuclear Society Annual Meeting, June 18–22, 1972, Las Vegas, Nevada (presented by J. E. Jobst).
- T. D. Jones  
*The Relationship of Some Work of ORNL to the Studies of ABCC*, Atomic Bomb Casualty Commission, September 3, 1971, Hiroshima, Japan.  
*Dose, LET, and Thermal Neutron Distributions for the Design of Dosimeters and Dosimetric Experiments in a Tissue-Equivalent Medium*, Health Physics Society Annual Meeting, June 12–16, 1972, Las Vegas, Nevada.
- M. J. Kelly, C. J. Barton, A. S. Meyer, E. W. Chew, and C. R. Bowman  
*Experimental Results from Processing Gasbuggy Gas in a Natural Gas Processing Plant*, Tritium Symposium, August 30–September 2, 1971, Las Vegas, Nevada.
- G. D. Kerr  
*Estimating Regional Radiological Impacts from the Nuclear Power Industry*, Georgia Institute of Technology, April 27, 1972, Atlanta, Georgia.
- G. D. Kerr, R. D. Birkoff, M. W. Williams, R. N. Hamm, and L. R. Painter  
*The Optical and Dielectric Properties of Water in the Vacuum Ultraviolet*, American Physical Society, November 4–6, 1971, Columbia, South Carolina.
- C. E. Klots  
*Quasi-Equilibrium Theory of Ionic Fragmentation: Further Considerations*, 20th Annual Conference on Mass Spectrometry and Allied Topics, June 4–9, 1972, Dallas, Texas.
- W. C. McClain  
*Demonstration Repository for Solidified Radioactive Wastes*, 16th Annual Meeting of Health Physics Society, July 13–14, 1971, New York.  
*Salt Mine Waste Repository*, Tenth Annual Region IV Radiological Health Symposium, October 8, 1971, Louisville, Kentucky.
- D. L. McCorkle and L. G. Christophorou  
*Electron Attachment to Polyatomic Molecules Below 1 eV; Determination of Absolute Cross Section Functions at Very High Gas Densities*, Radiation Research Society, May 14–18, 1972, Portland, Oregon.
- J. S. Nagpal, J. S. Cheka, R. B. Gammage, and K. Becker  
*Some Further Studies on the Effect of Activators on TSEE from Ceramic BeO*, Health Physics Society Annual Meeting, June 12–16, 1972, Las Vegas, Nevada (presented by J. S. Nagpal).

- D. R. Nelson and F. J. Davis  
*Determination of Electron Transport Coefficients near Thermal Energies in Oxygen*, 24 Annual Gaseous Electronics Conference, October 5--8, 1971, Gainesville, Florida.
- M. N. Pisanias, L. G. Christophorou, and J. G. Carter  
*Threshold-Electron Excitation and Compound Negative Ion Formation in Methane, Ethane, and Propane*, American Physical Society, December 1--3, 1971, Atlanta, Georgia.
- J. W. Poston  
*Calculation of the HPRR Neutron Spectrum for Simulated Nuclear Accident Conditions*, Health Physics Society Annual Meeting, June 12--16, 1972, Las Vegas, Nevada.
- R. H. Ritchie  
*Collective Electron Resonances in Solids*, U.S.--Japan Seminar on Wave and Plasma Effects in Solids, September 8--10, 1971, Philadelphia, Pennsylvania.  
*Low-Energy Electron Penetration in Condensed Matter*, Health Physics Society, June 12--16, 1972, Las Vegas, Nevada.  
*Surface Plasmons in Solids*, Surface State Conference, June 19--21, 1972, Rolla, Missouri.
- P. S. Rohwer, M. J. Kelly, and R. S. Booth  
*Guidance for Limiting Environmental Releases of Tritium*, Tritium Symposium, August 30--September 2, 1971, Las Vegas, Nevada.
- J. G. Skofronick, J. P. Aldridge, D. B. Greene, and R. N. Compton  
*Chemical Accelerator for Producing a Neutral Heavy Particle Molecular Beam*, American Physical Society, Southeastern Section, November 4--6, 1971, Columbia, South Carolina.
- W. S. Snyder  
*Mathematical Procedures for Estimating Dose from an Internally Deposited Emitter*, Second European Congress on Radiation Protection, May 3--5, 1972, Budapest, Hungary.  
*A Method of Interpreting Excretion Data which Allows for Statistical Fluctuations of the Data*, Symposium on the Assessment of Radioactive Organ and Body Burdens, November 22--26, 1971, Stockholm, Sweden.
- W. S. Snyder and L. T. Dillman  
*Dose to Individuals of Different Ages from a Semi-Infinite Cloud of Gamma Emitter*, Health Physics Society, June 12--16, 1972, Las Vegas, Nevada.
- W. S. Snyder and T. D. Jones  
*Depth Dose Due to Neutrons as Calculated for a Tissue Phantom and Man*, Symposium on Neutron Dosimetry in Biology and Medicine, May 15--19, 1972, Munich, Germany.
- B. L. Sowers, R. D. Birkoff, and E. T. Arakawa  
*Transmission Measurements on Thin Organic Liquid Samples in the Vacuum Ultraviolet*, Southeastern Section, American Physical Society, November 4--6, 1971, Columbia, South Carolina.
- J. A. D. Stockdale  
*Condensation Reactions in Benzene Vapor*, 20th Annual Conference on Mass Spectrometry and Allied Topics, June 4--9, 1972, Dallas, Texas.
- Tsuneo Tamura  
*Sorption Phenomena Significant in Radioactive Waste Disposal*, Symposium on Underground Waste Management and Environmental Implications Sponsored by American Association of Petroleum Geologists and United States Geological Survey, December 6--9, 1971, Houston, Texas.
- J. E. Turner, R. N. Hamm, J. Dutrannois, H. A. Wright, A. H. Sullivan, and J. Baarli  
*Nuclear Reaction Data for Assessing Biological Effectiveness of Negative and Positive Ions*, Health Physics Society, June 12--17, 1972, Las Vegas, Nevada.
- J. E. Turner and C. E. Klots  
*State of the Theory of Delta-Ray Production*, Conference on Microdosimetry, October 18--22, 1971, Stresa, Italy.

## Publications

- G. A. Andrews and F. F. Haywood  
 "Clinical and Biological Consequences of Nuclear Explosions," *Practitioner* **207** (1239), 331–42 (1971).
- E. T. Arakawa and M. W. Williams  
 "Optical Properties of Uranium Mononitride from 0 to 74 eV," *J. Nucl. Mater.* **41**, 91–95 (1971).
- J. C. Ashley, V. E. Anderson, R. H. Ritchie, and Werner Brandt  
 " $Z_1^3$ -Effect in the Stopping Power of Matter for Charged Particles: Tabular Presentation of the Functions  $I(\xi)$ ,  $L(x)$ , and  $F(w)/\chi$ ," submitted for publication in *Atomic Data*.
- J. C. Ashley and R. H. Ritchie  
 "Contribution of Surface Losses to the Stopping Power of Matter for Charged Particles," *Phys. Rev.* (in press).
- J. C. Ashley, R. H. Ritchie, and Werner Brandt  
 " $Z_1^3$  Effect in the Stopping Power of Charged Particles in Matter," *Phys. Rev. B* **5**, 2393–97 (1972).
- J. A. Auxier  
 "The Outcry Over Exposure Guidelines," *Nucl. Safety* **12**, 456–60 (1971).  
 Book Review: "Personnel Dosimetry Systems for External Radiation Exposures," IAEA Technical Reports Series No. 109, *Health Phys.* **21**, 613–14 (1971).
- J. A. Auxier, Z. G. Burson, R. L. French, F. F. Haywood, L. G. Mooney, and E. A. Straker  
*Nuclear Weapons Free-Field Environment Recommended for Initial Radiation Shielding Calculations*, ORNL-TM-3396 (February 1972).
- C. J. Barton, H. M. Butler, R. B. Cumming, and P. S. Rohwer  
 "The 1971 Tritium Symposium at Las Vegas," *Nucl. Safety* **13**(3), 225–35 (May–June 1972).
- C. J. Barton, D. G. Jacobs, M. J. Kelly, and E. G. Struxness  
 "Radiological Considerations in the Use of Natural Gas from Nuclearly Stimulated Wells," *Nucl. Technol.* **11**, 335–44 (July 1971).
- C. J. Barton, R. E. Moore, and S. R. Hanna  
*Quarterly Progress Report on Radiological Safety of Peaceful Uses of Nuclear Explosives: Hypothetical Exposures to Rulison Gas*, ORNL-TM-3601 (October 1971).
- K. Becker  
 "Application of the Track Etching Process in Radiation Protection," p. V3 in *Proceedings of International Topical Conference on Nuclear Track Registration in Insulating Solids, May 6-9, 1969*, Clermont-Ferrand, France, 1969.  
*Report of Trip to Europe During Period October 5, 1971 – October 23, 1971*, ORNL-CF 71-11-36 (November 24, 1971).  
*Health Physics and Dosimetry in Taiwan*, IAEA Report to the Government of the Republic of China (1971).  
*Health Physics in Brazil*, IAEA Report to the Government of Brazil (1972).  
 Book Review: "The Photographic Action of Ionizing Radiation in Dosimetry and Medical, Industrial, Neutron, Auto- and Microradiography," R. H. Herz, Wiley, 1969, *Rev. Sci. Instrum.* **42**, 1096 (1971).  
 "Personnel Neutron Dosimetry Research at ORNL" in *Proceedings of the Second AEC Workshop on Personnel Neutron Dosimetry, July 8 and 9, 1971*, New York (to be published).  
 "New Developments in Solid-State Dosimetry," in *Proceedings of the First Latin American Conference on Physics in Medicine and Radiation Protection, February 28 to March 3, 1972*, Sao Paulo, Brazil (to be published).  
 "Stimulated Exoelectron Emission from the Surface of Insulating Solids," *Crit. Rev. Solid State Sci.* **3**(1), 39–81 (1972).  
 "Dosimetric Applications of Track Etching," in *Progress in Radiation Dosimetry*, ed. by F. H. Attix (in publication).

- "The Future of Personnel Dosimetry," to be published in *Health Physics*.
- "Progress in Luminescence Dosimetry," to be published in *Science*.
- "Environmental Monitoring with TLD," to be published in *Nuclear Instruments and Methods*.
- K. Becker, J. S. Cheka, K. W. Crase, and R. B. Gammage  
 "New Exoelectron Dosimeters," pp. 25–36 in *Proceedings of a Symposium on New Developments in Physical and Biological Radiation Detectors, November 23 through 27, 1970*, Vienna, Austria, IAEA-SM-143/37, STI/PUB/269, Vienna, 1971.
- K. Becker, J. S. Cheka, and R. B. Gammage  
 "Progress in Exoelectron Dosimetry," pp. 318–54 in *Proceedings of the Third International Symposium on Exoelectrons, July 6 thru 8, 1970*, Braunschweig, Germany (W), PTB-Mitteilungen 80, Nr5, 1970.
- K. Becker and R. B. Gammage  
 "Exoelectron Emission and Surface Characteristics of Lunar Materials," vol. 3, pp. 2057–67 in *Proceedings of the Second Lunar Science Conference, January 11 to 14, 1971*, Houston, Texas, M.I.T. Press, 1971.
- K. Becker, R. B. Gammage, K. W. Crase, and J. S. Cheka  
 "Recent Advances in TSEE Dosimetry and Its Potentials in Microdosimetry," pp. 675–95 in *Proceedings of the Third Symposium on Microdosimetry, October 18 to 22, 1971*, Stresa, Italy, EUR 4810 d-f-e, 1972.
- K. Becker, Rosa Hong-Wei Lu, and Pao-Shan Weng  
 "Environmental and Personnel Dosimetry in Tropical Countries," part III, p. 960 in *Proceedings of the Third International Conference on Luminescence Dosimetry, October 11 to 14, 1971*, Risø, Denmark, Risø Report No. 249, Danish AEC, 1971.
- S. R. Bernard  
 "Estimates of Microcurie-Days Residence, Bone Dose Equivalent, and  $(MPC)_w$  for Thorium-232 in Man Using a Mammary Model," to be published in *The Bulletin of Mathematical Biophysics*.
- R. P. Blaunstein and L. G. Christophorou  
 "On Molecular Parameters of Physical, Chemical, and Biological Interest," *Radiat. Res. Rev.* 3, 69–118 (1971).
- R. S. Booth, O. W. Burke, and S. V. Kaye  
 "Dynamics of the Forage-Cow-Milk Pathway for Transfer of Radioactive Iodine, Strontium, and Cesium to Man," *Proceedings of American Nuclear Society Topical Meeting on Nuclear Methods in Environmental Research Columbia, Missouri, August 22–25, 1971* (in press).
- R. S. Booth and S. V. Kaye  
*A Preliminary Systems Analysis Model of Radioactivity Transfer to Man from Deposition in a Terrestrial Environment*, ORNL-TM-3135 (October 1971).
- A. J. Braundmeier, Jr., M. W. Williams, E. T. Arakawa, and R. H. Ritchie  
 "Radiation Decay of Surface Plasmons from Al," *Phys. Rev.* (in press).
- D. G. Brown and F. F. Haywood  
 "14 MeV Neutron Irradiation of Swine," to be published in *Health Physics*.
- D. G. Brown, D. F. Johnson, and J. A. Auxier  
 "Unilateral and Bilateral Exposure of Swine to Fission Neutrons," *Health Phys.* 21, 537–45 (1971).
- A. A. Christodoulides and L. G. Christophorou  
 "Electron Attachment to Aliphatic Hydrocarbons of the Form  $n-C_NH_{2N+1}Br$  ( $N = 1$  to 6, 8 and 10). Part 1: An Electron Swarm Study," *J. Chem. Phys.* 54, 4691–4705 (1971).
- L. G. Christophorou  
*Atomic and Molecular Radiation Physics*, Wiley, Sussex, England, 1971.
- "Intermediate Phase Studies for Understanding Radiation Interaction with Condensed Media: The Electron Attachment Process," submitted for publication in the *Journal of Chemical Physics*.
- "Recent Studies on Electron Attachment," in *Proceedings Third Tihany Conference on Radiation Chemistry* (in press).

- L. G. Christophorou and R. P. Blaunstein  
"Electron Attachment in Gases and Liquids," *Chem. Phys. Lett.* **12**, 173-79 (1971).
- L. G. Christophorou, J. G. Carter, E. L. Chaney, and P. M. Collins  
"Long-Lived Parent Negative Ions Formed by Capture of Low-Energy Electrons (0 to 3 eV) in the Field of the Ground and Excited Electronic States of Organic Molecules, in *Advances in Radiation Research* (Duplan and Chapiro, eds.), Gordon and Breach, 1972 (in press).
- L. G. Christophorou, J. G. Carter, P. M. Collins, and A. A. Christodoulides  
"Electron Attachment to Aliphatic Hydrocarbons of the Form  $n\text{-C}_N\text{H}_{2N+1}\text{Br}$  ( $N = 2-6$ , and 8). II. A Swarm-Beam Study," *J. Chem. Phys.* **54**, 4706-14 (1971).
- L. G. Christophorou, D. L. McCorkle, and V. E. Anderson  
"Swarm-Determined Electron Attachment Cross Sections as a Function of Electron Energy," *J. Phys. B: At. Mol. Phys.* **4**, 1163-72 (1971).
- C. D. Cooper and R. N. Compton  
"Metastable Anions of  $\text{CO}_2$ ," to be published in *Chemical Physics Letters*.
- K. W. Crase, K. Becker, and R. B. Gammage  
*Parameters Affecting the Radiation-Induced Thermally Stimulated Exoelectron Emission from Ceramic Beryllium Oxide*, ORNL-TM-3572 (November 1971).
- K. W. Crase, R. G. Gammage, and K. Becker  
"High Dose-Level Response of Ceramic  $\text{BeO}$ ," *Health Phys.* **22**, 402-405 (1972).
- H. J. Dunster and E. G. Struxness  
*Radiological Safety Evaluations Related to Planned and Unplanned Releases of Radioactive Materials Into the Natural Environment*, a report by Committee 4 of the International Commission on Radiological Protection, Oslo, Norway, June 19-22, 1972.
- J. L. Durham, B. R. Fish, Jack Wagman, and F. G. Seeley  
"Radiochemical Analysis of  $^{35}\text{SO}_2$  Adsorbed on  $\text{PbO}_2$ ," *Anal. Lett.* (July 1972).
- J. R. Dutrannois, R. N. Hamm, J. E. Turner, and H. A. Wright  
"Analysis of Energy Deposition in Water Around the Site of Capture of a Negative Pion by an Oxygen or Carbon Nucleus," submitted for publication in *Physics of Medicine and Biology*.
- J. M. Elson and R. H. Ritchie  
"Photon Interactions at a Rough Metal Surface," *Phys. Rev. B* **4**, 4129-38 (1971).  
"The Damping Rate of Plasma Waves in Condensed Matter," *Surface Sci.* **30**, 178-84 (1972).
- L. C. Emerson  
"Automatic Data Processing Using Tape Cassettes," submitted for publication in *Programmer*.
- L. C. Emerson, R. D. Birkhoff, V. E. Anderson, and R. H. Ritchie  
"Electron Slowing-Down Spectrum in Irradiated Silicon," submitted for publication in *The Physical Review*.
- B. R. Fish  
"Electrical Generation of Natural Aerosols from Vegetation," *Science* **175**, 1239 (1972).
- B. R. Fish and J. L. Durham  
"Diffusion Coefficient of  $\text{SO}_2$  in Air," *Environ. Lett.* **2**(1), 13 (1971).
- C. W. Francis and D. F. Grigal  
"A Rapid and Simple Procedure Using  $^{85}\text{Sr}$  for Determining Cation Exchange Capacities of Soils and Clays," *Soil Sci.* **112**(1), 17-21 (1971).
- R. B. Gammage and K. Becker  
"Search for Exoelectrons in Apollo 12 Materials," *Earth Planet Sci. Lett.* **12**, 155-58 (1971).

- R. B. Gammage, K. Becker, K. W. Crase, and A. Moreno y Moreno  
 "Chemically, Thermally and Radiation-Induced Changes in the TSEE Characteristics of Ceramic BeO," part II, p. 573 in *Proceedings of the Third International Conference on Luminescence Dosimetry, October 11 thru 14, 1971*, Risø, Denmark, Risø Report No. 249, 1971.
- R. B. Gammage, K. W. Crase, and K. Becker  
 "Role of Silicon Activator in Exoelectron Emission from BeO," *Health Phys.* 22, 56--63 (1972).
- W. R. Garrett  
 "Low-Energy Electron Scattering by Polar Molecules," submitted for publication in *Molecular Physics*.  
 "Re-examination of Scattering by a Pair of Fixed Dipolar Charges," *Phys. Rev. A* 4, 2229--35 (1971).
- T. F. Gesell and E. T. Arakawa  
 "Volume Plasmon Energy of Mg from Photoelectric Measurements," *Phys. Lett.* 36A, 79--80 (1971).
- J. T. Grissom, R. N. Compton, and W. R. Garrett  
 "Slow Electrons from Electron Impact Ionization of He, Ne, and Ar," submitted for publication in *The Physical Review*.
- W. F. Hanson and E. T. Arakawa  
 "High Energy X-Ray Satellites of the  $L_{2,3}$  Emission Bands of Na, Mg, Al, and Si," *Z. Physik* 251, 278--88 (1972).
- W. F. Hanson, E. T. Arakawa, and M. W. Williams  
 "Optical Properties of MgO and MgF<sub>2</sub> in the Extreme Ultraviolet Region," *J. Appl. Phys.* (in press).
- F. F. Haywood  
 Book Review: "Nuclear Accident Dosimetry Systems," IAEA, Vienna, STI/PUB/241, 1970, *Health Phys.* 21, 721--22 (1971).  
 "High Yield, Long-Lived Tritium Targets," Conference Proceedings for the 1971 Particle Accelerator Conference, March 1--3, 1971, Chicago, Illinois, *IEEE Trans. Nucl. Sci.* NS-8(3) (June 1971).  
 "Intercomparison Studies in Nuclear Accident Dosimetry at Oak Ridge National Laboratory," News Section, *Health Phys.* 22, 305 (1972).  
 1970 Intercomparison of Nuclear Accident Dosimetry Systems at the Oak Ridge National Laboratory, ORNL-TM-3551 (February 1972).
- F. F. Haywood, Z. G. Burson, and H. E. Banta  
 A Self-Replenishing Tritium Target for Neutron Generators, ORNL-TM-3397 (June 1972).
- F. F. Haywood, P. T. Perdue, and J. H. Thorngate  
 Low Energy X-Ray Spectrometry, CF-72-3-23 (March 15, 1972).
- F. F. Haywood and J. W. Poston  
 Second IAEA Nuclear Accident Dosimetry Coordination Meeting and Intercomparison Experiment, May 3--15, 1971, ORNL-TM-3770 (in publication).
- H. H. Hubbell, Jr.  
 Book Review: "Radiation Dosimetry: X Rays Generated at Potentials of 5 to 150 kV," ICRU Report 17, *Health Phys.* 21, 341 (1971).
- H. H. Hubbell, Jr., T. D. Jones, and J. S. Cheka  
 The Epicenters of the Atomic Bombs in Japan, Part II. Reevaluation of all Available Data and Our Recommended Values, ABCC-TR 3-69 (1972).
- G. S. Hurst  
 Book Review: "Radiation Protection Instrumentation and Its Application," ICRU Report 20. *Nucl. Safety* 13(3), 261 (1972).
- D. G. Jacobs  
 "Tritium," pp. 423--25 in *McGraw-Hill Yearbook of Science and Technology*, McGraw-Hill, New York, 1971.

- D. G. Jacobs, C. J. Barton, C. R. Bowman, G. R. Briggs, W. M. Culkowski,  
M. J. Kelly, P. S. Rohwer, and E. G. Struxness  
*Theoretical Evaluation of Consumer Products from Project Gasbuggy, Final Report, Phase I: Impact of Hypothetical Releases of Contaminated Gas in the San Juan Basin*, ORNL-4646 (Sept. 1971).
- D. G. Jacobs, C. J. Barton, C. R. Bowman, S. R. Hanna, M. J. Kelly, W. M. Culkowski, and F. A. Gifford, Jr.  
*Theoretical Evaluation of Consumer Products from Project Gasbuggy – Final Report, Phase II: Hypothetical Population Exposures Outside San Juan Basin*, ORNL-4748 (February 1972).
- D. G. Jacobs and E. G. Struxness  
“Radiological Safety Considerations in the Distribution of Natural Gas That Contains Radionuclides,” pp. 319–39 in *Peaceful Nuclear Explosions II*, International Atomic Energy Agency, Vienna, Austria, 1971.
- D. G. Jacobs, E. G. Struxness, M. J. Kelly, and C. R. Bowman  
“Consideration of the Radiological Impact from the Hypothetical Use of Contaminated Natural Gas from Nuclearly Stimulated Reservoirs,” *Health Phys.* 22, 429–440 (May 1972).
- T. D. Jones  
“Dose and LET in a Rabbit and a Rat,” *Health Phys.* 21, 553–62 (1971).  
*Report of Trip to Japan During Period August 13 thru September 25, 1971*, CF-71-10-17 (October 18, 1971).  
*Health Physics Division – Oak Ridge National Laboratory and Atomic Bomb Casualty Commission Liaison Pool Activities, Period August 13 thru September 25, 1971* (in preparation).  
“Solid Geometry vs. Plane Geometry for  $^{252}\text{Cf}$  Sources,” to be published in *Health Physics*.
- T. D. Jones and J. A. Auxier  
“Absorbed Dose and Linear Energy Transfer Distributions from Therapeutic Sources of  $^{252}\text{Cf}$ ,” *Phys. Med. Biol.* 17, 206–17 (1972).  
“Local Dose from Neutron Produced Recoil Ions in the Region of a Therapeutic  $^{252}\text{Cf}$  Needle,” to be published in *Radiology*.
- T. D. Jones, J. S. Auxier, W. S. Snyder, and G. G. Warner  
“Dose to Standard Reference Man from External Sources of Monoenergetic Photons,” to be published in *Health Physics*.
- T. D. Jones, W. S. Snyder, and J. A. Auxier  
“Absorbed Dose, Dose Equivalent, and LET Distributions in Cylindrical Phantoms Irradiated by a Collimated Beam of Monoenergetic Neutrons,” *Health Phys.* 21, 253–72 (1971).
- S. V. Kaye, R. S. Booth, P. S. Rohwer, and E. G. Struxness  
“A Cumulative Index (CUEx) for Assessing Environmental Releases of Radioactivity,” *Proceedings of International Symposium on Radioecology Applied to the Protection of Man and His Environment, Rome, Italy, September 7–10, 1971* (in press).
- M. J. Kelly, C. J. Barton, A. S. Meyer, E. W. Chew, and C. R. Bowman  
*Theoretical Evaluation of Consumer Products from Project Gasbuggy – Final Report: Tritium Behavior in a Natural Gas Processing Plant*, ORNL-4775 (July 1972).
- G. D. Kerr, J. T. Cox, L. R. Painter, and R. D. Birkhoff  
“A Reflectometer for Studying Liquids in the Vacuum Ultraviolet,” *Rev. Sci. Instrum.* 42, 1418–22 (1971).
- G. D. Kerr, J. W. Poston, and E. M. Robinson  
*Health Physics and Safety Guidelines for the DOSAR Facility*, ORNL-TM-1981 (Revision 1) (April 1972).
- G. D. Kerr, M. W. Williams, R. D. Birkhoff, and L. R. Painter  
“Optical Properties of Some Silicone Diffusion-Pump Oils in the Vacuum Ultraviolet – Using an Open-Dish Technique,” *J. Appl. Phys.* 42, 4258–61 (1971).

C. E. Klots

"Comparison of Photoabsorption and Resonance Energy Transfer Processes," in *Advances in Radiation Research* (Duplan and Chapiro, eds.), Gordon and Breach, 1972 (in press).

"Ionic Fragmentation through Centrifugal Barriers," *Chem. Phys. Lett.* **10**, 422-23 (1971).

"Photosensitized Ionization of Molecules by Argon: Comparison with the Photoionization Mechanism," *J. Chem. Phys.* **56**, 124-31 (1972).

"Quasi-Equilibrium Theory of Ionic Fragmentation: Further Considerations," *Z. Naturforsch.* **27A**, 553 (1972).

C. E. Klots and V. E. Anderson

"Monte Carlo Investigation of the Imprisonment of Resonance Radiation: The Doppler-Broadened Line," *J. Chem. Phys.* **56**, 120-24 (1972).

D. L. McCorkle, L. G. Christophorou, and V. E. Anderson

"Low-Energy ( $\lesssim 1$  eV) Electron Attachment to Molecules at Very High Gas Densities: O<sub>2</sub>," Submitted for publication in the *Journal of Physics B*.

R. E. Moore and C. J. Barton

*Progress Report on Radiological Safety of Peaceful Uses of Nuclear Explosives: Preliminary Equations and Computer Techniques for Estimating and Controlling Tritium Doses from Nuclearily Stimulated Natural Gas*, ORNL-TM-3755 (June 1971).

A. Moreno y Moreno, J. S. Cheka, J. S. Nagpal, R. B. Gammage, and K. Becker

*Further Studies on TSEE Activators in BeO*, ORNL-TM-3668 (March 1972).

K. Z. Morgan

"Radioactivity from Possible Accidents," Chap. 2 in *Nuclear Power and the Environment*, WHO/IAEA Booklet on the Environmental Aspects of Nuclear Power Production, January 1972.

"Public Health and Environmental Aspects of Nuclear Power Production," Chap. 5 in *Nuclear Power and the Environment*, WHO/IAEA Booklet on the Environmental Aspects of Nuclear Power Production, January 1972.

K. Z. Morgan and J. E. Turner

"Health Physics," to be published in *American Institute of Physics Handbook*.

W. T. Naff, R. N. Compton, and C. D. Cooper

"Electron Attachment and Excitation Processes in Selected Carbonyl Compounds," submitted for publication in the *Journal of Chemical Physics*.

S. J. Nalley, R. N. Compton, and H. C. Schweinler

"Cesium Charge Exchange," submitted for publication in the *Journal of Chemical Physics*.

D. R. Nelson and F. J. Davis

"Thermal and Near Thermal Electron Transport Coefficients in O<sub>2</sub> Determined with a Time-of-Flight Swarm Experiment Using a Drift-Dwell-Drift Technique," submitted for publication in the *Journal of Chemical Physics*.

D. R. Nelson, F. J. Davis, and V. E. Anderson

"Analysis of Time-of-Flight Data from a Pulsed-Field Electron Swarm Experiment," ORNL-TM-3742 (in preparation).

J. Neufeld

"Absorbed Dose and Tissue Dose," to be published in *Health Physics*.

"Dose Equivalent Index," to be published in *Health Physics*.

"Dosimetric Field Quantities in Health Physics," *Health Phys.* **21**, 97-104 (1971).

"Metrology in Health Physics and the ICRU," *Health Phys.* **21**, 715-18 (1971).

"Reply to Comments on 'Radiation Quantities and their Significance in Health Physics - Parts 1 and 2'," *Health Phys.* **22**, 416-17 (1972).

"What is Energy Imparted?" *Health Phys.* **21**, 317-21 (1971).

- J. Neufeld and Harvel Wright  
 "Radiation Levels and Fluence Conversion Factors," *Health Phys.* (in press).
- J. E. Parks, G. S. Hurst, T. E. Stewart, and H. L. Weidner  
 "Ionization of Noble Gases by Protons: Jesse Effects as a Function of Pressure," to be published in *The Physical Review*.
- P. T. Perdue  
 "Hazards of Irradiated Liquid Nitrogen -- A Brief Bibliography," *Health Phys.* **23**, 117 (1972).
- P. T. Perdue and J. H. Thorngate  
*A Paper Tape to Typewriter Translator that Suppresses Insignificant Zeros*, ORNL-TM-3692 (March 1972).
- M. N. Pisanias, L. G. Christophorou, and J. G. Carter  
 "Compound Negative Ion Resonances and Threshold-Electron Excitation Spectra of Quinoline and Isoquinoline," *Chem. Phys. Lett.* (in press).
- J. W. Poston  
 "A Detector for the Measurement of Dose Distributions at a Bone-Tissue Interface," pp. 299--310 in *Advances in Physical and Biological Radiation Detectors*, Vienna, 1971, IAEA-SM-143/36.  
 Book Review: "Protection Against Neutron Radiation," NCRP Report No. 38, 1971, *Nucl. Safety* **12**(4), 337 (July--August 1971).  
 Book Review: "Health Physics Aspects of Nuclear Facility Siting, Proceedings of the Fifth Annual Health Physics Society, Midyear Topical Symposium," 1970, to be published in *Health Physics*.  
*Report of Trip to Sao Paulo, Brazil, September 2--25, 1971*, ORNL-CF-71-11-38 (November 29, 1971).
- R. H. Ritchie  
 "Electron Slowing-Down-Cascade Spectra in Solids," *Nucl. Sci.* **NS-18**(6), 141--49 (1971).  
 "Plasmons in Solids," in *Proceedings NATO Advanced Study Institute* (in press).  
 "Surface Plasmons and the Image Force in Metals," *Phys. Lett.* **38A**, 189--90 (1972).
- P. S. Rohwer  
 "Responding to Public Concern Over Man-Made Radioactivity in the Environment," *Trans. Amer. Nucl. Soc.* **15**(1), 545--46 (June 1972).  
 "IAEA-WHO Symposium on Handling of Radiation Accidents," *Nucl. Safety* **12**(4), 338--48 (July--August 1971).
- P. S. Rohwer and E. G. Struxness  
 "Development of Radiation Safety Indices for Environmental Releases of Radioactivity," submitted for publication in *Health Physics*.
- W. S. Snyder  
 "Nuclear Safety at Geneva: A Review of the Nuclear Safety Aspects of the Fourth Geneva Conference," *Nucl. Safety* **13**(3), 198--99 (1972).
- M. Sohrabi and K. Becker  
*Some Studies on the Application of Track Etching in Personnel Fast Neutron Dosimetry*, ORNL-TM-3605 (December 1971).  
 "Fast Neutron Personnel Monitoring by Fission Fragment Registration from  $^{237}\text{Np}$ ," to be published in *Nuclear Instruments and Methods*.
- B. L. Sowers, R. D. Birkhoff, and E. T. Arakawa  
 "Optical Properties of Liquid Carbon Tetrachloride, n-Hexane, and Cyclohexane in the Vacuum Ultraviolet."  
 "Optical Absorption of Liquid Water in the Vacuum Ultraviolet," submitted for publication in the *Journal of Chemical Physics*.

- B. L. Sowers, M. W. Williams, R. N. Hamm, and E. T. Arakawa  
 "Optical Properties of Some Silicon Diffusion Pump Oils in the Vacuum Ultraviolet, Using a Closed Cell Technique," *J. Appl. Phys.* **42**, 4252--57 (1971).  
 "Optical Properties of  $\text{CCl}_4$ ,  $\text{C}_6\text{H}_6$ , and  $\text{C}_6\text{H}_6$  in the Vacuum Ultraviolet," submitted for publication in the *Journal of Chemical Physics*.
- T. E. Stewart, G. S. Hurst, J. E. Parks, and D. M. Bartell  
 "Vacuum Ultraviolet Emission from Proton Excited Helium Gas," *Phys. Rev. A* **3**, 1991--97 (1971).
- J. A. Stockdale, D. R. Nelson, F. J. Davis, and R. N. Compton  
 "Studies of Electron Impact Excitation, Negative Ion Formation, and Negative Ion-Molecule Reactions in Boron Trifluoride and Boron Trichloride," *J. Chem. Phys.* **56**, 3336--41 (1972).
- D. R. Stone and J. H. Thorngate  
 "The Development of a Spectrometer and the Measurement of the Neutron Spectrum from the Health Physics Research Reactor between 50 keV and 450 keV," *Health Phys.* **21**, 441--48 (1971).
- N. Thonnard and G. S. Hurst  
 "Time-Dependent Study of Vacuum-Ultraviolet Emission in Argon," *Phys. Rev. A* **5**, 1110--21 (1972).
- J. H. Thorngate  
 Book Review: "Neutron Capture Gamma Ray Spectroscopy, Proceedings of the International Symposium on Neutron Capture Gamma Ray Spectroscopy, Studsvik, August 11 thru 15, 1969," IAEA, Vienna, 1969, *Health Phys.* **21**, 482--83 (1971).  
 Book Review: "Gamma-Ray Spectrometry of Rocks," Elsevier Publishing Company, New York, 1970, *Health Phys.* **22**, 420 (1972).  
 Book Review: "Advances in Physical and Biological Radiation Detectors, Proceedings of a Symposium, Vienna, November 23--27, 1970," IAEA, Vienna, 1971, to be published in *Health Physics*.
- J. H. Thorngate and C. P. Littleton  
*An Interval Timer Designed for Use During Irradiations at the Health Physics Research Reactor*, ORNL-TM-1559 (Revision 1) (June 1972).
- J. H. Thorngate and P. T. Perdue  
 "A Stable Pulsed Light Source Using Low-Cost Light Emitting Diodes," to be published in *Nuclear Instruments and Methods*.
- J. E. Turner  
 Book Review: "Current Topics in Radiation Research," M. Ebert and A. Howard, eds., American Elsevier Publishing Co., Inc., 1970, *Health Phys.* **21**, 483--84 (1971).  
 "Microdosimetry" (Third Symposium on Microdosimetry -- Report prepared by J. E. Turner), *Health Phys.* **22**, 421--23 (1972).  
 "Meaning and Assessment of Radiation Quality for Radiation Protection," in *Biophysical Aspects of Radiation Quality*, International Atomic Energy Agency IAEA-SM-145/3, Vienna, 1971.  
 "Review of ICRU Report 19, Radiation Quantities and Units," *Nucl. Safety* **13**, 135 (1972).
- J. E. Turner, J. Dutrannois, H. A. Wright, R. N. Hamm, J. Baarli, A. H. Sullivan, M. J. Berger, and S. M. Seltzer  
 "The Computation of Pion Depth-Dose Curves in Water and Comparison with Experiment," submitted for publication in *Radiation Research*.
- J. E. Turner and C. E. Klots  
 "Status of the Theory of Delta-Ray Production," pp. 31--69 in *Proceedings Third Symposium on Microdosimetry*, EUR 4810-d-f-e, 1972.

U. S. Whang, E. T. Arakawa, and T. A. Callcott

“Optical Properties of Cs for Photons of Energy 3.6 to 9.6 eV,” *J. Opt. Soc. Amer.* **61**, 740–45 (1971).

“Optical Properties of K between 4 and 10.7 eV and Comparison with Na, Rb, and Cs,” submitted to *Physical Review*.

“Optical Properties of Rb for Photons of Energy 3.3 to 10.5 eV,” *Phys. Rev. B* **5**, 2118-24 (1972).

M. W. Williams and E. T. Arakawa

“Optical Properties of Glassy Carbon from 0 to 82 eV,” submitted for publication in the *Journal of Applied Physics*.

Harvel Wright and W. S. Snyder

“On the Differentiability of Arbitrary Real-Valued Set Functions-II,” *Trans. Amer. Math. Soc.* **161**, 111–22 (1971).

## Lectures

C. J. Barton

*Dose Estimates for Nuclearly Stimulated Natural Gas*, Ten-Week Health Physics Course of the Oak Ridge Associated Universities, June 3, 1972, Oak Ridge, Tennessee.

*Safe Handling of Tritium and Carbon-14 in the Laboratory*, Seminar at Gulf Research and Development Laboratory, February 7, 1971, Merriam, Kansas.

K. Becker

*Recent Progress in Solid-State Dosimetry*, National Atomic Research Center, July 1, 1971, Seoul, South Korea.

*Advances in Exoelectron Research*, University of Osaka, July 2, 1971, Osaka, Japan.

*Progress in Solid-State Dosimetry*, Japan Radioisotope Society, July 3, 1971, Tokyo, Japan.

*Dosimetric Applications of Track Etching*, Institute of Biophysics, Federal University of Rio de Janeiro, February 17, 1972, Rio de Janeiro, Brazil.

*Thermoluminescence and Exoelectron Emission*, Institute of Biophysics, Federal University of Rio de Janeiro, February 24, 1972, Rio de Janeiro, Brazil.

*Thermally Stimulated Exoelectron Emission*, Division of Solid-State Physics, Institute of Atomic Energy, March 7, 1972, Sao Paulo, Brazil.

*Measurement of External Radiation Personnel Exposure*, Division of Solid-State Physics, Institute of Atomic Energy, March 15, 1972, Sao Paulo, Brazil.

*Track Etching and Its Application for Radiation Measurements*, National Institute for Scientific Research, March 27, 1972, Rio de Janeiro, Brazil.

*Radiophotoluminescence and Other Techniques of Solid-State Dosimetry*, Institute of Biophysics, Federal University of Rio de Janeiro, March 29, 1972, Rio de Janeiro, Brazil.

*Inside South America*, Health Physics Division Seminar, May 1, 1972, Oak Ridge, Tennessee.

L. G. Christophorou

*Low-Energy Electron-Molecule Interaction Processes*, Hahn-Meitner Institute, June 5, 1972, Berlin, West Germany.

*Recent Studies on the Interaction of Slow Electrons with Molecules*, Institute fur Physikalische Chemie, June 6, 1972, Julich, West Germany.

*Electron Attachment Studies at Very High Densities*, Interuniversity Reactor Institute, June 7, 1972, Delft, Netherlands.

*Recent Studies on Electron Attachment*, The Hebrew University, June 13, 1972, Jerusalem, Israel.

*Recent Studies on Low-Energy Electron-Molecule Interaction Processes*, Soreq Nuclear Research Center, June 16, 1972, Jerusalem, Israel.

- Low-Energy Electron-Molecule Interaction Processes*, University of California, May 19, 1972, Los Angeles, California.
- R. N. Compton  
*Chemi-Ionizing Collisions Between Cesium and Molecules*, University of North Carolina, March 7, 1972, Chapel Hill, North Carolina.  
*Mechanisms for Formation of Singly and Doubly Charged Negative Ions*, Florida State University, October 5, 1971, Tallahassee, Florida.
- B. R. Fish  
*Present State of the Atmosphere*, Oak Ridge Associated Universities, October 1971 and June 23, 1972, and Ritta Community Club, February 1972.
- H. H. Hubbell, Jr.  
*The Calculation of Radiation Doses to Survivors of the Nuclear Bombing of Japan*, Oak Ridge Associated Universities Medical Division Staff Seminar, October 12, 1971, Oak Ridge, Tennessee.
- K. Z. Morgan  
*Panel Discussion on Radiation Standards and the Population*, Oak Ridge Associated Universities, Atomic Museum, August 3, 1971, Oak Ridge, Tennessee.  
*Radiation Tolerance Levels*, Oak Ridge Associated Universities, August 13, 1971, Oak Ridge, Tennessee.  
*Health Physics Lecture Course*, Sao Paulo Institute, September 27–October 15, 1971, Sao Paulo, Brazil.  
*The Changing Role of the Health Physicist*, Brookhaven National Laboratory Health Physics Symposium, October 28, 1971, Upton, L.I., New York.  
*Proper Use of Information on Organ and Body Burdens of Radioactive Materials*, IAEA/WHO Symposium on the Assessment of Radioactive Organ and Body Burdens, November 22–26, 1971, Stockholm, Sweden.  
*Linear Versus Threshold Hypothesis for Low Radiation Exposure*, University of North Carolina, January 19, 1972, Charlotte, North Carolina.  
*The Need for Radiation Protection*, Southeastern Conference of Radiologic Technologists, January 22, 1972, Durham, North Carolina.  
*Linear Versus Threshold Hypothesis for Low Radiation Exposure*, Georgia Institute of Technology, January 25, 1972, Atlanta, Georgia.  
*Effects of Low Levels of Exposure to Man*, Lenoir Rhyne College, January 17, 1972, Hickory, North Carolina.  
*Effects of Low Levels of Exposure to Man*, Davidson College, January 20, 1972, Davidson, North Carolina.  
*Criteria for the Control of Radioactive Effluents Appropriate for Nuclear Power Reactors and Other Peaceful Applications of Radiation*, Puerto Rico Nuclear Center, April 4, 1972, Mayaguez, Puerto Rico.  
*The Basis of Standards for Radiation Protection*, University of Puerto Rico, April 4, 1972, Mayaguez, Puerto Rico.  
*Criteria for the Control of Radioactive Effluents Appropriate for Nuclear Power Reactors and Other Peaceful Applications of Radiation*, University of Florida, April 6, 1972, Gainesville, Florida.  
*University of Tennessee Internal Dose Lectures*, University of Tennessee, April 25, 1972, April 27, 1972, May 9, 1972, May 11, 1972, May 16, 1972, and May 18, 1972, Knoxville, Tennessee.  
*Health Physics Measures to Implement New USAEC Regulations Relating to Radiation Exposure of the General Public*, Second European Congress of IRPA, May 3–5 1972, Budapest, Hungary.  
*The Need to Reduce Medical Exposure in the United States*, Testimony on Senate Bill S.3327, May 15, 1972, Washington, D.C.  
*Biological Effects of Radioactive Isotopes*, University of California, May 23, 1972, Santa Barbara, California.  
*Biological Effects of Radioactive Isotopes*, University of California, May 24, 1972, Los Angeles, California.

*Problems Relating to Medical Exposure*, Southeastern Radiological Health Laboratory and the Alabama Chapter of the Health Physics Society, May 26, 1972, Birmingham, Alabama.

*Comparison of Radiation Exposure of the Population from Medical Diagnosis and the Nuclear Energy Industry*, American Nuclear Society Meeting, June 18–22, 1972, Las Vegas, Nevada.

J. W. Poston

*Interaction of Radiation with Matter*, Health Physics Course, University of Sao Paulo, Instituto of Atomic Energy, September 6–24, 1971, Sao Paulo, Brazil.

*Radiation Quantities and Units*, Health Physics Course, University of Sao Paulo, Instituto of Atomic Energy, September 6–24, 1971, Sao Paulo, Brazil.

*The Physical Basis of Radiation Dosimetry*, Health Physics Course, University of Sao Paulo, Instituto of Atomic Energy, September 6–24, 1971, Sao Paulo, Brazil.

*Detection and Measurement of Radiation*, Health Physics Course, University of Sao Paulo, Instituto of Atomic Energy, September 6–24, 1971, Sao Paulo, Brazil.

*Mixed Radiation Dosimetry*, Health Physics Course, University of Sao Paulo, Instituto of Atomic Energy, September 6–24, 1971, Sao Paulo, Brazil.

*Special Methods in Radiation Dosimetry*, Health Physics Course, University of Sao Paulo, Instituto of Atomic Energy, September 6–24, 1971, Sao Paulo, Brazil.

*Dose from Electrons and Beta Rays*, Health Physics Course, University of Sao Paulo, Instituto of Atomic Energy, September 6–24, 1971, Sao Paulo, Brazil.

*Introduction to Radiation Biology*, Health Physics Course, University of Sao Paulo, Instituto of Atomic Energy, September 6–24, 1971, Sao Paulo, Brazil.

*The Health Physics Research Reactor*, Seminar, University of Sao Paulo, Instituto of Atomic Energy, September 6–24, 1971, Sao Paulo, Brazil.

*Operation BREN and HENRE*, Seminar, University of Sao Paulo, Instituto of Atomic Energy, September 6–24, 1971, Sao Paulo, Brazil.

*Nuclear Accident Dosimetry Systems and Intercomparisons*, Seminar, University of Sao Paulo, Instituto of Atomic Energy, September 6–24, 1971, Sao Paulo, Brazil.

*Dose Distributions at the Bone-Tissue Interface*, Seminar, University of Sao Paulo, Instituto of Atomic Energy, September 6–24, 1971, Sao Paulo, Brazil.

*Recent Developments in the Radiation Dosimetry Section*, Seminar, University of Sao Paulo, Instituto of Atomic Energy, September 6–24, 1971, Sao Paulo, Brazil.

*Depth Dose Distributions in Homogeneous Tissue-Equivalent Phantoms*, Seminar, University of Sao Paulo, Instituto of Atomic Energy, September 6–24, 1971, Sao Paulo, Brazil.

*Intercomparison of Survey Instruments in Common Use in Health Physics*, Seminar, University of Sao Paulo, Instituto of Atomic Energy, September 6–24, 1971, Sao Paulo, Brazil.

*Dose-Effect Relationships Among Survivors of the Atomic Bombings in Hiroshima and Nagasaki*, Seminar, University of Sao Paulo, Instituto of Atomic Energy, September 6–24, 1971, Sao Paulo, Brazil.

*Depth Dose Calculations*, Seminar, University of Sao Paulo, Instituto of Atomic Energy, September 6–24, 1971, Sao Paulo, Brazil.

R. H. Ritchie

*The Theory of Plasmon Excitation by Swift Electrons*, NATO Advanced Study Institute, August 16–27, 1971, Istanbul, Turkey.

*The Theory of Optical Plasma Resonances in Solids*, NATO Advanced Study Institute, August 16–27, 1971, Istanbul, Turkey. The  $Z_1^3$  Effect in Stopping Power, Institute of Physics, Aarhus University, September 7, 1971, Aarhus, Denmark.

*Surface Plasmons*, Stevens Institute of Technology, November 17, 1971, Hoboken, New Jersey.

*Surface Plasmons in Solids*, University of North Carolina, February 16, 1972, Chapel Hill, North Carolina.

P. S. Rohwer

*Assessment of Environmental Releases of Radioactivity – Impact Statements*, Invited Guest Seminar Program, Lawrence Livermore Laboratory, January 17, 1972, Livermore, California.

H. C. Schweinler

*A New Way to Get Molecular Potential Energy Curves*, University of Tennessee, October 5, 1971, Knoxville, Tennessee.

W. S. Snyder

*Historical Development of Radiation Standards*, ORAU Course on Radiation Protection and Health Physics, July 20, 1971, Oak Ridge, Tennessee.

*Present Standards of Radiation Protection*, ORAU Course on Radiation Protection and Health Physics, July 21, 1971, Oak Ridge, Tennessee.

*Principles of Dosimetry of Internal Emitters; The Use of Reference Man for Estimation of Dose; General Models for Dosimetry; Calculations of Depth Dose from External Sources of Radiation; Principles of Environmental Monitoring; Radiological Safety Assessment of Environmental Releases; Reactor Accidents and Emergency Planning; Radioactive Waste Management; Interpretation of an Exposure to Tritium; Monitoring of the Individual, Vivo Counting, Excretion Analysis; Monitoring for Exposure to Plutonium; The Clinch River Study: A Comprehensive Survey after 20 Years of Use for Disposal of Low Level Waste; Disposal of Radioactive Wastes at Oak Ridge National Laboratory by Hydraulic Fracturing; A Review of Some Accidents Involving Potentially Serious Exposure; Project Salt Vault: A Demonstration of High-Activity Waste Storage in Salt Mines; A Study of the Feasibility of Constructing a Sea-Level Canal with Nuclear Explosives; An Assessment of the Dose Resulting from Uses of Natural Gas Produced from Nuclearly Stimulated Wells*; Health Physics Course, University of Sao Paulo Institute of Atomic Energy, November 1–19, 1971, Sao Paulo, Brazil. *Absorbed Fractions of Gamma Energy for Organs of the Human Body: A Monte Carlo Study*, Department of Physics, Emory University, January 28, 1972, Atlanta, Georgia.

E. G. Struxness

*Assessing the Environmental Impact of Nuclear Power Plants*, 38th Annual Meeting of Southeastern Section of ASEE, University of Tennessee, April 5, 1972, Knoxville, Tennessee.



# HEALTH PHYSICS DIVISION

AUGUST 1, 1971-JUNE 30, 1972

K. Z. MORGAN, DIRECTOR  
 W. S. SNYDER, ASSISTANT DIRECTOR  
 E. G. STRUXNESS, ASSISTANT DIRECTOR THROUGH MAY 15, 1972  
 JEANNE S. CARVER  
 GWEN L. DAGLEY  
 NATALIE E. TARR

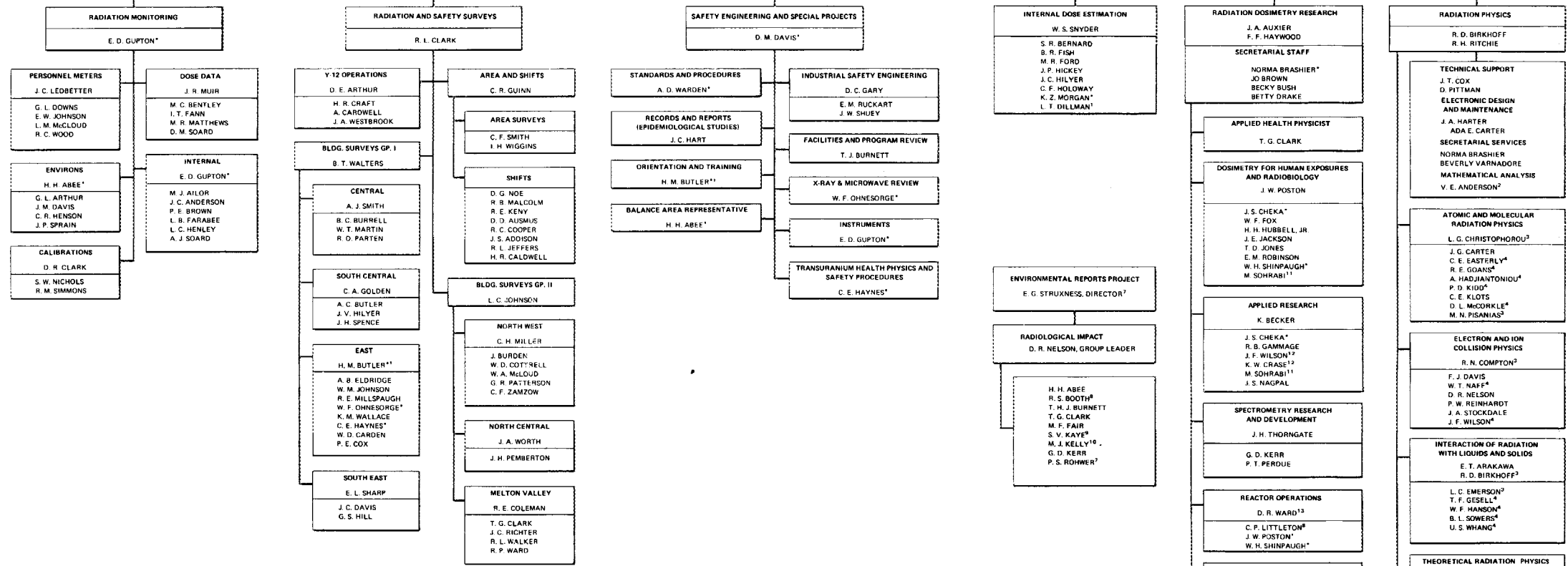
DRAFTING AND MAINTENANCE  
 E. T. LOY  
 J. L. MALONE

ADMINISTRATIVE ASSISTANT  
 W. D. GHORMLEY

OUTSIDE ASSIGNMENTS  
 K. E. COWSER  
 B. L. HOUSER  
 D. G. JACOBS

APPLIED HEALTH PHYSICS AND SAFETY  
 D. M. DAVIS\* - DEPARTMENT HEAD  
 A. D. WARDEN\* - ASST DEPARTMENT HEAD  
 DOT GADDIS  
 CAROLYN MILLER

RADIATION PHYSICS AND DOSIMETRY  
 W. S. SNYDER\*  
 SALLY STOCKSTILL



\* DUAL CAPACITY  
 † RADIATION CONTROL OFFICER DIVISION SAFETY OFFICER  
 ‡ CONSULTANT, OHIO WESLEYAN UNIVERSITY  
 § ON LOAN FROM CENTRAL DATA PROCESSING  
 ¶ DUAL ASSIGNMENT  
 †† GRADUATE STUDENT  
 ‡‡ ASSISTANT DIVISION DIRECTOR  
 §§ DIVISION DIRECTOR  
 ¶¶ ENVIRONMENTAL SCIENCES BEGINNING MAY 15, 1972  
 ††† INSTRUMENTATION AND CONTROLS DIVISION  
 ‡‡‡ ENVIRONMENTAL SCIENCES  
 §§§ REACTOR DIVISION  
 ¶¶¶ ALIEN GUEST  
 †††† STUDENT  
 ‡‡‡‡ NEUTRON PHYSICS DIVISION  
 §§§§ CONSULTANT

# HEALTH PHYSICS DIVISION

JULY 1, 1972

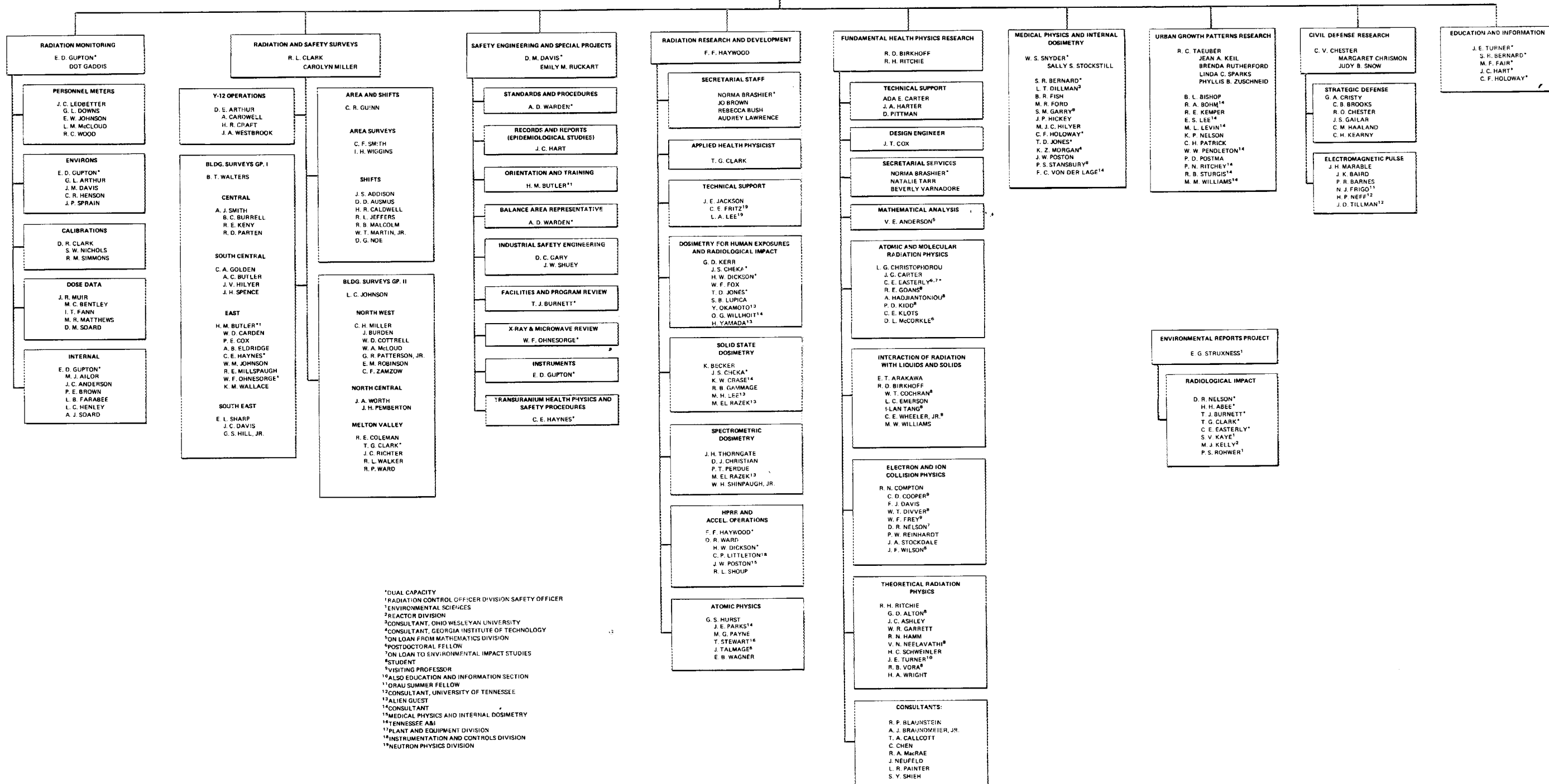
J. A. AUXIER, DIRECTOR  
 W. S. SNYDER, ASSISTANT DIRECTOR  
 D. M. DAVIS, ASSISTANT DIRECTOR  
 JEANNE S. CARVER  
 GWEN L. DAGLEY

ADMINISTRATIVE ASSISTANT  
 W. D. GHORMLEY

OUTSIDE ASSIGNMENTS  
 K. E. COWSER  
 B. L. HOUSER  
 D. G. JACOBS

DRAFTING AND MAINTENANCE  
 C. H. ABNER  
 E. T. LOY  
 J. L. MALONE

SENIOR RESEARCH ADVISORS  
 K. Z. MORGAN  
 E. P. WIGNER



\*DUAL CAPACITY  
 †RADIATION CONTROL OFFICER DIVISION SAFETY OFFICER  
 ‡ENVIRONMENTAL SCIENCES  
 §REACTOR DIVISION  
 ¶CONSULTANT, OHIO WESLEYAN UNIVERSITY  
 \*\*CONSULTANT, GEORGIA INSTITUTE OF TECHNOLOGY  
 ††ON LOAN FROM MATHEMATICS DIVISION  
 ‡‡POSTDOCTORAL FELLOW  
 †††ON LOAN TO ENVIRONMENTAL IMPACT STUDIES  
 §§STUDENT  
 ¶¶VISITING PROFESSOR  
 ††††ALSO EDUCATION AND INFORMATION SECTION  
 †††††ORAU SUMMER FELLOW  
 †††††CONSULTANT, UNIVERSITY OF TENNESSEE  
 †††††ALIEN GUEST  
 †††††CONSULTANT  
 †††††MEDICAL PHYSICS AND INTERNAL DOSIMETRY  
 †††††TENNESSEE A&I  
 †††††PLANT AND EQUIPMENT DIVISION  
 †††††INSTRUMENTATION AND CONTROLS DIVISION  
 †††††NEUTRON PHYSICS DIVISION